Oxidative Medicine and Cellular Longevity

# Brain Injury Due to Mechanical Trauma and Ischemic-Hypoxic Insult: Biomarkers of Brain Injury and Oxidative Stress

Lead Guest Editor: Margherita Neri
Guest Editors: Andreas Büttner and Vittorio Fineschi

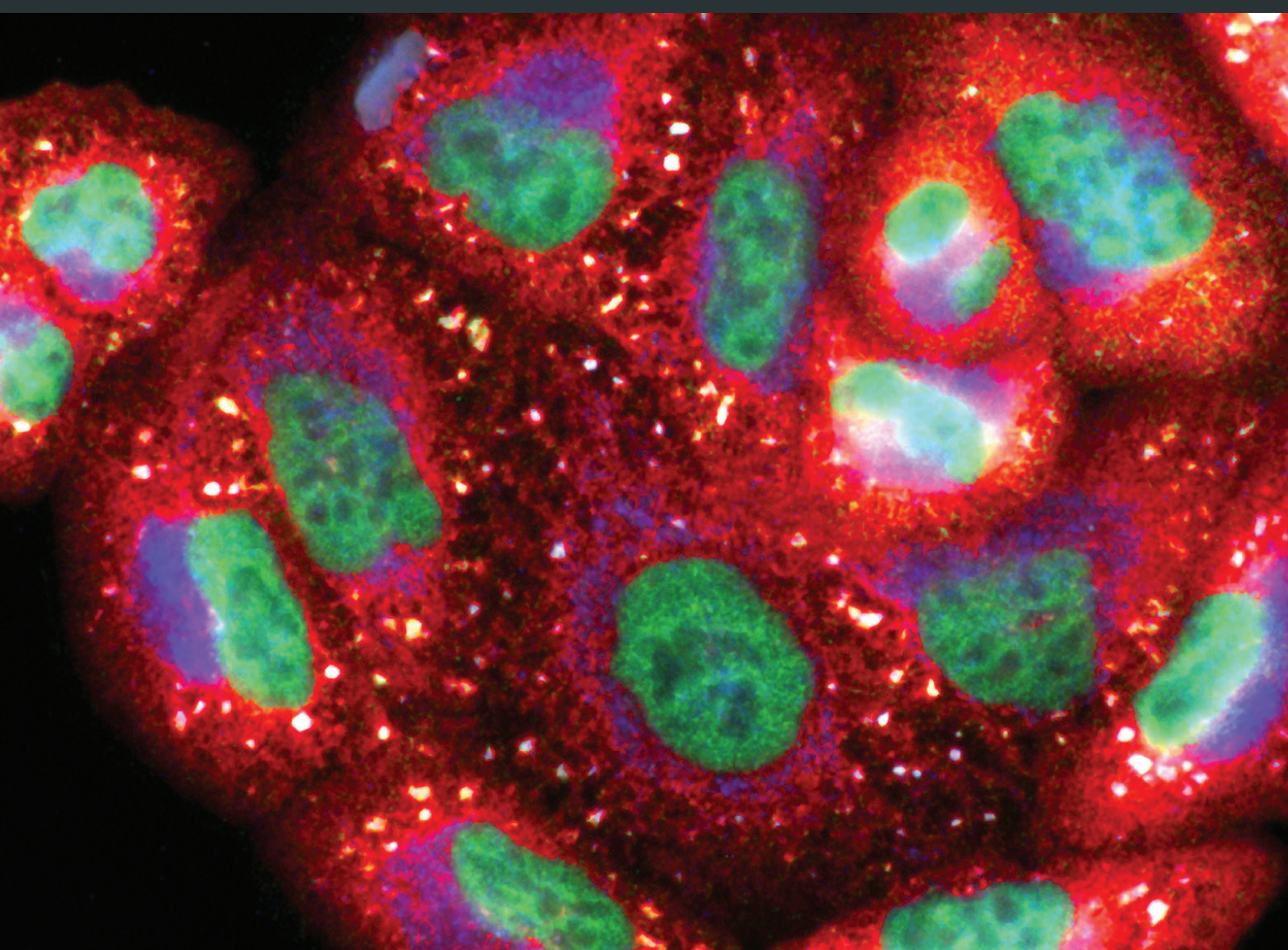

# Brain Injury Due to Mechanical Trauma and Ischemic-Hypoxic Insult: Biomarkers of Brain Injury and Oxidative Stress

Oxidative Medicine and Cellular Longevity

# Brain Injury Due to Mechanical Trauma and Ischemic-Hypoxic Insult: Biomarkers of Brain Injury and Oxidative Stress

Lead Guest Editor: Margherita Neri
Guest Editors: Andreas Büttner and Vittorio Fineschi

# Editorial Board

# Contents

Hindawi
Oxidative Medicine and Cellular Longevity
Volume 2017, Article ID 8923472, 2 pages
https://doi.org/10.1155/2017/8923472

*Editorial*

# Brain Injury due to Mechanical Trauma and Ischemic-Hypoxic Insult: Biomarkers of Brain Injury and Oxidative Stress

**Margherita Neri,[1] Andreas Büttner,[2] and Vittorio Fineschi[3]**

[1]*Department of Morphology, Surgery and Experimental Medicine, University of Ferrara, Via Fossato di Mortara, 70 44100 Ferrara, Italy*
[2]*Institute of Forensic Medicine, Rostock University Medical Center, Rostock, Germany*
[3]*Department of Anatomical, Histological, Forensic and Orthopaedic Sciences (SAIMLAL), Sapienza University of Rome, Viale Regina Elena 336, 00185 Rome, Italy*

Correspondence should be addressed to Margherita Neri; margheritaneri@hotmail.com

Received 22 August 2017; Accepted 22 August 2017; Published 24 September 2017



Brain injury (BI) due to mechanical trauma represents one of the major causes of mortality and disability in the world. The pathophysiology of BI is composed of two different pathogenetic moments: primary damage due directly to trauma, with mechanical forces applied to the head, and subsequent biochemical events due to a complex cell response that leads to the death of neuronal cells and classified as secondary damage. Accumulating evidence suggests that the extent of brain injury and the clinical outcome after BI are modulated, to some degree, by genetic variants. In the literature, the existence of a rather precise chronology of expression of the different markers of hypoxic-ischemic brain damage has been shown, which is correlated to the duration of the same insult and is to be ascribed, essentially, to a different stimulation of the different cellular types and also to a different response by the same cells to the ischemic insult.

In brain injury cases, there is a cross-talking network of cellular processes that involves the combination of the two major cell deaths: necrosis and apoptosis. Apoptosis plays an important role in brain development, as immature cells tend to apoptosis even in physiological conditions. In the face of a hypoxic-ischemic injury, apoptosis and necrosis overlap so much so that today it is normal to consider it a continuum of apoptosis-necrosis in a certain injured brain area.

As noted by J. I. Romero et al., it is apparent from the literature that various neuroprotective agents, described as effective from previous studies, have been used to improve the damage caused by hypoxia/ischemia in the central nervous system (CNS); however, none of them have been shown to be effective against damage induced by hypoxia/ischemia in the CNS. Their experimental paper aims to demonstrate the neuroprotective effects of Grx2 and Trx1 expressed exogenously, recombinantly in an animal model of neonatal hypoxia/ischemia, which was designed to look for potential new therapeutic strategies. By performing an elegant experimental procedure, the authors used a common carotid artery binding model in the P7 Sprague-Dawley P7 male rats subjected to a 100% nitrogen environment to induce anoxia. Grx2 and Trx1 were administered to examine the role of Grx2 and Trx1 recombinant as therapeutics after perinatal asphyxiation. The results are encouraging because the authors suggest that Grx2 administration first and Trx1 administration, in a small way, have the potential to significantly mitigate the neuronal damage caused by PA, including cell damage response, glutamate excitotoxicity, axonal integrity, and astrogliosis.

The therapeutic potential of another substance, SCM-198, was used to protect against ischemia-reperfusion injury and possible underlying mechanisms as studied by Q.-Y. Zhang et al. experimentally in rats by inhibition of transient cerebral artery in vivo (tMCAO).

The authors have shown that SCM-198 significantly decreased the volume of infarction and improved the neurologic deficit in the tMCAO model. In addition, SCM-198 could also reduce cellular lesion caused by OGD/R in vitro. Further studies on the mechanism have shown that HDAC4

could inhibit the expression of NOX4 and MMP9 and thus improve TJ levels and protect against blood-brain barrier (BBB) breakdown. This study therefore revealed that HDAC4 was involved in regulating BBB's integrity and that SCM-198 had protective effects against BBB destruction by improving HDAC4 expression. In the genesis of delayed permanent damage to the central nervous system, a primary role is due to oxidative stress. Among the major sources of reactive oxygen species (ROS) in the brain, one should remember that NADPH oxidases (Nox) and ubiquitary membrane multisubunit enzymes are involved in many neurological degenerative diseases. NOX isoforms have been examined as fundamental in the context of TBI-induced NLRP3 inflammasome pathway activation. Recent literature evidence shows that Nox-2 is upregulated after TBI; this objective finding therefore assumes a critical role both at the initial stage and in the subsequent development of this pathology.

M. W. Ma et al. organized an experiment with Nox-2 KO mouse: mice were anesthetized with isoflurane and subjected to an injury or controlled cortical impact. The study has shown that oxidative stress derived from NOX2 induces TXNIP interaction with NLRP3 to induce inflammation of NLRP3, which enhances inflammation in the wounded cortex after TBI. From this study, it is concluded that inflammation of NLRP3 may be useful as an effective treatment for TBI. NLRP3 may also be useful in other acute and chronic cerebral lesions involving inflammation of NLRP3.

A model of lesion of the spinal cord reperfusion (SCIR) was created by L. Xie et al. to evaluate the role of autophagy and its potential signaling path in SCIR and protective effect and internal mechanism of NAD+ involved in SCIR and to explore the underlying relationship between autophagy and NAD+. In conclusion, this study suggests excessive and sustained autophagic activation in SCIR. NAD+ administration can reduce the damage caused by I/R and inhibit neuronal cell apoptosis.

Another fundamental field of research is the neuropathological characteristics of blast polytrauma, a general aspect to better understand the body's response and reflexes on cerebral pathophysiology. In this regard, an interesting line of research has been put in place to document the effects of blast polytrauma with an animal model that also investigates the behavioral response, hypoxic effects, and the consequences of hypoxia itself on brain cellularity. In W. B. Hubbard et al.'s study, by studying reactive astrocytic response (GFAP), apoptosis, cleaved caspase-3 expression, and microglial activation, both in traumatic brain injury and in mild brain injury, and by comparing with the control group, we can explain the organism responses. In addition, by analyzing the integrity of the BBB and hypoxic and angiogenesis expressions, a comprehensive view is obtained to identify concrete and useful polytraumatic-specific injury markers that may be of practical and immediate utility in clinical routine.

The practical development of this experimental model is to examine the role of oxidative stress in a pathophysiological system governed by hypoxia.

Oxidative stress and aberrant deimination are part of the pathology that accompany brain damage. Blast traumatic brain injury causes protein deimination, and this is a reversible process. Basically, by activating calcium-dependent enzymes, aberrant protein deimination is caused causally by traumatic brain injury, in which the pathological response of the adaptive immune system is still largely the case.

In summary, the effects of brain injury due to mechanical trauma represent one of the major causes of mortality and disability in the world. A review of studies from the literature indicates that cell responses and pathological consequences seem to be more or less the same in most animal models, but the models diverge widely when it comes to their ability to produce the changes induced by combined effects due to trauma and/or hypoxia/ischemia in the CNS. The epidemiological importance of the underlying disease makes a thorough knowledge of its direct and indirect traumatic effects fundamental from the research, pathological, and emergency therapy points of view. This special issue wants to contribute for a better understanding on brain injury due to mechanical trauma-related pathophysiology, cellular responses, behavioral response, hypoxic effects, and the consequences of hypoxia itself on brain cellularity.

*Margherita Neri*
*Andreas Büttner*
*Vittorio Fineschi*

Hindawi
Oxidative Medicine and Cellular Longevity
Volume 2017, Article ID 6057609, 18 pages
https://doi.org/10.1155/2017/6057609

*Research Article*

# NADPH Oxidase 2 Regulates NLRP3 Inflammasome Activation in the Brain after Traumatic Brain Injury

**Merry W. Ma,[1,2] Jing Wang,[1,2] Krishnan M. Dhandapani,[1,3] and Darrell W. Brann[1,2]**

[1]*Charlie Norwood VA Medical Center, One Freedom Way, Augusta, GA 30904, USA*
[2]*Department of Neuroscience and Regenerative Medicine, Medical College of Georgia, Augusta University, Augusta, GA, USA*
[3]*Department of Neurosurgery, Medical College of Georgia, Augusta University, Augusta, GA, USA*

Correspondence should be addressed to Darrell W. Brann; dbrann@augusta.edu

Received 21 February 2017; Revised 2 May 2017; Accepted 1 June 2017; Published 12 July 2017

Academic Editor: Jacek Zielonka



Traumatic brain injury (TBI) is a leading cause of death and disability worldwide. After the initial primary mechanical injury, a complex secondary injury cascade involving oxidative stress and neuroinflammation follows, which may exacerbate the injury and complicate the healing process. NADPH oxidase 2 (NOX2) is a major contributor to oxidative stress in TBI pathology, and inhibition of NOX2 is neuroprotective. The NLRP3 inflammasome can become activated in response to oxidative stress, but little is known about the role of NOX2 in regulating NLRP3 inflammasome activation following TBI. In this study, we utilized NOX2 knockout mice to study the role of NOX2 in mediating NLRP3 inflammasome expression and activation following a controlled cortical impact. Expression of NLRP3 inflammasome components NLRP3 and apoptosis-associated speck-like protein containing a CARD (ASC), as well as its downstream products cleaved caspase-1 and interleukin-1$\beta$ (IL-1$\beta$), was robustly increased in the injured cerebral cortex following TBI. Deletion of NOX2 attenuated the expression, assembly, and activity of the NLRP3 inflammasome via a mechanism that was associated with TXNIP, a sensor of oxidative stress. The results support the notion that NOX2-dependent inflammasome activation contributes to TBI pathology.

## 1. Introduction

Traumatic brain injury (TBI) is a major cause of disability in young adults and contributes to over 30% of injury-related deaths [1]. In addition to the serious financial burden on the families and society, TBI can lead to grave long-term impairments for the survivors [2, 3]. TBI is a highly complex disorder that involves a primary injury resulting in neuronal death and a secondary injury cascade involving, but not limited to, edema, excitotoxicity, mitochondrial dysfunction, oxidative stress, and inflammation [4–7]. This secondary injury can extend past the initially damaged tissue and lead to further neurological deterioration for months after the primary injury [8]. Due to the heterogeneity of TBI patients and the complex nature of secondary injury cascades following TBI, translation of neuroprotective strategies or pharmacological treatments to the clinic has proven to be a challenge.

Oxidative stress is one of the major mediators of the secondary injury following TBI. Many sources may contribute toward the cellular production of reactive oxygen species (ROS); however, NADPH oxidases (NOX) are the only family of enzymes solely devoted to the production of ROS whereas other enzymes, such as xanthine oxidase, lipooxygenase, cyclooxygenase, nitric oxide synthase, and cyp450, generate ROS as a byproduct [9]. NOX has essential physiological functions for many cellular signaling pathways and immune defense [10]. However, sustained activation, such as that involved in chronically activated microglia after TBI, is detrimental to recovery and exacerbates the primary injury [11]. Several NOX isoforms have been studied in the context of TBI pathology both in humans and in rodents [12]. Postmortem analysis demonstrated a correlation between elevated NOX2 and NOX4 expression and clinical TBI severity [13, 14], and circulating neutrophils of TBI patients show increased NOX2 expression [15]. In rodents, our laboratory showed acutely increased NOX2 expression in the cortex and CA1 hippocampus in the days following TBI [16]. Other studies reported chronically elevated NOX2 expression

following TBI [11, 17], and a recent study also showed elevated NOX4 expression after TBI [14]. Inhibition of NOX2 has been shown to be neuroprotective by reducing lesion severity, apoptosis, oxidative damage, and inflammation [12, 16, 18].

Neuroinflammation is associated with the progression of neurodegenerative disorders and contributes to the secondary injury after TBI [19–22]. Inflammasomes, such as NOD-like receptors (NLRP) and absent in melanoma 2- (AIM 2-) like receptors, are innate immune system sensors of damage-associated molecular patterns (DAMPs) and pathogen-associated molecular patterns (PAMPs) that regulate the activation of caspase-1 and promote secretion of proinflammatory cytokines, such as IL-1$\beta$ and IL-18 [23–25]. NLRP3 is the most abundant and most studied inflammasome in brain injury [26–28]. Upon sensing stimuli, NLRP3 nucleotide-binding domain (NBD) oligomerizes the pyrin domain (PYD), which serves to nucleate apoptosis-associated speck-like protein containing a CARD (ASC) proteins through PYD-PYD interactions. Long ASC filaments then form and caspase activation recruitment domain (CARD) interactions recruit pro-caspase-1 to this multimeric protein complex. The proximity of pro-caspase-1 to one another induces an autoproteolytic cleavage that activates caspase-1, leading to further release of proinflammatory cytokines [24]. Although not extensively studied, there is growing evidence that inflammasomes play a role in TBI pathology. In support of this contention, high NLRP1, ASC, AIM 2, and caspase-1 expression was detected in the CSF of TBI patients [29–31] and correlated with severity of TBI [30]. Recent studies have reported elevated NLRP3 inflammasome expression in rat [32] and in human brains after TBI [33]. Furthermore, ATP and other ROS-induced DAMPs that are released after TBI [34] can activate the NLRP3 inflammasome, suggesting a potential therapeutic role for NLRP3 after TBI.

Mitochondrial ROS reportedly can activate NLRP3 inflammasomes [35]. In particular, NOX isoforms may serve as a source of ROS for inflammasome activation, as p22phox knockdown, apocynin, and DPI all independently diminished IL-1$\beta$ secretion [36]. ROS induction of NLRP3 activation would suggest potential involvement of redox-sensing proteins in the mechanism of ROS regulation of the inflammasome. In support of this possibility, thioredoxin-interacting protein (TXNIP) can directly activate NLRP3 inflammasome via dissociation of TXNIP from thioredoxin and subsequent binding to NLRP3 [37]. However, this has not yet been examined in the context of TBI.

The above studies suggest that NOX2 can potentially regulate NLRP3 inflammasome activation; however, several important questions remain unanswered. What is the temporal expression of the NLRP3 inflammasome in the mouse brain after TBI? Does NOX2 regulate NLRP3 inflammasome expression and complex formation, as well as downstream proinflammatory cytokines? If so, what is the mechanism mediating NOX2-derived ROS crosstalk with NLRP3 inflammasome-mediated neuroinflammation? To address these key questions, we used a NOX2 knockout (KO) mouse model to examine whether NOX2 is an essential regulator of NLRP3 inflammasome activation in TBI. The results of the study reveal that NLRP3 expression, complex formation, and activation are robustly increased in the injured mouse cerebral cortex after TBI—an effect paralleled by increased cleavage of caspase-1 with associated IL-1$\beta$ activation. Furthermore, NOX2 appears critical for TBI-induced NLRP3 inflammasome pathway activation, as NOX2 deletion strongly attenuates the expression, complex formation, and activation of NLRP3, as well as cleavage of caspase-1 and IL-1$\beta$ activation after TBI. Finally, the results also provide evidence that TXNIP may be a key factor mediating the crosstalk between oxidative stress and neuroinflammation.

## 2. Materials and Methods

*2.1. Animals.* Adult 3-month-old C5BL/6N male mice were obtained from Envigo (Prattville, AL) for use in this study. NOX2 KO (B6.129S-*Cybbtm1Din*/J; Stock number 002365) and WT (000664) mice of equivalent age and weight were obtained from Jackson Labs (Bar Harbor, ME). Mice were housed under humidity- and temperature-controlled conditions with free access to food and water. All animal experiments were approved by the Charlie Norwood VA Medical Center Institutional Animal Care and Use Committee.

*2.2. Controlled Cortical Impact.* Mice were anesthetized with isoflurane (2–4%) and subjected to a sham injury or controlled cortical impact as detailed previously by our laboratory [16, 38, 39]. Mice were placed in a stereotaxic frame (Leica Impact One™ Stereotaxic Impactor for CCI, Buffalo Grove, IL, USA), and a 3.5 mm craniotomy was made in the right parietal bone midway between the lambda and the bregma with the medial edge 1 mm lateral from the midline. The dura was left intact. TBI mice, but not shams, were impacted at 4.5 m/s impactor with 20 ms dwell time and 1 mm depression using a 3 mm diameter convex tip to produce a moderate TBI. Bone wax was used to cover the cranial window, and the scalp incision was closed with surgical staples. Mice were allowed to recover before being placed back in to their housing environment. Throughout the procedure, body temperature was monitored and maintained at 37°C using a small thermometer (Kopf Instruments, Tujunga, CA, USA). In experiments that utilized the NADPH oxidase inhibitor, apocynin (Sigma-Aldrich, 5 mg/kg) or saline was administered by intraperitoneal (IP) injections beginning at 23 hours after TBI and administered every 24 hours until the time of sacrifice. Sham-operated mice received identical treatment except for the cortical impact. Control animals did not undergo any procedures. Fewer mice were utilized for the sham and control groups due to their low variability within each group. WT TBI, KO TBI, and APO TBI groups indicate wild-type, NOX2 knockout, or apocynin-treated mice sacrificed at time points indicated in the text.

*2.3. Tissue Collection.* All animals were transcardially perfused with ice-cold saline and decapitated at the desired time point after TBI. For RT-PCR and Western blot analysis, the brains were dissected and processed, as described in subsequent sections. For coronal sections, mice were transcardially

perfused with saline and then 4% paraformaldehyde before decapitation. The perfused brains were removed, fixed in 4% paraformaldehyde for 24 hours, then cryoprotected in 30% sucrose, and sectioned on a cryostat to obtain 20 $\mu$M coronal sections for further staining, immunohistochemistry, or proximity ligation assay. Figure 1 outlines the perilesional area from where all confocal images were taken.

*2.4. BV2 Cell Experiments.* BV2, immortalized murine microglia, cells were cultured in RPMI 1640 media supplemented with 10% heat-inactivated FBS at 37°C in a humidified incubator with a 5% $CO_2$ atmosphere. Samples for inflammasome-positive control were collected after cells were treated with 500 ng/mL LPS (Sigma-Aldrich, L4130) for 3 hours. 20 $\mu$g protein was applied to each lane for Western blot analysis.

*2.5. Quantification of Lesion Volume and NeuN.* To quantify cortical tissue loss following CCI, coronal sections taken from the middle of the brain lesion showing the largest damage were stained with cresyl violet and imaged using a digital camera integrated with a light microscope. Using a similar method as previously described [40, 41], we took coronal sections from the center of the lesion for each mouse and assessed the area of the ipsilateral and contralateral cortices using NIH ImageJ software. The cortical lesion size was expressed as a percentage, calculated as follows: (Ac−Ai)/(Ac) × 100, where Ac is the contralateral cortical area and Ai is the ipsilateral cortical area. This method allows the quantification of lesion size as a percentage of the contralateral (uninjured) cortex of the same coronal section for each mouse. $NeuN^+$ cells were counted using a method similar to that previously reported [42]. $\%NeuN^+$ cells were calculated as (number of $NeuN^+$ cells)/(number of $DAPI^+$ cells) in a consistent and set area using 40x confocal images as described below. The percentages of $\%NeuN^+$ cells were reported relative to that of sham mice. Sections from 4 mice (4 sections per mouse) per experimental group were examined for the lesion analysis and for quantification of neuronal survival.

*2.6. RT-PCR.* Injured cortical tissue from the perilesional area (or an anatomically matched cortical area on sham/control mice) averaging 50–60 mg per mouse was collected at various time points after TBI. RNA was isolated using the SV total RNA isolation system (Promega). Superscript III one-step RT-PCR system with platinum Taq DNA Polymerase (Invitrogen) was used for reverse transcriptase-PCR. Primers are as listed in Table 1 (Integrated DNA Technologies). Gene expression analyses were done using the comparative ΔΔCt method, and mRNA changes were expressed as fold change as compared to control animals. 18S was used as the housekeeping gene for normalization. Group average ΔCt values for NLRP3, ASC, caspase-1, and IL-1$\beta$ are shown in Table 2.

*2.7. Western Blot Analysis.* 50–60 mg of injured cortical tissue from the perilesional area (or a similar cortical area on sham/control mice) was collected at various time points after TBI as previously described by our laboratory [16, 43]. The tissue was immediately frozen in dry ice or kept on ice for immediate homogenization using a tissue tear or with ice-cold RIPA buffer. The homogenate was centrifuged at 12,000 RPM for 20 minutes at 4°C, and the supernatant was aliquoted for further analysis. Protein concentrations were determined by the BCA Protein Assay (Thermo Fisher Scientific, Carlsbad, CA). 40 $\mu$g samples of protein was separated on a 4–20% SDS-PAGE gel and transferred onto 0.2 $\mu$M nitrocellulose membranes. Blots were blocked with 5% bovine serum albumin for 1 hour at room temperature with gentle shaking. After blocking, the blots were incubated overnight in 4°C with the following antibodies: NLRP3 (1 : 1000, Adipogen, AG-20B-0014), ASC (1 : 200, Santa Cruz, sc-22,514-R), cleaved caspase-1 p20 (1 : 1000, Adipogen, AG-20B-0042), and IL-1$\beta$ (1 : 1000, Abcam, ab9722). $\beta$-actin (1 : 4000, Sigma-Aldrich, A5441) was used as a loading control. The membrane was then washed with 1x TBST and then incubated with the secondary antibodies. Bound proteins were visualized using the Odyssey Imaging System (LI-COR Bioscience, Lincoln, NB) and analyzed with NIH ImageJ analysis software. The immunoblot densities were corrected based on corresponding $\beta$-actin-loading controls.

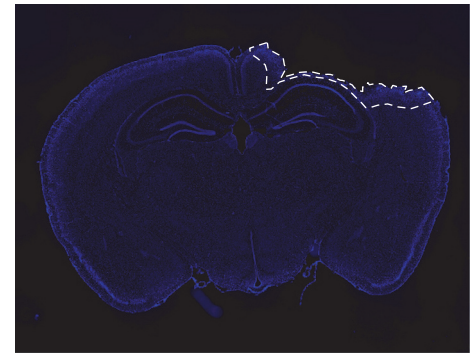

Figure 1: Demarcated perilesional area. Representative DAPI-stained confocal image of whole-brain slice showing perilesional area used for WB, IHC, and PCR analyses. Whole-brain image was created by stitching together 20 images taken at 4x of WT mouse at 4 d post-TBI. White-dotted outline demarcates perilesional area from where all confocal images have been taken.

*2.8. Confocal Microscopy and Image Analysis.* Three to four coronal sections from each mouse were washed with PBS and permeabilized with 0.4% Triton-X PBS for 20 minutes. The sections were then blocked with 10% normal donkey serum for 1 hour at room temperature in a buffer containing 0.1% Triton. Sections were incubated for 2 nights with the primary antibody at 4°C in the same buffer using the following antibodies: NeuN (1 : 200, Millipore MAB377), ASC (1 : 50, Santa Cruz, sc-22,514-R), NLRP3 (1 : 50, Santa Cruz, sc-66,846), cleaved caspase-1 p20 (1 : 50, Santa Cruz, sc-22,165), cleaved IL-1$\beta$ (1 : 50, Santa Cruz, sc-23,459), and TXNIP (1 : 50, Santa Cruz, sc-33,099). After the primary antibody incubation, the sections were washed in PBS and incubated with the appropriate secondary antibodies (1 : 500, Alexa Fluor 488/568) for 1 hour at room temperature. Sections were then mounted with water-based DAPI-mounting medium containing antifading agents and observed using confocal microscopy. All images were captured on a confocal laser

Table 1: List of RNA primers used for RT-PCR.

| Gene | Forward | Reverse |
|---|---|---|
| 18S | 5′ GTAACCCGTTGAACCCCATT 3′ | 5′ CCATCCAATCGGTAGTAGCG 3′ |
| NLRP3 | 5′ GTTCTGAGCTCCAACCATTCT ′3 | 5′ CACTGTGGGTCCTTCATCTTT 3′ |
| ASC | 5′ CAGAGTACAGCCAGAACAGGACAC 3′ | 5′ GTGGTCTCTGCACGAACTGCCTG 3′ |
| Caspase-1 | 5′ GGGCAAAGAGGAAGCAATTTATC 3′ | 5′ GTGCCTTGTCCATAGCAGTAA 3′ |
| IL-1$\beta$ | 5′ AGAGCATCCAGCTTCAAATCTC 3′ | 5′ CAGTTGTCTAATGGGAACGTCA 3′ |

Table 2: Average ΔCt values from RT-PCR studies comparing WT versus KO.

| | Ctrl | Sham | WT 4d TBI | KO 4d TBI |
|---|---|---|---|---|
| NLRP3 | 18.982 | 18.836 | 17.645 | 18.739 |
| ASC | 17.186 | 16.774 | 14.953 | 15.652 |
| Caspase-1 | 17.097 | 17.010 | 15.832 | 17.836 |
| IL-1$\beta$ | 28.456 | 26.964 | 23.441 | 26.411 |

microscope (Carl Zeiss, Germany) using Zen software at 40x magnification. The intensity above threshold of the fluorescent signal of the bound antibodies was analyzed using NIH ImageJ software. Data were expressed as fold change from sham.

*2.9. Proximity Ligation (Duolink) Assay.* The proximity ligation (Duolink) assay was performed, as described by our laboratory [44]. Briefly, coronal brain sections were blocked in 5% (vol/vol) donkey serum for 1 hour at room temperature and incubated overnight with the following pairs of primary antibodies: goat-NLRP3 (Santa Cruz, sc-34,408) and rabbit-ASC (Santa Cruz, sc-22,514-R); or rabbit-NLRP3 (Santa Cruz, sc-66,846) and goat-TXNIP (Santa Cruz, sc-33,099) at 4°C. These sections were then incubated for 1 hour at 37°C with the following Duolink PLA probes: anti-Rabbit MINUS (Sigma-Aldrich, DUO92005) and anti-goat PLUS (Sigma-Aldrich, DUO92003). Duolink in situ detection reagent kit (Sigma-Aldrich, DUO92008) was used for ligation and amplification at 37°C using the according to the manufacturer's protocol. All sections were then mounted on a slide using DAPI-mounting media, and all images were captured on a confocal laser microscope (Carl Zeiss, Germany) using the Zen software at 40x magnification. Fluorescence of PLA indicating interacting proteins was analyzed as intensity above threshold using NIH ImageJ software and represented as fold change from shams.

*2.10. Statistical Analysis.* An independent two-sample *t*-test was conducted to investigate the difference between lesion volume of WT versus KO TBI mice. The one-way ANOVA test was conducted to analyze the differences within control, sham, and the different time points following TBI. The one-way ANOVA test was also used to investigate whether there is a significant difference among control, sham, WT, KO, and APO (apocynin) mice for all proteins in the study. Whenever an ANOVA test was found to be significant, the post hoc Tukey's test was conducted to make pairwise comparisons between the groups of animals. Statistical significance was accepted at the 95% confidence level ($P < 0.05$) using GraphPad Prism. Data was expressed as mean ± standard error (SEM).

## 3. Results

*3.1. Mice Deficient in NOX2 Have Reduced Lesion Size and Neuronal Cell Death after TBI.* Figure 2(a) shows representative cresyl violet staining of brain sections from sham, WT, and NOX2 KO mice to examine lesion size. As shown in Figure 2(a), sham-injured mice show no gross lesion or noticeable damage to the cerebral cortex. In contrast, WT animals undergoing CCI exhibit a moderately sized lesion, which is significantly reduced in NOX2 KO mice. To further quantitate the findings, lesion volume was calculated at the center of the lesion on the largest injured area (outlined in black) and compared to anatomically matched cortical sections. As shown in Figure 2(a), NOX2 KO mice have a significant reduction in lesion size, as compared to WT mice. Closer examination of the injured cortex under confocal microscopy revealed that TBI decreases the number of $NeuN^+$ neurons in the injured cortex in WT, whereas mice deficient in NOX2 retain similar neuronal densities as sham mice (Figure 2(b)). These findings indicate that the deletion of NOX2 offers robust neuroprotection after TBI.

*3.2. TBI Induces NLRP3 Inflammasome Expression in the Cortex.* We next hypothesized that NOX2 may play a role in NLRP3 inflammasome activation after TBI. To test this hypothesis, we first performed a time course examining expression of NLRP3 inflammasome pathway factors in the cerebral cortex after TBI. As shown in Figure 3(a), RT-PCR analysis revealed that NLRP3 mRNA levels in the cortex increased 2.6-fold at 4 days and 3-fold at 7 days after TBI in WT mice (relative to uninjured sham mice). Similarly, ASC mRNA expression was significantly increased at 2–7 days after TBI, showing a 6-fold increase at peak elevation compared to sham. Expression of pro-caspase-1, a substrate of the NLRP3 inflammasome, also was significantly elevated at 4 days after TBI showing a 2.5-fold increase. In line with the RT-PCR results, Western blot analysis revealed that NLRP3 and ASC protein levels were elevated in the cortex at 4, 7, and 14 days after TBI (Figure 3(b)). Furthermore, p20, the cleaved product of caspase-1, showed a time-dependent increase in cleaved caspase-1 expression within the cerebral cortex following TBI.

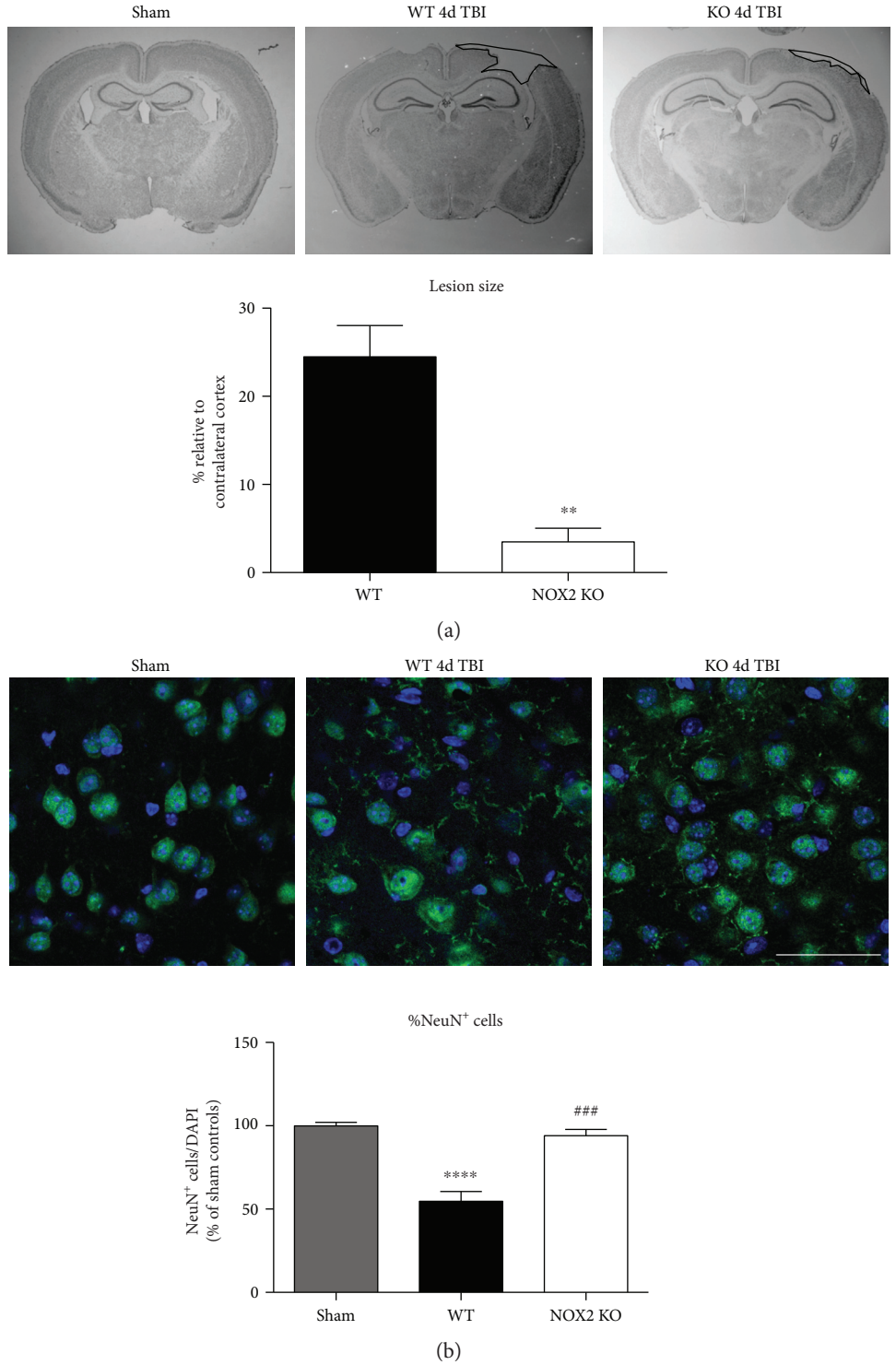


Figure 2: Mice deficient in NOX2 have both reduced lesion size and reduced neuronal damage after TBI. (a) Representative cresyl violet staining on day 4 after TBI from sham, WT TBI, and NOX2 KO TBI mice show neurons. Images have been converted to grayscale for added clarity. Mice were sacrificed at 4 days after TBI, and the brains of sham, WT TBI, and NOX2 KO TBI were collected for sectioning into 20 $\mu$M slices. Lesion size of TBI mice was calculated as a percent relative to a similarly affected area from the contralateral cortex of the same section. Lesion areas used for quantification are outlined in black. NOX2 KO mice show reduced lesion volume on gross examination throughout the injured cortex as quantified to the right. $n = 4$–6 mice/group. ($^{**}p < 0.01$ WT versus NOX2 KO) (b) Representative confocal images showing NeuN (green) and DAPI (blue) fluorescent signal of the injured cortex in sham, WT, and NOX2 KO mice at the 4-day post-TBI. NeuN/DAPI double-positive cells were counted and analyzed as a percent of total DAPI$^+$ cells, which is shown below the representative panel. TBI reduces NeuN-positive cells in the injured cortex, which is attenuated with deletion of NOX2. $n = 4$ mice/group. Scale bar represents 50 $\mu$M. ($^{****}p < 0.0001$ sham versus WT; $^{###}p < 0.001$ WT versus KO).

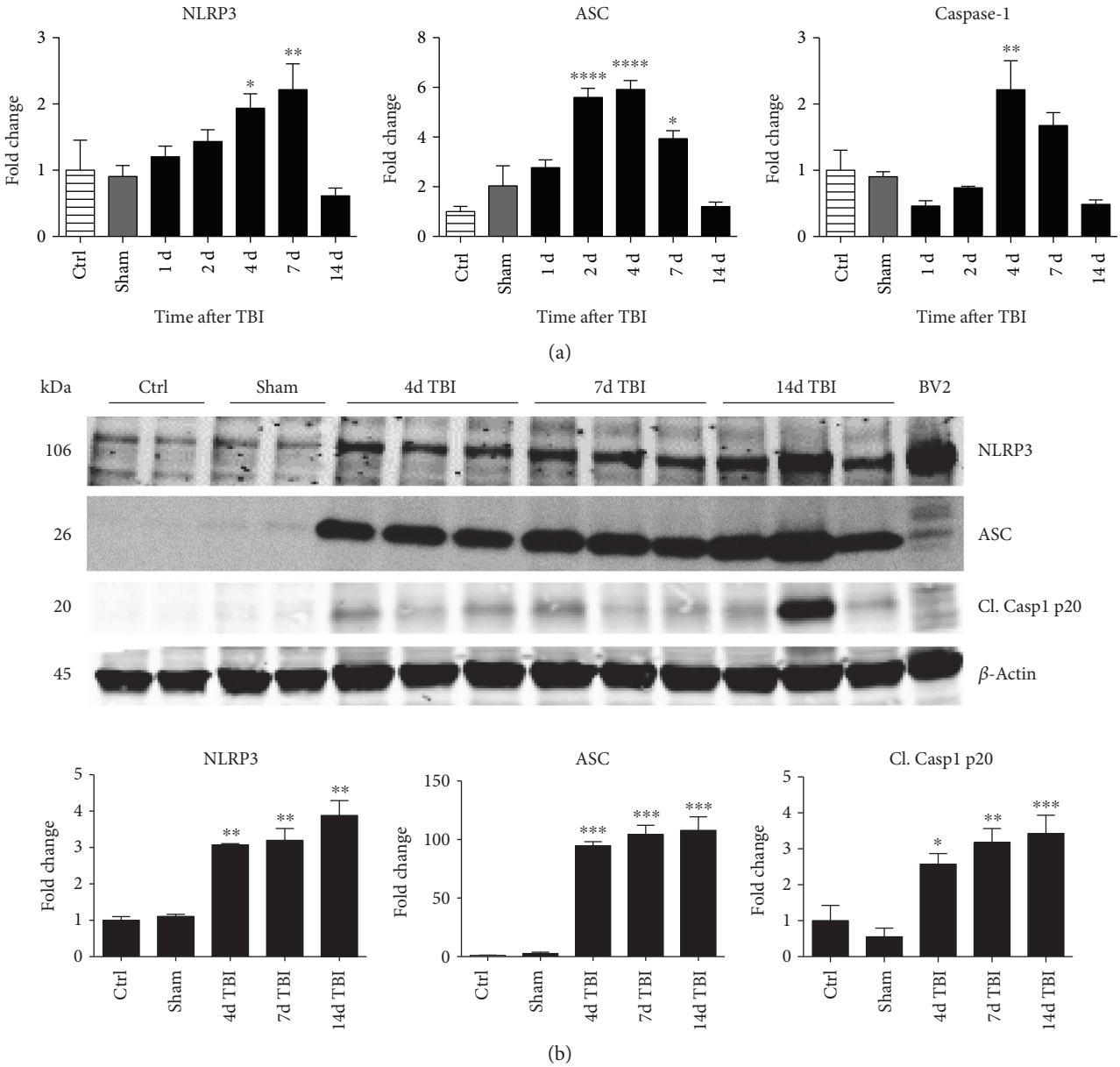


Figure 3: Time course gene and protein expression of NLRP3 inflammasome components in the mouse cerebral cortex after TBI. (a) Temporal pattern of NLRP3, ASC, and caspase-1 gene expression after TBI in WT mice between 1- and 14-day post-TBI showing peak increased mRNA expression between 4 and 7 days after TBI. $n = 4, 7, 4, 7, 6, 13$, and 4 mice (ctrl, sham, 1d, 2d, 4d, 7d, and 14d, resp.). (b) Representative Western blots showing temporal protein expression of NLRP3, ASC, and cleaved caspase-1 p20 after TBI in WT mice at 4, 7, and 14 days after TBI. Quantification of all blots shown below the image indicating increased protein expression of NLRP3, ASC, and cleaved caspase-1 after TBI (data normalized to $\beta$-actin and presented as fold change relative to ctrl mice). BV2 sample included as positive control. $n = 4, 4, 6, 6$, and 6 mice (ctrl, sham, 4d, 7d, and 14d, resp.). ($^{*}p < 0.05$, $^{**}p < 0.01$, $^{***}p < 0.001$, and $^{****}p < 0.0001$ sham versus TBI).

*3.3. NOX2 Deletion or Inhibition Leads to a Significantly Reduced Induction of NLRP3 Inflammasome Pathway Factor Expression in the Injured Cortex Following TBI.* Since ROS can stimulate NLRP3 inflammasome activation in vivo and in vitro [45], and NOX2 is a major generator of superoxide; we therefore sought to determine the role of NOX2 in induction of NLRP3 inflammasome pathway factor expression after TBI. Based on our current findings, the NLRP3 inflammasome appears to be strongly induced at the 4-day post-TBI time point. We examined the effects of NOX2 deletion on NLRP3 inflammasome components using NOX2 KO mice. We saw no significant baseline differences between WT and KO mice (Figure 4). NOX2 KO mice exhibited a significant reduction in NLRP3 and ASC gene expression at the day-4 post-TBI, as compared to WT mice (Figure 5(a)). Furthermore, increased immunoreactivity of NLRP3 and ASC within the perilesional cortex at the 4-day post-TBI in WT mice was significantly attenuated in NOX2 KO mice (Figure 5(b)). Examination of cortical sections at the 7-day post-TBI time point showed similar attenuation of NLRP3 and ASC immunoreactivity with deletion of NOX2 (Figure 6). To further confirm these results, we subjected

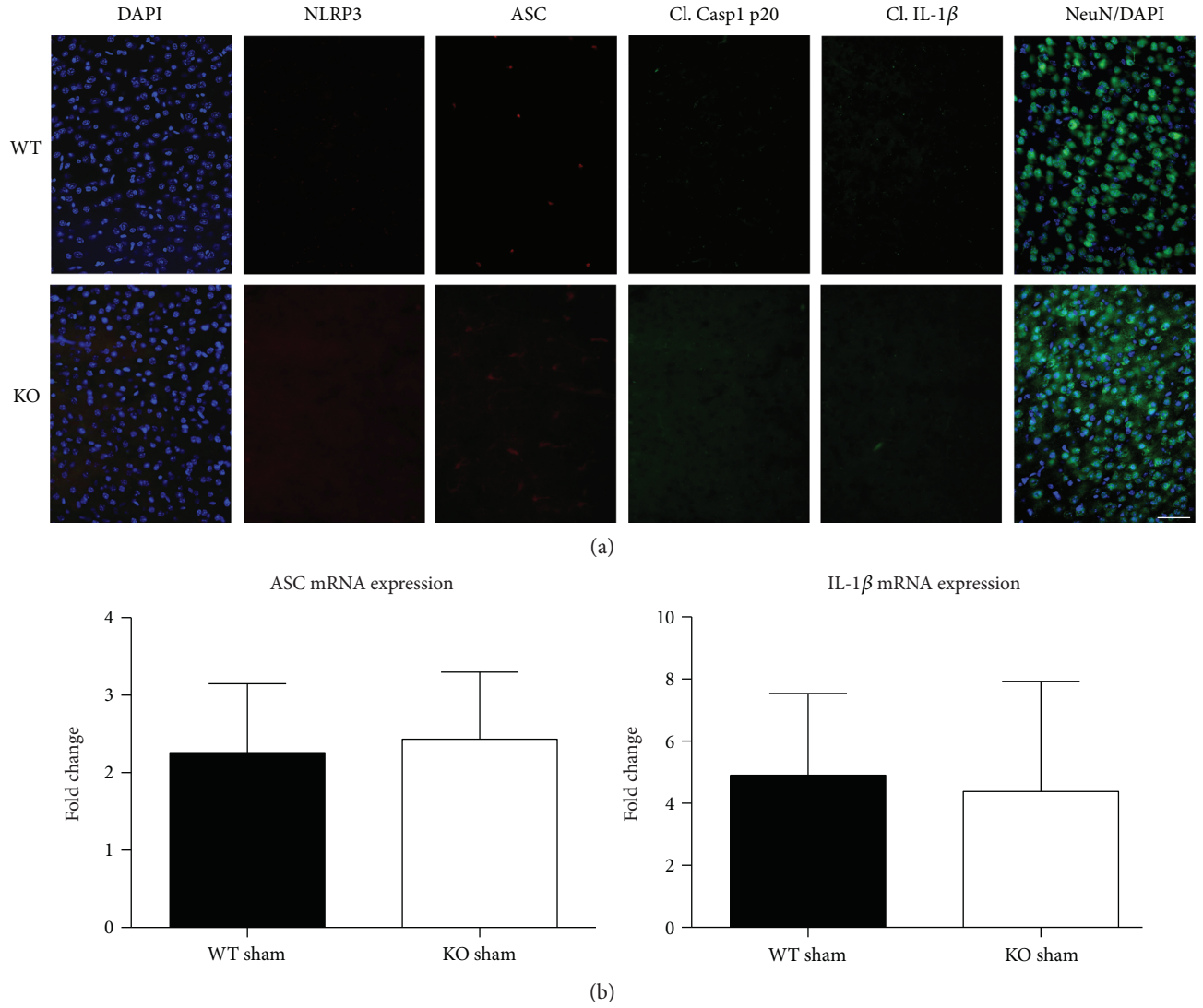


Figure 4: WT and KO mice show no differences in expression of NLRP3 inflammasome components at baseline. (a) Representative confocal images show baseline immunoreactivity of NLRP3, ASC, cleaved caspase-1 (p2), cleaved IL-1$\beta$, and NeuN in WT and KO sham mice. No differences in the expression of inflammasome components were observed between WT and KO sham mice. Scale bar represents 50 $\mu$M. (b) Quantitative RT-PCR results for ASC and IL-1$\beta$, genes that appeared slightly elevated due to sham surgery. No differences were observed between WT and KO sham mice at the 4-day postinjury in the mRNA expression of ASC and IL-1$\beta$. $n = 4$, 3 mice (WT, sham, and KO sham, resp.).

cortical lysates from WT and NOX2 KO groups to Western blot analysis. We also included an additional group in which animals were treated with a NOX inhibitor, apocynin, so as to further confirm our NOX2 KO findings. Representative Western blots and densitometric analysis show that both NOX2 deletion and inhibition of NOX2 by apocynin significantly attenuated NLRP3 and ASC protein expression at 4 days after TBI, as compared to the WT group (Figure 5(c)). Similar Western blot results were obtained at 7 days after TBI where NOX2 KO mice showed attenuation of NLRP3 and ASC protein expression as compared to WT mice (Figure 7).

*3.4. Reduced NLRP3 Inflammasome Complex Formation in the Injured Cortex of NOX2 KO Mice Following TBI.* Assembly of NLRP3 inflammasome components into a complex is necessary for functional activation. We therefore used an in situ Duolink coimmunoprecipitation assay to measure the protein-protein interaction of NLRP3 and ASC in the injured mouse cortex at 4 days after TBI. TBI increased NLRP3-ASC complex formation, as visualized using confocal microscopy, in the injured cerebral cortex at the 4-day post-TBI, as compared to sham controls (Figure 8). Examination at 7 days after TBI revealed similar reduction in the NLRP3 inflammasome complex formation with deletion of NOX2 (Figure 9). Notably, deletion of NOX2 significantly suppressed the TBI-induced NLRP3-ASC complex formation in the injured cortex, indicating that NOX2 regulates both NLRP3 inflammasome expression and the complex formation after TBI.

*3.5. NOX2 Regulates Caspase-1 Expression and Activity after TBI.* We next sought next to examine the gene expression

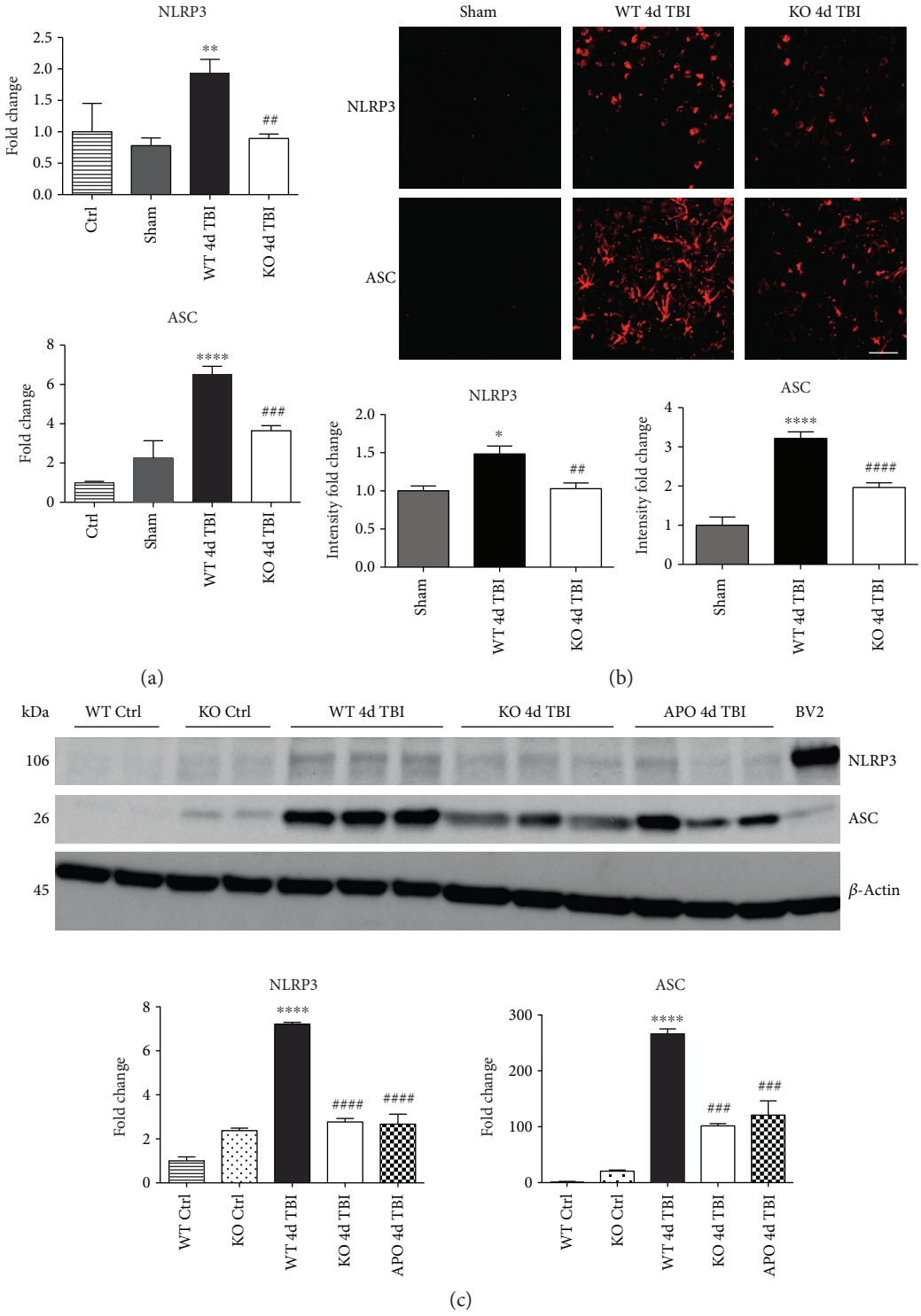


Figure 5: Deficiency of NOX2 reduces gene and protein expression of NLRP3 and ASC in the mouse cerebral cortex after TBI. (a) Deletion of NOX2 attenuates mRNA gene expression of NLRP3 and ASC at 4 days after TBI as compared to WT mice. $n = 4, 6, 6$, and 8 mice (ctrl, sham, WT, and KO, resp.). (b) Representative confocal images show that NLRP3 and ASC immunoreactivity is increased at the 4-day post-TBI in the WT-injured cortex. Deletion of NOX2 attenuates the expression of NLRP3 and ASC in the injured cortex following TBI. All images quantified below representative panel (data presented as fold change relative to sham mice). $n = 4, 6$, and 6 mice (sham, WT, and KO, resp.). Scale bar represents 50 $\mu$M. (c) Representative Western blot and quantification of all blots show the protein expression of NLRP3 and ASC in WT, NOX2 KO, and apocynin-treated mice at the 4-day post-TBI (data normalized to $\beta$-actin and presented as fold change relative to WT ctrl mice). Both the deletion of NOX2 and inhibition of NOX attenuated NLRP3 and ASC protein levels. BV2 sample included as positive control. $n = 4, 4, 7, 7$, and 4 mice (WT ctrl, KO ctrl, WT, KO, and APO, resp.). ($^{*}p < 0.05$, $^{**}p < 0.01$, and $^{****}p < 0.0001$ sham versus WT TBI; $^{\#\#}p < 0.01$, $^{\#\#\#}p < 0.001$, and $^{\#\#\#\#}p < 0.0001$ WT TBI versus KO or APO TBI).

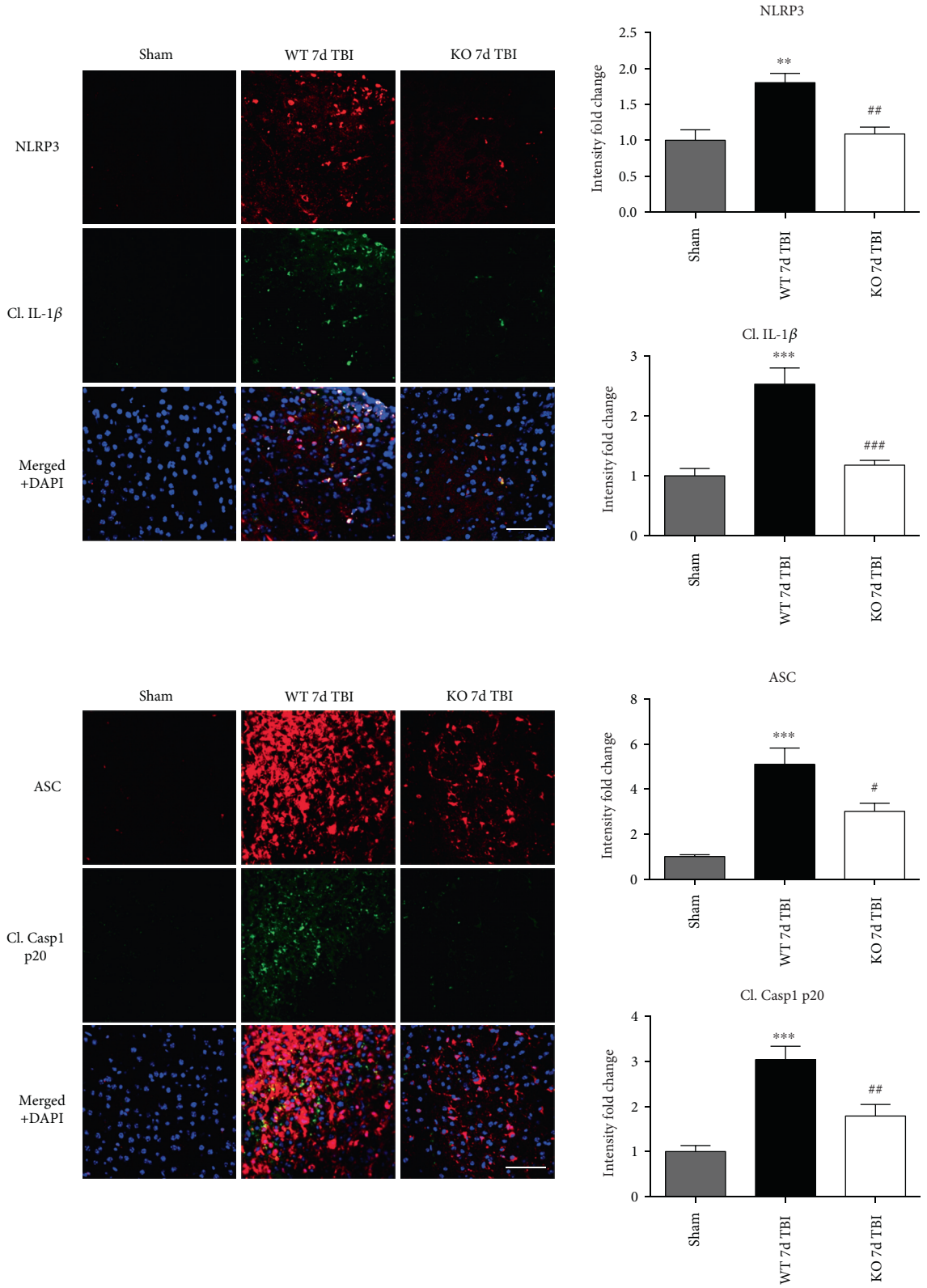


Figure 6: Deletion of NOX2 attenuates immunoreactivity of the injured mouse cortex to NLRP3 inflammasome and its products at the7-day post-TBI. Representative confocal images show that NLRP3, ASC, cleaved caspase-1 (p20), and cleaved IL-1$\beta$ are elevated at the 7-day post-TBI in WT-injured mouse cortex. Deletion of NOX2 attenuates the expression of both the inflammasome and its products in the injured cortex at the 7-day post-TBI. All confocal images were quantified to the right of the representative panel of images (presented as fold change relative to shams). $n = 4, 5,$ and 4 mice (sham, WT, and KO, resp.). Scale bar represents 50 $\mu$M. ($^{**}p < 0.01$, $^{***}p < 0.001$, sham versus WT TBI; $^{\#}p < 0.05$, $^{\#\#}p < 0.01$, and $^{\#\#\#}p < 0.001$ WT TBI versus KO TBI).

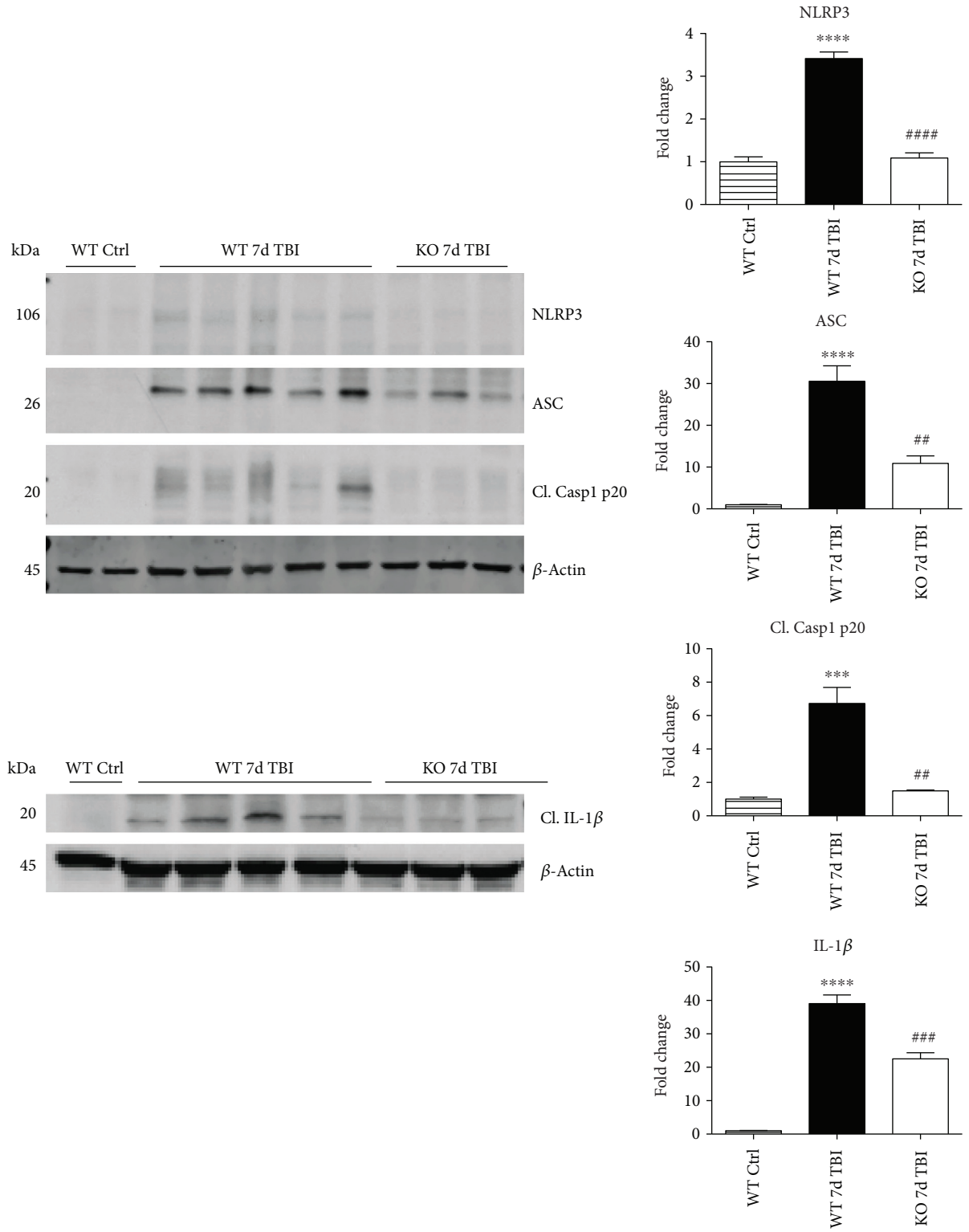


Figure 7: Deletion of NOX2 suppresses protein expression of NLRP3 inflammasome and its products at the 7-day post-TBI. Representative Western blots and quantification of all blots show the protein expression of NLRP3, ASC, cleaved caspase-1 (p20), and IL-1$\beta$ in WT and NOX2 KO mice at the 7-day post-TBI. Deletion of NOX2 was able to suppress expression of the NLRP3 inflammasome and its products caspase-1 and IL-1$\beta$ at this later time point. Values presented as fold change relative to WT ctrl mice. $n = 4$, 5, and 3 mice (sham, WT, and KO, resp.). ($^{***}p < 0.001$, $^{****}p < 0.0001$ sham versus WT TBI; $^{\#\#}p < 0.01$, $^{\#\#\#}p < 0.001$, and $^{\#\#\#\#}p < 0.0001$ WT TBI versus KO TBI).

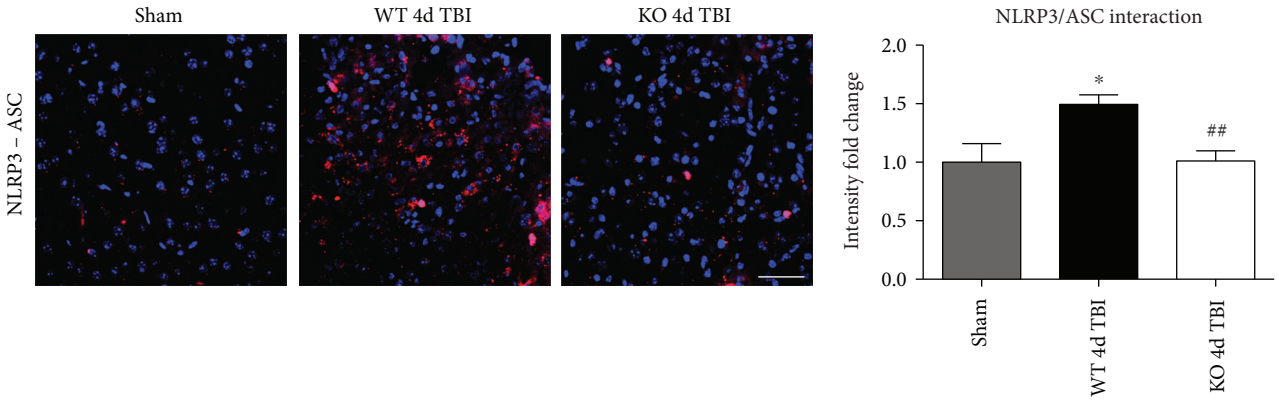


Figure 8: NOX2 deletion leads to a decrease in NLRP3 inflammasome complex formation in the injured mouse cortex after TBI. Proximity ligation assay (PLA) demonstrates NLRP3-ASC complex formation after TBI and regulation by NOX2. Representative confocal images of Duolink in situ co-IP show red fluorescence indicative of NLRP3-ASC protein-protein interaction in the injured cortex at the 4-day post-TBI. Deletion of NOX2 attenuates NLRP3-ASC complex formation at the 4-day post-TBI in the injured cortex. Quantification of all images shows a significant increase in NLRP3 inflammasome complex formation after TBI that is significantly attenuated by NOX2 deletion (data presented as fold change relative to sham mice). $n = 4$, 7, and 8 mice (sham, WT, and KO, resp.). Scale bar represents 50 $\mu$M. ($^{*}p < 0.05$ sham versus WT TBI; $^{\#\#}p < 0.01$ WT TBI versus KO TBI).

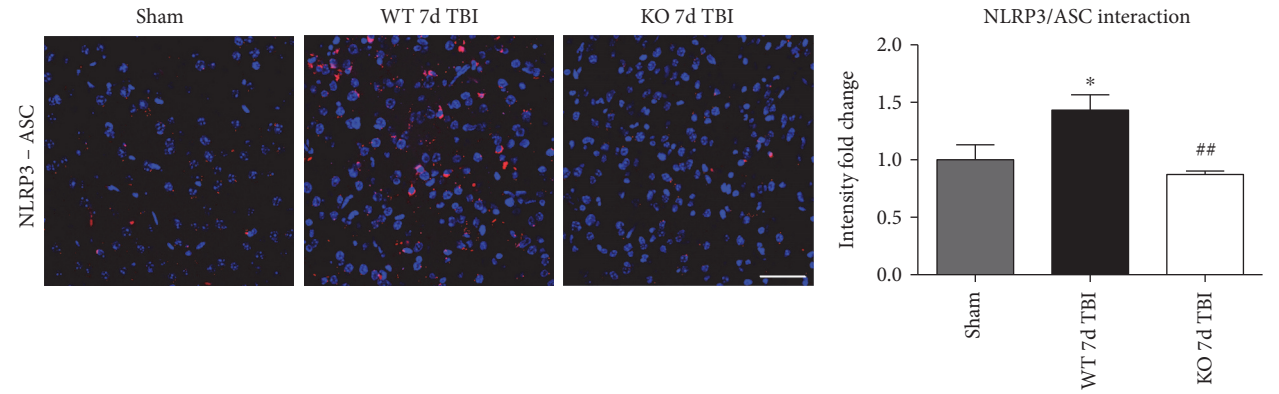


Figure 9: Deletion of NOX2 attenuates NLRP3 inflammasome complex formation in the injured mouse cortex at the 7-day post-TBI. Representative confocal images of Duolink in situ co-IP show red fluorescence indicative of NLRP3-ASC protein-protein interaction in the injured cortex at the 7-day post-TBI. Deletion of NOX2 attenuates the NLRP3-ASC complex formation at the 7-day post-TBI in the injured cortex. Quantification of all images shows a significant increase in NLRP3 inflammasome complex formation after TBI that is significantly attenuated by NOX2 deletion (presented as fold change relative to shams). $n = 4$, 6, and 6 mice (sham, WT, and KO, resp.). Scale bar represents 50 $\mu$M. ($^{*}p < 0.05$ sham versus WT TBI; $^{\#\#}p < 0.01$ WT TBI versus KO TBI).

of the NLRP3 downstream effectors, caspase-1 and IL-1$\beta$ in the injured cerebral cortex at the 4-day post-TBI. As shown in Figure 10(a), mRNA expression of caspase-1 and IL-1$\beta$ was increased at the 4-day post-TBI in the injured cerebral cortex of WT, but not NOX2 KO, mice. Since the activation of the inflammasome leads to increased caspase-1 cleavage, which in turn cleaves IL-1$\beta$ into the mature form, we next utilized Western blot analysis to assess the cleavage of caspase-1 and IL-1$\beta$ into their mature forms in the injured cortex at the 4-day post-injury. TBI significantly increased the cleavage of both caspase-1 and IL-1$\beta$ in the injured cortex, effects that were significantly attenuated in NOX2 KO mice or by apocynin treatment (Figure 10(b)). Additional blots confirming these results for expression of cleaved IL-1$\beta$ in WT, KO, and apocynin-treated groups are shown in Figure 11. This attenuation in cleavage is also observed at the 7-day post-TBI time point (Figure 7). The cleavage of caspase-1 and IL-1$\beta$ is further confirmed via immunofluorescent labeling of their cleaved products (Figure 10(c)). Similarly, immunoreactivity of the cleaved caspase-1 subunit, p20, and of cleaved IL-1$\beta$ was reduced within the perilesional cortex of NOX2 KO mice after TBI (Figure 10(c)). The examination of the 7-day post-TBI sections also showed similar attenuation of caspase-1 and IL-1$\beta$ cleavage (Figure 6).

*3.6. TXNIP Links NOX2-Dependent Oxidative Stress and NLRP3 Inflammasome Activation.* TXNIP, which directly links oxidative stress to NLRP3 inflammasome formation [37], was next examined by dual immunofluorescent labeling of NLRP3 (red) and TXNIP (green). As shown in Figure 12(a), TBI significantly increased expression of TXNIP in the injured cortex of WT mice at the 4-day post-TBI, as compared to sham mice; however, this effect was significantly attenuated in NOX2 KO mice (Figure 12(a)).

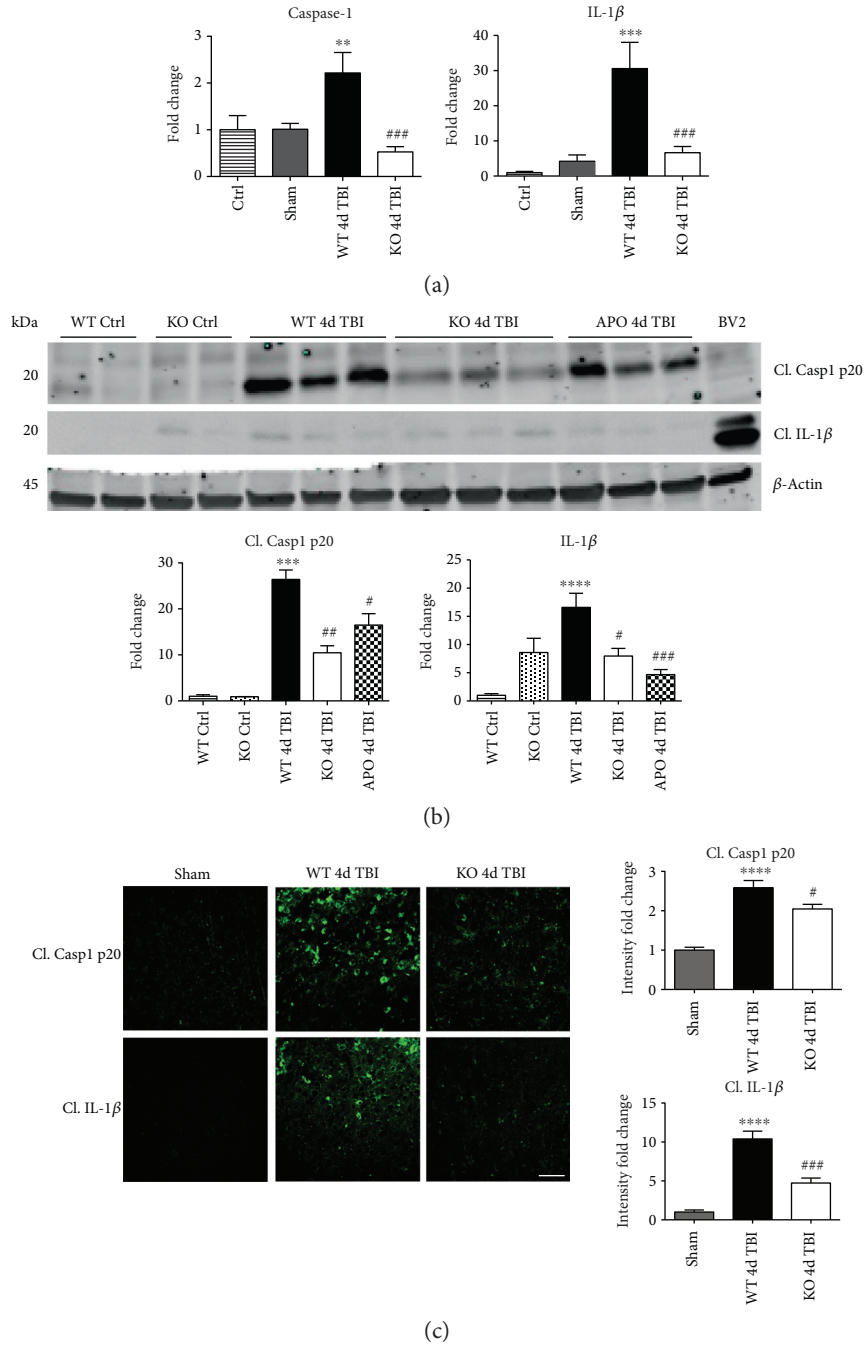


FIGURE 10: NOX2 deletion leads to a decrease in expression and activation of the NLRP3 inflammasome effectors, caspase-1 and IL-1$\beta$ in the injured cortex after TBI. (a) Quantitative RT-PCR for inflammasome components and downstream interleukins caspase 1 and IL-1$\beta$. mRNA samples were collected from the injured cortex at the 4-day post-TBI in WT and NOX2 KO mice. Caspase-1 and IL-1$\beta$ mRNA show increased gene expression at the 4-day post-TBI. Deletion of NOX2 significantly attenuates these changes. $n = 4, 6, 6$, and 9 mice (ctrl, sham, WT, and KO, resp.). (b) Representative Western blot showing protein expression of NLRP3 inflammasome products cleaved caspase-1 p20 and cleaved IL-1$\beta$. At 4 days after TBI, WT mice show increased expression of both cleaved effectors. However, mice deficient in NOX2 show attenuated cleavage of caspase-1 and IL-1$\beta$. Inhibition of NOX using apocynin also produces similar attenuated cleavage. Quantification of blots shown below representative image (data normalized to $\beta$-actin and presented as fold change relative to WT ctrl mice). BV2 sample included as positive control. $n = 4, 4, 7, 7$, and 4 mice (WT ctrl, KO ctrl, WT, KO, and APO, resp.). (c) Representative confocal images showing immunoreactivity of cleaved caspase 1 p20 and cleaved IL-1$\beta$ in the injured cortex after TBI for WT and NOX2 KO mice. All images have been quantified to the right of the representative panel (data presented as fold change relative to sham mice). TBI increased cleavage of caspase-1 and IL-1$\beta$ as detected by immunoreactivity of its cleaved products in WT mice at the 4-day post-TBI. Deletion of NOX2 attenuates this cleavage of caspase-1 and IL-1$\beta$ at the 4-day post-TBI. $n = 4, 6$, and 6 mice (sham, WT, and KO, resp.). Scale bar represents 50 $\mu$M. ($^{**}p < 0.01$, $^{***}p < 0.001$, $^{****}p < 0.0001$ sham versus WT TBI; $^{\#}p < 0.05$, $^{\#\#}p < 0.01$, and $^{\#\#\#}p < 0.001$ WT TBI versus KO or APO TBI).

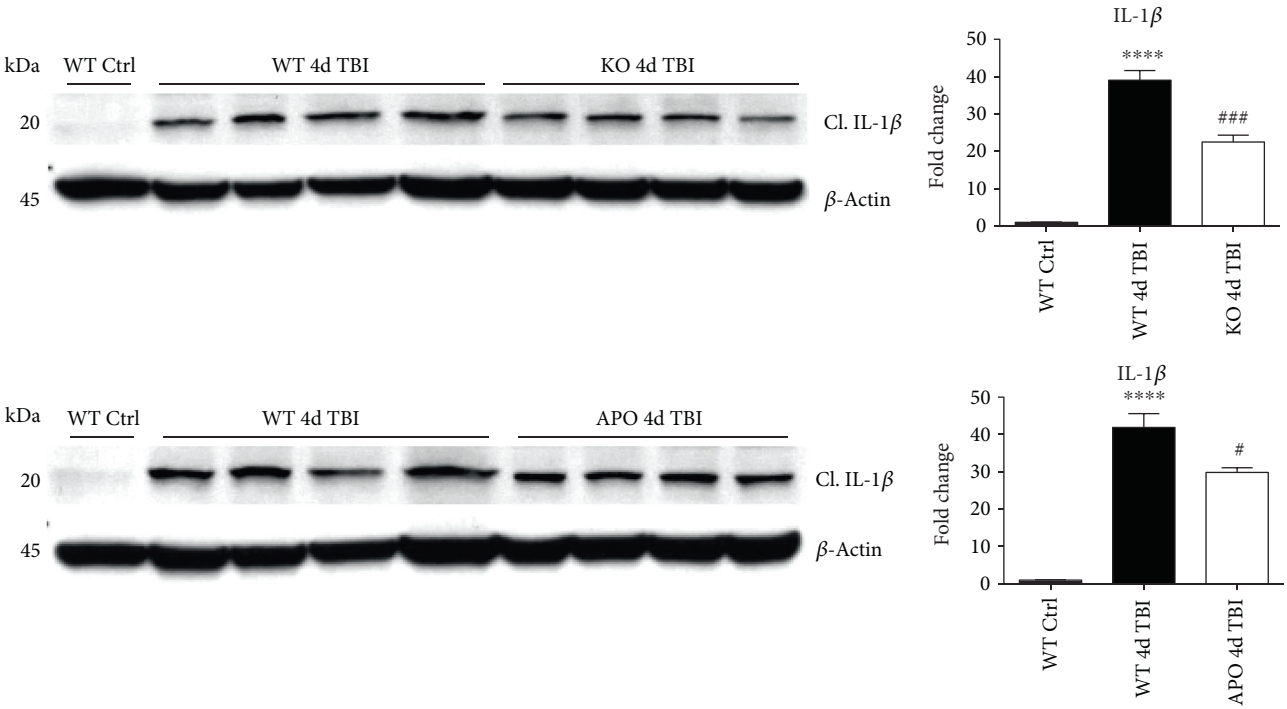


Figure 11: Additional Western blots for IL-1$\beta$. Blot showing cleaved IL-1$\beta$ product in different set of WT ctrl, WT 4d TBI, and KO 4d TBI mice and an additional APO 4d TBI mouse from those depicted in Figure 10. Densitometry quantification represents samples in this set of blots relative to respective loading controls. Inhibition of NOX2 via either knockout or apocynin reduces protein expression of cleaved IL-1$\beta$. Data presented as fold change relative to WT ctrl mice. ($^{****}p < 0.0001$ WT ctrl versus WT TBI; $^{\#}p < 0.05$ WT TBI versus APO TBI; $^{\#\#\#}p < 0.001$ WT TBI versus KO TBI).

Of note, a NOX2-dependent colocalization of TXNIP and NLRP3 was observed after TBI. We next examined protein-protein interaction between TXNIP and NLRP3 using the Duolink proximity ligand assay. The increased interaction of TXNIP and NLRP3 after TBI was reversed in NOX KO mice at 4 days after injury (Figure 12(b)). Examination of injured brain sections at the 7-day post-TBI also showed attenuated TXNIP-NLRP3 interaction in NOX2-deficient mice (Figure 13). Thus, TXNIP may link NOX2-dependent oxidative stress and NLRP3 inflammasome activation in TBI.

## 4. Discussion

The current study provides several important findings. First, it demonstrates that NLRP3 inflammasome expression and activation are strongly induced in the injured mouse cerebral cortex after TBI. Secondly, it demonstrates that the induction of the NLRP3 inflammasome after TBI is coupled with increased interaction with TXNIP, a known activator of NLRP3. Thirdly, it provides the novel insight that NOX2 deletion strongly attenuates NLPR3 inflammasome activation after TBI, an effect that correlated with a reduced interaction of NLRP3 and TXNIP. The results of our studies were confirmed using multiple approaches, which demonstrated that NOX2 regulation of the NLRP3 inflammasome is exerted at levels of gene, protein, and complex assembly.

The complex secondary cascade of injury following TBI involves oxidative stress and inflammation. NOX2 and microglial activation are detrimental after TBI [11, 12, 16, 18, 46, 47]. Though the study of inflammasomes in the context of TBI is relatively recent, the detrimental role of elevated IL-1$\beta$ after TBI is well documented [48–50]. Our results demonstrate that therapeutic targeting of NOX2 after TBI may attenuate this inflammatory secondary injury cascade involving IL-1$\beta$ via a mechanism involving the NLRP3 inflammasome. We and others previously showed that NOX2 expression and NADPH oxidase activity increase rapidly in the mouse cerebral cortex and hippocampal CA1 region after TBI with a prolonged peak from 24–96 hours after TBI that occurs in microglia [12, 16, 18]. That NOX2 has a critical role in TBI outcome is evidenced by our finding that cortical lesion size is significantly decreased and neuronal survival robustly increased in NOX2 deletion mice, which agrees with previous studies by our group and others showing a similar protective effect of NOX2 deletion and NOX2 inhibitors after TBI [16, 18]. Furthermore, NOX2 inhibition has been shown to lead to improved neurological outcome after TBI [46].

We utilized a NOX2 KO mouse model of TBI to elucidate the role of NOX2 in inflammasome activation following TBI. We also utilized a selective NOX inhibitor, apocynin, to further confirm the NOX2 genetic deletion results. Both deletion and inhibition of NOX2 decreased the expression and activation of the NLRP3 inflammasome following TBI. These changes were paralleled by a concomitant reduction in IL-1$\beta$, supporting a regulatory role of NOX2 in proinflammatory

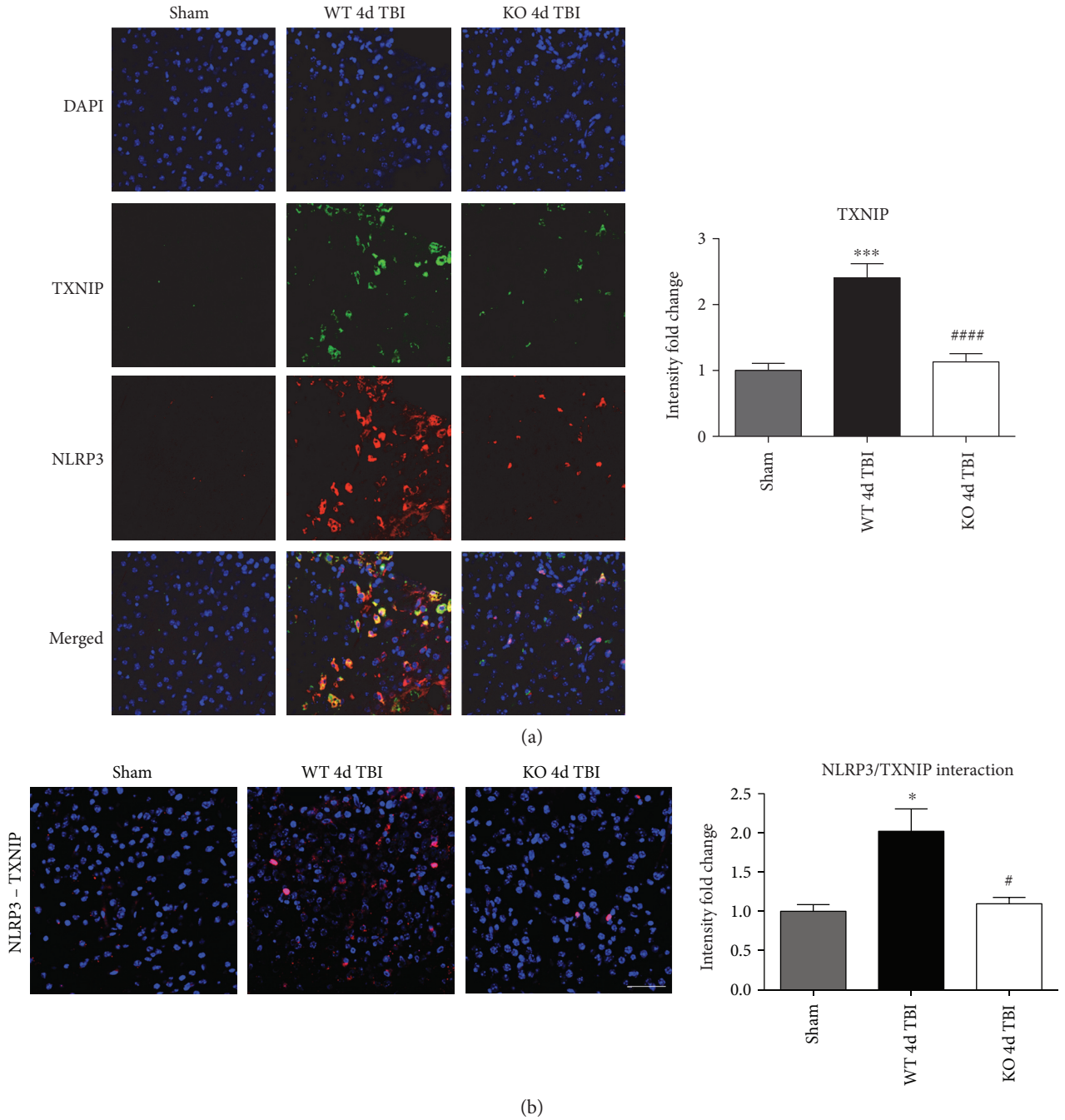


Figure 12: NOX2 deletion significantly attenuates TBI-induced TXNIP expression and complex formation within the injured mouse cortex. (a) Expression of TXNIP in the injured cortex after TBI. Representative images from sham, WT, and NOX2 KO mice show that TBI increases expression of TXNIP in the injured cortex after TBI, and TXNIP colocalizes with NLRP3 expression. Deletion of NOX2 attenuates the expression of TXNIP in the injured cortex at the 4-day post-TBI. Immunoreactivity from all images has been quantified to the right of the representative panel (data presented as fold change relative to shams). $n = 4$, 6, and 6 mice (sham, WT, and KO, resp.). (b) In situ PLA demonstrating NLRP3-TXNIP complex formation after TBI and regulation by NOX2. Representative confocal images of Duolink in situ co-IP show red fluorescence indicative of NLRP3-TXNIP protein-protein interaction in the injured cortex at the 4-day post-TBI. Mice deficient in NOX2 show reduced NLRP3-TXNIP complex formation at the 4-day post-TBI in the injured cortex. Quantification of all Duolink images shows significantly increased NLRP3-TXNIP interaction after TBI that is attenuated by NOX2 deletion. $n = 4$, 6, and 6 mice (sham, WT, and KO, resp.). Scale bar represents 50 $\mu$M. Data for (a) and (b) presented as fold change relative to sham mice. ($^{*}p < 0.05$, $^{***}p < 0.001$ sham versus WT TBI; $^{\#}p < 0.05$, $^{\#\#\#\#}p < 0.0001$ WT TBI versus KO TBI).

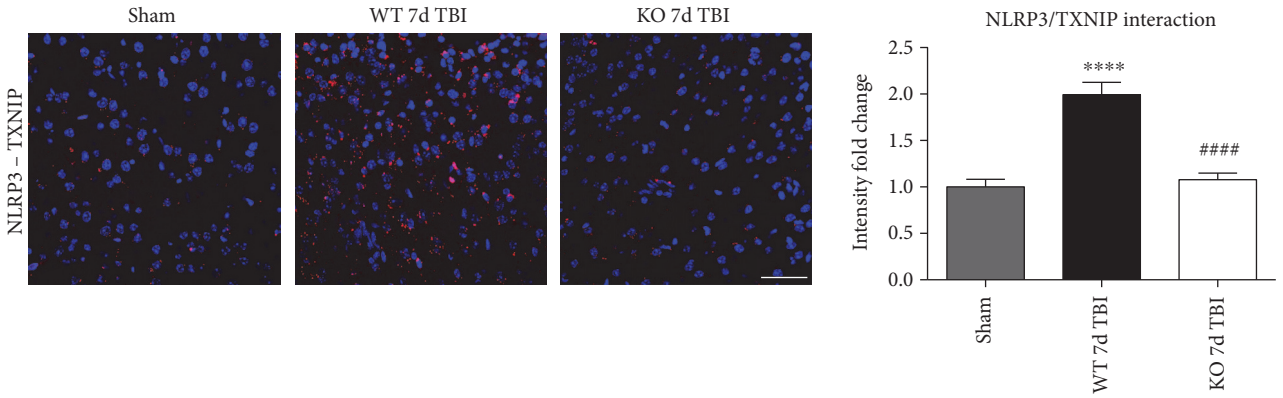


Figure 13: Deletion of NOX2 attenuates NLRP3-TXNIP complex formation at the 7-day post-TBI in the injured mouse cortex. Representative confocal images of Duolink in situ co-IP show red fluorescence indicative of NLRP3-TXNIP complex formation in the injured cortex at the 7-day post-TBI. Mice deficient in NOX2 show reduced NLRP3-TXNIP interaction at the 7-day post-TBI in the injured cortex. Quantification of all Duolink images shows significantly increased NLRP3-TXNIP interaction after TBI that is attenuated by NOX2 deletion (presented as fold change relative to shams). $n = 4$ mice/group. Scale bar represents 50 $\mu$M. ($^{****}p < 0.0001$ sham versus WT TBI; $^{\#\#\#\#}p < 0.0001$ WT TBI versus KO TBI).

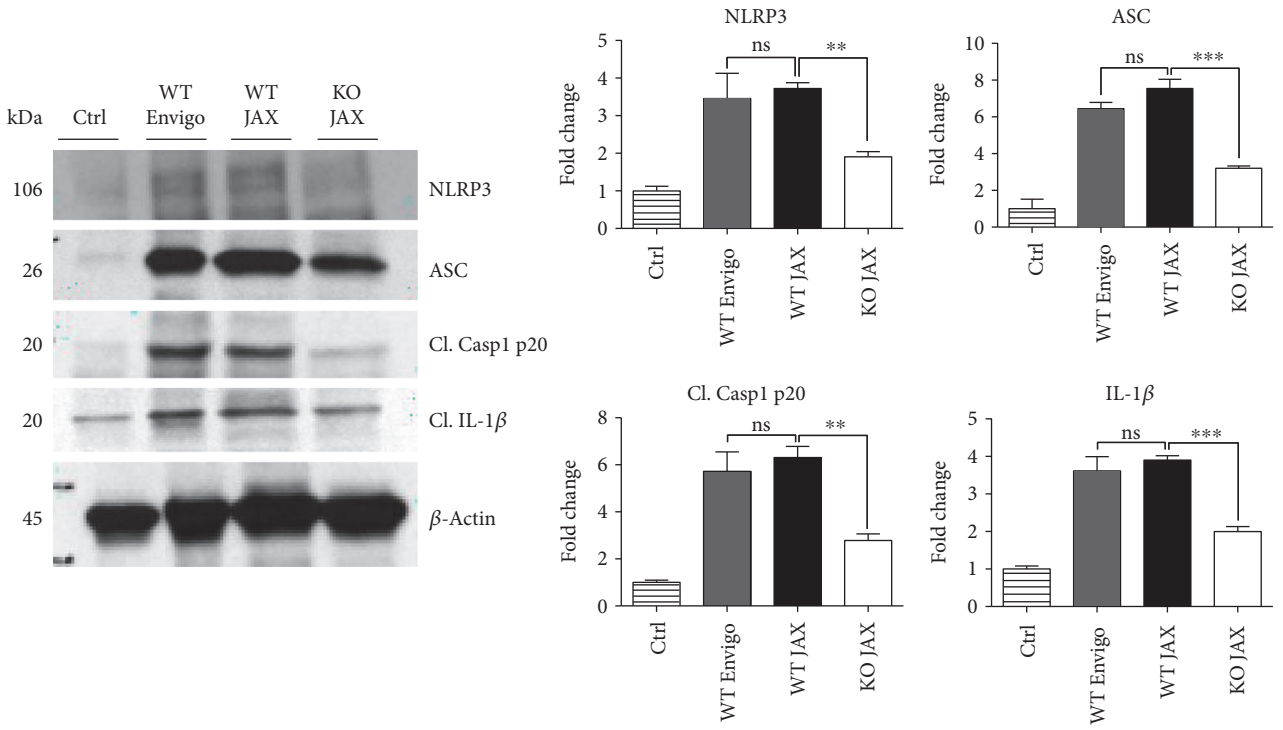


Figure 14: Effect of NOX2 deletion on NLRP3 inflammasome expression is conserved in both littermate and nonlittermate C57BL/6 mice at the 4-day post-TBI. Representative Western blots showing expression of NLRP3, ASC, cleaved caspase-1 (p20), and cleaved IL-1$\beta$ in ctrl, WT TBI mice from Envigo (nonlittermate) and Jackson Labs (JAX, littermate to KO mice), and NOX2 KO TBI mice from JAX at the 4-day post-TBI. Densitometry quantification (normalized to $\beta$-actin and represented as fold change to ctrl) is shown to the right of the images. No differences were observed between WT mice from Envigo and JAX after TBI. Deletion of NOX2 still reduced expression of NLRP3 inflammasome components when compared to WT Jackson Labs mice at the 4-day post-TBI. $n = 3, 3, 5,$ and 3 (ctrl, WT Envigo, WT JAX, KO JAX, resp.). ($^{**}p < 0.01$, $^{***}p < 0.001$, ns = not significant).

activation after TBI. While suggestive of a role for NOX2 in NLRP3 regulation, the use of apocynin may be a caveat. Although apocynin inhibits NOX2 assembly [51–53] and requires NOX2 to elicit protection after cerebral infarction [54], apocynin also may produce anti-inflammatory and antioxidant effects independent of NOX2 [55, 56]. Despite this mechanistic limitation, apocynin exhibits documented clinical safety in asthma and chronic obstructive pulmonary disease patients [57, 58] and reduced inflammasome formation, even when administered up to 24 hours post-TBI. As 24 hours is beyond the peak expression of NOX2 in neurons [16], the delayed NOX2 elevation in immune cells may

mediate release of proinflammatory cytokines, such as IL-1$\beta$, to exacerbate the secondary injury after TBI. Thus, our studies provide translational value supporting the therapeutic use of apocynin to reduce neuroinflammation within a delayed, clinically relevant therapeutic window after TBI.

Based on the results of our study, we propose that NOX2-derived oxidative stress induces TXNIP interaction with NLRP3 to lead to NLRP3 inflammasome activation, which exacerbates inflammation in the injured cortex after TBI. It is possible that NOX2 may indirectly regulate inflammasome-mediated neuroinflammation via altering migratory behavior and/or inflammatory phenotype of peripheral immune cells that infiltrate the injured cortex [59–61]. However, Kumar et al. reported previously that $CD45^{hi}$ cell numbers did not vary between WT and $NOX2^{-/-}$ mice when examining the injured cortex at the 3-day post-TBI, suggesting that NOX2 did not affect the numbers of infiltrating peripheral macrophages [60]. The same study also determined NOX2 involvement in microglial polarization following TBI [60], but whether polarization differences contribute to NLRP3 activation is unknown. Since both resident and peripheral immune cells are implicated in neuroinflammation after TBI, further studies are needed to address the involvement of inflammasomes in the infiltrating macrophages that migrate to the injured cortex following TBI.

While our findings suggest that NOX2 mediates NLRP3 inflammasome activation following TBI, we cannot rule out the possibility that other NOX isoforms may also contribute to inflammasome activation, as NOX4 is elevated in both rodent and human cortex after TBI [14]. Furthermore, NOX4 has been reported to regulate NLRP3 inflammasome activation in human umbilical vein endothelial cells under high-glucose environment and to modulate TXNIP [62]. Although NOX2 did not regulate NLRP3 or TXNIP in the umbilical vein endothelial cells [62], NOX2 deletion attenuated NLRP3 induction in the cerebral cortex of mice after ischemic stroke [63], as we observed after TBI. The reason for the divergent effects is not clear, but it could suggest that NOX isoform regulation of NLRP3 inflammasome activation may be tissue- and/or context specific. Importantly, these observed effects were independent of strain and supplier, further supporting the notion that NOX2 inhibition on NLRP3 inflammasome is a conserved mechanism of injury after TBI (Figure 14), and this relationship may apply to other disease models utilizing different mouse strains.

An interesting question is whether NOX2 regulates other types of inflammasomes in addition to the NLRP3 inflammasome. While our study did not address this issue, correlational human studies suggested involvement of NLRP1 and AIM 2 in the pathogenesis of TBI [29–31]; however, these findings remain to be demonstrated in mechanistic experimental models. In addition, while there is significant evidence that ROS can regulate the NLRP3 inflammasome, there is little evidence of similar ROS regulation of NLRP1 and AIM 2. Thus, further work is needed to elucidate the role of other inflammasome complexes in TBI and determine any potential regulation by NOX.

In conclusion, the results of our study demonstrate that increased NLRP3 inflammasome activation is in the injured cortex after TBI. Notably, we show that NOX2 regulates NLRP3 inflammasome expression and activation. Furthermore, we show that NOX2 regulation of the NLRP3 inflammasome may be through oxidative stress sensing of TXNIP. These findings provide new insight into the anti-inflammatory effects of NOX2 inhibition and support the potential translational value for NOX inhibitors in the clinical management of TBI. Thus, therapeutic targeting of NLRP3 inflammasome may provide a novel and efficacious treatment for TBI, as well as other acute and chronic brain injuries involving the activation of the NLRP3 inflammasome.

## Abbreviations

ASC: Apoptosis-associated speck-like protein containing a CARD
CCI: Controlled cortical impact
IL-1$\beta$: Interleukin-1$\beta$
KO: Knockout
NLRP3: NOD-like receptor with a pyrin domain-3
ROS: Reactive oxygen species
TBI: Traumatic brain injury
TXNIP: Thioredoxin-interacting protein
WT: Wild-type.

## Disclosure

US Government Disclaimer: "The contents do not represent the views of the U.S. Department of Veteran Affairs or the United States Government."

## Conflicts of Interest

The authors declare that they have no competing interests.

## Acknowledgments

This research presented in this article was conducted in partial fulfillment of the Ph.D. degree requirements set forth for Merry W. Ma and was supported by a VA Merit Review Award (5l101BX001117) from the United States Department of Veteran's Affairs, Biomedical Laboratory Research, and Development Service.

## References

[1] V. G. Coronado, L. Xu, S. V. Basavaraju et al., "Surveillance for traumatic brain injury-related deaths—United States, 1997-2007," *MMWR Surveillance Summaries*, vol. 60, no. 5, pp. 1–32, 2011.

[2] N. Stocchetti and E. R. Zanier, "Chronic impact of traumatic brain injury on outcome and quality of life: a narrative review," *Critical Care*, vol. 20, no. 1, p. 148, 2016.

[3] A. C. McKee and M. E. Robinson, "Military-related traumatic brain injury and neurodegeneration," *Alzheimers Dement*, vol. 10, no. 3 Suppl, pp. S242–S253, 2014.

[4] T. K. McIntosh, D. H. Smith, D. F. Meaney, M. J. Kotapka, T. A. Gennarelli, and D. I. Graham, "Neuropathological sequelae of traumatic brain injury: relationship to neurochemical and

biomechanical mechanisms," *Laboratory Investigation*, vol. 74, no. 2, pp. 315–342, 1996.

[5] L. H. Mbye, I. N. Singh, P. G. Sullivan, J. E. Springer, and E. D. Hall, "Attenuation of acute mitochondrial dysfunction after traumatic brain injury in mice by NIM811, a non-immunosuppressive cyclosporin A analog," *Experimental Neurology*, vol. 209, no. 1, pp. 243–253, 2008.

[6] A. Chodobski, B. J. Zink, and J. Szmydynger-Chodobska, "Blood-brain barrier pathophysiology in traumatic brain injury," *Translational Stroke Research*, vol. 2, no. 4, pp. 492–516, 2011.

[7] A. Rodriguez-Rodriguez, J. J. Egea-Guerrero, F. Murillo-Cabezas, and A. Carrillo-Vico, "Oxidative stress in traumatic brain injury," *Current Medicinal Chemistry*, vol. 21, no. 10, pp. 1201–1211, 2014.

[8] R. B. Borgens and P. Liu-Snyder, "Understanding secondary injury," *The Quarterly Review of Biology*, vol. 87, no. 2, pp. 89–127, 2012.

[9] S. Altenhofer, P. W. Kleikers, K. A. Radermacher et al., "The NOX toolbox: validating the role of NADPH oxidases in physiology and disease," *Cellular and Molecular Life Sciences*, vol. 69, no. 14, pp. 2327–2343, 2012.

[10] K. Bedard and K. H. Krause, "The NOX family of ROS-generating NADPH oxidases: physiology and pathophysiology," *Physiological Reviews*, vol. 87, no. 1, pp. 245–313, 2007.

[11] D. J. Loane, A. Kumar, B. A. Stoica, R. Cabatbat, and A. I. Faden, "Progressive neurodegeneration after experimental brain trauma: association with chronic microglial activation," *Journal of Neuropathology and Experimental Neurology*, vol. 73, no. 1, pp. 14–29, 2014.

[12] M. W. Ma, J. Wang, Q. Zhang et al., "NADPH oxidase in brain injury and neurodegenerative disorders," *Molecular Neurodegeneration*, vol. 12, no. 1, p. 7, 2017.

[13] Z. Li, F. Tian, Z. Shao et al., "Expression and clinical significance of non-phagocytic cell oxidase 2 and 4 after human traumatic brain injury," *Neurological Sciences*, vol. 36, no. 1, pp. 61–71, 2015.

[14] B. P. Lucke-Wold, Z. J. Naser, A. F. Logsdon et al., "Amelioration of nicotinamide adenine dinucleotide phosphate-oxidase mediated stress reduces cell death after blast-induced traumatic brain injury," *Translational Research*, vol. 166, no. 6, pp. 509–528, 2015, e1.

[15] Y. Liao, P. Liu, F. Guo, Z. Y. Zhang, and Z. Zhang, "Oxidative burst of circulating neutrophils following traumatic brain injury in human," *PloS One*, vol. 8, no. 7, article e68963, 2013.

[16] Q. G. Zhang, M. D. Laird, D. Han et al., "Critical role of NADPH oxidase in neuronal oxidative damage and microglia activation following traumatic brain injury," *PloS One*, vol. 7, no. 4, article e34504, 2012.

[17] S. J. Cooney, S. L. Bermudez-Sabogal, and K. R. Byrnes, "Cellular and temporal expression of NADPH oxidase (NOX) isotypes after brain injury," *Journal of Neuroinflammation*, vol. 10, p. 155, 2013.

[18] K. Dohi, H. Ohtaki, T. Nakamachi et al., "Gp91phox (NOX2) in classically activated microglia exacerbates traumatic brain injury," *Journal of Neuroinflammation*, vol. 7, p. 41, 2010.

[19] C. C. Chiu, Y. E. Liao, L. Y. Yang et al., "Neuroinflammation in animal models of traumatic brain injury," *Journal of Neuroscience Methods*, vol. 272, pp. 38–49, 2016.

[20] G. Singhal, E. J. Jaehne, F. Corrigan, C. Toben, and B. T. Baune, "Inflammasomes in neuroinflammation and changes in brain function: a focused review," *Frontiers in Neuroscience*, vol. 8, p. 315, 2014.

[21] A. Kumar and D. J. Loane, "Neuroinflammation after traumatic brain injury: opportunities for therapeutic intervention," *Brain, Behavior, and Immunity*, vol. 26, no. 8, pp. 1191–1201, 2012.

[22] R. M. Ransohoff, "How neuroinflammation contributes to neurodegeneration," *Science*, vol. 353, no. 6301, pp. 777–783, 2016.

[23] W. P. Arend, G. Palmer, and C. Gabay, "IL-1, IL-18, and IL-33 families of cytokines," *Immunological Reviews*, vol. 223, pp. 20–38, 2008.

[24] H. Guo, J. B. Callaway, and J. P. Ting, "Inflammasomes: mechanism of action, role in disease, and therapeutics," *Nature Medicine*, vol. 21, no. 7, pp. 677–687, 2015.

[25] S. Chakraborty, D. K. Kaushik, M. Gupta, and A. Basu, "Inflammasome signaling at the heart of central nervous system pathology," *Journal of Neuroscience Research*, vol. 88, no. 8, pp. 1615–1631, 2010.

[26] J. P. de Rivero Vaccari, W. D. Dietrich, and R. W. Keane, "Activation and regulation of cellular inflammasomes: gaps in our knowledge for central nervous system injury," *Journal of Cerebral Blood Flow and Metabolism*, vol. 34, no. 3, pp. 369–375, 2014.

[27] L. C. Freeman and J. P. Ting, "The pathogenic role of the inflammasome in neurodegenerative diseases," *Journal of Neurochemistry*, vol. 136, Supplement 1, pp. 29–38, 2016.

[28] J. G. Walsh, D. A. Muruve, and C. Power, "Inflammasomes in the CNS," *Nature Reviews Neuroscience*, vol. 15, no. 2, pp. 84–97, 2014.

[29] J. P. de Rivero Vaccari, F. Brand 3rd, S. Adamczak et al., "Exosome-mediated inflammasome signaling after central nervous system injury," *Journal of Neurochemistry*, vol. 136, Supplement 1, pp. 39–48, 2016.

[30] S. Adamczak, G. Dale, J. P. de Rivero Vaccari, M. R. Bullock, W. D. Dietrich, and R. W. Keane, "Inflammasome proteins in cerebrospinal fluid of brain-injured patients as biomarkers of functional outcome: clinical article," *Journal of Neurosurgery*, vol. 117, no. 6, pp. 1119–1125, 2012.

[31] S. E. Adamczak, J. P. de Rivero Vaccari, G. Dale et al., "Pyroptotic neuronal cell death mediated by the AIM2 inflammasome," *Journal of Cerebral Blood Flow and Metabolism*, vol. 34, no. 4, pp. 621–629, 2014.

[32] H. D. Liu, W. Li, Z. R. Chen et al., "Expression of the NLRP3 inflammasome in cerebral cortex after traumatic brain injury in a rat model," *Neurochemical Research*, vol. 38, no. 10, pp. 2072–2083, 2013.

[33] C. Lin, H. Chao, Z. Li et al., "Omega-3 fatty acids regulate NLRP3 inflammasome activation and prevent behavior deficits after traumatic brain injury," *Experimental Neurology*, vol. 290, pp. 115–122, 2017.

[34] L. Cristofori, B. Tavazzi, R. Gambin et al., "Biochemical analysis of the cerebrospinal fluid: evidence for catastrophic energy failure and oxidative damage preceding brain death in severe head injury: a case report," *Clinical Biochemistry*, vol. 38, no. 1, pp. 97–100, 2005.

[35] M. E. Heid, P. A. Keyel, C. Kamga, S. Shiva, S. C. Watkins, and R. D. Salter, "Mitochondrial reactive oxygen species induces NLRP3-dependent lysosomal damage and inflammasome activation," *Journal of Immunology*, vol. 191, no. 10, pp. 5230–5238, 2013.

[36] C. Dostert, V. Pétrilli, R. Van Bruggen, C. Steele, B. T. Mossman, and J. Tschopp, "Innate immune activation

through Nalp3 inflammasome sensing of asbestos and silica," *Science*, vol. 320, no. 5876, pp. 674–677, 2008.

[37] R. Zhou, A. Tardivel, B. Thorens, I. Choi, and J. Tschopp, "Thioredoxin-interacting protein links oxidative stress to inflammasome activation," *Nature Immunology*, vol. 11, no. 2, pp. 136–140, 2010.

[38] M. D. Laird, S. Sukumari-Ramesh, A. E. Swift, S. E. Meiler, J. R. Vender, and K. M. Dhandapani, "Curcumin attenuates cerebral edema following traumatic brain injury in mice: a possible role for aquaporin-4?," *Journal of Neurochemistry*, vol. 113, no. 3, pp. 637–648, 2010.

[39] C. Wakade, S. Sukumari-Ramesh, M. D. Laird, K. M. Dhandapani, and J. R. Vender, "Delayed reduction in hippocampal postsynaptic density protein-95 expression temporally correlates with cognitive dysfunction following controlled cortical impact in mice," *Journal of Neurosurgery*, vol. 113, no. 6, pp. 1195–1201, 2010.

[40] R. C. Hoover, M. Motta, J. Davis et al., "Differential effects of the anticonvulsant topiramate on neurobehavioral and histological outcomes following traumatic brain injury in rats," *Journal of Neurotrauma*, vol. 21, no. 5, pp. 501–512, 2004.

[41] H. J. Thompson, N. Marklund, L. B. DG et al., "Tissue sparing and functional recovery following experimental traumatic brain injury is provided by treatment with an anti-myelin-associated glycoprotein antibody," *The European Journal of Neuroscience*, vol. 24, no. 11, pp. 3063–3072, 2006.

[42] X. Gao and J. Chen, "Mild traumatic brain injury results in extensive neuronal degeneration in the cerebral cortex," *Journal of Neuropathology and Experimental Neurology*, vol. 70, no. 3, pp. 183–191, 2011.

[43] Q. G. Zhang, R. Wang, M. Khan, V. Mahesh, and D. W. Brann, "Role of Dickkopf-1, an antagonist of the Wnt/beta-catenin signaling pathway, in estrogen-induced neuroprotection and attenuation of tau phosphorylation," *The Journal of Neuroscience*, vol. 28, no. 34, pp. 8430–8441, 2008.

[44] G. R. Sareddy, Q. Zhang, R. Wang et al., "Proline-, glutamic acid-, and leucine-rich protein 1 mediates estrogen rapid signaling and neuroprotection in the brain," *Proceedings of the National Academy of Sciences of the United States of America*, vol. 112, no. 48, pp. E6673–E6682, 2015.

[45] L. Minutoli, D. Puzzolo, M. Rinaldi et al., "ROS-mediated NLRP3 inflammasome activation in brain, heart, kidney, and testis ischemia/reperfusion injury," *Oxidative Medicine and Cellular Longevity*, vol. 2016, Article ID 2183026, 10 pages, 2016.

[46] X. Y. Lu, H. D. Wang, J. G. Xu, K. Ding, and T. Li, "NADPH oxidase inhibition improves neurological outcome in experimental traumatic brain injury," *Neurochemistry International*, vol. 69, pp. 14–19, 2014.

[47] C. Angeloni, C. Prata, F. V. Dalla Sega, R. Piperno, and S. Hrelia, "Traumatic brain injury and NADPH oxidase: a deep relationship," *Oxidative Medicine and Cellular Longevity*, vol. 2015, Article ID 370312, 10 pages, 2015.

[48] K. T. Lu, Y. W. Wang, J. T. Yang, Y. L. Yang, and H. I. Chen, "Effect of interleukin-1 on traumatic brain injury-induced damage to hippocampal neurons," *Journal of Neurotrauma*, vol. 22, no. 8, pp. 885–895, 2005.

[49] K. Kamm, W. Vanderkolk, C. Lawrence, M. Jonker, and A. T. Davis, "The effect of traumatic brain injury upon the concentration and expression of interleukin-1beta and interleukin-10 in the rat," *The Journal of Trauma*, vol. 60, no. 1, pp. 152–157, 2006.

[50] S. M. Allan, P. J. Tyrrell, and N. J. Rothwell, "Interleukin-1 and neuronal injury," *Nature Reviews. Immunology*, vol. 5, no. 8, pp. 629–640, 2005.

[51] G. J. Gatto Jr et al.Z. Ao, M. G. Kearse, M. Zhou et al., "NADPH oxidase-dependent and -independent mechanisms of reported inhibitors of reactive oxygen generation," *Journal of Enzyme Inhibition and Medicinal Chemistry*, vol. 28, no. 1, pp. 95–104, 2013.

[52] J. Stolk, T. J. Hiltermann, J. H. Dijkman, and A. J. Verhoeven, "Characteristics of the inhibition of NADPH oxidase activation in neutrophils by apocynin, a methoxy-substituted catechol," *American Journal of Respiratory Cell and Molecular Biology*, vol. 11, no. 1, pp. 95–102, 1994.

[53] D. K. Johnson, K. J. Schillinger, D. M. Kwait et al., "Inhibition of NADPH oxidase activation in endothelial cells by ortho-methoxy-substituted catechols," *Endothelium*, vol. 9, no. 3, pp. 191–203, 2002.

[54] K. A. Jackman, A. A. Miller, T. M. De Silva, P. J. Crack, G. R. Drummond, and C. G. Sobey, "Reduction of cerebral infarct volume by apocynin requires pretreatment and is absent in Nox2-deficient mice," *British Journal of Pharmacology*, vol. 156, no. 4, pp. 680–688, 2009.

[55] S. Heumuller, S. Wind, E. Barbosa-Sicard et al., "Apocynin is not an inhibitor of vascular NADPH oxidases but an antioxidant," *Hypertension*, vol. 51, no. 2, pp. 211–217, 2008.

[56] E. Cifuentes-Pagano, D. N. Meijles, and P. J. Pagano, "The quest for selective nox inhibitors and therapeutics: challenges, triumphs and pitfalls," *Antioxidants & Redox Signaling*, vol. 20, no. 17, pp. 2741–2754, 2014.

[57] J. Stefanska, A. Sarniak, A. Wlodarczyk et al., "Apocynin reduces reactive oxygen species concentrations in exhaled breath condensate in asthmatics," *Experimental Lung Research*, vol. 38, no. 2, pp. 90–99, 2012.

[58] J. Stefanska, A. Sarniak, A. Wlodarczyk et al., "Hydrogen peroxide and nitrite reduction in exhaled breath condensate of COPD patients," *Pulmonary Pharmacology & Therapeutics*, vol. 25, no. 5, pp. 343–348, 2012.

[59] S. Chaubey, G. E. Jones, A. M. Shah, A. C. Cave, and C. M. Wells, "Nox2 is required for macrophage chemotaxis towards CSF-1," *PloS One*, vol. 8, no. 2, article e54869, 2013.

[60] A. Kumar, J. P. Barrett, D. M. Alvarez-Croda, B. A. Stoica, A. I. Faden, and D. J. Loane, "NOX2 drives M1-like microglial/macrophage activation and neurodegeneration following experimental traumatic brain injury," *Brain, Behavior, and Immunity*, vol. 58, pp. 291–309, 2016.

[61] J. P. Barrett, R. J. Henry, S. Villapol et al., "NOX2 deficiency alters macrophage phenotype through an IL-10/STAT3 dependent mechanism: implications for traumatic brain injury," *Journal of Neuroinflammation*, vol. 14, no. 1, p. 65, 2017.

[62] W. Wang, Q. H. Wu, Y. Sui, Y. Wang, and X. Qiu, "Rutin protects endothelial dysfunction by disturbing Nox4 and ROS-sensitive NLRP3 inflammasome," *Biomedicine & Pharmacotherapy*, vol. 86, pp. 32–40, 2016.

[63] F. Yang, Z. Wang, X. Wei et al., "NLRP3 deficiency ameliorates neurovascular damage in experimental ischemic stroke," *Journal of Cerebral Blood Flow and Metabolism*, vol. 34, no. 4, pp. 660–667, 2014.

Hindawi
Oxidative Medicine and Cellular Longevity
Volume 2017, Article ID 4162465, 14 pages
https://doi.org/10.1155/2017/4162465

*Research Article*

# Neuronal Damage Induced by Perinatal Asphyxia Is Attenuated by Postinjury Glutaredoxin-2 Administration

**Juan Ignacio Romero,[1] Mariana Inés Holubiec,[1] Tamara Logica Tornatore,[1] Stéphanie Rivière,[1] Eva-Maria Hanschmann,[2,3] Rodolfo Alberto Kölliker-Frers,[1] Julia Tau,[4] Eduardo Blanco,[5] Pablo Galeano,[6] Fernando Rodríguez de Fonseca,[7] Christopher Horst Lillig,[3] and Francisco Capani[1,8,9]**

[1]*Instituto de Investigaciones Cardiológicas "Prof. Dr. Alberto C. Taquini" (ININCA), Facultad de Medicina, UBA-CONICET, Marcelo T. de Alvear 2270, C1122AAJ, Ciudad de Buenos Aires, Argentina*
[2]*Department of Neurology, Medical Faculty, Heinrich-Heine-University, Düsseldorf, Germany*
[3]*Institute for Medical Biochemistry and Molecular Biology, Universitätsmedizin Greifswald, Ernst-Moritz-Arndt-Universität Greifswald, 17475 Greifswald, Germany*
[4]*Laboratory of Ocular Investigation, Department of Pathology, School of Medicine, University of Buenos Aires, Buenos Aires, Argentina*
[5]*Departament de Pedagogia i Psicologia, Facultat d'Educació, Psicologia i Treball Social, Universitat de Lleida, Avda. de l'Estudi General 4, 25001 Lleida, Spain*
[6]*Fundación Instituto Leloir, Av. Patricias Argentinas 435, C1405BWE, Ciudad Autónoma de Buenos Aires, Argentina*
[7]*Unidad de Gestión Clínica de Salud Mental, Instituto de Investigación Biomédica de Málaga, Hospital Regional Universitario de Málaga, Universidad de Málaga, Avda. Carlos Haya 82, 29010 Málaga, Spain*
[8]*Departamento de Biología, Universidad Argentina JF Kennedy, Buenos Aires, Argentina*
[9]*Investigador Asociado, Universidad Autónoma de Chile, Santiago, Chile*

Correspondence should be addressed to Juan Ignacio Romero; juanromero63@gmail.com and Fernando Rodríguez de Fonseca; fernando.rodriguez@ibima.eu

Received 2 March 2017; Accepted 23 April 2017; Published 15 June 2017

Academic Editor: Reiko Matsui



The general disruption of redox signaling following an ischemia-reperfusion episode has been proposed as a crucial component in neuronal death and consequently brain damage. Thioredoxin (Trx) family proteins control redox reactions and ensure protein regulation via specific, oxidative posttranslational modifications as part of cellular signaling processes. Trx proteins function in the manifestation, progression, and recovery following hypoxic/ischemic damage. Here, we analyzed the neuroprotective effects of postinjury, exogenous administration of Grx2 and Trx1 in a neonatal hypoxia/ischemia model. P7 Sprague-Dawley rats were subjected to right common carotid ligation or sham surgery, followed by an exposure to nitrogen. 1 h later, animals were injected i.p. with saline solution, 10 mg/kg recombinant Grx2 or Trx1, and euthanized 72 h postinjury. Results showed that Grx2 administration, and to some extent Trx1, attenuated part of the neuronal damage associated with a perinatal hypoxic/ischemic damage, such as glutamate excitotoxicity, axonal integrity, and astrogliosis. Moreover, these treatments also prevented some of the consequences of the induced neural injury, such as the delay of neurobehavioral development. To our knowledge, this is the first study demonstrating neuroprotective effects of recombinant Trx proteins on the outcome of neonatal hypoxia/ischemia, implying clinical potential as neuroprotective agents that might counteract neonatal hypoxia/ischemia injury.

## 1. Introduction

One of the main causes of neonatal death and neurological deficits in children is an insufficient oxygen supply during birth, known as perinatal asphyxia (PA). The central nervous system (CNS), particularly the brain, is damaged as a result of the combination of hypoxia, blood flow reduction (ischemia), and reoxygenation [1]. This pathology is associated with an increase in the levels of glutamate [2] and the consequent release of nitric oxide (NO) [3, 4]. Moreover, an increase of the superoxide anion radical (O2-·) which can rapidly react with NO to form peroxynitrite anions (ONOO-) has been described [5]. The excess of these molecules and the unspecific damage to various biomolecules have been described as oxidative stress in the 80th and have been linked to cell death, inflammation and might even explain the high mortality risk. Nowadays, the definition of oxidative stress has been paraphrased, acknowledging the function of different reactive species in physiological signaling cascades as well as their dysregulation in pathological conditions [6].

Redox signaling is regulated by proteins of the thioredoxin (Trx) family such as Trxs, glutaredoxins (Grxs) and peroxiredoxins (Prxs), that use thiol groups of cysteinyl residues within their active site motifs to catalyze for example thiol-disulfide exchange reactions [7, 8] (for an overview, see [6]). These redox proteins show tissue- and cell type-specific distributions. For instance, our work demonstrates specific differences in terms of protein abundance and distribution in the murine CNS [9, 10]. Trx family proteins possess the representative common structural motif, known as the Trx fold [11]. Trxs and Grxs are small oxidoreductases that contain the characteristic and highly conserved dithiol Cys-X-X-Cys motif in their active site that is essential for the reduction of specific disulfide bonds via the dithiol mechanism. Moreover, Trxs can catalyze the de-/nitrosylation of substrates and Grxs can catalyze the de-/glutathionylation of target proteins via the monothiol mechanism (reviewed in [12]). Trxs and Grxs can reduce Prxs, which are not only highly abundant peroxidases but rather regulators of the levels of the second messenger hydrogen peroxide and therefore essential for redox signaling [6, 12].

Interestingly, these proteins were shown to be altered in terms of expression, cellular distribution, and/or activity in various disorders. Also in diseases linked to hypoxia/ischemia, Trxs, Grxs, and Prxs and thereby cellular signaling within distinct cell types and tissues are significantly altered (for an overview, see [6]). Following cerebral ischemia induced by middle cerebral artery occlusion, Trx1 was reduced in ischemic areas and increased in perifocal ischemic regions [13]. Trx1 was induced in hippocampal glial cells during reperfusion following a transient cerebral ischemia in gerbils [14]. Transgenic mice overexpressing human Trx1 showed attenuated ischemic neuronal injury and significantly smaller infarct sizes when subjected to focal cerebral ischemia [15]. Moreover, Trx1 overexpression was shown to protect mice from neuronal apoptosis following mild focal ischemia [16]. In accordance with this evidence, the knock-down of Trx1 led to more pronounced neurological dysfunction, brain infarct size, brain edema, and overall peroxidation [17], as well as exacerbated apoptosis of neurons, behavioral deficits, and mortality [18]. Interestingly, the overexpression of the mitochondrial Trx2 attenuated ROS-induced TNF-$\alpha$ expression and subsequent NF-$\kappa$B activation and apoptosis [19]. Additionally, the protein levels of the cytosolic Grx1 were diminished after middle cerebral artery occlusion, correlating with neuronal damage [20]. Moreover, the overexpression of Prx2 was shown to protect cortical neuronal cell cultures from oxidative and ischemic damage [21]. Furthermore, exogenous administration of human Trx1 was shown to be able to pass the blood-brain barrier and exert a positive effect on neurogenesis promotion and cognitive recovery following cerebral ischemia in adult mice [22].

We have recently shown an increase in the hippocampal protein levels of Trx1 and Grx2 following a neonatal hypoxic/ischemic event. The specific knock-down of these proteins in a neuron-like cell model allowed us to characterize the importance of these proteins in neuronal differentiation and maturation after a hypoxic/ischemic reperfusion event. Particularly, both Grx2 and Trx1 seem to protect neuronal cells from hypoxia-induced damage, while Trx1 knock-down decreases cellular proliferation and viability. Moreover, the absence of either Grx2 or Trx1 following hypoxia and reoxygenation triggers differentiation into a glial-like cell type [23]. Interestingly, it was shown before in zebra fish that the loss of glutaredoxin leads to neuronal apoptosis and loss of an axonal scaffold, making Grx an essential protein for embryonic brain development [24].

Several potential neuroprotective agents have been used in the past to ameliorate the hypoxia/ischemia-induced damage in the CNS; however, neither of them has shown to be effective against hypoxia/ischemia-induced damage in the CNS. Here, we demonstrate the neuroprotective effects of exogenously administered, recombinantly expressed Grx2 and Trx1 (particularly in the hippocampus) in an animal model of neonatal hypoxia/ischemia, implying potential new therapeutic strategies.

## 2. Experimental Procedures

*2.1. Animals.* All experiments were conducted according to the principles of the guide for the care and use of laboratory animals (NIH publication no. 80-23, revised 1996) and approved by the institutional animal care and use committee at the University of Buenos Aires (School of Medicine). All efforts were made to reduce the number of animals used and to minimize suffering. Pregnant rats were obtained from the "School of Veterinary Sciences" central *vivarium* at the University of Buenos Aires. All animals were kept in a temperature ($21 \pm 2^{\circ}$C) and humidity ($65 \pm 5\%$) controlled environment on a 12 h light/dark cycle. Animals had ad libitum access to food (Purina chow) and tap water.

*2.2. Model for Common Carotid Artery Ligation and Treatment.* The model for common carotid artery ligation used in this study has been previously developed and validated [23, 25]. P7 male Sprague-Dawley rats were anesthetized (40 mg/kg ketamine and 4 mg/kg xylazine) and placed

on a heat plate to keep their body temperature at constant 37°C. The right common carotid artery (CCA) was exposed through an incision on the neck and was then isolated and permanently ligated with a 6-0 surgical silk thread (carotid group $n = 27$). Afterwards, the wound was closed and pups were returned to their dams for 4-5 h to recover. Subsequently, the animals were subjected to a 100% nitrogen environment at 37°C for 3 minutes to induce anoxia. Sham-operated rats (sham group $n = 27$) had their right CCA exposed but not ligated, and no nitrogen was applied. One hour after nitrogen exposure, animals were injected intraperitoneally (i.p.) with either saline solution (vehicle group $n = 9$), 10 mg/kg of recombinantly expressed and purified human Grx2 (Grx2 group $n = 9$), or 10 mg/kg of recombinantly expressed and purified human Trx1 (Trx1 group $n = 9$). At 72 h postinjury (postnatal day 10 (P10)), animals were sacrificed and their blood plasma and brains were collected for further analysis. The cloning, recombinant expression, and purification of hGrx2 and hTrx1 are described in Lundberg et al. [26] and Godoy et al. [9] and were produced in Dr Lillig's laboratory. All human recombinant Grx2 and Trx1 were processed to exchange the original buffer for phosphate-buffered saline (PBS) and increase protein concentration. Before injection, each concentrate was diluted (at least 10-fold) with sterile saline solution in order to reach a 10 mg/kg dosage.

*2.3. Western Blotting.* Western blot analysis was performed as previously described in Romero et al. [23]. Animals were euthanized by decapitation, and brains were dissected, homogenized in ice-cold lysis buffer (10 mM Tris/HCl, pH 7.4, 10 mM NaCl, 3 mM $MgCl_2$, 0.1% NP-40, protease inhibitors), and fast frozen in liquid nitrogen. The tissues were then thawn on ice and centrifuged at 13000 rpm for 15 min at 4°C. The supernatants were analyzed for total protein concentration using Bradford solution (Biorad, Munich, Germany) in 96-well plates with bovine serum albumin (BSA) as standard. 10–20 $\mu$g of total protein were diluted in sample buffer (0.3 M Tris/HCl, pH 7, 50% glycerol, 5% SDS, 1 mM EDTA, 0.1% bromphenol blue) and were treated with 100 mM DTT for 30 min at room temperature followed by 10 min at 94°C. Samples were subjected to SDS–PAGE using the Mini-Protean TGX stain-free 4–20% precast gels (Biorad) and were transferred to PVDF membranes according to the manufacturer's instructions.

Membranes were blocked with 5% nonfat milk powder and 1% BSA in Tris-buffered saline containing 0.05% Tween 20 and incubated with specific primary antibodies at 4°C overnight. Antigen-antibody complexes were stained using horseradish peroxidase- (HRP-) coupled antibodies (Biorad, Richmond, CA, USA) and the enhanced chemiluminescence method. Luminescence was recorded using a gel documentation system (ChemiDoc™ XRS+ System). The total protein amount in each lane was quantified using the stain-free technology of Biorad and was used for normalization of the blotting data obtained from densitometric analysis [27, 28]. Antibodies detecting HSP70 (4873S, dil 1 : 1000) and PSD95 (ab18258, dil 1 : 1000) were purchased from Cell Signaling Technology (Danvers, USA) and Abcam (Cambridge, USA), respectively.

*2.4. ELISA.* A specific sandwich ELISA kit (NS170, Chemicon International, USA-Canada) was used to quantify the heavy chain of phosphorylated neurofilaments (pNF-H) according to the manufacturer's instructions. Briefly, a 96-well immunoplate precoated with chicken anti-pNF-H polyclonal antibody was used to capture pNF-H in plasma samples, as well as specific standards with known pNF-H concentrations. Captured pNF-H was then detected by a rabbit anti-pNF-H polyclonal antibody (1 : 100) and followed by an alkaline phosphatase-conjugated goat anti-rabbit polyclonal antibody. After the addition of the substrate pNPP (p-nitrophenyl phosphatase), the amount of pNF-H was determined by absorbance at 405 nm.

*2.5. Immunohistochemistry and Cell Counting.* Immunohistochemistry was performed as previously described in Romero et al. [23]. Animals were anesthetized with 28% (*w*/*v*) chloral hydrate, 0.1 ml/100 g of body weight, and intracardially perfused with 4% paraformaldehyde (Sigma-Aldrich, St. Louis, MO, USA) freshly prepared in 0.1 M phosphate buffer, pH 7.4. Brains were dissected and postfixed in the same solution for 2 h. Coronal brain sections (4 $\mu$m thick) were cut using a Leica sliding microtome and then recovered for light microscopy studies. Prior to the staining, sections were incubated in 3% hydrogen peroxide for 10 min to quench endogenous peroxidases. After three washing steps in PBS, nonspecific antibody binding sites were blocked with 10% goat serum (Invitrogen Corporation, Camarillo, CA, USA) in PBS and sections were incubated overnight with anti-GFAP rabbit polyclonal antibody (1 : 500, Z0334, Dako, Germany) at 4°C. Then, sections were washed three times with PBS and subsequently incubated with a goat anti-rabbit biotinylated secondary antibody (1 : 500, BA-1000, Vector Laboratories Inc., USA) for 60 min at room temperature. The streptavidin/HRP detection system (P0397, Dako, Germany) was used for antigen staining according to the manufacturer's recommendations. Sections were incubated with the substrate diaminobenzidine (11718096001, Roche Life Science, USA) for 5 min at room temperature. Finally, sections were dehydrated and were mounted with Canada balsam (Sigma-Aldrich, St. Louis, MO, USA). Sections without incubation with the primary antibody were used as a control to verify the specificity of the secondary antibody. Samples were examined by light microscopy using a Leitz Laborlux S microscope (Heidelberg, Germany) equipped with a CCD video camera (Canon). Images were analyzed and compiled using Adobe Photoshop 11.0 CS4. Note that for protein staining, all samples (both sham and carotid groups) were processed together in the same batch, using the same antibody dilutions and the same time for DAB development.

Cell counting analysis was carried out in 5 to 6 coronal sections obtained from −3.14 mm to −4.30 mm Bregma levels (dorsal hippocampus) [29], for a total of 4 animals per group. In every section, the number of GFAP positive cells was quantified in both hemispheres and averaged. A mean was calculated for each animal and used for subsequent statistical analysis. We determined the cell number per area using the "Cell Counter" Image J 1.38X plugin tool (NIH, USA). In sections stained with GFAP containing *Cornu Ammonis* 1 (CA1),

we set 0.02 $mm^2$ squares along the *Stratum pyramidale* (sp) of CA1 in such a manner that the whole area was represented. Subsequently, we manually determined the number of cells in each square and calculated the number of cells per $mm^2$. All quantifications were performed in a blind approach.

*2.6. Neurobehavioral Studies.* Neurobehavioral development studies were carried out from the first day after hypoxia-ischemia induction (P8), till the last animal showed the appearance or disappearance of the analyzed reflex (~P19). Animals were evaluated every day at the same time (10 a.m.) for approximately 3 hours each time. All scoring was performed blindly by two observers. In order to evaluate the possible effect of the treatment in the neurobehavioral development of the animals, pups were subjected to a series of tests previously described by Kiss et al. [30], Shahrokhi et al. [31], and Giriko et al. [32], which assess the manifestation of different reflexes such as surface righting reflex, negative geotaxis, crossed extensor reflex, ear and eyelid twitching, and auditory startle. Additionally, ear unfolding and eye opening were assessed as a measurement of physical development.

*2.7. Statistical Analysis.* Band intensities obtained from Western blots were quantified using GelPro 3.1 and were expressed as percentage of the control levels (sham-operated rats injected with saline solution). Total protein amount, visualized using the stain-free technology of Biorad was quantified using the ImageLab 5.0 software (Biorad). Bar diagrams depict the mean of four independent quantifications for each experiment, consisting of sham-operated (sham-veh, $n = 5$; sham-Grx2, $n = 5$; and sham-Trx1, $n = 5$) and ischemic (carotid-veh, $n = 5$; carotid-Grx2, $n = 5$; and carotid-Trx1, $n = 5$) animals + SEM, correlated to total protein. Two-way ANOVA tests with condition (sham, carotid) and treatment (vehicle, Grx2, and Trx1) as between-subject factors, followed by Tukey's post hoc tests, were employed to analyze the biochemical parameters and protein levels. For the neurobehavioral analysis, bar diagrams depict the mean of the day of appearance of the assessed reflexes for each group, consisting of sham-operated (sham-veh, $n = 10$; sham-Grx2, $n = 10$; and sham-Trx1, $n = 10$) and ischemic (carotid-veh, $n = 10$; carotid-Grx2, $n = 10$; and carotid-Trx1, $n = 10$) animals + SEM. Kruskal-Wallis tests, followed by Mann–Whitney tests for pair-wise multiple comparisons, were employed to analyze neurodevelopmental parameters. In all cases, the level of significance was set up at 5%. All analyses were performed using SPSS 15.0 (Chicago, IL, USA).

## 3. Results

We have previously shown that Grx2 and Trx1 are induced in the hippocampus upon perinatal asphyxia [23]. Interestingly, Grx2 and Trx1 are essential for the neuronal integrity, since the knock-down of these redoxins in the neuroblastoma cell line SH-SY5Y affected cell morphology and viability during hypoxia and reoxygenation [23]. Within this study, we investigated whether recombinant Grx2 and Trx1 can be used as therapeutics following perinatal asphyxia, using the well-established murine carotid ligation model.

*3.1. Grx2 Administration Decreases Neuronal Damage after Neonatal Hypoxia/Ischemia.* Perinatal asphyxia was induced in rats by carotid ligation and 3 min nitrogen treatment. Following the treatment with recombinantly expressed and purified Grx2, Trx1, or saline solution 1 h after the hypoxic/ischemic event, animals were sacrificed and their brains analyzed. We observed that animals from the carotid ligation group that only received a saline injection displayed an approximately 3-fold higher immunoreactivity against the neuronal damage marker heat shock protein 70 (HSP70) than the sham group with the same treatment ($p < 0.01$) (Figure 1). The carotid ligation group treated with recombinant human Grx2 presented an approximately 3-fold lower immunoreactivity against HSP70 than the carotid ligation group with saline injection ($p < 0.01$) and did not differ from both, the sham group treated with Grx2 nor the sham group treated with saline solution (Figure 1). Treatment with recombinant human Trx1 did not affect the protein levels of HSP70 in both, sham ($p < 0.01$) and carotid ligation animals ($p < 0.01$). The carotid ligation group treated with Trx1 also presented a 3-fold higher immunoreactivity against HSP70, comparable to the sham carotid ligation group (Figure 1).

*3.2. Exogenous Administration of Grx2 or Trx1 Interferes with the Glutamate Excitotoxicity Pathway after Neonatal Hypoxia/Ischemia.* To determine whether Grx2 or Trx1 treatments affect the excitotoxic effects of glutamate associated with PA, we analyzed the protein levels of the postsynaptic density protein 95 (PSD95). High levels of PSD95 have been linked to increase glutamate excitotoxicity, while its reduction has been linked to a neuroprotective effect in neonatal models of hypoxia/ischemia [33–35]. Western blotting analysis showed that animals subjected to neonatal hypoxia/ischemia and injected with saline solution presented over 5-fold higher levels of PSD95 in comparison to the sham group with the same treatment ($p < 0.01$) (Figure 2). After injection of 10 mg/kg of Grx2 1 hour after the hypoxic/ischemic insult, the carotid ligation group displayed no differences compared to the sham group that was also treated with Grx2. Furthermore, neither the sham group nor the carotid group treated with Grx2 showed any significant differences when compared to the sham group that only received the saline injection (Figure 2). The carotid ligation group treated with Grx2 presented an approximately 6-fold reduction in the levels of PSD95 compared with the saline-treated carotid ligation group ($p < 0.01$) (Figure 2). The carotid ligation group treated with Trx1 presented a 3-fold increase in PSD95 levels in comparison to both the sham group treated with Grx2 ($p < 0.05$) and the sham group with saline injection ($p < 0.05$). Nonetheless, Trx1 treatment significantly attenuated the increase in PSD95 levels in the carotid ligation group by 3-fold in comparison to the carotid group treated with saline solution ($p < 0.01$) (Figure 2).

*3.3. Exogenous Administration of Grx2 or Trx1 Helps in Maintaining Structural Integrity after Neonatal Hypoxia/Ischemia.* The structural integrity of axons was evaluated in hypoxic/ischemic animals 72 h after the hypoxia/ischemia event by analyzing the plasma levels of phosphorylated

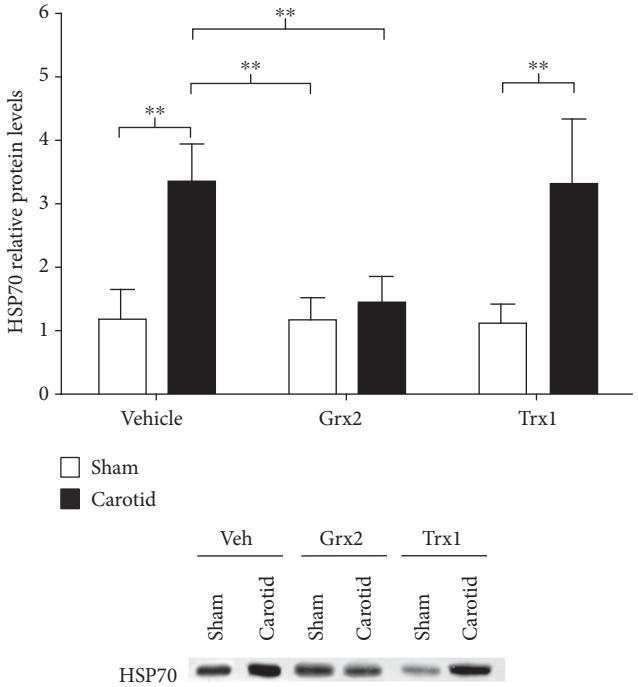


Figure 1: Grx2 reduces neuronal damage following perinatal hypoxia/ischemia. Perinatal asphyxia was induced in rats by carotid ligation and 3 min nitrogen treatment. During 1 h postischemia, the animals were treated with recombinant Grx2 or Trx1. Hippocampi were isolated and analyzed for changes in the protein levels of the neuronal damage marker HSP70 by Western blot. The diagram depicts the relative protein levels compared to sham-operated rats that only received a saline solution (vehicle). Representative Western blots demonstrate the significant changes. Bars depict the mean + SEM of 5 rats per group. Two-way ANOVA test [condition (sham, carotid): $F_{(1,24)} = 49.85$, $p < 0.001$; treatment (veh, Grx2, and Trx1): $F_{(2,24)} = 8.05$, $p < 0.01$; and interaction: $F_{(2,24)} = 8.39$, $p < 0.01$] followed by Tukey's post hoc tests was employed to analyze the data. $^{**}p < 0.01$.

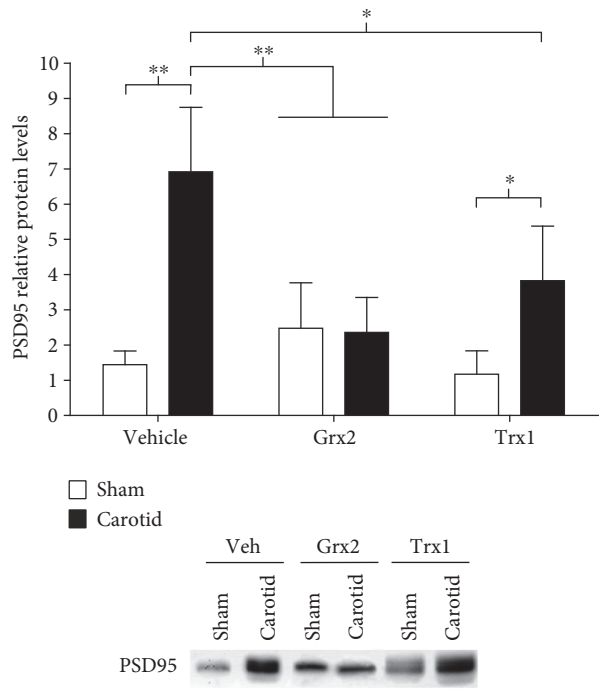


Figure 2: Grx2 and Trx1 interfere with the glutamate excitotoxicity pathway following neonatal hypoxia/ischemia. Perinatal asphyxia was induced in rats by carotid ligation and 3 min nitrogen treatment. During 1 h postischemia, the animals were treated with recombinant Grx2 or Trx1. Hippocampi were isolated and analyzed for changes in the protein levels of PSD95 by Western blot, as a reporter for the induction of glutamate exitotoxicity. The diagram depicts the relative protein levels compared to sham-operated rats that only received a saline solution (vehicle). Bars show the mean + SEM of 5 rats per group. Two-way ANOVA test [condition (sham, carotid): $F_{(1,24)} = 29.07$, $p < 0.001$; treatment (veh, Grx2, and Trx1): $F_{(2,24)} = 58.36$, $p < 0.05$; and interaction: $F_{(2,24)} = 10.61$, $p < 0.001$] followed by Tukey's post hoc tests was employed to analyze the data. $^{*}p < 0.05$, $^{**}p < 0.01$.

neurofilament heavy protein (pNF-H). In fact, animals of the CCA ligation group with the saline injection had a 50% increase in the levels of pNF-H in plasma in comparison to the sham group treated only with saline solution ($p < 0.05$) (Figure 3). Animals subjected to an injection of 10 mg/kg of Grx2 one hour after the hypoxic/ischemic event did not show the increase in pNF-H levels in plasma normally associated with structural axon damage. Moreover, both the carotid ligation and sham groups treated with Grx2 did not display differences in the levels of pNF-H, compared to the sham group that only received a saline injection (Figure 3). Similarly, animals from the carotid ligation group treated with Trx1 did not present an increase in pNF-H plasma levels. Interestingly, the levels of pNF-H in plasma in the groups treated with Trx1 were still another 50% lower than those detected in the sham group that only received a saline injection ($p < 0.05$) (Figure 3).

*3.4. Exogenous Administration of Grx2 and Trx1 Avoids the Astrogliosis Caused by Neonatal Hypoxia/Ischemia.* The effect of Grx2 and Trx1 treatment on astrogliosis development following the hypoxic/ischemic event was analyzed by glial fibrillary acidic protein (GFAP) immunostaining in the *stratum radiatum* of the hippocampal CA1 area, which previously has been reported as a particularly susceptible area in neural plasticity and development of astrogliosis [36–38]. As expected, hypoxic/ischemic rats injected with saline solution presented an approximately 30% increase in the number of GFAP positive (GFAP+) astrocytes, in comparison to sham rats treated with saline solution ($p < 0.01$) (Figure 4). Animals from the carotid ligated group treated with Grx2 did not present an increase in the number of GFAP+ cells when compared to the carotid ligated group treated with saline solution ($p < 0.05$), while it did not show any differences in comparison with the sham group treated with Grx2 (Figure 4). Likewise, the carotid group treated with Trx1 did not show an increase in GFAP+ astrocytes in comparison to the carotid group that only received the saline solution injection ($p < 0.01$). No significant difference was detected between the carotid ligation and sham

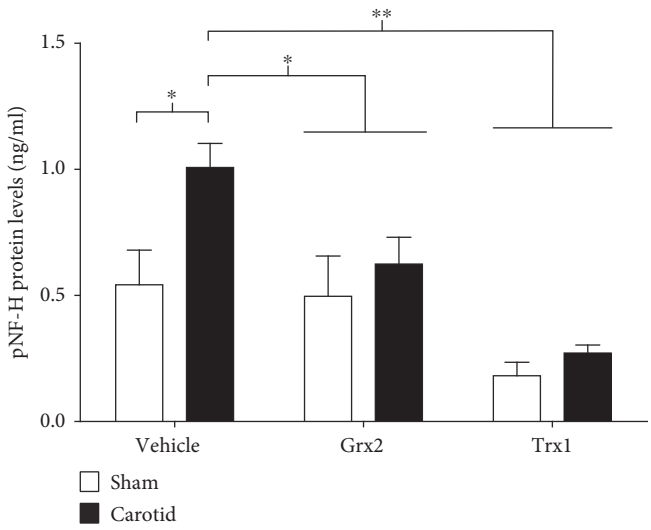


Figure 3: Grx2 and Trx1 help to maintain the structural integrity following neonatal hypoxia/ischemia. Plasma from 10-day-old rats that were subjected to a carotid ligation or sham operation and subsequent 3 min nitrogen treatment and received a treatment with either saline solution, Grx2, or Trx1 one hour postinjury, was screened for pNF-H as a measurement of structural damage to the axons. The levels of pNF-H were analyzed by a specific ELISA. Bars represent the mean + SEM of 5 rats per group. Two-way ANOVA test [condition (sham, carotid): $F_{(1,24)} = 27.20$, $p < 0.001$; treatment (veh, Grx2, and Trx1): $F_{(2,24)} = 53.34$, $p < 0.001$; and interaction: $F_{(2,24)} = 7.47$, $p < 0.01$] followed by Tukey post hoc tests was employed to analyze the data. $^{*}p < 0.05$, $^{**}p < 0.01$.

groups treated with Trx1 (Figure 4). Moreover, all groups treated with either Grx2 or Trx1 did not show significant differences when compared with the sham group treated only with the saline solution (Figure 4), suggesting that the treatment with either Grx2 or Trx1 protects from the astrogliosis associated with the hypoxic/ischemic event during birth.

*3.5. Grx2 and Trx1 Administration Reverts Some of the Early Developmental Alterations Associated with Neonatal Hypoxia/Ischemia.* In order to assess both the effects of the hypoxic/ischemic event and the treatment with Grx2 or Trx1 on the neurodevelopment of pups, a series of reflexes and physical developmental parameters were measured from postnatal day 8 (P8) until ~P19. There were no significant differences between group conditions (sham or carotid) or between treatments (saline, Grx2, or Trx1 administration) for the tasks evaluating surface righting reflex, negative geotaxis, crossed extensor reflex, ear twitching, auditory startle, and ear unfolding (see Supplementary Figure 1 available online at https://doi.org/10.1155/2017/4162465). Nevertheless, carotid animals that only received a saline injection displayed a significant delay in eye opening and eyelid twitching in comparison with sham-operated animals ($p < 0.05$ in both cases, see Figures 5(a) and 5(b), resp.). Interestingly, Grx2 administration reverted the delayed eye opening observed in the carotid group treated with saline (Figure 5(a)). Trx1 administration had no effect on this developmental parameter. Interestingly, Grx2 had no effect on the delay in eyelid twitching observed after the injury, while Trx1 treatment reverted the delay in relation with the sham group (Figure 5(b)).

## 4. Discussion

Recently, we have analyzed the changes in the levels of 14 members of the Trx family in the brains of rats subjected to the carotid ligation model [23], showing that Grx2 and Trx1 are crucial for the recovery following hypoxia/ischemia and reoxygenation. In fact, silencing of these proteins in neuron-like cell cultures (SH-SY5Y) plays an important role in maintaining the neuronal phenotype of these cells [23]. These studies prompted us to investigate the effects of protein administration on the neuronal damage caused by PA. The results presented suggest that the administration of Grx2, and to some extent the administration of Trx1, has the potential to significantly attenuate the neuronal damage caused by PA, including the cellular damage response, glutamate excitotoxicity, axonal integrity, and astrogliosis. It is worth mentioning that the reoxygenation phase following a hypoxic/ischemic event comprises the early, acute phase that is induced by $O_2$, $O_2-$, and overall changes in cellular redox properties, and the late subacute phase that is rather induced by the overall immune response [39]. Here, we have focused on the short-term changes (72 h posthypoxic/ischemic event) induced by PA, because (i) the CNS is especially susceptible to oxidative damage due to its high metabolic rate, its oxygen consumption, and its low capacity for regeneration and (ii) these changes correlate with the mortality rate of patients [40–43].

Interestingly, Prxs, substrates for Trxs and Grxs, are significantly altered as a result of stroke-related insults [21, 44–46]. Overexpression of Prx6 decreased hypoxia-induced retinal ganglion cell death [47]. Prx3, which was shown to be reduced and regenerated by Grx2 [48], showed elevated protein levels in the hippocampus of gerbils following cerebral hypoxia/ischemia and reoxygenation and protected CA1 pyramidal neurons against the induced damage [49]. It is thus tempting to speculate that the protective mechanism of Grx2 could involve the reduction of Prxs and therefore the regulation of intracellular levels of peroxides and cellular signaling, as well as the molecular damage that can occur in the presence of high peroxide levels.

Cellular damage derived from an ischemic insult induces the expression of heat shock proteins, one of the groups of proteins involved in the overall stress response [50]. HSP70 is constitutively expressed and is the most abundant heat shock protein present in the cell, and it is produced as a response to several stimuli, such as heat, heavy metals, toxins, and ischemia [51]. Increased HSP70 expression has been reported as a response to ischemic damage in neurons, astrocytes, and endothelial cells [52]. Interestingly, cerebral ischemia in rats induces HSP70 expression, mainly in the

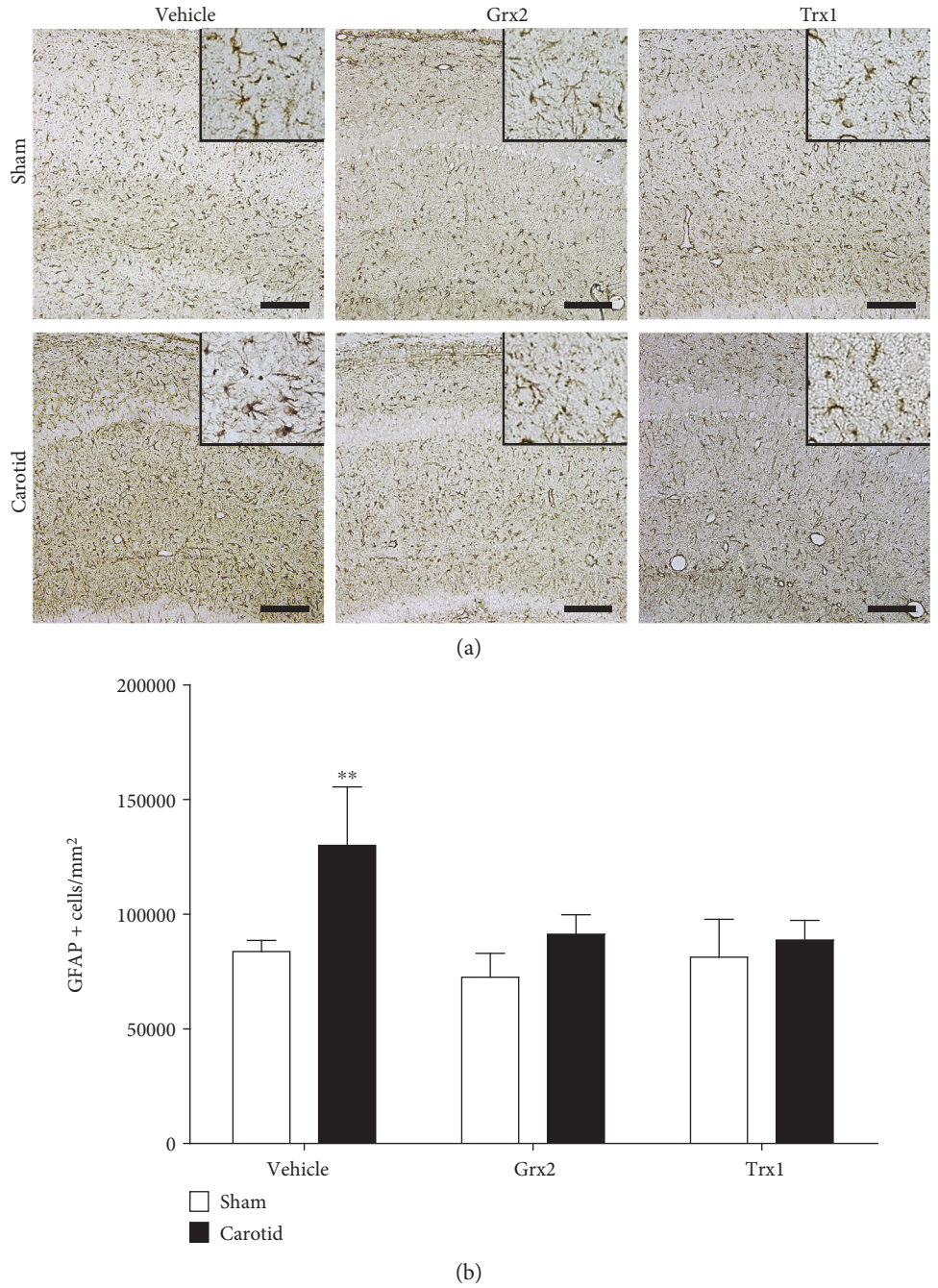


Figure 4: Grx2 and Trx1 prevent the characteristic astrogliosis that follows neonatal hypoxia/ischemia. (a) Representative immunostainings of GFAP in the CA1 area of the hippocampus. Insets show the morphological details of astrocytes. (b) Quantification of GFAP+ cells as number of positive cells by $mm^2$ was used as a measurement of the reactive gliosis response. Bars represent the mean + SEM of 4 rats per group. Two-way ANOVA test [condition (sham, carotid): $F_{(1,18)} = 17.52$, $p < 0.001$; treatment (veh, Grx2, and Trx1): $F_{(2,18)} = 7.42$, $p < 0.001$; and interaction: $F_{(2,18)} = 3.97$, $p < 0.05$] followed by Tukey's post hoc tests was employed to analyze the data. $^{**}p < 0.01$. Scale bars 10 $\mu$m.

hippocampus and the cerebral cortex, correlating with the vulnerability of the CNS to ischemic damage [53]. Since carotid animals that were treated with Grx2 presented significantly lower levels of HSP70 compared to control animals that only received saline solution, it can be inferred that Grx2 can significantly reduce the immediate cellular response towards the hypoxic/ischemic event associated with the HSP70 response (Figure 1).

The protein-protein interactions, mediated by the PPDZ domain of the postsynaptic density 95 protein, are key elements in intracellular signaling [54]. The structural postsynaptic protein PSD95 binds simultaneously to the

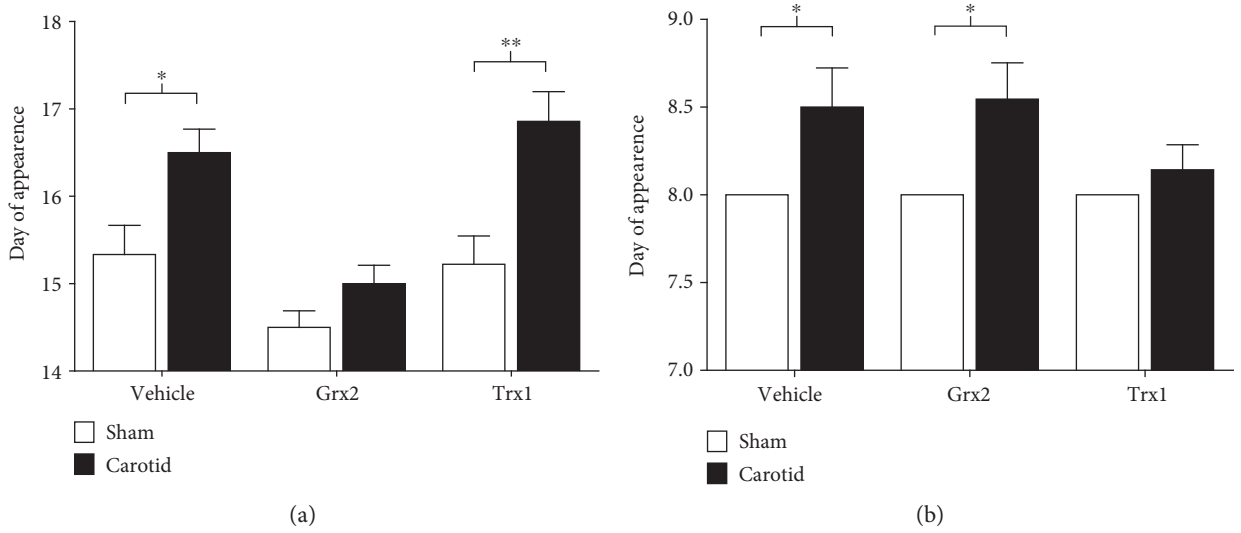


Figure 5: Grx2 and Trx1 revert the delay in the appearance of eye neurodevelopment milestones present after neonatal hypoxia/ischemia. Pups were evaluated for the detection of variation in the appearance of different reflexes and motor skills. (a) Quantification of the eye opening in pups expressed as the day of the first appearance (both eyes presented completed separation of the eyelids). (b) Quantification of the eye twitching reflex in pups expressed as the day of the first appearance (day in which both eyelids twitch for the first time). Bars represent the mean + SEM of 10 rats per group. Kruskal-Wallis tests [eye opening: $H = 25.35$, d.f. = 5, $p < 0.001$; eye twitching: $H = 15.72$, d.f. = 5, $p < 0.01$], followed by post hoc Mann–Whitney tests were employed to analyze the data. $^{*}p < 0.05$, $^{**}p < 0.01$.

ionotropic glutamate receptor NMDA and the enzyme nNOS through its PDZ1 and PDZ2 domains [55]. The activation of the NMDA receptor causes the influx of intracellular $Ca^{2+}$ which, in turn, produces the activation of nNOS with the consequent generation of NO [35], one of the most common promoters of glutamate excitotoxicity [56, 57]. Considering that PSD95 inhibition does not affect the overall ion flux [58] or the signaling pathways that favor survival [59], which are mediated by the NMDA receptor, it has been speculated that PSD95 could be a safe and efficient target for the treatment of cerebral ischemic damage [60]. Hence, neurons deficient for PSD95 or nNOS show a reduction in the vulnerability to glutamate excitotoxicity [61]. Previous studies have shown that the reduction of PSD95 expression is linked to a reduction of the damage associated with a neonatal hypoxic/ischemic event [33–35]. As expected, the levels of PSD95 were significantly elevated in the carotid group compared to the sham animal group (about 7-fold increase). Interestingly, no significant increase of PSD95 was detected in the carotid animals injected with Grx2 compared to the sham animal groups injected with saline solution or Grx2. Thus, Grx2 might not only counteract the HSP70 response but also the damage associated to glutamate excitotoxicity after the hypoxic/ischemic injury (Figure 2). Even though Trx1 treatment did not show a significant effect on HSP70 protein levels following the hypoxia/ischemia (Figure 1), a significant 3-fold decrease in the protein levels of PSD95 compared with the carotid group treated with saline solution was detected. However, Trx1 treatment was not as efficient as Grx2 in preventing or counteracting the induction of PSD95 (Figure 2).

The screening of specific components in tissues and biological fluids secreted upon pathological conditions is commonly used as a therapeutic and diagnostic tool [62]. Neurofilaments are highly abundant proteins in neurons and are found in the axons of all neurons. Their main function is the maintenance of the axonal gauge, which is essential for the morphological integrity and the conduction velocity of neuronal impulses [63]. Three types of neurofilaments (light neurofilaments (NF-L), medium neurofilaments (NF-M), and heavy neurofilaments (NF-H)) make up the nerve fibers and are eliminated to the extracellular space in considerable amounts following axonal damage or neuronal degeneration [64–66]. The perturbation of the axonal membrane expels neurofilaments to the interstitial space and eventually to the cerebrospinal fluid and the blood. In this manner, the levels of neurofilaments in the blood can be used for both the prediction and monitoring of the progress of a disease and the evaluation of the efficacy and/or toxicity of neuroprotective treatments [67–70]. The phosphorylated form of NF-H is axon-specific and is used as a specific marker for neuronal damage and degeneration [71]. pNF-H levels are, for instance, elevated following acute hypoxic/ischemic damage [72]. It has been further shown that the levels of pNF-H in serum and cerebrospinal fluid are increased after a variety of damages to the CNS, both in animal models and in humans [71]. Moreover, the increment of pNF-H levels in serum is a good indicator of the degree of the lesion in the white matter of the CNS [73]. In our model, we could confirm that acute hypoxia/ischemia leads to neuronal damage and elevated levels of pNF-H in serum compared to sham animals (Figure 3). Interestingly, when the carotid animals were treated with Grx2 or Trx1 following the hypoxic/ischemic event, no such increase was detectable via specific ELISA (Figure 3). It is worth to notice that in the case of Trx1 administration, pNF-H levels both in sham and

carotid animals were well below those found in the sham group treated only with saline solution. This effect could be the consequence of a higher effect in axonal integrity produced by Trx1. In this regard, previous studies have linked Trx1 to a strong protection against axonal damage in a model of retinal nerve damage [74, 75], as well as to the regulation of axonal regeneration [76]. The excess of Trx1 in the system could thus contribute to lower the basal levels of pNF-H by tipping the balance toward axonal regeneration rather than disruption.

Reactive gliosis can be triggered in response to several CNS pathologies, such as trauma, stroke, and neurodegenerative diseases [77]. Following injury, astrocytes proliferate and their GFAP expression increases [78]. Experimental data suggest that reactive gliosis can be detrimental for neuroplasticity and regeneration of the CNS. Therefore, the prevention of reactive gliosis has become an essential issue in the development of therapeutic interventions [79]. Previous studies have shown that perinatal hypoxia/ischemia triggers reactive gliosis in neonatal rats [36, 80]. In this study, we have shown that hypoxia/ischemia induces the characteristic reactive gliosis. Sham-treated animals, as well as animals that were treated with either Grx2 or Trx1 one hour after the injury, did not develop astrogliosis (Figure 4).

The rat postnatal development is characterized by the appearance of a series of reflexes and motor skills through the first three weeks of life [81]. During this period, different insults, such as a hypoxic/ischemic event, can affect the normal development of those reflexes and physical skills [30, 82–84]. Previous studies have shown that glutamate neurotoxicity plays a key role in the impairment of the development of neurological reflexes and motor skills [82, 85]. This excitotoxicity has shown to be most severe in the retina, in the cortex, and in the hippocampus [82, 85–88]. Moreover, glutamate excitotoxicity has also been previously linked to neurobehavioral delays [82, 85]. Interestingly, the biochemical findings of this study showed that both Grx2 and Trx1 acted in the biomarker reduction associated with the glutamate excitotoxicity pathway which was increased after hypoxia/ischemia (Figure 2). In this regard, neurodevelopmental analyses have shown that Grx2 treatment was able to revert the developmental delay presented in the opening of the eye in carotid pups (Figure 5(a)), while Trx1 administration reverted the neurodevelopmental delay presented in the appearance of the eye twitching reflex (Figure 5(b)).

Both of the thioredoxin family proteins investigated here, Grx2 and Trx1, have been characterized as crucial for cell survival under various conditions when expressed intracellularly (summarized, for instance in Holmgren et al. [89] and Hanschmann et al. [6]). Since Trx1 is known to be secreted by cells via an unconventional mechanism and to function, for instance, in the activation of immune cells (summarized in Nakamura [90]), Trx1 administration has been discussed as a potential therapeutic strategy against cellular damage [91]. In fact, the perfusion, but not the inhalation, of recombinant human Trx1 protected rat lungs from ischemia-reperfusion injury [92]. An intravitreous injection of recombinant Trx1 was also shown to attenuate the damage produced to the retina by ischemia and glaucoma, induced by N-methyl-D-aspartate, which stimulates glutamate receptors [93]. Both Grxs and Trxs have shown to protect from dopamine-induced neuronal damage in vitro [94, 95]. Recently, Tian and coworkers demonstrated that treatment with recombinant Trx1 can improve the neurogenesis via the regulation of the ERK signaling pathway in mice following global cerebral ischemia, improving spatial learning and memory [22].

In the present study, we have shown that even though Grx2 and Trx1 are both part of the thioredoxin family of proteins, they do not necessarily behave in the same manner. This can be exemplified by the differences observed in response to Grx2 and Trx1 treatments, regarding HSP70, PSD95, and pNF-H markers as well as the different outcomes in the neurodevelopmental evaluation after the treatments. These differences could be explained through the possible distinct mechanisms involved in each protein intervention. In this regard, it is known that Grx2, as part of the glutaredoxin subfamily, plays a key role in redox-dependent cellular processes [96]. Particularly, glutaredoxins (Grxs) are able to reduce both disulfides and mixed disulfides, while they can be restored by glutathione reductase which is directly coupled to the GSH/GSSG ratio (the main indicator of the cell redox state and its redox potential) [97, 98]. Grxs are also capable of catalyzing S-glutathionylation of proteins (a key regulatory mechanism of biological processes) [99, 100]. It is generally accepted that Grxs are a key component in response to an oxidative imbalance through the regulation of mix disulfides [101, 102]. In addition, due to the mitochondrial localization of Grx2, it has been proved that it prevents apoptosis by avoiding the leak of cytochrome c from mitochondria and cardiolipin oxidation [89, 103, 104]. By contrast, Trx1 shows no activity towards mixed disulfides and it is thought to have a more prominent role in redox regulation of cell signaling rather than direct participation in redox-dependent reactions as a consequence of its low levels in comparison with other endogenous antioxidants, and its multifunctional role as a cytosolic protein. In this compartment, Trx1 can function as a growth factor and enzyme cofactor and, under different stresses, can translocate to the nucleus and regulate several transcription factors [96, 105–109]. Taking this data into account, the observed differences in the measurements performed in the present study could be associated with the biological processes in which each redoxin is more important. One could hypothesize that those processes more related to an imbalance of the redox state could respond better to a Grx2 treatment, while Trx1 could be more prominent in processes where it functions as a regulator of transcription factors.

## 5. Conclusion

Taken together, the results presented in this study suggest that the delivery of recombinant Grx2, and to some extend of Trx1, has the potential to attenuate the severe neurological damage induced by PA. If not the delivery of these proteins themselves, a detailed understanding of the underlying redox regulated signaling pathways, may put in evidence the need

for new therapeutic strategies to improve CNS recovery after PA and potentially other stroke associated pathologies.

## Disclosure

The current address of Juan Ignacio Romero is Fundación Instituto Leloir, Av. Patricias Argentinas 435, C1405BWE, Ciudad Autónoma de Buenos Aires, Argentina.

## Conflicts of Interest

None of the authors have any conflict of interest to report related to this manuscript.

## Acknowledgments

This work was supported by the Deutsche Forschungsgemeinschaft (SFB593-N01, LI984/3-1, and GRK1947-A1) to Christopher Horst Lillig; the Federal Ministry for Science and Education (BMBF: 01DN13023-PAREDOX) and MINCYT to Christopher Horst Lillig and Francisco Capani; the German Academic Exchange Service DAAD and MINCYT (PROALAR program) to Christopher Horst Lillig and Francisco Capani; the National Scientific and Technical Research Council (PIP 11420100100159, CONICET, Argentina) to Francisco Capani; Instituto de Salud Carlos III, Ministerio de Economía y Competitividad UE/ERDF grants PI16/01698 and Red de Trastornos Adictivos RD16/0017/0001, and Fundació "La Marató de TV3" (Grant no. 386/C/2011) to Fernando Rodríguez de Fonseca; and the University of Buenos Aires (UBACYT 20020090100118) to Francisco Capani. Juan Ignacio Romero, Mariana Inés Holubiec, Stéphanie Rivière, and Tamara Logica Tornatore are fellowship holders from the National Scientific and Technical Research Council (CONICET, Argentina). Francisco Capani and Pablo Galeano are researchers from the National Scientific and Technical Research Council (CONICET, Argentina). Eduardo Blanco is an associate professor of the Serra-Hunter Programme from the Catalan Government.

## References

[1] J. E. Rice 3rd, R. C. Vannucci, and J. B. Brierley, "The influence of immaturity on hypoxic-ischemic brain damage in the rat," *Annals of Neurology*, vol. 9, no. 2, pp. 131–141, 1981.

[2] D. W. Choi and S. M. Rothman, "The role of glutamate neurotoxicity in hypoxic-ischemic neuronal death," *Annual Review of Neuroscience*, vol. 13, no. 1, pp. 171–182, 1990.

[3] F. Capani, F. Loidl, J. J. Lopez-Costa, A. Selvin-Testa, and J. P. Saavedra, "Ultrastructural changes in nitric oxide synthase immunoreactivity in the brain of rats subjected to perinatal asphyxia: neuroprotective effects of cold treatment," *Brain Research*, vol. 775, no. 1, pp. 11–23, 1997.

[4] C. F. Loidl, J. De Vente, M. M. van Ittersum et al., "Hypothermia during or after severe perinatal asphyxia prevents increase in cyclic GMP-related nitric oxide levels in the newborn rat striatum," *Brain Research*, vol. 791, no. 1, pp. 303–307, 1998.

[5] F. Capani, C. F. Loidl, F. Aguirre et al., "Changes in reactive oxygen species (ROS) production in rat brain during global perinatal asphyxia: an ESR study," *Brain Research*, vol. 914, no. 1, pp. 204–207, 2001.

[6] E. M. Hanschmann, J. R. Godoy, C. Berndt, C. Hudemann, and C. H. Lillig, "Thioredoxins, glutaredoxins, and peroxiredoxins—molecular mechanisms and health significance: from cofactors to antioxidants to redox signaling," *Antioxidants & Redox Signaling*, vol. 19, no. 13, pp. 1539–1605, 2013.

[7] A. Holmgren, "Thioredoxin and glutaredoxin systems," *The Journal of Biological Chemistry*, vol. 264, no. 24, pp. 13963–13966, 1989.

[8] W. W. Wells, Y. Yang, T. L. Deits, and Z. R. Gan, "Thioltransferases," *Advances in Enzymology and Related Areas of Molecular Biology*, vol. 66, pp. 149–201, 1993.

[9] J. R. Godoy, M. Funke, W. Ackermann et al., "Redox atlas of the mouse. Immunohistochemical detection of glutaredoxin-, peroxiredoxin-, and thioredoxin-family proteins in various tissues of the laboratory mouse," *Biochimica et Biophysica Acta*, vol. 1810, no. 1, pp. 2–92, 2011.

[10] M. L. Aon-Bertolino, J. I. Romero, P. Galeano et al., "Thioredoxin and glutaredoxin system proteins-immunolocalization in the rat central nervous system," *Biochimica et Biophysica Acta*, vol. 1810, no. 1, pp. 93–110, 2011.

[11] J. L. Martin, "Thioredoxin—a fold for all reasons," *Structure*, vol. 3, no. 3, pp. 245–250, 1995.

[12] C. H. Lillig and A. Holmgren, "Thioredoxin and related molecules—from biology to health and disease," *Antioxidants & Redox Signaling*, vol. 9, no. 1, pp. 25–47, 2007.

[13] Y. Takagi, T. Tokime, K. Nozaki, Y. Gon, H. Kikuchi, and J. Yodoi, "Redox control of neuronal damage during brain ischemia after middle cerebral artery occlusion in the rat: immunohistochemical and hybridization studies of thioredoxin," *Journal of Cerebral Blood Flow and Metabolism: Official Journal of the International Society of Cerebral Blood Flow and Metabolism*, vol. 18, no. 2, pp. 206–214, 1998.

[14] H. Tomimoto, I. Akiguchi, H. Wakita, J. Kimura, K. Hori, and J. Yodoi, "Astroglial expression of ATL-derived factor, a human thioredoxin homologue, in the gerbil brain after transient global ischemia," *Brain Research*, vol. 625, no. 1, pp. 1–8, 1993.

[15] Y. Takagi, A. Mitsui, A. Nishiyama et al., "Overexpression of thioredoxin in transgenic mice attenuates focal ischemic brain damage," *Proceedings of the National Academy of Sciences of the United States of America*, vol. 96, no. 7, pp. 4131–4136, 1999.

[16] F. Zhou, M. Gomi, M. Fujimoto et al., "Attenuation of neuronal degeneration in thioredoxin-1 overexpressing mice after mild focal ischemia," *Brain Research*, vol. 1272, pp. 62–70, 2009.

[17] L. Li, K. Zhu, Y. Liu et al., "Targeting thioredoxin-1 with siRNA exacerbates oxidative stress injury after cerebral ischemia/reperfusion in rats," *Neuroscience*, vol. 284, pp. 815–823, 2015.

[18] X. Wu, L. Li, L. Zhang et al., "Inhibition of thioredoxin-1 with siRNA exacerbates apoptosis by activating the ASK1-JNK/p38 pathway in brain of a stroke model rats," *Brain Research*, vol. 1599, pp. 20–31, 2015.

[19] J. M. Hansen, H. Zhang, and D. P. Jones, "Mitochondrial thioredoxin-2 has a key role in determining tumor necrosis

factor-alpha-induced reactive oxygen species generation, NF-kappaB activation, and apoptosis," *Toxicological Sciences: An Official Journal of the Society of Toxicology*, vol. 91, no. 2, pp. 643–650, 2006.

[20] S. A. Stroev, T. S. Gluschenko, E. I. Tjulkova et al., "Preconditioning enhances the expression of mitochondrial antioxidant thioredoxin-2 in the forebrain of rats exposed to severe hypobaric hypoxia," *Journal of Neuroscience Research*, vol. 78, no. 4, pp. 563–569, 2004.

[21] S. Boulos, B. P. Meloni, P. G. Arthur, C. Bojarski, and N. W. Knuckey, "Peroxiredoxin 2 overexpression protects cortical neuronal cultures from ischemic and oxidative injury but not glutamate excitotoxicity, whereas Cu/Zn superoxide dismutase 1 overexpression protects only against oxidative injury," *Journal of Neuroscience Research*, vol. 85, no. 14, pp. 3089–3097, 2007.

[22] L. Tian, H. Nie, Y. Zhang et al., "Recombinant human thioredoxin-1 promotes neurogenesis and facilitates cognitive recovery following cerebral ischemia in mice," *Neuropharmacology*, vol. 77, pp. 453–464, 2014.

[23] J. I. Romero, E. M. Hanschmann, M. Gellert et al., "Thioredoxin 1 and glutaredoxin 2 contribute to maintain the phenotype and integrity of neurons following perinatal asphyxia," *Biochimica et Biophysica Acta*, vol. 1850, no. 6, pp. 1274–1285, 2015.

[24] L. Brautigam, L. D. Schutte, J. R. Godoy et al., "Vertebrate-specific glutaredoxin is essential for brain development," *Proceedings of the National Academy of Sciences of the United States of America*, vol. 108, no. 51, pp. 20532–20537, 2011.

[25] F. Lopez-Aguilera, M. G. Plateo-Pignatari, V. Biaggio, C. Ayala, and A. M. Seltzer, "Hypoxic preconditioning induces an AT2-R/VEGFR-2(Flk-1) interaction in the neonatal brain microvasculature for neuroprotection," *Neuroscience*, vol. 216, pp. 1–9, 2012.

[26] M. Lundberg, C. Johansson, J. Chandra et al., "Cloning and expression of a novel human glutaredoxin (Grx2) with mitochondrial and nuclear isoforms," *The Journal of Biological Chemistry*, vol. 276, no. 28, pp. 26269–26275, 2001.

[27] J. E. Gilda and A. V. Gomes, "Stain-free total protein staining is a superior loading control to beta-actin for Western blots," *Analytical Biochemistry*, vol. 440, no. 2, pp. 186–188, 2013.

[28] A. Gurtler, N. Kunz, M. Gomolka et al., "Stain-free technology as a normalization tool in Western blot analysis," *Analytical Biochemistry*, vol. 433, no. 2, pp. 105–111, 2013.

[29] G. Paxinos and C. Watson, *The Rat Brain: In Stereotaxic Coordinates*, Academic Press, Cambridge, MA, USA, 1998.

[30] P. Kiss, D. Szogyi, D. Reglodi et al., "Effects of perinatal asphyxia on the neurobehavioral and retinal development of newborn rats," *Brain Research*, vol. 1255, pp. 42–50, 2009.

[31] A. Shahrokhi, G. Hassanzadeh, N. Vousooghi, M. T. Joghataei, S. Eftekhari, and M. R. Zarrindast, "The effect of tiagabine on physical development and neurological reflexes and their relationship with the gamma-aminobutyric acid switch in the rat cerebral cortex during developmental stages," *Behavioural Pharmacology*, vol. 24, no. 7, pp. 561–568, 2013.

[32] C. A. Giriko, C. A. Andreoli, L. V. Mennitti et al., "Delayed physical and neurobehavioral development and increased aggressive and depression-like behaviors in the rat offspring of dams fed a high-fat diet," *International Journal of Developmental Neuroscience: The Official Journal of the International Society for Developmental Neuroscience*, vol. 31, no. 8, pp. 731–739, 2013.

[33] B. Xu, A. J. Xiao, W. Chen et al., "Neuroprotective effects of a PSD-95 inhibitor in neonatal hypoxic-ischemic brain injury," *Molecular Neurobiology*, vol. 53, no. 9, pp. 5962–5970, 2016.

[34] X. Jiang, D. Mu, R. A. Sheldon, D. V. Glidden, and D. M. Ferriero, "Neonatal hypoxia-ischemia differentially upregulates MAGUKs and associated proteins in PSD-93-deficient mouse brain," *Stroke; a Journal of Cerebral Circulation*, vol. 34, no. 12, pp. 2958–2963, 2003.

[35] R. Sattler, Z. Xiong, W. Y. Lu, M. Hafner, J. F. MacDonald, and M. Tymianski, "Specific coupling of NMDA receptor activation to nitric oxide neurotoxicity by PSD-95 protein," *Science*, vol. 284, no. 5421, pp. 1845–1848, 1999.

[36] G. E. Saraceno, M. L. Bertolino, P. Galeano, J. I. Romero, L. M. Garcia-Segura, and F. Capani, "Estradiol therapy in adulthood reverses glial and neuronal alterations caused by perinatal asphyxia," *Experimental Neurology*, vol. 223, no. 2, pp. 615–622, 2010.

[37] J. M. Cho, Y. J. Shin, J. M. Park, J. Kim, and M. Y. Lee, "Characterization of nestin expression in astrocytes in the rat hippocampal CA1 region following transient forebrain ischemia," *Anatomy & Cell Biology*, vol. 46, no. 2, pp. 131–140, 2013.

[38] L. Gu, S. Kleiber, L. Schmid et al., "Long-term in vivo imaging of dendritic spines in the hippocampus reveals structural plasticity," *The Journal of Neuroscience: The Official Journal of the Society for Neuroscience*, vol. 34, no. 42, pp. 13948–13953, 2014.

[39] C. Fan, R. M. Zwacka, and J. F. Engelhardt, "Therapeutic approaches for ischemia/reperfusion injury in the liver," *Journal of Molecular Medicine*, vol. 77, no. 8, pp. 577–592, 1999.

[40] R. C. Vannucci and J. M. Perlman, "Interventions for perinatal hypoxic-ischemic encephalopathy," *Pediatrics*, vol. 100, no. 6, pp. 1004–1014, 1997.

[41] R. Berger and Y. Garnier, "Perinatal brain injury," *Journal of Perinatal Medicine*, vol. 28, no. 4, pp. 261–285, 2000.

[42] A. J. Gunn, "Cerebral hypothermia for prevention of brain injury following perinatal asphyxia," *Current Opinion in Pediatrics*, vol. 12, no. 2, pp. 111–115, 2000.

[43] S. Shankaran, "Neonatal encephalopathy: treatment with hypothermia," *Journal of Neurotrauma*, vol. 26, no. 3, pp. 437–443, 2009.

[44] P. O. Koh, "Proteomic analysis of focal cerebral ischemic injury in male rats," *The Journal of Veterinary Medical Science/the Japanese Society of Veterinary Science*, vol. 72, no. 2, pp. 181–185, 2010.

[45] D. Brea, R. Rodriguez-Gonzalez, T. Sobrino, M. Rodriguez-Yanez, M. Blanco, and J. Castillo, "Proteomic analysis shows differential protein expression in endothelial progenitor cells between healthy subjects and ischemic stroke patients," *Neurological Research*, vol. 33, no. 10, pp. 1057–1063, 2011.

[46] J. Rashidian, M. W. Rousseaux, K. Venderova et al., "Essential role of cytoplasmic cdk5 and Prx2 in multiple ischemic injury models, in vivo," *The Journal of Neuroscience: The Official Journal of the Society for Neuroscience*, vol. 29, no. 40, pp. 12497–12505, 2009.

[47] N. Fatma, E. Kubo, M. Sen et al., "Peroxiredoxin 6 delivery attenuates TNF-alpha-and glutamate-induced retinal ganglion cell death by limiting ROS levels and maintaining Ca2+ homeostasis," *Brain Research*, vol. 1233, pp. 63–78, 2008.

[48] E. M. Hanschmann, M. E. Lonn, L. D. Schutte et al., "Both thioredoxin 2 and glutaredoxin 2 contribute to the reduction

of the mitochondrial 2-Cys peroxiredoxin Prx3," *The Journal of Biological Chemistry*, vol. 285, no. 52, pp. 40699–40705, 2010.

[49] I. K. Hwang, K. Y. Yoo, D. W. Kim et al., "Changes in the expression of mitochondrial peroxiredoxin and thioredoxin in neurons and glia and their protective effects in experimental cerebral ischemic damage," *Free Radical Biology & Medicine*, vol. 48, no. 9, pp. 1242–1251, 2010.

[50] T. S. Nowak Jr., "Protein synthesis and the heart shock/stress response after ischemia," *Cerebrovascular and Brain Metabolism Reviews*, vol. 2, no. 4, pp. 345–366, 1990.

[51] F. R. Sharp, S. M. Massa, and R. A. Swanson, "Heat-shock protein protection," *Trends in Neurosciences*, vol. 22, no. 3, pp. 97–99, 1999.

[52] F. R. Sharp, D. Lowenstein, R. Simon, and K. Hisanaga, "Heat shock protein hsp72 induction in cortical and striatal astrocytes and neurons following infarction," *Journal of Cerebral Blood Flow and Metabolism: Official Journal of the International Society of Cerebral Blood Flow and Metabolism*, vol. 11, no. 4, pp. 621–627, 1991.

[53] Y. Li, M. Chopp, J. H. Garcia, Y. Yoshida, Z. G. Zhang, and S. R. Levine, "Distribution of the 72-kd heat-shock protein as a function of transient focal cerebral ischemia in rats," *Stroke; a Journal of Cerebral Circulation*, vol. 23, no. 9, pp. 1292–1298, 1992.

[54] L. L. Blazer and R. R. Neubig, "Small molecule protein-protein interaction inhibitors as CNS therapeutic agents: current progress and future hurdles," *Neuropsychopharmacology: Official Publication of the American College of Neuropsychopharmacology*, vol. 34, no. 1, pp. 126–141, 2009.

[55] K. S. Christopherson, B. J. Hillier, W. A. Lim, and D. S. Bredt, "PSD-95 assembles a ternary complex with the N-methyl-D-aspartic acid receptor and a bivalent neuronal NO synthase PDZ domain," *The Journal of Biological Chemistry*, vol. 274, no. 39, pp. 27467–27473, 1999.

[56] V. L. Dawson, T. M. Dawson, E. D. London, D. S. Bredt, and S. H. Snyder, "Nitric oxide mediates glutamate neurotoxicity in primary cortical cultures," *Proceedings of the National Academy of Sciences of the United States of America*, vol. 88, no. 14, pp. 6368–6371, 1991.

[57] Z. Huang, P. L. Huang, N. Panahian, T. Dalkara, M. C. Fishman, and M. A. Moskowitz, "Effects of cerebral ischemia in mice deficient in neuronal nitric oxide synthase," *Science*, vol. 265, no. 5180, pp. 1883–1885, 1994.

[58] M. Aarts, Y. Liu, L. Liu et al., "Treatment of ischemic brain damage by perturbing NMDA receptor- PSD-95 protein interactions," *Science*, vol. 298, no. 5594, pp. 846–850, 2002.

[59] F. X. Soriano, M. A. Martel, S. Papadia et al., "Specific targeting of pro-death NMDA receptor signals with differing reliance on the NR2B PDZ ligand," *The Journal of Neuroscience: The Official Journal of the Society for Neuroscience*, vol. 28, no. 42, pp. 10696–10710, 2008.

[60] M. Tymianski, "Emerging mechanisms of disrupted cellular signaling in brain ischemia," *Nature Neuroscience*, vol. 14, no. 11, pp. 1369–1373, 2011.

[61] H. Cui, A. Hayashi, H. S. Sun et al., "PDZ protein interactions underlying NMDA receptor-mediated excitotoxicity and neuroprotection by PSD-95 inhibitors," *The Journal of Neuroscience: The Official Journal of the Society for Neuroscience*, vol. 27, no. 37, pp. 9901–9915, 2007.

[62] N. Norgren, L. Rosengren, and T. Stigbrand, "Elevated neurofilament levels in neurological diseases," *Brain Research*, vol. 987, no. 1, pp. 25–31, 2003.

[63] P. N. Hoffman, D. W. Cleveland, J. W. Griffin, P. W. Landes, N. J. Cowan, and D. L. Price, "Neurofilament gene expression: a major determinant of axonal caliber," *Proceedings of the National Academy of Sciences of the United States of America*, vol. 84, no. 10, pp. 3472–3476, 1987.

[64] N. Geisler and K. Weber, "Self-assembly in vitro of the 68,000 molecular weight component of the mammalian neurofilament triplet proteins into intermediate-sized filaments," *Journal of Molecular Biology*, vol. 151, no. 3, pp. 565–571, 1981.

[65] K. Weber, G. Shaw, M. Osborn, E. Debus, and N. Geisler, "Neurofilaments, a subclass of intermediate filaments: structure and expression," *Cold Spring Harbor Symposia on Quantitative Biology*, vol. 48, Part 2, pp. 717–729, 1983.

[66] M. K. Lee, Z. Xu, P. C. Wong, and D. W. Cleveland, "Neurofilaments are obligate heteropolymers in vivo," *The Journal of Cell Biology*, vol. 122, no. 6, pp. 1337–1350, 1993.

[67] J. Gaiottino, N. Norgren, R. Dobson et al., "Increased neurofilament light chain blood levels in neurodegenerative neurological diseases," *PloS One*, vol. 8, no. 9, article e75091, 2013.

[68] L. Robelin and J. L. Gonzalez De Aguilar, "Blood biomarkers for amyotrophic lateral sclerosis: myth or reality?" *BioMed Research International*, vol. 2014, Article ID 525097, 11 pages, 2014.

[69] L. E. Rosengren, J. E. Karlsson, J. O. Karlsson, L. I. Persson, and C. Wikkelso, "Patients with amyotrophic lateral sclerosis and other neurodegenerative diseases have increased levels of neurofilament protein in CSF," *Journal of Neurochemistry*, vol. 67, no. 5, pp. 2013–2018, 1996.

[70] J. Sellner, A. Patel, P. Dassan, M. M. Brown, and A. Petzold, "Hyperacute detection of neurofilament heavy chain in serum following stroke: a transient sign," *Neurochemical Research*, vol. 36, no. 12, pp. 2287–2291, 2011.

[71] M. Douglas-Escobar, C. Yang, J. Bennett et al., "A pilot study of novel biomarkers in neonates with hypoxic-ischemic encephalopathy," *Pediatric Research*, vol. 68, no. 6, pp. 531–536, 2010.

[72] P. Singh, J. Yan, R. Hull et al., "Levels of phosphorylated axonal neurofilament subunit H (pNfH) are increased in acute ischemic stroke," *Journal of the Neurological Sciences*, vol. 304, no. 1, pp. 117–121, 2011.

[73] C. Hjalmarsson, M. Bjerke, B. Andersson et al., "Neuronal and glia-related biomarkers in cerebrospinal fluid of patients with acute ischemic stroke," *Journal of Central Nervous System Disease*, vol. 6, pp. 51–58, 2014.

[74] Y. Kitaoka, M. Tanito, K. Kojima et al., "Axonal protection by thioredoxin-1 with inhibition of interleukin-1beta in TNF-induced optic nerve degeneration," *Experimental eye Research*, vol. 152, pp. 71–76, 2016.

[75] Y. Kitaoka, Y. Munemasa, Y. Hayashi et al., "Axonal protection by 17beta-estradiol through thioredoxin-1 in tumor necrosis factor-induced optic neuropathy," *Endocrinology*, vol. 152, no. 7, pp. 2775–2785, 2011.

[76] D. Tonge, K. Chan, N. Zhu et al., "Enhancement of axonal regeneration by in vitro conditioning and its inhibition by cyclopentenone prostaglandins," *Journal of Cell Science*, vol. 121, no. 15, pp. 2565–2577, 2008.

[77] M. Pekny and M. Nilsson, "Astrocyte activation and reactive gliosis," *Glia*, vol. 50, no. 4, pp. 427–434, 2005.

[78] L. F. Eng and R. S. Ghirnikar, "GFAP and astrogliosis," *Brain Pathology*, vol. 4, no. 3, pp. 229–237, 1994.

[79] M. Pekny and M. Pekna, "Astrocyte reactivity and reactive astrogliosis: costs and benefits," *Physiological Reviews*, vol. 94, no. 4, pp. 1077–1098, 2014.

[80] J. Romero, J. Muniz, T. Logica Tornatore et al., "Dual role of astrocytes in perinatal asphyxia injury and neuroprotection," *Neuroscience Letters*, vol. 565, pp. 42–46, 2014.

[81] G. Horvath, D. Reglodi, G. Vadasz, J. Farkas, and P. Kiss, "Exposure to enriched environment decreases neurobehavioral deficits induced by neonatal glutamate toxicity," *International Journal of Molecular Sciences*, vol. 14, no. 9, pp. 19054–19066, 2013.

[82] P. Kiss, A. Tamas, A. Lubics et al., "Development of neurological reflexes and motor coordination in rats neonatally treated with monosodium glutamate," *Neurotoxicity Research*, vol. 8, no. 3-4, pp. 235–244, 2005.

[83] J. Farkas, D. Reglodi, B. Gaszner et al., "Effects of maternal separation on the neurobehavioral development of newborn Wistar rats," *Brain Research Bulletin*, vol. 79, no. 3, pp. 208–214, 2009.

[84] A. Lubics, D. Reglodi, A. Tamas et al., "Neurological reflexes and early motor behavior in rats subjected to neonatal hypoxic-ischemic injury," *Behavioural Brain Research*, vol. 157, no. 1, pp. 157–165, 2005.

[85] P. Kiss, D. Hauser, A. Tamas et al., "Changes in open-field activity and novelty-seeking behavior in periadolescent rats neonatally treated with monosodium glutamate," *Neurotoxicity Research*, vol. 12, no. 2, pp. 85–93, 2007.

[86] V. Chaparro-Huerta, M. C. Rivera-Cervantes, B. M. Torres-Mendoza, and C. Beas-Zarate, "Neuronal death and tumor necrosis factor-alpha response to glutamate-induced excitotoxicity in the cerebral cortex of neonatal rats," *Neuroscience Letters*, vol. 333, no. 2, pp. 95–98, 2002.

[87] C. Beas-Zarate, M. Perez-Vega, and I. Gonzalez-Burgos, "Neonatal exposure to monosodium L-glutamate induces loss of neurons and cytoarchitectural alterations in hippocampal CA1 pyramidal neurons of adult rats," *Brain Research*, vol. 952, no. 2, pp. 275–281, 2002.

[88] A. Tamas, R. Gabriel, B. Racz et al., "Effects of pituitary adenylate cyclase activating polypeptide in retinal degeneration induced by monosodium-glutamate," *Neuroscience Letters*, vol. 372, no. 1, pp. 110–113, 2004.

[89] A. Holmgren, C. Johansson, C. Berndt, M. E. Lonn, C. Hudemann, and C. H. Lillig, "Thiol redox control via thioredoxin and glutaredoxin systems," *Biochemical Society Transactions*, vol. 33, no. 6, pp. 1375–1377, 2005.

[90] H. Nakamura, "Extracellular functions of thioredoxin," *Novartis Foundation Symposium*, vol. 291, pp. 184–192, 2008, discussion 192-185, 221-184.

[91] H. Nakamura, Y. Hoshino, H. Okuyama, Y. Matsuo, and J. Yodoi, "Thioredoxin 1 delivery as new therapeutics," *Advanced Drug Delivery Reviews*, vol. 61, no. 4, pp. 303–309, 2009.

[92] J. Zhang, F. Chen, T. Nakamura et al., "Protective effect of thioredoxin perfusion but not inhalation in warm ischemic-reperfused rat lungs," *Redox Report: Communications in Free Radical Research*, vol. 14, no. 2, pp. 75–81, 2009.

[93] Y. Inomata, H. Nakamura, M. Tanito et al., "Thioredoxin inhibits NMDA-induced neurotoxicity in the rat retina," *Journal of Neurochemistry*, vol. 98, no. 2, pp. 372–385, 2006.

[94] L. Arodin, A. Miranda-Vizuete, P. Swoboda, and A. P. Fernandes, "Protective effects of the thioredoxin and glutaredoxin systems in dopamine-induced cell death," *Free Radical Biology & Medicine*, vol. 73, pp. 328–336, 2014.

[95] D. Daily, A. Vlamis-Gardikas, D. Offen et al., "Glutaredoxin protects cerebellar granule neurons from dopamine-induced apoptosis by activating NF-kappa B via Ref-1," *The Journal of Biological Chemistry*, vol. 276, no. 2, pp. 1335–1344, 2001.

[96] E. V. Kalinina, N. N. Chernov, and A. N. Saprin, "Involvement of thio-, peroxi-, and glutaredoxins in cellular redox-dependent processes," *Biochemistry. Biokhimiia*, vol. 73, no. 13, pp. 1493–1510, 2008.

[97] J. H. Bushweller, M. Billeter, A. Holmgren, and K. Wuthrich, "The nuclear magnetic resonance solution structure of the mixed disulfide between *Escherichia coli* glutaredoxin(C14S) and glutathione," *Journal of Molecular Biology*, vol. 235, no. 5, pp. 1585–1597, 1994.

[98] K. Nordstrand, F. Åslund, A. Holmgren, G. Otting, and K. D. Berndt, "NMR structure of *Escherichia coli* glutaredoxin 3-glutathione mixed disulfide complex: implications for the enzymatic mechanism," *Journal of Molecular Biology*, vol. 286, no. 2, pp. 541–552, 1999.

[99] D. Daily, A. Vlamis-Gardikas, D. Offen et al., "Glutaredoxin protects cerebellar granule neurons from dopamine-induced apoptosis by dual activation of the ras-phosphoinositide 3-kinase and jun n-terminal kinase pathways," *The Journal of Biological Chemistry*, vol. 276, no. 24, pp. 21618–21626, 2001.

[100] P. Klatt, E. P. Molina, M. G. De Lacoba et al., "Redox regulation of c-Jun DNA binding by reversible S-glutathiolation," *FASEB Journal: Official Publication of the Federation of American Societies for Experimental Biology*, vol. 13, no. 12, pp. 1481–1490, 1999.

[101] S. A. Gravina and J. J. Mieyal, "Thioltransferase is a specific glutathionyl mixed disulfide oxidoreductase," *Biochemistry*, vol. 32, no. 13, pp. 3368–3376, 1993.

[102] S. Yoshitake, H. Nanri, M. R. Fernando, and S. Minakami, "Possible differences in the regenerative roles played by thioltransferase and thioredoxin for oxidatively damaged proteins," *Journal of Biochemistry*, vol. 116, no. 1, pp. 42–46, 1994.

[103] C. H. Lillig, M. E. Lonn, M. Enoksson, A. P. Fernandes, and A. Holmgren, "Short interfering RNA-mediated silencing of glutaredoxin 2 increases the sensitivity of HeLa cells toward doxorubicin and phenylarsine oxide," *Proceedings of the National Academy of Sciences of the United States of America*, vol. 101, no. 36, pp. 13227–13232, 2004.

[104] M. Enoksson, A. P. Fernandes, S. Prast, C. H. Lillig, A. Holmgren, and S. Orrenius, "Overexpression of glutaredoxin 2 attenuates apoptosis by preventing cytochrome c release," *Biochemical and Biophysical Research Communications*, vol. 327, no. 3, pp. 774–779, 2005.

[105] T. Sasada, S. Iwata, N. Sato et al., "Redox control of resistance to cis-diamminedichloroplatinum (II) (CDDP): protective effect of human thioredoxin against CDDP-induced cytotoxicity," *The Journal of Clinical Investigation*, vol. 97, no. 10, pp. 2268–2276, 1996.

[106] T. Andoh, P. B. Chock, and C. C. Chiueh, "The roles of thioredoxin in protection against oxidative stress-induced apoptosis in SH-SY5Y cells," *The Journal of Biological Chemistry*, vol. 277, no. 12, pp. 9655–9660, 2002.

[107] Y. Gon, T. Sasada, M. Matsui et al., "Expression of thioredoxin in bleomycin-injured airway epithelium: possible role of protection against bleomycin induced epithelial injury," *Life Sciences*, vol. 68, no. 16, pp. 1877–1888, 2001.

[108] K. Shioji, C. Kishimoto, H. Nakamura et al., "Overexpression of thioredoxin-1 in transgenic mice attenuates adriamycin-induced cardiotoxicity," *Circulation*, vol. 106, no. 11, pp. 1403–1409, 2002.

[109] T. Tanaka, H. Nakamura, A. Nishiyama et al., "Redox regulation by thioredoxin superfamily; protection against oxidative stress and aging," *Free Radical Research*, vol. 33, no. 6, pp. 851–855, 2000.

Hindawi
Oxidative Medicine and Cellular Longevity
Volume 2017, Article ID 7150376, 17 pages
https://doi.org/10.1155/2017/7150376

*Research Article*

# Novel Therapeutic Effects of Leonurine On Ischemic Stroke: New Mechanisms of BBB Integrity

**Qiu-Yan Zhang,[1,2] Zhi-Jun Wang,[1,2] De-Miao Sun,[2] Ying Wang,[1] Peng Xu,[1] Wei-Jun Wu,[1] Xin-Hua Liu,[1] and Yi-Zhun Zhu[1,2]**

[1]*Department of Pharmacology, School of Pharmacy and Institute of Biomedical Science, Fudan University, Shanghai, China*
[2]*Department of Pharmacology, School of Pharmacy, Macau University of Science & Technology, Macau*

Correspondence should be addressed to Yi-Zhun Zhu; yzzhu@must.edu.mo

Received 7 January 2017; Revised 10 April 2017; Accepted 16 April 2017; Published 13 June 2017

Academic Editor: Margherita Neri



Stroke is a leading cause of morbidity and mortality globally. Leonurine (also named SCM-198), a compound extracted from *Herba leonuri*, was effective on the prevention of various cardiovascular and brain diseases. The purpose of this study was to explore the possible therapeutic potential of SCM-198 against ischemia reperfusion injury and underlying mechanisms. In the in vivo transient middle cerebral artery occlusion (tMCAO) rat model, we found that treatment with SCM-198 could decrease infarct volume and improve neurological deficit by protecting against blood-brain barrier (BBB) breakdown. In the in vitro model of cell oxygen-glucose deprivation and reoxygenation (OGD/R), consistent results were obtained with decreased reactive oxygen species (ROS) production and maintained the BBB integrity. Further study demonstrated that SCM-198 increased the expression of histone deacetylase- (HDAC-) 4 which could inhibit NADPH oxidase- (NOX-) 4 and matrix metalloproteinase- (MMP-) 9 expression, resulting in the elevation of tight junction proteins, including claudin-5, occludin, and zonula occluden- (ZO-) 1. These results indicated SCM-198 protected BBB integrity by regulating the HDAC4/NOX4/MMP-9 tight junction pathway. Our findings provided novel insights into the protective effects and mechanisms of SCM-198 on ischemic stroke, indicating SCM-198 as a new class of potential drug against acute onset of ischemic stroke.

## 1. Introduction

Stroke is a main cause of morbidity and mortality throughout the world. In the clinic, stroke is divided into two forms: ischemic stroke which accounts for ~85% and hemorrhagic stroke, including intracerebral (~10%) and subarachnoidal (~3%) bleedings [1]. Ischemic stroke is mainly caused by blockage of the blood vessels, while hemorrhagic stroke by rupture of blood vessels. Currently, tissue-type plasminogen activator (tPA) serves as the priority remedy for ischemic stroke, from which only about 10% patients are suitable for this therapy. In addition, concerns have been raised regarding its limited therapeutic time window and safety issue, which result in less than 5% of clinical efficiency in patients [1, 2]. Meanwhile, the secondary damage caused by reperfusion will bring worse results, such as blood-brain barrier (BBB) breakdown, inflammation, and postischemic neuronal injury [1].

The BBB is composed of three main elements: brain microvessel endothelium, astrocyte endfeet, and pericytes, forming neurovascular unit (NVU). BBB was damaged in early critical event in ischemia-reperfusion (I/R) which causes the edema formation, inflammatory cascade, and ultimately serious outcomes [3]. BBB dysfunction is a peculiar character of many neurological conditions, for instance, ischemic and hemorrhagic stroke, multiple sclerosis, and brain tumours [4]. Currently, many researchers focus on neurons and brain parenchyma, whereas straight BBB protection has attracted little attention. The results show that early BBB disruption is the cause rather than the result of parenchymal cell injury [5]. Mounting evidences have suggested that brain microvessel endothelium cells (BMECs)

are the basis of BBB which form a barrier that restricts diffusion of blood-borne solutes. BMECs play a central role in maintaining the BBB integrity by tight junctional proteins (TJs) and caveolin-1 (Cav1)—mediated trans-endothelia vesicular transport [6–9]. TJs contain occludin, claudins, junctional adhesion molecules (JAM), and cytoplasm accessory zonula occluden (ZO) proteins. Among them, occludin, claudin-5, and ZO-1 are widely investigated and considered as essential factors for BBB integrity. Occludin and claudin-5 are the transmembrane proteins which are responsible for fence function and paracellular size selectivity, respectively, while ZO-1 is in charge of anchoring them to the actin cytoskeleton [10]. Following subjected to transient middle cerebral artery occlusion (tMCAO) or oxygen-glucose deprivation and reoxygenation (OGD/R), loss of BMECs evoked stress fibre formation and TJ redistribution resulted in shrinked cell morphology, enhancing permeability of BBB. Targeting the BMEC structural changes could prevent BBB insult and secondary tissue injury [6]. As to Cav1, a recent study revealed that transcellular mechanisms mediated by Cav1 do not exert a predominant role up to 24 h after ischemia induced BBB breakdown [9]. So we chose bEnd.3 (brain microvascular endothelial cell line) in our experiment. And we determined the effect of SCM-198 on BBB integrity by TJs.

Recently, a lot of attention has been focused on Leonurine which also named SCM-198. As we know, SCM-198 is a unique single compound existed only in *Herba leonuri*, which is widely used in gynecology. Previous research suggested SCM-198 could improve antioxidant capacity of myocardium, promote angiogenesis in ischemic myocardium, and ameliorate endothelial dysfunction caused by hyperlipidemia [11, 12]. SCM-198 was surprisingly found to be effective in permanent MCAO stroke models via modulating mitochondrial functions [13], which prompted us to further explore its possible therapeutic potential in more dangerous tMCAO models. Therefore, we investigated the protective effects of SCM-198 in both tMCAO rat model and OGD/R cell model. Furthermore, we addressed new mechanisms that contribute to the protective effects of SCM-198 and whether they occur via maintaining BBB functioning and permeability.

## 2. Materials and Methods

*2.1. Materials.* Antibodies were obtained from the following commercial sources: Matrix metalloproteinase- (MMP-) 9 and histone deacetylase- (HDAC-) 4 (Cell Signaling Technology), claudin-5 and ZO-1 (Invitrogen), occludin, the nicotinamide adenine dinucleotide phosphate oxidase- (NOX-) 4, and GAPDH (Proteintech), and rhodamine phalloidin was obtained from Cytoskeleton. GKT137831 and Tasquinimod (Taq) was from selleck. Lactate dehydrogenase (LDH) activity assay kit was bought from Beyotime Institute of Biotechnology. Cell counting kit 8 (CCK8) was from Dojindo. 2,3,5-Triphenyltetrazolium chloride (TTC), 2′,7′-dichlorofluorescin diacetate (DCFH-DA), diphenyleneiodonium (DPI), fluorescein isothiocyanate- (FITC-) labeled dextran, and other chemical reagents were from Sigma-Aldrich.

*2.2. Animal Treatment and Model.* The experiment protocol was approved by the institutional ethical committee with internationally accepted ethical standards. All protocols and animal handling were performed in accordance under the guidelines of National Institutes of Health Guide for the Care and Use of Laboratory Animals. Hundred male Sprague-Dawley (SD) rats were supplied by the Laboratory Animal Center, Fudan University. Rats weighing 180–220 g were housed with food and water ad libitum under diurnal lighting condition. Rats were anaesthetized with chloral hydrate (300 mg/kg, intraperitoneally) as our standard protocol.

Briefly, we performed the surgery as described previously [14]. 90 minutes later, we withdrew the filament to cause the reperfusion injury. At different time point of MCAO and reperfusion, occlusion was confirmed by laser Doppler imaging system (Moor Instruments, USA) to monitor cerebral blood flow (CBF).

All the animals mentioned above were randomly divided into five groups: control operation group, tMCAO group treated with saline, vehicle group with Edaravone (3 mg/kg/day) for tMCAO [15], and treatment groups which were posttreated (0.5 h and 2 h after operation) with SCM-198 (15 mg/kg/day in normal saline). All the drugs were given intravenous injection once daily for 3 days.

*2.3. Measurement of Infarct Volume and Brain Swelling after Ischemia-Reperfusion.* The TTC staining assay is one of the most common methods to measure infarct volume which was measured as previously described [16]. At the third day after I/R, animals were anesthetized with chloral hydrate (300 mg/kg, i.p.) and decapitated. Rat brains were immediately removed and then dissected into 2 mm-thick coronal slices using a brain slice matrix. Then the slices were stained with TTC solution (1% TTC in PBS) at 37°C for 15 min then photographed. Infarct sizes were quantified using ImageJ software. The relative infarction volume percentage (RIVP) was calculated as following equation: $\text{RIVP} = \text{IVA}/\text{TA} \times 100\%$, where IVA and TA were infarcted area and total area of the coronal sections, respectively.

The cerebral edema volume was also measured. Edema volume = ([volume of ipsilateral hemisphere − volume of contralateral hemisphere]/volume of contralateral hemisphere) × 100% [17].

*2.4. Behavioral Evaluation.* To evaluate neuronal function impairment after ischemic stroke insult, a neurological deficit grading system with a scale of zero to 5 was carried out on all of the animals as described previously [18].

*2.5. Brain Water Content.* Three days after tMCAO, rats were anesthetized by 10% chloral hydrate. The brains were removed and separated into contralateral and ipsilateral hemisphere. The wet weight of ipsilateral hemisphere was recorded immediately. After dried at 50°C for 48 hours, the dry weight of these samples were obtained by an electronic analytical balance. The formula for calculating brain

water content (BWC) was as follows: (wet weight − dry weight)/wet weight × 100% [19].

*2.6. Evaluation of Blood-Brain Barrier Integrity.* The effect of SCM-198 on BBB permeability was assessed by Evans blue (EB) test [20]. EB dye (80 mg/kg) in phosphate-buffered saline (PBS; pH 7.4) was injected into tail vein and allowed to circulate for 24 h. Then rats were anesthetized with chloral hydrate, and transcardially perfused with PBS, the brains were removed and divided into the right and left hemispheres. The left hemispheres were weighed and placed in 50% trichloroacetic acid solution to precipitate protein. The supernatant was diluted 4-fold with ethanol. The EB dye was measured by a microplate fluorescence reader (excitation 620 nm, emission 680 nm). We also measured the cerebral edema volume. Edema volume = ([volume of ipsilateral hemisphere − volume of contralateral hemisphere]/volume of contralateral hemisphere) × 100% [21].

*2.7. bEnd.3 Cell Culture and Treatment.* Mouse bEnd.3 cell was bought from American Type Culture Collection (ATCC). Cells were cultured with Dulbecco's modified Eagle medium (DMEM, Hyclone, USA), supplemented with 10% fetal bovine serum (FBS, Hyclone, USA) and 100 $\mu$g/ml penicillin/streptomycin (Gibco), and cultured at 37°C containing 5% $CO_2$ and 95% $O_2$. All the cells used in the experiments were performed from passages 2 to 10.

To mimic ischemic-like conditions in vitro, bEnd.3 cells were exposed to OGD as we described previously [22]. In brief, the cells were washed with PBS three times then replaced with serum- and glucose-free medium (Invitrogen). The cells were placed in a Biospherix incubator chamber (ProOx C21, USA), which was flushed with 95% $N_2$ and 5% $CO_2$ for 6 h then transferred to 95% air, 5% $CO_2$, and continued to be cultured in glucose-containing medium for 4 h each time. Control cells were cultured with norm-oxygenated and glucose-containing medium for the same period of time in normal condition. The cells were divided into five groups: control, OGD, and cells treated with SCM-198 (0.1 $\mu$M, 1 $\mu$M, and 10 $\mu$M) 2 h before OGD. The inhibitors were added 1 h before OGD until the end of the experiment.

*2.8. Cellular Viability.* Cell viability was determined using the CCK8 assay in accordance with the manufacturer's instructions [23]. In briefly, cells were seeded into 96-well plate at a density of $1.0 \times 10^4$ cells/well and cultured for 24 h, and then 10 $\mu$l CCK-8 solution was added to each well after reperfusion and incubated for 1 h. The absorbance was measured at 450 nm for each well using a multiwell spectrophotometer. The experiment was performed in triplicate.

*2.9. Lactate Dehydrogenase Assay.* LDH activity was detected using a LDH activity assay kit according to the manufacturer's instructions [24]. Absorbance values were measured at 490 nm with a reference wavelength of 655 nm, using a 96-well microplate reader (Tecan Systems Inc., Oberdiessbach, Switzerland). The experiment was repeated at least three times.

*2.10. Reactive Oxygen Species Measurement.* The amount of intracellular ROS was measured by the change of fluorescence resulting from oxidation of DCFH-DA, a membrane-permeable fluorescent probe [23]. After treated with SCM-198 for 2 h and OGD/R injury, cells were washed in PBS and incubated with 10 $\mu$M of DCFH-DA for 30 min at 37°C in the dark. The cells were washed with serum-free DMEM to remove the free molecules of the dye. The fluorescence of intracellular ROS was detected by both fluorescence microscopy (Zeiss, Oberkochen, Germany) and microplate reader (TecanSystems Inc., Oberdiessbach, Switzerland).

*2.11. Measurement of BBB Permeability In Vitro.* Then we tested the putative function of SCM-198 in regulating the in vitro BBB permeability as previously described [25]. The bEnd.3 cells were seeded on 24-well transwell polycarbonate insert filters (diameter: 24 mm; pore size: 3 $\mu$m; BD, USA) at a confluent density of $2 \times 10^5$ cells/cm$^2$ and incubated for 2 days. At 1 h before the end of the reoxygen period, solutions of FITC-labeled dextran solution were added to the apical chamber. The fluorescence intensity of FITC-dextran was detected at the excitation wavelength of 485 nm and the emission wavelength of 520 nm with a microplate reader (Tecan Systems Inc., Oberdiessbach, Switzerland). All samples were performed in triplicate.

*2.12. Lentivirus Production and Transduction.* Lentiviral plasmids and packaging plasmids were cotransfected into HEK293 cells to generate lentivirus by lipofectamine 2000 (Life Technologies) according to the manufacturer's instructions. The recombinant virus-containing medium was collected 72 h after transfection, and then the media was centrifuged at 5000$g$ for 30 min to remove cell debris; at last, the supernatants were concentrated by PEG-it virus precipitation solution (SBI, USA) to obtain virus particles. After the bEnd.3 cells reached 60–70% confluence, the abovementioned lentiviral particles were used to transducer at a multiplicity of infection (MOI) of 50. The cells were used for the next experiment until at least 80%. The overexpression of adenovirus of HDAC4 was obtained from Gene Pharma (Shanghai, China). The efficiency of transduction was evaluated by the rate of GFP-positive cell number counted under a fluorescent microscope (Leica, Wetzlar, Germany).

*2.13. Western Blot.* Western blot analyses were performed as previously described [11]. The frozen tissues were cut into small pieces and homogenized in RIPA buffer and then centrifuged at 12,000$g$ for 10 min at 4°C to separate soluble from insoluble fractions. Equal amounts of proteins for each group mixed with loading buffer were separated by 10% SDS-polyacrylamine gel and transferred to nitrocellulose filter membranes.

Each membrane was incubated with specific antibodies as follows: MMP-9, ZO-1, occludin, claudin-5, HDAC4, NOX4, and GAPDH. Immunoreactive proteins were visualized using the ECL western blotting detection kit (Thermo Fisher Scientific Inc., Boston, USA), according to the manufacturer's instructions. To measure the expression of each

protein, the relative intensity was calculated by comparing with the intensity of GAPDH using densitometry (Bio-Rad, USA).

*2.14. Real-Time RT-PCR.* The total RNA was isolated from the brain cortex and striatum using TRIzol Reagent (Takara, Japan) as described in the manufacturer's instructions. After quantifying the amount of extracted total RNA, 500 ng template RNA was reversely transcribed to single-stranded cDNA with a Prime Script 1st strand cDNA synthesis kit (Takara, Japan) according to the manufacturer. Real-time PCR was performed on a BIO-RA- D IQ5 system (Bio-Rad, USA). The relative differences in gene expression between groups were expressed using cycle time (Ct) values. Briefly, the Ct values of the interested genes were first normalized with GAPDH of the same sample and then the relative differences between control and treatment groups. The primer sequences that were used in the real-time PCR analyses were provided in Supplementary Table 1 available online at https://doi.org/10.1155/2017/7150376.

*2.15. Immunofluorescent Staining.* Immunofluorescence was assessed as described earlier [26]. Following reoxygenation for 4 h, cells were washed with PBS and fixed in 4% paraformaldehyde for 30 min at room temperature, then washed with PBS 3 times. After permeabilizing with 0.1% Triton X-100, cells were blocked with 3% BSA for 30 min. Subsequently, the cells were incubated at 4°C overnight with the primary antibodies as follows: ZO-1 and occludin. After washing off the primary antibodies, the cells were incubated with Alexa Fluor 488- or 568-conjugated secondary antibodies (1 : 500, Thermo Fisher Scientific) at room temperature for 1 h. Following three times of PBS washes, the cell nuclei were stained using 4′,6-diamidino-2-phenylindole (DAPI, Beyotime).

To stain the F-actin stress fibres, cells were exposed to rhodamine phalloidin (1 : 50, Cytoskeleton) for 20 min, DAPI for staining the nuclei. Fluorescence staining was viewed with a laser scanning confocal microscope (Zeiss, Oberkochen, Germany).

*2.16. Statistical Analysis.* GraphPad Prism 5.0 software was used for analysis. Every two groups were compared by 1-way ANOVA with Tukey's post hoc test for $P$ values. The Mann–Whitney $U$ test was used for the statistical analysis of neurological deficits. All values are expressed as mean ± SEM. Values of $p < 0.05$ were considered to state statistical significance.

## 3. Results

*3.1. SCM-198 Ameliorated Ischemia-Reperfusion Injury.* To test the therapeutical effect of SCM-198 on I/R, rats were subjected to 90 min of ischemia followed by 72 h of reperfusion. We set three time points to determine the therapeutic window: treatment at 0.5, 2, and 6 h postreperfusion. The brain infarct size was examined by TTC staining (Figure 1(a)), and we found that I/R markedly increased the infarct volume approximately up to 38.00 ± 8.10%, while postinjection of SCM-198 could significantly decrease the infarct volume ($F$ (4, 31) = 35.04, $P < 0.0001$, Figure 1 (b)), notably at 0.5 h after reperfusion which was 13.13 ± 4.42%. SCM-198 revealed better protective effect against infarct volume than Edaravone which decreased the infarct volume only to 20.14 ± 8.86%. As neurological deficit caused by ischemia stroke is another big consequence, we observed and scored the behavior at 24, 48, and 72 h postsurgery. Compared with the tMCAO group, the neurological scores of treatment with SCM-198 and edaravone were significantly decreased at corresponding day (Figures 1(c)–1(e)). Moreover, we explored that treatment with SCM-198 at 0.5 h after surgery had the best effect. We also examined 6 h treatment after I/R, but there was no evident effect (data not shown). From the above results, we could safely conclude that SCM-198 improved neurological deficit, as well as decreased infarct volume.

*3.2. The Effect of SCM-198 on BBB Breakdown.* We know that stroke develops various damages to BBB integrity leading to the swell of brain tissue. Therefore, protection of BBB function can be a crucial aspect for reducing ischemic injury. To confirm the further mechanism of SCM-198 on stroke, we decided to focus on the protective effect against BBB breakdown. EB dye is always used as a marker of albumin effluxion to evaluate BBB permeability. EB can easily permeate the BBB after brain insult by I/R. We used EB to detect whether SCM-198 could maintain the intact BBB. Representative photos of EB dye in rat brain tissues are shown in Figure 1(f). We compared EB leakage in the ipsilateral hemisphere among all groups. SCM-198 could drastically reduce EB leakage when compared with the tMCAO group (Figure 1(f)). Treatment with SCM-198 at 2 h and 0.5 h after ischemic stroke markedly diminished EB leakage (Figure 1(f)). The quantitative analysis of EB leakage after I/R is shown in Figure 1(g) ($F$ (3, 39) = 59.33, $P < 0.0001$). Correspondingly, SCM-198 could decrease the brain edema volume ($F$ (3, 20) = 29.14, $P < 0.0001$, Figure 1(h)) and water content in the ipsilateral hemisphere subjected with I/R injury ($F$ (3, 52) = 18.06, $P < 0.0001$, Figure 1(i)). These results suggested that SCM-198 may offer the protection against onset of BBB leakage.

*3.3. SCM-198 Decreased the Degradation of Tight Junctions in Ischemic Brain.* As we know, the cortex and striatum are the most sensitive to reperfusion, so we divided the brain into peri-ischemic region in the cortex and striatum. I/R causes the degradation of TJs, such as ZO-1 and occludin, which results in the loss of BBB function [27]. We examined the mRNA and protein levels of ZO-1 and occludin in the peri-ischemic region and striatum of rat brains. Their protein and mRNA levels, in both peri-ischemic region and striatum, were sharply decreased after I/R injury, while SCM-198 could dramatically restore the degradation (Figure 2(a); $F$ (3, 12) = 18.65, $P < 0.0001$, Figure 2(b); $F$ (3, 22) = 38.22, $P < 0.0001$, Figure 2(c); Figure 2(d); $F$ (3, 8) = 8.228, $P = 0.0079$, Figure 2(e); $F$ (3, 16) = 17.23, $P < 0.0001$, Figure 2(f); $F$ (3, 6) = 25.11, $P = 0.0009$, Figure 2(g); $F$ (3, 8) = 7.631, $P = 0.0099$, Figure 2(h); $F$ (3, 8) = 10.04,

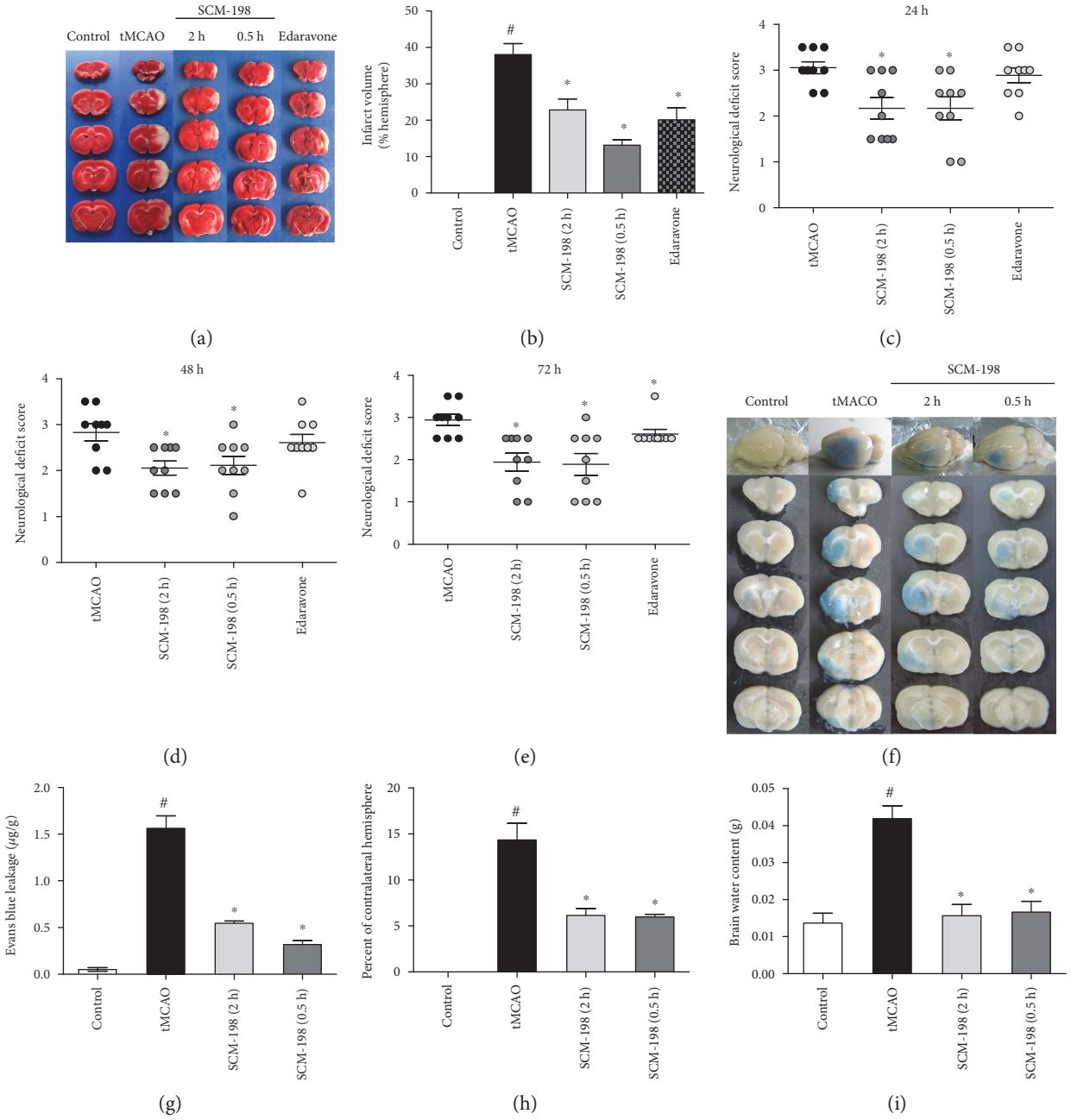


Figure 1: Posttreatment with SCM-198 significantly protected against the damage induced by tMCAO. The rats were subjected to 90 min MCAO before reperfusion. SCM-198 decreased the infarct volume and improved neurological scores. (a) Representative pictures of coronal sections from ischemic rat brain stained with TTC. (b) The quantitative analysis of the number of infarct size. $F$ (4, 31) = 35.04, $P < 0.0001$. (c–e) Neurological function was ameliorated by SCM-198 after ischemia reperfusion. Values are expressed as mean ± SEM. $^{\#}p < 0.05$ versus the control group, $^{*}p < 0.05$ versus the tMCAO group, $n = 8$. Posttreatment with SCM-198 maintained BBB integrity. (f, g) At the end of treatment, the Evans blue dye was injected into the vein following 24 h circulation. (f) Representative pictures of coronal sections from rat brain stained with Evans blue dye after ischemic reperfusion. (g) The quantitative analysis of Evans blue leakage after ischemia reperfusion, $F$ (3, 39) = 59.33, $P < 0.0001$. Edema volume ((h), $F$ (3, 20) = 29.14, $P < 0.0001$) and water content ((i), $F$ (3, 52) = 18.06, $P < 0.0001$) were decreased by SCM-198 after ischemia reperfusion. Values are expressed as mean ± SEM. $^{\#}p < 0.05$ versus the control group, $^{*}p < 0.05$ versus the tMCAO group, $n = 6$.

$P = 0.0044$, Figure 2(i); $F$ (3, 8) = 9.389, $P = 0.0053$, Figure 2(j)).

The TJs are reportedly degraded in I/R mainly by MMP-9 [28, 29] which is the predominant protease involving in BBB disruption following ischemic stroke [30]. It is also reported that MMP-9 is upregulated after ischemia and influences the delayed BBB opening which contributes to the irreversible increase in BBB permeability. So we speculated that SCM-198 may offer a protection through inhibiting the expression of MMP-9. The results confirmed our conjecture,

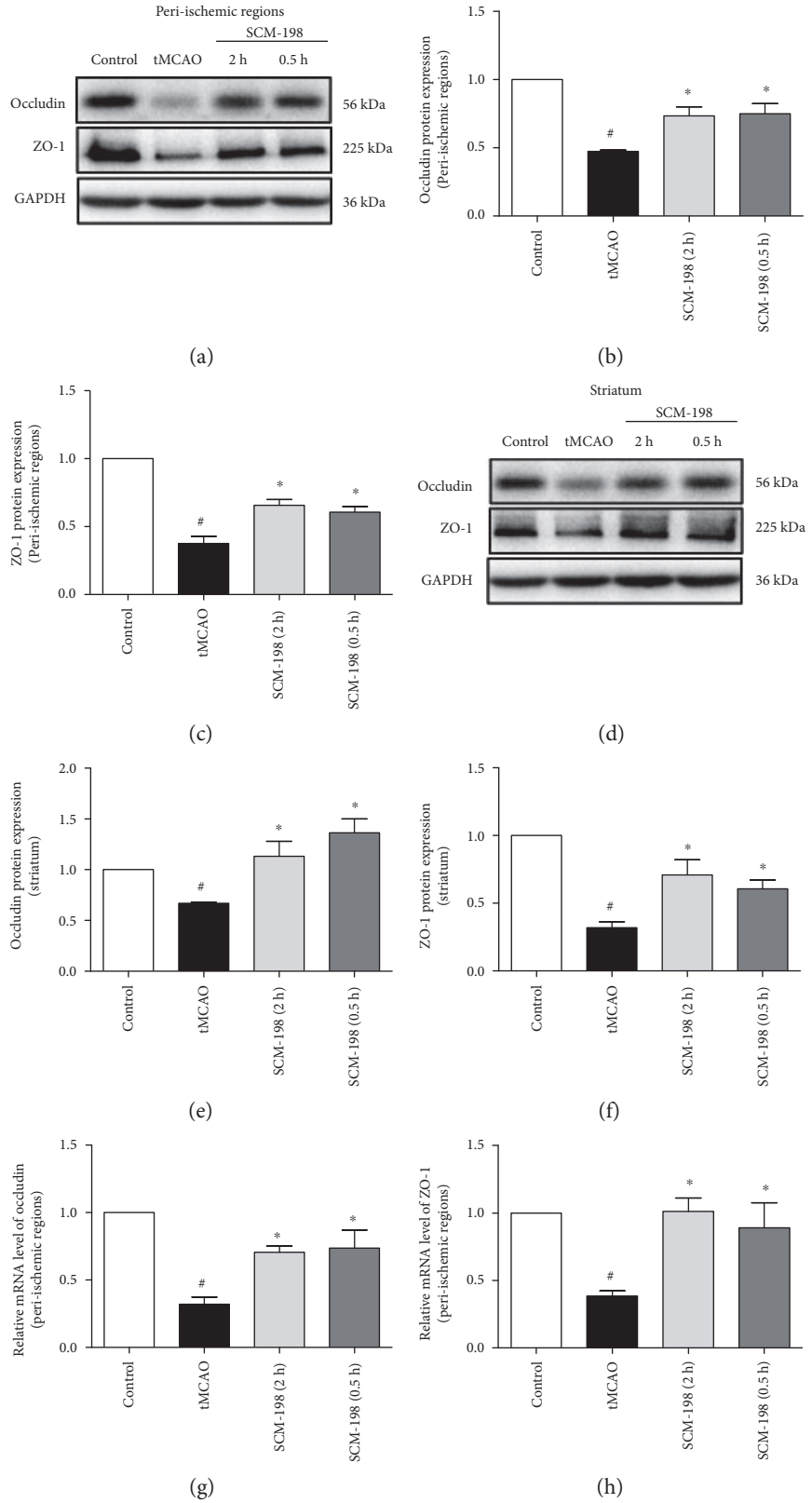


Figure 2: Continued.

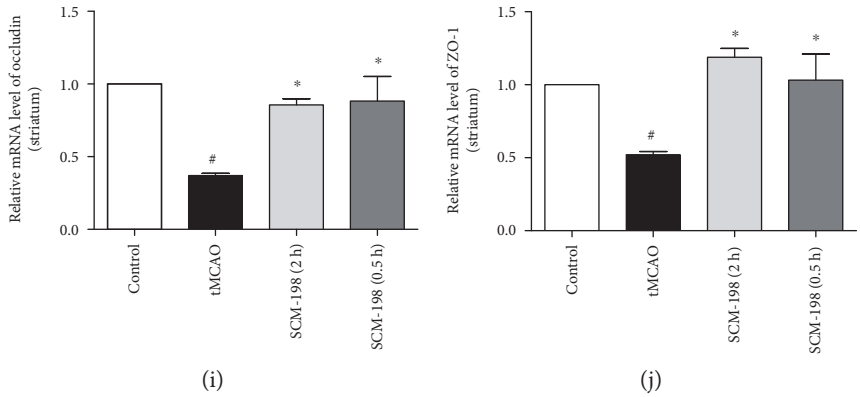


Figure 2: SCM-198 protected against TJ degradation induced by cerebral ischemic reperfusion. (a, d) Western blots of peri-ischemic region and striatum tissues in the tMCAO model showed increased the loss of occludin and ZO-1 levels, but reversed by SCM-198 treatment. GAPDH was used as the loading control. (b-c, e-f) The quantitative analysis occludin and ZO-1 levels were calculated and expressed relative to control. $F$ (3, 12) = 18.65, $P < 0.0001$, Figure 2(b); $F$ (3, 22) = 38.22, $P < 0.0001$, Figure 2(c); $F$ (3, 8) = 8.228, $P = 0.0079$, Figure 2(e); $F$ (3, 16) = 17.23, $P < 0.0001$, Figure 2(f). (g–j) Posttreatment with SCM-198 at 2 h and 0.5 h after reperfusion notably improved occludin and ZO-1 mRNA expression. SCM-198 revealed significantly protection. $F$ (3, 6) = 25.11, $P = 0.0009$, Figure 2(g); $F$ (3, 8) = 7.631, $P = 0.0099$, Figure 2(h); $F$ (3, 8) = 10.04, $P = 0.0044$, Figure 2(i); $F$ (3, 8) = 9.389, $P = 0.0053$, Figure 2(j). Values are expressed as mean ± SEM. $^{\#}p < 0.05$ versus the control group, $^{*}p < 0.05$ versus the tMCAO group, $n = 4$.

western blot (Figure 3(a); $F$ (3, 9) = 38.73, $P < 0.0001$, Figure 3(b); Figure 3(d); $F$ (3, 10) = 14.65, $P = 0.0005$, Figure 3(e)), and real-time RT-PCR assays ($F$ (3, 8) = 85.85, $P < 0.0001$, Figure 3(c), $F$ (3, 8) = 42.11, $P < 0.0001$, Figure 3(f)) revealed that MMP-9 levels were evoked in the peri-ischemic region and striatum in tMCAO group, and SCM-198 treatment after surgery could remarkably reduce the expressions of MMP-9.

NOX4 and HDAC4 involve in mediating BBB permeability, and their expressions are changed by I/R [2, 31]. To determine whether SCM-198 affected expressions of NOX4 and HDAC4, the protein levels were tested in the peri-ischemic region and striatum. Figure 3 (Figure 3(g); $F$ (3, 15) = 51.79, $P < 0.0001$, Figure 3(h); $F$ (3, 8) = 31, $P < 0.0001$, Figure 3(i); Figure 3(j); $F$ (3, 11) = 24.47, $P < 0.0001$, Figure 3(k); $F$ (3, 8) = 14.09, $P = 0.0015$, Figure 3(l)) suggested that I/R caused loss of HDAC4 but increase of NOX4 in both regions of the brain; treatment with SCM-198 enhanced the protein level of HDAC4 and inhibited the expression of NOX4. These results indicated that SCM-198 had a pivotal role in supporting BBB maintenance in vivo.

In order to confirm the protective action of SCM-198 against BBB breakdown and find out how SCM-198 exerted its effect, we used the OGD/R cell model for the further study.

*3.4. SCM-198 Provided Protective Effect against OGD/R Insult.* To clarify the mechanisms of the effect of SCM-198 on BBB disruption, we took an in vitro BBB model on bEnd.3 cell line followed OGD for 6 h and reoxygenation for 4 h. Meantime, we examined the expression of HIF-$\alpha$ to confirm the success of this model (Supplementary Figure 1). The cell viability was determined 4 h after reoxygenation by the CCK8 method. Results revealed that cell death in OGD/R group was significantly increased compared with the control group ($F$ (3, 14) = 12.57, $P = 0.0003$, Figure 4(a)). Pretreatment with different concentrations of SCM-198 had a dose-dependent protective effect, especially the 10 $\mu$M group which could increase the cell viability from 24.49 ± 5.84% to 55.24 ± 5.95%. At the same time, LDH assay was used for assessing cytotoxicity. We found that OGD/R under our condition increased LDH leakage into the cell culture media compared with the control group ($p < 0.05$). And SCM-198 treatment could markedly decrease the LDH release ($F$ (3, 4) = 39.25, $P = 0.002$, Figure 4(b)). These results indicated that SCM-198 provided protection against OGD/R injury.

*3.5. SCM-198 Decreased ROS Production in bEnd.3 Cell Line.* We detected OGD/R-induced ROS production by DCF-DA reagent, a fluorescent probe used for visualizing ROS. OGD/R enriched DCF-DA-positive cells compared with the control group ($p < 0.05$). SCM-198 notably cut ROS generation and reduced the positive cell number in a concentration-dependent manner compared with the OGD/R group. There was no apparent difference between the SCM-198 treatment group and control group (Figure 4(d)). We also calculated the fluorescent intensity by microplate reader. The graph showed that SCM-198 significantly decreased the fluorescent intensity compared with the OGD/R group ($F$ (4, 12) = 43.35, $P < 0.0001$, Figure 4(c)).

*3.6. SCM-198 Maintained the BBB Integrity In Vitro.* FITC-dextran is always used as a fluorescent tracer for evaluating BBB TJ function. Under physiological conditions, due to BBB, the endothelial membrane is impermeable for macromolecules to cross the barrier. But when the cell is subjected to OGD/R injury, FITC-dextran flux observably increased, which indicated disruption of the barrier. SCM-198 reduced the flux of FITC-dextran, suggesting SCM-198 could maintain the integrity of BBB in vitro ($F$ (4, 10) = 6.671, $P = 0.007$, Figure 5(a)).

Western blots showed that TJ proteins, claudin-5, occludin, and ZO-1 were dramatically degraded in the

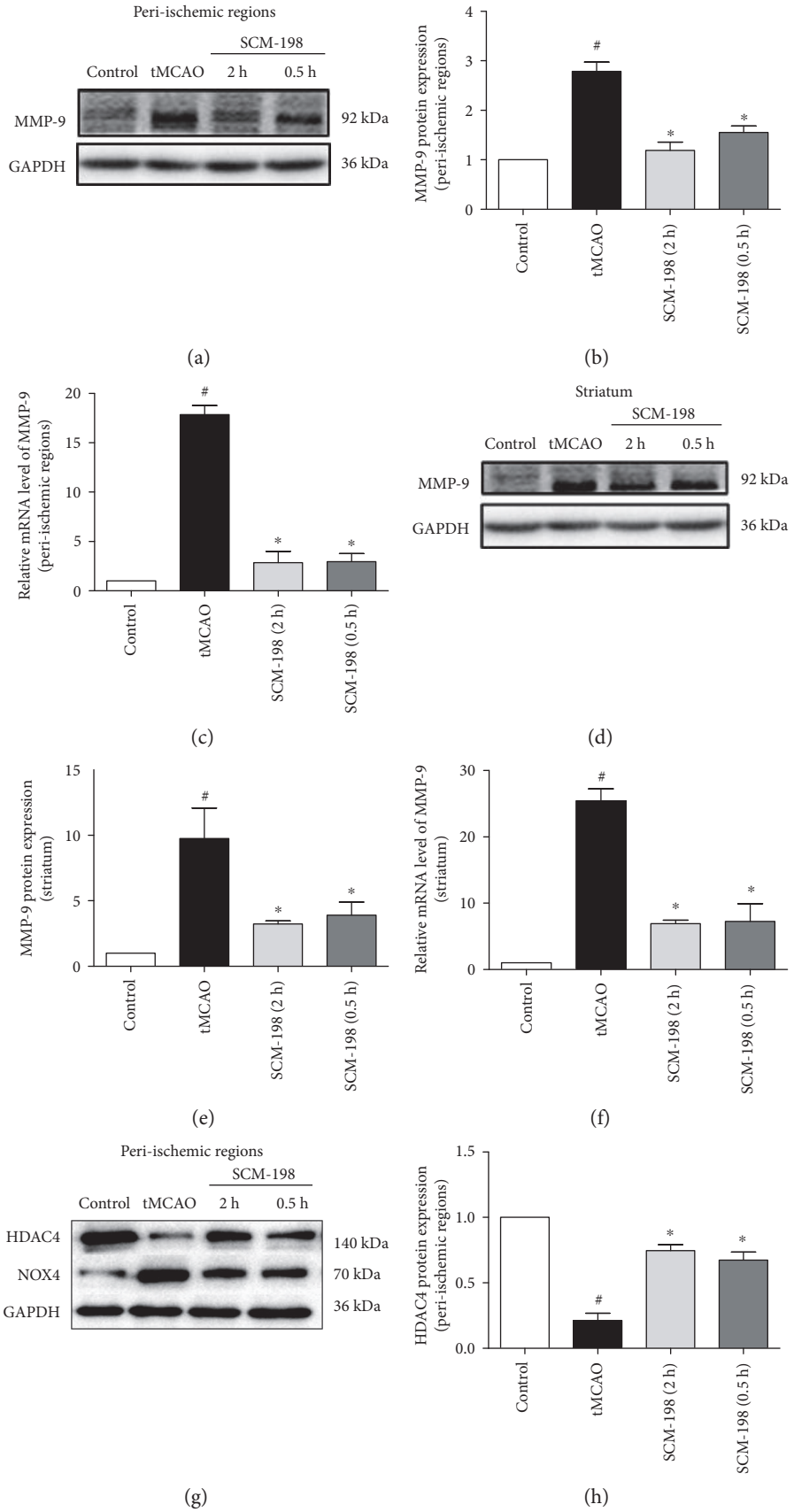


Figure 3: Continued.

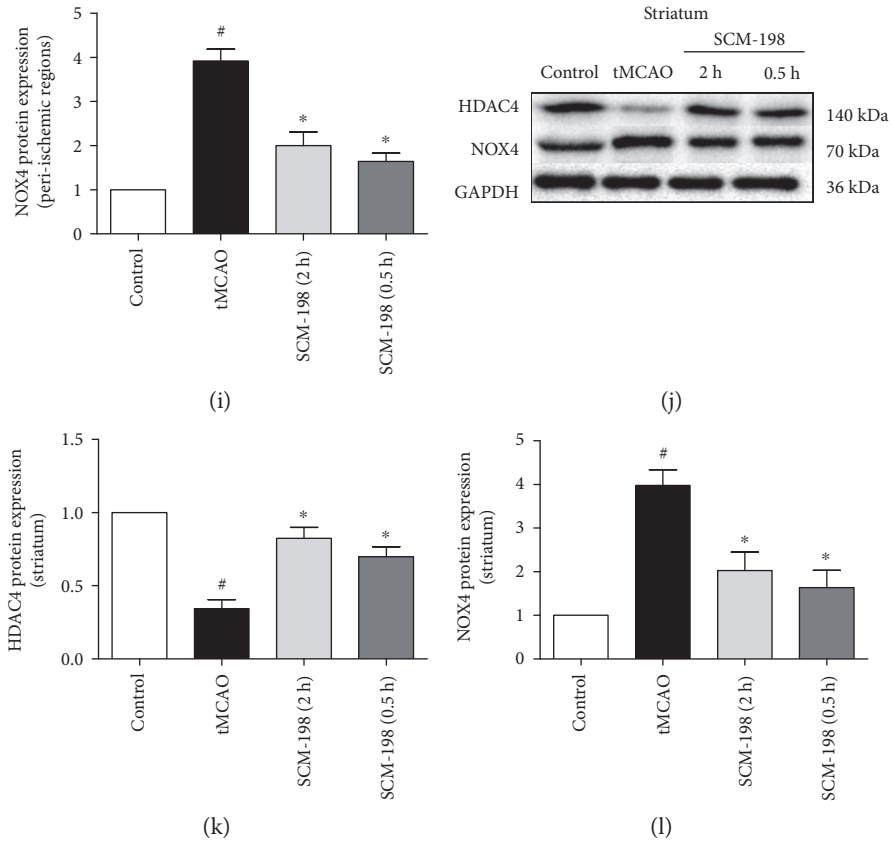


Figure 3: SCM-198 mediated the expression of MMP-9, NOX4, and HDAC4 in tMCAO rat. Reperfusion increased the loss of HDAC4 and the expression of MMP-9 and NOX4 in both peri-ischemic region and striatum tissues of the brain. (a–c) Reperfusion exacerbated the protein and mRNA expression of MMP-9 in peri-ischemic regions. SCM-198 significantly inhibited MMP-9 mRNA expression in the cortex. $F$ (3, 9) = 38.73, $P < 0.0001$, Figure 3(b); $F$ (3, 8) = 85.85, $P < 0.0001$, Figure 3(c). (d–f) Reperfusion improved the protein and mRNA expression of MMP-9 in the striatum. SCM-198 inhibited MMP-9 mRNA expression in the striatum. $F$ (3, 10) = 14.65, $P = 0.0005$, Figure 3(e); $F$ (3, 8) = 42.11, $P < 0.0001$, Figure 3(f); (g–l) Reperfusion increased the loss of HDAC4 and the expression of NOX4 in both peri-ischemic region and striatum tissues of the brain. GAPDH was used as the loading control. $F$ (3, 15) = 51.79, $P < 0.0001$, Figure 3(h); $F$ (3, 8) = 31, $P < 0.0001$, Figure 3(i); $F$ (3, 11) = 24.47, $P < 0.0001$, Figure 3(k); $F$ (3, 8) = 14.09, $P = 0.0015$, Figure 3(l). Values are expressed as mean ± SEM. $^{\#}p < 0.05$ versus the control group, $^{*}p < 0.05$ versus the tMCAO group, $n = 4$.

OGD/R group. This reduction of TJs may interpret the vast increase in barrier permeability. But SCM-198 could signally reverse the degradation of TJs (Figure 5(b); $F$ (4, 10) = 133.1, $P < 0.0001$, Figure 5(c); $F$ (4, 14) = 26.32, $P < 0.0001$, Figure 5(d); $F$ (4, 14) = 22.99, $P < 0.0001$, Figure 5(e)). The results were confirmed by real-time RT-PCR, and the mRNA expressions of claudin-5, occludin, and ZO-1 were markedly reduced at 4 h post-OGD/R. SCM-198 prevented the reduction of these three proteins ($F$ (4, 10) = 7.764, $P = 0.0041$, Figure 5(f); $F$ (4, 15) = 5.983, $P = 0.0044$, Figure 5(g); $F$ (4, 21) = 12.70, $P < 0.0001$, Figure 5(h)). Immunofluorescence analysis also showed that OGD/R weakened occludin and ZO-1 expression when compared with intact ZO-1 and occludin in the control group. But the loss of ZO-1 and occludin was recovered after treatment with SCM-198 (Figure 5(i)). According to the above findings, we also found abundant linear stress fibre formation, which accounts for cell contraction and hyperpermeability [32–35], which was stained by rhodamine dye after OGD/R (Figure 5(i)).

These data manifested that OGD/R touched off robust loss of occludin, claudin-5, and ZO-1 while SCM-198 could improve the expressions. These results were consistent with the findings in vivo.

*3.7. SCM-198 Ameliorated BBB Injury via Enhancing HDAC4.* To identify whether the signals causing BBB damage in vivo also occur in cell model in vitro, we measured the protein and mRNA levels of HDAC4, NOX4, and MMP-9. In the OGD/R group, both protein and mRNA levels of HDAC4 were notably reduced (Figures 6(a), 6(b), and 6(e)), while NOX4 and MMP-9 were significantly increased after reoxygenation (Figures 6(a), 6(c), 6(d), 6(f), and 6(g)). Consistent with the results in vivo, SCM-198 could exert the protection by enhancing the expression of HDAC4 and inhibiting the expression of NOX4 and MMP-9 (Figure 6(a); $F$ (4, 12) = 20.46, $P < 0.0001$, Figure 6(b); $F$ (4, 19) = 20.6, $P < 0.0001$, Figure 6(c); $F$ (4, 10) = 34.23, $P < 0.0001$, Figure 6(d); $F$ (4, 10) = 9.474, $P = 0.002$, Figure 6(e); $F$ (4, 10) = 7.831,

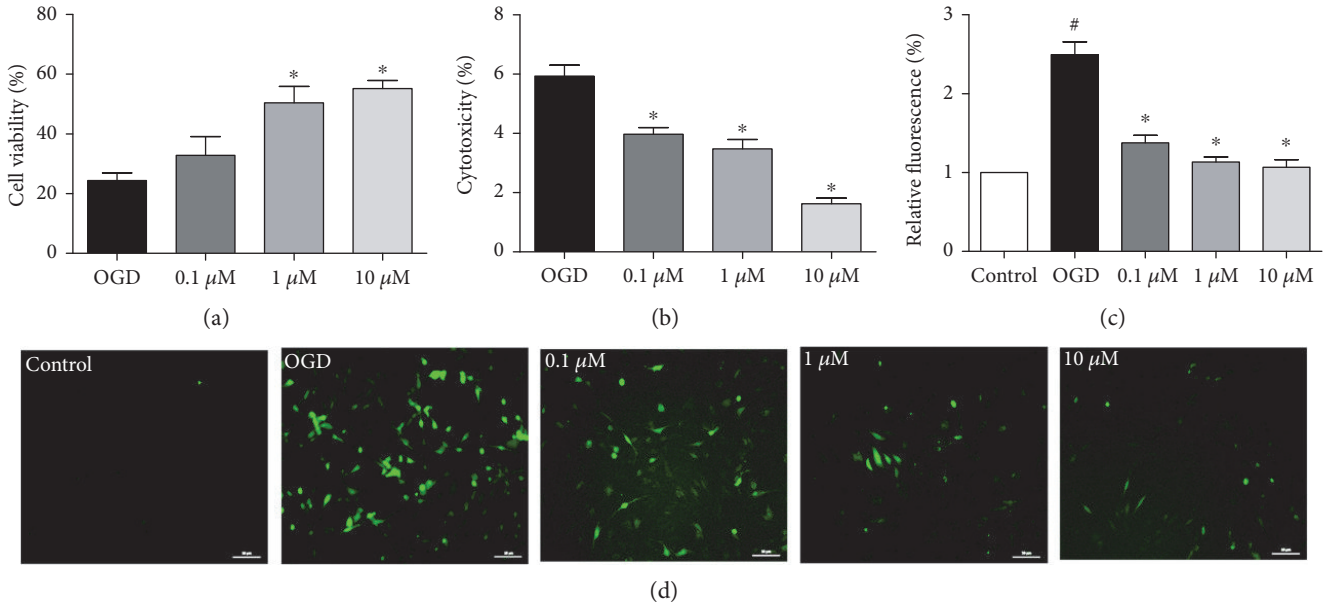


Figure 4: SCM-198 protected against ischemia-like injury in the in vitro BBB model. bEnd.3 cell line was exposed to 6 h of OGD followed by 4 h reperfusion after treated with different concentrations of SCM-198. (a) OGD/R markedly increased cell death, SCM-198 dose-dependently improved the cell viability, $F(3, 14) = 12.57$, $P = 0.0003$. (b) SCM-198 reduced the LDH leakage in the supernatant after OGD/R, $F(3, 4) = 39.25$, $P = 0.002$. (c) The fluorescence intensity of intracellular ROS, $F(4, 12) = 43.35$, $P < 0.0001$. (d) OGD/R produced abundant ROS in the cells, while SCM-198 significantly reduced the ROS formation, scale bar = 10 $\mu$m. Values are expressed as mean ± SEM. $^{\#}p < 0.05$ versus the control group, $^{*}p < 0.05$ versus the OGD group, $n = 3$.

$P = 0.004$, Figure 6(f); $F(4, 10) = 39.81$, $P < 0.0001$, Figure 6(g)). These results suggested that SCM-198 could also exhibit protective effect on BBB integrity in vitro by regulating the expression of HDAC4, NOX4, and MMP-9.

HDAC4 and NOX4 are two proteins which exist in the same signaling pathway, but the regulative relationship between HDAC4 and NOX4 is not clear. To explored whether HDAC4 was responsible for the expression of NOX4, we used adenovirus or specific inhibitor Taq to overexpress or inhibit HDAC4 in bEnd.3 cells and then exposed these cells to OGD/R. Western blot results revealed that overexpression of HDAC4 by adenovirus inhibited the increase of NOX4 (Supplementary Figure 2A-B), while Taq further increased the expression of NOX4 at 0.2 $\mu$M (Supplementary Figure 2C). On the other hand, overexpression of NOX4 by lentivirus or inhibition of NOX4 with DPI and GKT137831 could not influence the expression of HDAC4 (Supplementary 3). Therefore, we speculated that HDAC4 could inhibit the expression of NOX4 under our OGD/R condition.

Next, we examined whether HDAC4 was involved in the regulation of BBB integrity. The results showed that Taq enhanced the ROS formation ($F(4, 14) = 9.319$, $P = 0.0007$, Figure 6(h)) and increased the protein and mRNA levels of NOX4 and MMP-9 in bEnd.3 cells (Figure 7(a), $F(4, 15) = 13.24$, $P < 0.0001$, Figure 7(b); $F(4, 13) = 28.16$, $P < 0.0001$, Figure 7(c); $F(4, 10) = 43.70$, $P < 0.0001$, Figure 7(d); $F(4, 10) = 27.45$, $P < 0.0001$, Figure 7(e); $F(4, 10) = 50.05$, $P < 0.0001$, Figure 7(f); $F(4, 10) = 8.332$, $P = 0.0032$, Figure 7(g); $F(4, 10) = 39.14$, $P < 0.0001$, Figure 7(h)). Furthermore, Taq abolished the protection of HDAC4 on BBB integrity by decreasing the expression of TJ protein and mRNA such as claudin-5, occludin, and ZO-1 (Figures 7(a) and 7(d)–7(f), $F(4.10) = 401$, $P < 0.0001$, Figure 7(i); $F(4.10) = 144.9$, $P < 0.0001$, Figure 7(j); $F(4.10) = 39.03$, $P < 0.0001$, Figure 7(k)). Treatment with SCM-198 reduced the ROS production (Figure 6(h)) and the overexpression of NOX4 and MMP-9 induced by Taq (Figures 7(a)–7(c) and 7(g)-7(h)). Similarly, treatment with SCM-198 increased the mRNA and protein levels of these TJ proteins (Figures 7(a), 7(d)–7(f), and 7(i)–7(k)). Together these results indicated that SCM-198 may exert the protection effect on BBB through enhancing the expression of HDAC4 which could regulate NOX4 and MMP-9.

## 4. Discussion

In this article, we used classic tMCAO rat model in vivo and reperfusion post-OGD cell model in vitro to explore the potential of SCM-198 as a therapeutic approach for reperfusion-induced BBB disrupture. We found that SCM-198 significantly decreased infarct volume and ameliorated neurological deficit in the tMCAO model. Moreover, SCM-198 could also reduce the cell injury caused by OGD/R in vitro. Further study about the mechanism demonstrated that HDAC4 could inhibit the expression of NOX4 and MMP-9 and then improve TJ levels, therefore protect against BBB breakdown. In conclusion, we first revealed that HDAC4 was involved in regulating BBB integrity and SCM-198 had the protective effects against BBB leakage through enhancing the expression of HDAC4.

The brain suffers from ischemia-induced vast loss of oxygen and nutrient leading to tissue damage, especially the cortex and striatum regions [36], and reperfusion

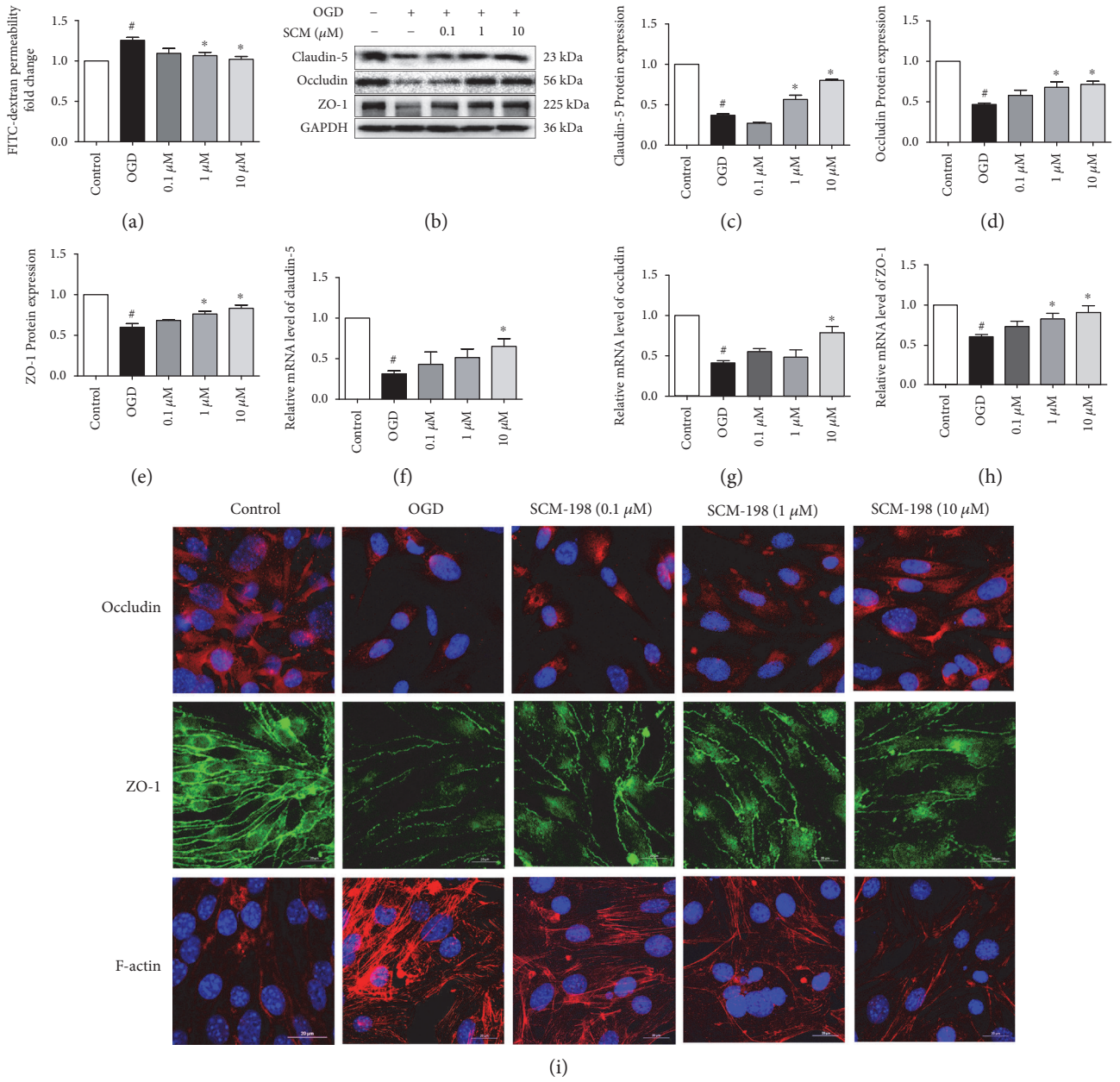


Figure 5: SCM-198 reduced the degradation of TJs induced by OGD/R. (a) FITC-dextran was used to determine BBB integrity. After reperfusion the leakage of dextran in the plate was remarkably increased. SCM-198 could reduce the leakage, $F\ (4, 10) = 6.671$, $P = 0.007$. (b) Expressions of TJs, occludin, claudin-5, and ZO-1 were evaluated by western blot 4 h after reperfusion. OGD/R induced the obvious loss of TJs, and SCM-198 reversed this loss. (c–e) The results were quantified and expressed relative to control, $F\ (4, 10) = 133.1$, $P < 0.0001$, Figure 5(c); $F\ (4, 14) = 26.32$, $P < 0.0001$, Figure 5(d); $F\ (4, 14) = 22.99$, $P < 0.0001$, Figure 5(e). (f–h) The expressions of mRNA levels were detected by real time RT-PCR. SCM-198 could reduce the degradation of TJs at the level of mRNA, $F\ (4, 10) = 7.764$, $P = 0.0041$, Figure 5(f); $F\ (4, 15) = 5.983$, $P = 0.0044$, Figure 5(g); $F\ (4, 21) = 12.70$, $P < 0.0001$, Figure 5(h). (i) Immunofluorescence analysis of occludin and ZO-1, and rhodamine-conjugated phalloidin for stress fibre. Scale bar = 20 μm. The expressions of occludin and ZO-1 were significantly reduced by OGD/R while SCM-198 prevented their reduction. SCM-198 also decreased the formation of stress fibre. Values are expressed as mean ± SEM. $^{\#}p < 0.05$ versus the control group, $^{*}p < 0.05$ versus the OGD group, $n = 3$.

exacerbates this insult because of the fresh oxygen [1]. We found that both cortex and striatum regions in the tMCAO animals appeared plenty of infarct volume, approximately 40% of the whole brain (Figures 1(a) and 1(b)). SCM-198 and Edaravone could significantly reduce the infarct area and reduce neurological deficit scores (Figures 1(c) and 1(e)). Furthermore, treatment with SCM-198 at 0.5 h postsurgery revealed better therapeutic effect on infarct area and neurological deficit score than Edaravone (Figure 1).

BBB is a specialized structure between the brain tissue and blood circulation to maintain the homeostasis of

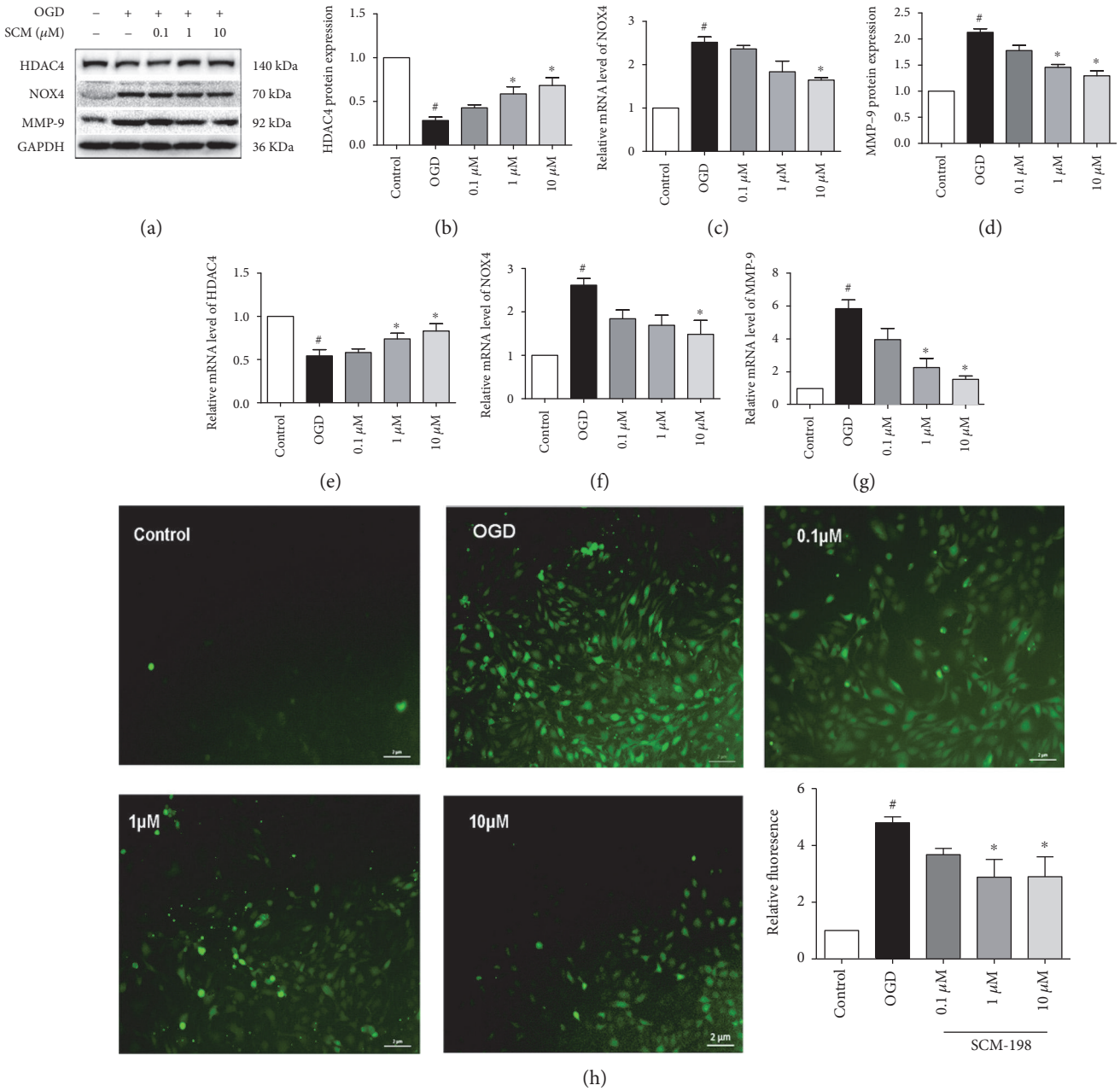


Figure 6: SCM-198 mediated the expression of MMP-9, NOX4, and HDAC4 in vitro. (a–d) Western blot images and quantitative analysis of MMP-9, NOX4, and HDAC4 were shown, $F(4, 12) = 20.46$, $P < 0.0001$, Figure 6(b); $F(4, 19) = 20.6$, $P < 0.0001$, Figure 6(c); $F(4, 10) = 34.23$, $P < 0.0001$, Figure 6(d). (e–g) The mRNA levels of HDAC4, NOX4, and MMP-9 were estimated by real-time RT-PCR, $F(4, 10) = 9.474$, $P = 0.002$, Figure 6(e); $F(4, 10) = 7.831$, $P = 0.004$, Figure 6(f); $F(4, 10) = 39.81$, $P < 0.0001$, Figure 6(g). (h) The HDAC4 inhibitor Taq (0.2 $\mu$M) or vehicle was applied 1 h before until the end of the experiment. Taq exacerbated the production of ROS, while SCM-198, 1 and 10 $\mu$M, could still reduce the ROS formation, $F(4, 14) = 9.319$, $P = 0.0007$, scale bar = 2 $\mu$m. Values are expressed as mean ± SEM. $^{\#}p < 0.05$ versus the control group, $^{*}p < 0.05$ versus the OGD group, $n = 3$.

microenvironment and avoid the harm from the exogenous compounds. Study showed that treatment with tPA often accompanies with lethal complication of brain edema due to reperfusion insult which contribute to the disrupture of BBB. In our study, I/R-induced BBB disruption was confirmed by EB dye which crossed from blood into parenchyma (Figure 1(f)). Furthermore, the increase of bEnd.3 cells permeability induced by OGD/R in the in vitro model was tested by FITC-dextrans. SCM-198 remarkably decreased EB and FITC-dextran leakage (Figure 5(a)). Besides, we also detected that I/R significantly increased the water content and edema volume of the ipsilateral brain compared with the control rats. SCM-198 decreased the brain edema volume and water content in the ipsilateral hemisphere (Figures 1(h) and 1(i)). These results indicated that SCM-198 played the protective effect against BBB breakdown both in vivo and in vitro.

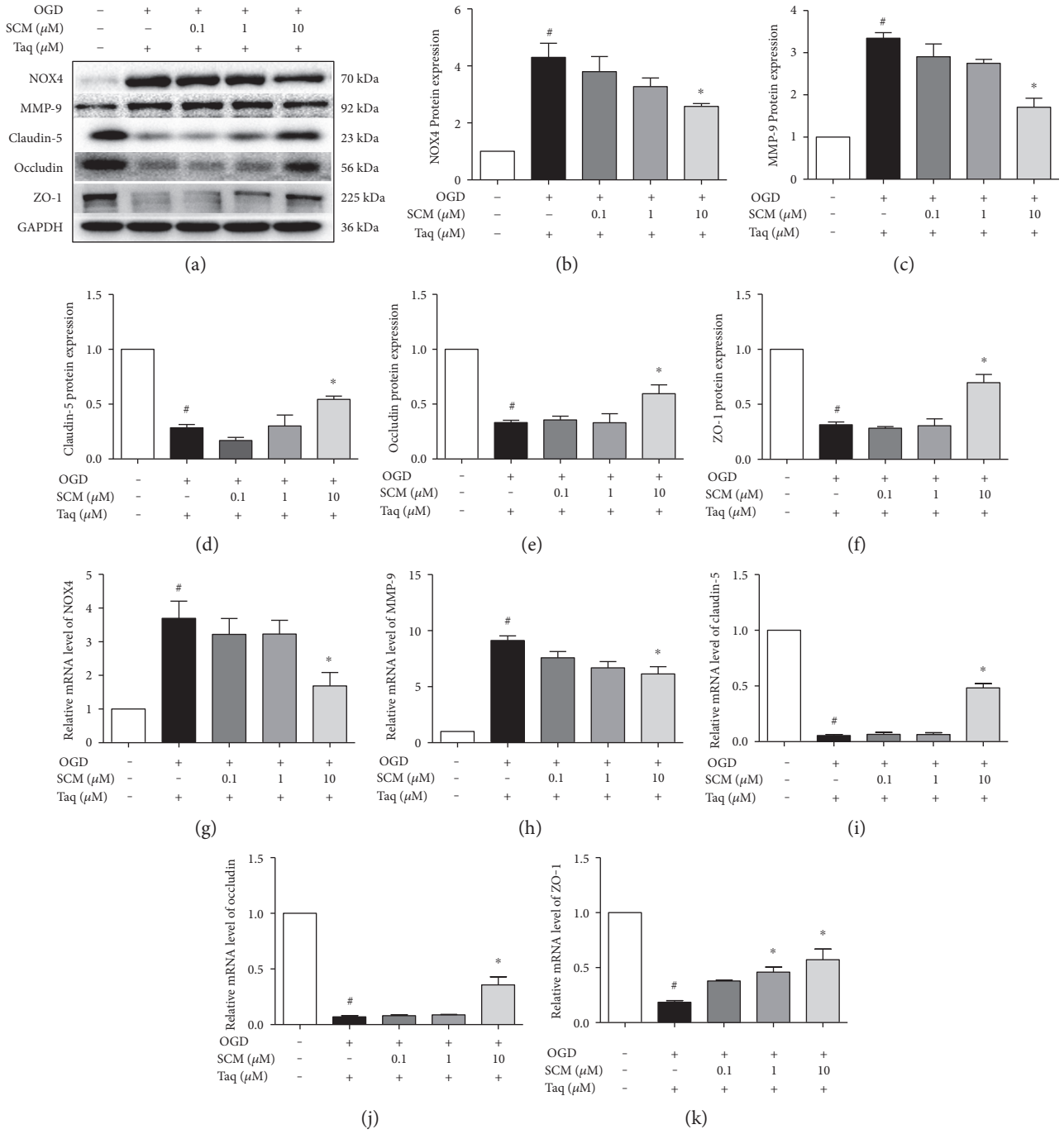


Figure 7: SCM-198 maintained the BBB integrity via enhancing the expression of HDAC4. The HDAC4 inhibitor Taq (0.2 $\mu$M) or vehicle was applied 1 h before until the end of the experiment. (a–f) Western blot images and quantitative analysis suggested inhibition of HDAC4 increased the expression of NOX4 and MMP-9, and treatment with 10 $\mu$M SCM-198 reduced the raised levels of NOX4 and MMP-9. Meanwhile, SCM-198 decreased the loss of TJs. The results revealed SCM-198 could protect against the degradation of TJs via improving the expression of HDAC4, $F$ (4, 15) = 13.24, $P < 0.0001$, Figure 7(b); $F$ (4, 13) = 28.16, $P < 0.0001$, Figure 7(c); $F$ (4, 10) = 43.70, $P < 0.0001$, Figure 7(d); $F$ (4, 10) = 27.45, $P < 0.0001$, Figure 7(e); $F$ (4, 10) = 50.05, $P < 0.0001$, Figure 7(f); (g–k) The mRNA levels of NOX4, MMP-9, and TJs were estimated by real-time RT-PCR, $F$ (4, 10) = 8.332, $P = 0.0032$, Figure 7(g); $F$ (4, 10) = 39.14, $P < 0.0001$, Figure 7(h); $F$ (4.10) = 401, $P < 0.0001$, Figure 7(i); $F$ (4.10) = 144.9, $P < 0.0001$, Figure 7(j); $F$ (4.10) = 39.03, $P < 0.0001$, Figure 7(k). Values are expressed as mean ± SEM. $^{\#}p < 0.05$ versus the control group, $^{*}p < 0.05$ versus the OGD group, $n = 3$.

Following stroke, BBB disrupture has two phases: the initial opening occurs within hours after stroke onset and the second phase comes 24–48 h later. MMPs, especially MMP-2 and MMP-9, are involved in such early and late phases. The early BBB breakdown is mainly caused by MMP-2 which increased in the early phase of the tMCAO model [37]. But in our condition, the mRNA expression of MMP2 was unchanged between each group (Supplementary

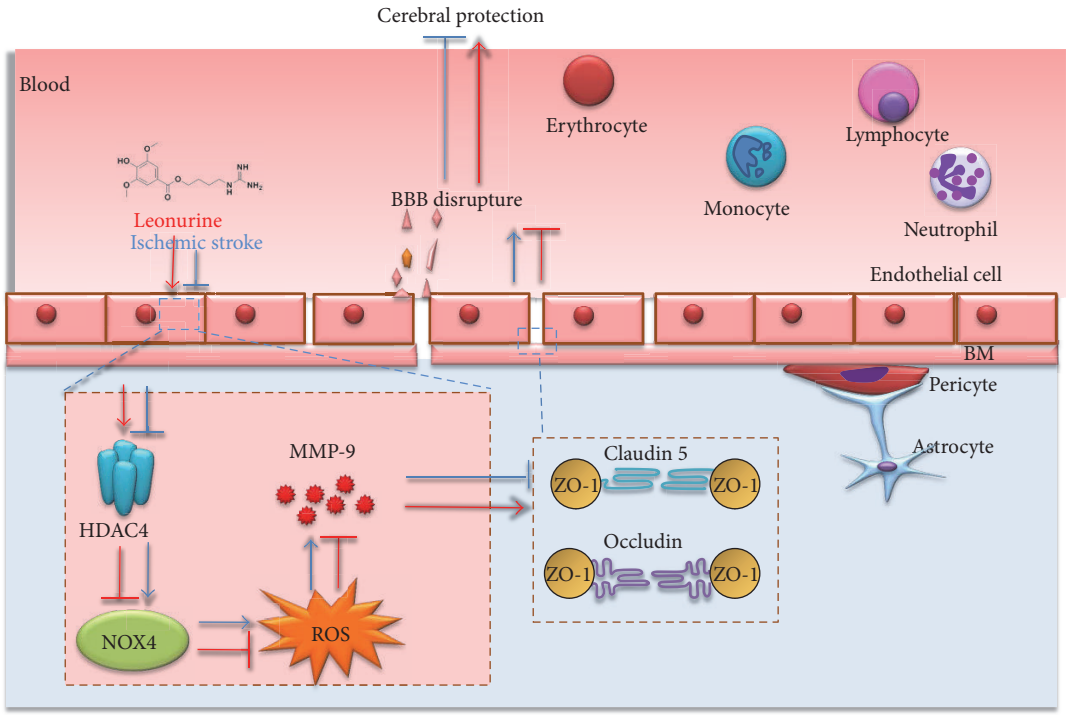


Figure 8: Schematic representation of the mechanisms of SCM-198 protection against ischemic stroke. SCM-198 protected BBB integrity by regulating the HDAC4/NOX4/MMP-9 tight junction pathway.

Figure 4). Correspondingly, MMP-9 was elevated during the delayed barrier disruption, from 4 h to 4 days. The upregulation of MMP-9 leads to the production of stress fibre and entire degradation of TJs, in addition to complete disrupture of BBB and brain edema [38].

In the clinic, MMP-9 is mainly derived from infiltrating neutrophils and microvessel endothelium after ischemic stroke in humans [39]. MMP-9 is considered as the predominant protease which can break the integrity of BBB following ischemic stroke. We supposed that SCM-198 may protect the further lesion by regulating the expression of MMP-9. We examined the expression of MMP-9 and found that MMP-9 was indeed declined by SCM-198 treatment. While TJs, which could be regulated by MMP-9, play critical function in maintaining BBB integrity. In our study, we found SCM-198 could enhance the mRNA and protein levels of them and then defend the insult induced by I/R. These suggested that SCM-198 has a beneficial effect on BBB damage by inhibiting MMP-9 levels and improve TJ expression (Figures 2, 3, 5, and 6).

It is well known that nuclear factor kappa-B (NF-$\kappa$B) and reactive oxygen species (ROS) are involving of MMP-9 activation during ischemia [40]. ROS, including hydrogen peroxide, superoxide anion, and hydroxyl radical, are induced by ischemia following reperfusion which contributes to the critical injury to the brain tissue and BBB disruption [41–43]. When the brain is subjected to oxidative stress, NOXs are activated and then the electrons are transferred from NADPH to oxygen producing abundant ROS. NOX family is the primary source of ROS [44], which comprises seven members: NOX1, NOX2, NOX3, NOX4, NOX5, dual oxidase- (Duox-) 1, and Duox-2. Of these NOX isoforms identified hitherto [45–47], NOX1, NOX2, and NOX4 are expressed in the brain and involved in BBB dysfunction after cerebral ischemia and reperfusion. The recent research had proved that NOX4$^{-/-}$ mice exhibited the decrease of infarct volume, oxidative stress, BBB disruption, and neuronal apoptosis in the tMCAO model. But the absent of NOX2 had no effect on infarct area, BBB leakage, neuronal apoptosis, or functional outcome after tMCAO. So the researchers concluded that deletion of NOX4, not NOX1 or NOX2, exerted the protective effect [48]. In our study, we found that the expression of NOX2 did not change in the tMCAO model (Supplementary Figure 5), suggesting that NOX2 did not play a predominant role in our situation. As we know, NOX4 is considered as the major source of ROS. NOX4, first discovered in the kidney, is mainly distributed in neuron and endothelial cells of the brain [1, 43]. Ischemic stroke induces NOX4 activated [48], and previous research revealed that inhibition of NOX4 could suppress the enhanced level of MMP-9 induced by tMCAO [47].

Based on these results, we believed that NOX4 may exert a main role in our tMCAO and OGD/R models. Our results showed that NOX4 expression was increased in both tMCAO and OGD/R models. Treatment with SCM-198 would reduce the expression of NOX4 and then protect against I/R and OGD/R injury (Figures 3 and 6). A number of transcription factors, for instance, NF-$\kappa$b[49], SMAD proteins [50], HIF1$\alpha$ [51], E2F [52], Nrf2 [53], Nrf3 [54] and STAT1/3 [55] have been shown to regulate NOX4 gene expression. However, few researchers focused on the epigenetic regulation of NOX4. Some studies confirmed that HDAC inhibition

provided neuroprotection after cerebral ischemic insult or intracerebral hemorrhage [56–58]. Histone deacetylases (HDACs) are a protein family consisted of 18 proteins which could be categorized into 4 groups according to their structural and functional resemblance: class I (HADCs 1, 2, 3, and 8), class IIa (HDACs 4, 5, 7, and 9), class IIb (HDACs 6 and 10), class III (sirtuins 1–7), and class IV (HDAC 11) [59]. HDAC dysregulation is associated with brain disorders such as Huntington's disease, Alzheimer's disease, and ischemic stroke [60, 61]. Therefore, it could be a potential therapeutic target. He et al. examined the change of HDACs 1–11 induced by ischemia and reperfusion; the results suggested that only HDAC4/5 mRNA levels were significantly decreased while HDAC9 was prominently increased in ischemic hemisphere [31].

In our study, in both rat and cell model groups, the levels of HDAC4 were notably decreased, and treatment with SCM-198 could enhance the expression of HDAC4 (Figures 6(a) and 6(b)). Furthermore, we overexpressed or inhibited HDAC4 to clarify the regulative relationship between HDAC4 and NOX4. The results showed that HDAC4 could regulate the expression of NOX4 in the opposite direction. Therefore, we demonstrated that SCM-198 could regulate the expression of HDAC4 which modulated NOX4 level and then influenced the downstream of BBB disrupture (Figure 7).

## 5. Conclusion

In summary, our research implied that SCM-198 reduced the infarct volume, ameliorated the neurological deficit, and protected against BBB leakage in vivo and in vitro. The underlying mechanism may be that SCM-198 could improve the level of HDAC4 which could regulate the expression of NOX4 and further influence the downstream pathway to exert the protective effect on BBB disrupture (Figure 8). SCM-198 may be a promising candidate for the treatment of cerebral ischemia and reperfusion.

## Abbreviations

tMCAO: Transient middle cerebral artery occlusion
BBB: Blood-brain barrier
OGD/R: Oxygen-glucose deprivation and reoxygenation
ROS: Reactive oxygen species
ZO: Zonula occludens
NOX: Nicotinamide adenine dinucleotide phosphate oxidases
MMPs: Matrix metalloproteinases
HDACs: Histone deacetylases
tPA: Tissue-type plasminogen activator
NVU: Neurovascular unit
TJs: Tight junctional proteins
Cav1: Caveolin-1
JAM: Junctional adhesion molecules
BMECs: Brain microvessel endothelium cells
NF-$\kappa$B: Nuclear factor kappa-B
CNS: Central nervous system
I/R: Ischemic reperfusion
CBF: Cerebral blood flow
TTC: 2,3,5-Triphenyltetrazolium chloride
BWC: Brain water content
LDH: Lactate dehydrogenase
EB: Evans blue
DPI: Diphenyleneiodonium
Taq: Tasquinimod.

## Conflicts of Interest

The authors declare no competing financial interests.

## Acknowledgments

This work was supported by grants from the National Natural Science Foundation of China (no. 81330080), Shanghai Committee of Science and Technology of China (no. 14JC1401100), a key laboratory program of the Education Commission of Shanghai Municipality (no. ZDSYS14005), and National Major Scientific and Technological Special Project (no. 2012ZX09103101i-064; 2012ZX 09501001-001-003).

## References

[1] K. A. Radermacher, K. Wingler, F. Langhauser et al., "Neuroprotection after stroke by targeting NOX4 as a source of oxidative stress," *Antioxidants & Redox Signaling*, vol. 18, pp. 1418–1427, 2013.

[2] Y. Wang, J. Jia, G. Ao et al., "Hydrogen sulfide protects blood-brain barrier integrity following cerebral ischemia," *Journal of Neurochemistry*, vol. 129, pp. 827–838, 2014.

[3] M. Khan, T. S. Dhammu, H. Sakakima et al., "The inhibitory effect of S-nitrosoglutathione on blood-brain barrier disruption and peroxynitrite formation in a rat model of experimental stroke," *Journal of Neurochemistry*, vol. 123, Supplement 2, pp. 86–97, 2012.

[4] E. A. Neuwelt, B. Bauer, C. Fahlke et al., "Engaging neuroscience to advance translational research in brain barrier biology," *Nature Reviews. Neuroscience*, vol. 12, pp. 169–182, 2011.

[5] Y. Shi, L. Zhang, H. Pu et al., "Rapid endothelial cytoskeletal reorganization enables early blood-brain barrier disruption and long-term ischaemic reperfusion brain injury," *Nature Communications*, vol. 7, p. 10523, 2016.

[6] W. Shi, X. Wei, Z. Wang et al., "HDAC9 exacerbates endothelial injury in cerebral ischaemia/reperfusion injury," *Journal of Cellular and Molecular Medicine*, vol. 20, pp. 1139–1149, 2016.

[7] T. Zhang, S. Fang, C. Wan et al., "Excess salt exacerbates blood-brain barrier disruption via a p38/MAPK/SGK1-dependent pathway in permanent cerebral ischemia," *Scientific Reports*, vol. 5, p. 16548, 2015.

[8] P. Huang, C. M. Zhou, H. Qin et al., "Cerebralcare granule(R) attenuates blood-brain barrier disruption after middle cerebral artery occlusion in rats," *Experimental Neurology*, vol. 237, pp. 453–463, 2012.

[9] D. Knowland, A. Arac, K. J. Sekiguchi et al., "Stepwise recruitment of transcellular and paracellular pathways underlies blood-brain barrier breakdown in stroke," *Neuron*, vol. 82, pp. 603–617, 2014.

[10] M. M. Tenreiro, R. Ferreira, L. Bernardino, and M. A. Brito, "Cellular response of the blood-brain barrier to injury: potential biomarkers and therapeutic targets for brain regeneration," *Neurobiology of Disease*, vol. 91, pp. 262–273, 2016.

[11] X. Liu, L. Pan, X. Wang, Q. Gong, and Y. Z. Zhu, "Leonurine protects against tumor necrosis factor-alpha-mediated inflammation in human umbilical vein endothelial cells," *Atherosclerosis*, vol. 222, pp. 34–42, 2012.

[12] X. H. Liu, L. L. Pan, H. Y. Deng et al., "Leonurine (SCM-198) attenuates myocardial fibrotic response via inhibition of NADPH oxidase 4," *Free Radical Biology & Medicine*, vol. 54, pp. 93–104, 2013.

[13] K. P. Loh, J. Qi, B. K. Tan, X. H. Liu, B. G. Wei, and Y. Z. Zhu, "Leonurine protects middle cerebral artery occluded rats through antioxidant effect and regulation of mitochondrial function," *Stroke*, vol. 41, pp. 2661–2668, 2010.

[14] F. J. Ortega, J. Jolkkonen, N. Mahy, and M. J. Rodriguez, "Glibenclamide enhances neurogenesis and improves long-term functional recovery after transient focal cerebral ischemia," *Journal of Cerebral Blood Flow and Metabolism : Official Journal of the International Society of Cerebral Blood Flow and Metabolism*, vol. 33, pp. 356–364, 2013.

[15] H. Hu, X. Sun, F. Tian, H. Zhang, Q. Liu, and W. Tan, "Neuroprotective effects of Isosteviol sodium injection on acute focal cerebral ischemia in rats," *Oxidative Medicine and Cellular Longevity*, vol. 2016, Article ID 1379162, 10 pages, 2016.

[16] K. P. Loh, S. H. Huang, B. K. Tan, and Y. Z. Zhu, "Cerebral protection of purified Herba Leonuri extract on middle cerebral artery occluded rats," *Journal of Ethnopharmacology*, vol. 125, pp. 337–343, 2009.

[17] S. Fu, Y. Gu, J. Q. Jiang et al., "Calycosin-7-O-beta-D-glucoside regulates nitric oxide/caveolin-1/matrix metalloproteinases pathway and protects blood-brain barrier integrity in experimental cerebral ischemia-reperfusion injury," *Journal of Ethnopharmacology*, vol. 155, pp. 692–701, 2014.

[18] N. Li, K. Ragheb, G. Lawler et al., "Mitochondrial complex I inhibitor rotenone induces apoptosis through enhancing mitochondrial reactive oxygen species production," *The Journal of Biological Chemistry*, vol. 278, pp. 8516–8525, 2003.

[19] D. Han, W. Fang, R. Zhang et al., "Clematichinenoside protects blood brain barrier against ischemic stroke superimposed on systemic inflammatory challenges through up-regulating A20," *Brain, Behavior, and Immunity*, vol. 51, pp. 56–69, 2016.

[20] M. Li, R. N. Ma, L. H. Li, Y. Z. Qu, and G. D. Gao, "Astragaloside IV reduces cerebral edema post-ischemia/reperfusion correlating the suppression of MMP-9 and AQP4," *European Journal of Pharmacology*, vol. 715, pp. 189–195, 2013.

[21] S. Garbuzova-Davis, E. Haller, S. N. Williams et al., "Compromised blood-brain barrier competence in remote brain areas in ischemic stroke rats at the chronic stage," *The Journal of Comparative Neurology*, vol. 522, pp. 3120–3137, 2014.

[22] J. Liu, X. Jin, K. J. Liu, and W. Liu, "Matrix metalloproteinase-2-mediated occludin degradation and caveolin-1-mediated claudin-5 redistribution contribute to blood-brain barrier damage in early ischemic stroke stage," *The Journal of Neuroscience : The Official Journal of the Society for Neuroscience*, vol. 32, pp. 3044–3057, 2012.

[23] J. Wu, W. Guo, S. Z. Lin et al., "Gp130-mediated STAT3 activation by S-propargyl-cysteine, an endogenous hydrogen sulfide initiator, prevents doxorubicin-induced cardiotoxicity," *Cell Death & Disease*, vol. 7, article e2339, 2016.

[24] S. Wu, Y. Yue, H. Tian et al., "Tramiprosate protects neurons against ischemic stroke by disrupting the interaction between PSD95 and nNOS," *Neuropharmacology*, vol. 83, pp. 107–117, 2014.

[25] C. M. Zehendner, L. Librizzi, J. Hedrich et al., "Moderate hypoxia followed by reoxygenation results in blood-brain barrier breakdown via oxidative stress-dependent tight-junction protein disruption," *PloS One*, vol. 8, article e82823, 2013.

[26] L. L. Pan, X. H. Liu, Y. Q. Shen et al., "Inhibition of NADPH oxidase 4-related signaling by sodium hydrosulfide attenuates myocardial fibrotic response," *International Journal of Cardiology*, vol. 168, pp. 3770–3778, 2013.

[27] S. M. Gloor, M. Wachtel, M. F. Bolliger, H. Ishihara, R. Landmann, and K. Frei, "Molecular and cellular permeability control at the blood-brain barrier," *Brain Research. Brain Research Reviews*, vol. 36, pp. 258–264, 2001.

[28] D. Amantea, G. Micieli, C. Tassorelli et al., "Rational modulation of the innate immune system for neuroprotection in ischemic stroke," *Frontiers in Neuroscience*, vol. 9, p. 147, 2015.

[29] M. Asahi, K. Asahi, J. C. Jung, G. J. del Zoppo, M. E. Fini, and E. H. Lo, "Role for matrix metalloproteinase 9 after focal cerebral ischemia: effects of gene knockout and enzyme inhibition with BB-94," *Journal of Cerebral Blood Flow and Metabolism : Official Journal of the International Society of Cerebral Blood Flow and Metabolism*, vol. 20, pp. 1681–1689, 2000.

[30] E. Dejonckheere, R. E. Vandenbroucke, and C. Libert, "Matrix metalloproteinases as drug targets in ischemia/reperfusion injury," *Drug Discovery Today*, vol. 16, pp. 762–778, 2011.

[31] M. He, B. Zhang, X. Wei et al., "HDAC4/5-HMGB1 signalling mediated by NADPH oxidase activity contributes to cerebral ischaemia/reperfusion injury," *Journal of Cellular and Molecular Medicine*, vol. 17, pp. 531–542, 2013.

[32] K. Burridge and E. S. Wittchen, "The tension mounts: stress fibers as force-generating mechanotransducers," *The Journal of Cell Biology*, vol. 200, pp. 9–19, 2013.

[33] E. Vandenbroucke, D. Mehta, R. Minshall, and A. B. Malik, "Regulation of endothelial junctional permeability," *Annals of the new York Academy of Sciences*, vol. 1123, pp. 134–145, 2008.

[34] D. Mehta and A. B. Malik, "Signaling mechanisms regulating endothelial permeability," *Physiological Reviews*, vol. 86, pp. 279–367, 2006.

[35] S. M. Stamatovic, P. Shakui, R. F. Keep et al., "Monocyte chemoattractant protein-1 regulation of blood-brain barrier permeability," *Journal of Cerebral Blood Flow and Metabolism : Official Journal of the International Society of Cerebral Blood Flow and Metabolism*, vol. 25, pp. 593–606, 2005.

[36] F. Chen, Z. Qi, Y. Luo et al., "Non-pharmaceutical therapies for stroke: mechanisms and clinical implications," *Progress in Neurobiology*, vol. 115, pp. 246–269, 2014.

[37] Y. Yang, E. Y. Estrada, J. F. Thompson, W. Liu, and G. A. Rosenberg, "Matrix metalloproteinase-mediated disruption of tight junction proteins in cerebral vessels is reversed by synthetic matrix metalloproteinase inhibitor in focal ischemia in rat," *Journal of Cerebral Blood Flow and Metabolism : Official Journal of the International Society of Cerebral Blood Flow and Metabolism*, vol. 27, pp. 697–709, 2007.

[38] S. E. Lakhan, A. Kirchgessner, D. Tepper, and A. Leonard, "Matrix metalloproteinases and blood-brain barrier disruption in acute ischemic stroke," *Frontiers in Neurology*, vol. 4, p. 32, 2013.

[39] A. Rosell, A. Ortega-Aznar, J. Alvarez-Sabin et al., "Increased brain expression of matrix metalloproteinase-9 after ischemic and hemorrhagic human stroke," *Stroke*, vol. 37, pp. 1399–1406, 2006.

[40] G. C. Jickling, D. Liu, B. Stamova et al., "Hemorrhagic transformation after ischemic stroke in animals and humans," *Journal of Cerebral Blood Flow and Metabolism : Official Journal of the International Society of Cerebral Blood Flow and Metabolism*, vol. 34, pp. 185–199, 2014.

[41] P. H. Chan, "Role of oxidants in ischemic brain damage," *Stroke*, vol. 27, pp. 1124–1129, 1996.

[42] P. H. Chan, "Reactive oxygen radicals in signaling and damage in the ischemic brain," *Journal of Cerebral Blood Flow and Metabolism*, vol. 21, pp. 2–14, 2001.

[43] S. Sciarretta, D. Yee, P. Ammann et al., "Role of NADPH oxidase in the regulation of autophagy in cardiomyocytes," *Clinical Science*, vol. 128, pp. 387–403, 2015.

[44] S. P. Gray and K. Jandeleit-Dahm, "The pathobiology of diabetic vascular complications–cardiovascular and kidney disease," *Journal of Molecular Medicine*, vol. 92, pp. 441–452, 2014.

[45] B. Lassegue, A. San Martin, and K. K. Griendling, "Biochemistry, physiology, and pathophysiology of NADPH oxidases in the cardiovascular system," *Circulation Research*, vol. 110, pp. 1364–1390, 2012.

[46] Y. Maejima, J. Kuroda, S. Matsushima, T. Ago, and J. Sadoshima, "Regulation of myocardial growth and death by NADPH oxidase," *Journal of Molecular and Cellular Cardiology*, vol. 50, pp. 408–416, 2011.

[47] Y. Suzuki, K. Hattori, J. Hamanaka et al., "Pharmacological inhibition of TLR4-NOX4 signal protects against neuronal death in transient focal ischemia," *Scientific Reports*, vol. 2, article 896, 2012.

[48] C. Kleinschnitz, H. Grund, K. Wingler et al., "Post-stroke inhibition of induced NADPH oxidase type 4 prevents oxidative stress and neurodegeneration," *PLoS Biology*, vol. 8, 2010.

[49] A. Manea, L. I. Tanase, M. Raicu, and M. Simionescu, "Transcriptional regulation of NADPH oxidase isoforms, Nox1 and Nox4, by nuclear factor-kappaB in human aortic smooth muscle cells," *Biochemical and Biophysical Research Communications*, vol. 396, pp. 901–907, 2010.

[50] A. Sturrock, B. Cahill, K. Norman et al., "Transforming growth factor-beta1 induces Nox4 NAD(P)H oxidase and reactive oxygen species-dependent proliferation in human pulmonary artery smooth muscle cells," *American Journal of Physiology. Lung Cellular and Molecular Physiology*, vol. 290, pp. L661–L673, 2006.

[51] I. Diebold, A. Petry, J. Hess, and A. Gorlach, "The NADPH oxidase subunit NOX4 is a new target gene of the hypoxia-inducible factor-1," *Molecular Biology of the Cell*, vol. 21, pp. 2087–2096, 2010.

[52] L. Zhang, O. R. Sheppard, A. M. Shah, and A. C. Brewer, "Positive regulation of the NADPH oxidase NOX4 promoter in vascular smooth muscle cells by E2F," *Free Radical Biology & Medicine*, vol. 45, pp. 679–685, 2008.

[53] S. Pendyala, J. Moitra, S. Kalari et al., "Nrf2 regulates hyperoxia-induced Nox4 expression in human lung endothelium: identification of functional antioxidant response elements on the Nox4 promoter," *Free Radical Biology & Medicine*, vol. 50, pp. 1749–1759, 2011.

[54] A. E. Pepe, Q. Xiao, A. Zampetaki et al., "Crucial role of nrf3 in smooth muscle cell differentiation from stem cells," *Circulation Research*, vol. 106, pp. 870–879, 2010.

[55] A. Manea, L. I. Tanase, M. Raicu, and M. Simionescu, "Jak/STAT signaling pathway regulates nox1 and nox4-based NADPH oxidase in human aortic smooth muscle cells," *Arteriosclerosis, Thrombosis, and Vascular Biology*, vol. 30, pp. 105–112, 2010.

[56] B. Wang, X. Zhu, Y. Kim et al., "Histone deacetylase inhibition activates transcription factor Nrf2 and protects against cerebral ischemic damage," *Free Radical Biology & Medicine*, vol. 52, pp. 928–936, 2012.

[57] H. J. Kim, M. Rowe, M. Ren, J. S. Hong, P. S. Chen, and D. M. Chuang, "Histone deacetylase inhibitors exhibit anti-inflammatory and neuroprotective effects in a rat permanent ischemic model of stroke: multiple mechanisms of action," *The Journal of Pharmacology and Experimental Therapeutics*, vol. 321, pp. 892–901, 2007.

[58] D. I. Sinn, S. J. Kim, K. Chu et al., "Valproic acid-mediated neuroprotection in intracerebral hemorrhage via histone deacetylase inhibition and transcriptional activation," *Neurobiology of Disease*, vol. 26, pp. 464–472, 2007.

[59] R. N. Saha and K. Pahan, "HATs and HDACs in neurodegeneration: a tale of disconcerted acetylation homeostasis," *Cell Death and Differentiation*, vol. 13, pp. 539–550, 2006.

[60] A. Fischer, F. Sananbenesi, A. Mungenast, and L. H. Tsai, "Targeting the correct HDAC(s) to treat cognitive disorders," *Trends in Pharmacological Sciences*, vol. 31, pp. 605–617, 2010.

[61] B. Chen and C. L. Cepko, "HDAC4 regulates neuronal survival in normal and diseased retinas," *Science*, vol. 323, pp. 256–259, 2009.

Hindawi
Oxidative Medicine and Cellular Longevity
Volume 2017, Article ID 8398072, 9 pages
https://doi.org/10.1155/2017/8398072

*Research Article*

# The Effects of Blast Exposure on Protein Deimination in the Brain

**Peter J. Attilio,[1] Michael Flora,[2] Alaa Kamnaksh,[2] Donald J. Bradshaw,[1] Denes Agoston,[2] and Gregory P. Mueller[2]**

[1]*Neuroscience Program, Uniformed Services University of the Health Sciences, Bethesda, MD, USA*
[2]*Department of Anatomy, Physiology and Genetics, Uniformed Services University of the Health Sciences, Bethesda, MD, USA*

Correspondence should be addressed to Gregory P. Mueller; gregory.mueller@usuhs.edu

Received 19 January 2017; Accepted 16 March 2017; Published 24 May 2017

Academic Editor: Francisco J. Romero



Oxidative stress and calcium excitotoxicity are hallmarks of traumatic brain injury (TBI). While these early disruptions may be corrected over a relatively short period of time, long-lasting consequences of TBI including impaired cognition and mood imbalances can persist for years, even in the absence of any evidence of overt injury based on neuroimaging. This investigation examined the possibility that disordered protein deimination occurs as a result of TBI and may thus contribute to the long-term pathologies of TBI. Protein deimination is a calcium-activated, posttranslational modification implicated in the autoimmune diseases rheumatoid arthritis and multiple sclerosis, where aberrant deimination creates antigenic epitopes that elicit an autoimmune attack. The present study utilized proteomic analyses to show that blast TBI alters the deimination status of proteins in the porcine cerebral cortex. The affected proteins represent a small subset of the entire brain proteome and include glial fibrillary acidic protein and vimentin, proteins reported to be involved in autoimmune-based pathologies. The data also indicate that blast injury is associated with an increase in immunoglobulins in the brain, possibly representing autoantibodies directed against novel protein epitopes. These findings indicate that aberrant protein deimination is a biomarker for blast TBI and may therefore underlie chronic neuropathologies of head injury.

## 1. Introduction

Central features in traumatic brain injury (TBI) include oxidative stress [1–4], breakdown of the blood brain barrier [5, 6], and a protracted period of $Ca^{2+}$ excitotoxicity [7, 8]. These early consequences of brain injury set the stage for the progressive development of long-term pathologies including impaired learning and memory, as well as emotional and mood imbalances [9–13]. These long-term consequences of TBI can be complex and may increase in severity over months and years, even though the injury may have been classified as clinically mild, and there is no evidence of physical injury using the most sensitive of imaging techniques [14, 15]. At present, there is a gap in our knowledge linking the acute events of mild TBI to chronic pathology. Importantly, repeated mild TBI has now been identified as the most significant environmental factor for developing chronic neuropsychiatric symptoms [16–18].

The purpose of this study was to determine if aberrant deimination of brain proteins occurs in response to TBI and, therefore, potentially contributes to the long-term consequences of TBI. Deimination, or citrullination, is a post-translational modification involving the calcium-dependent conversion of peptidyl-arginine to peptidyl-citrulline catalyzed by peptidylarginine deiminase (PAD) (Figure 1). This modification can result in the creation of novel, potentially antigenic epitopes that can elicit autoimmune responses [19, 20] (Figure 1). Specifically, disordered deimination of the joint proteins, filaggrin [21] and vimentin [22], generates antigenic epitopes [23] which can trigger a sustained autoimmune attack that eventually destroys the synovial compartment [24]. Disorders in protein deimination are also implicated in the diseases of the central nervous system, most notably multiple sclerosis [25–27], where the deimination of myelin basic protein appears to underlie a sustained autoimmune attack against the deiminated protein [28]. There is

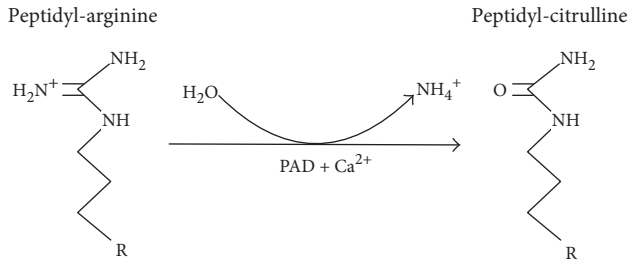


Figure 1: Protein deimination is catalyzed by a family of structurally related, calcium-dependent enzymes known as peptidylarginine deiminases (PADs). Protein deimination involves the conversion of an intraprotein arginine residue to a citrulline residue, resulting in the loss of a positively charged amine group and 1 Da in molecular mass.

increasing interest in the possibility that the immune system plays a role in the long-term pathogenesis of TBI [29, 30].

It was previously reported that controlled cortical impact in rodents selectively alters the deimination status of a subset of proteins constituting the brain proteome [31], presumably due to injury-induced conditions of oxidative stress and calcium excitotoxicity. The present investigation was designed to extend these findings to a large animal model using blast injury as a noninvasive form of TBI. As seen with direct cortical injury in rodents [31], only a small subset of the entire brain proteome underwent blast-induced deimination in the porcine brain. Two of the six proteins identified as being deiminated were vimentin and glial fibrillary acidic protein (GFAP). The deimination sites found within vimentin and GFAP corresponded to previously reported sites of deimination, respectively, in rheumatoid arthritis and in multiple sclerosis [32] and Alzheimer's disease [33, 34]. Moreover, the levels of immunoglobulin G (IgG) detected in the brains of blast-exposed animals were markedly elevated as compared to those present in control animals, possibly representing autoantibodies directed against novel protein epitopes. These findings indicate that aberrant protein deimination may be a biomarker for blast TBI and may therefore underlie chronic neuropathologies through mechanisms involving the adaptive immune system.

## 2. Materials and Methods

*2.1. Animals.* Studies were conducted in adult male Yucatan miniature and Yorkshire swines (Sinclair BioResources, LLC., and Archer Farms, Darlington, MD, respectively) weighing 40–50 kg, $N = 4$/group). Animals were cared for and treated in accordance with guidelines approved by the US Department of Agriculture and the Medical Research and Material Command of the US Army.

Anesthetized pigs in the injured group were positioned in sternal recumbency and equipped with a specially made Kevlar and lead body armor as well as head and face protection. Animals were then transferred to a blast tube, simulating free-field blast, where they received a single moderate blast overpressure exposure (40–52 psi, average = 46 psi). Details pertaining to anesthesia, pre- and postprocedural treatments, and blast structure were as described earlier [5, 35–37]. Immediately after blast exposure, animals were removed from the blast structure and returned to the adjacent procedure facility for recovery. The endotracheal tube was maintained until animals exhibited normal pharyngeal function via cough reflex. Physiological parameters were electronically recorded by the monitoring system until animals were fully recovered from anesthesia and returned to their holding cages. In the days that followed, animals were assessed for pain or distress and monitored for general health as well as cranial nerve and neurologic and respiratory functions.

All animals were euthanized 2 weeks after exposure, and whole brains were collected and rinsed in physiologic saline. Coronal sections were prepared (0.75 inches thick), snap frozen on dry ice, and stored at −80°C until used.

*2.2. Sample Preparation.* Brain sections of frontal cortex were thawed and further dissected to produce wedges of tissue that contained an equivalent representation of all layers of the cerebral cortex frontal lobe. Tissue samples were homogenized in 5 volumes/tissue weight of 0.1 M Tris buffer (pH 7.4) containing 1x complete protease inhibitors using a Polytron (setting 6; 3 × 15 second pulses, with chilling in between) (Roche, Basel, Switzerland) followed by 3 freeze-thaw cycles and centrifugation (20000 ×g, 15 min, 4°C). The resulting supernatants were removed and stored at −80°C until used.

*2.3. Liquid-Phase Isoelectric Focusing.* Liquid-phase isoelectric focusing (LP-IEF) of brain supernatants was carried out as previously described [31]. Briefly, treatment group pools (naïve and blast, $N = 4$/group) underwent concentration and buffer exchange to water/1x protease inhibitors by Vivaspin (10 kDa molecular weight cut off (MWCO); General Electric, Fairfield, CT), removing TRIS which interferes with LP-IEF. Samples were then diluted in 1.1x IEF running solution (7.7 M urea, 2.2 M thiourea, and 4.4% CHAPS) and 1x complete protease inhibitor (1 part sample/9 parts IEF buffer). Samples were further adjusted for IEF fractionation by combining 900 $\mu$L pooled sample with ampholytes (150 $\mu$L, pH 3–10; Novex, Thermo Fisher, ZM0021; Waltham, MA), dithiolthreitol (DTT; 25 $\mu$L, 4 M), and bromphenol blue (20 $\mu$L, 10 mg/mL). IEF fractionation was performed under the following conditions: (1) 100 V, 2 mA, 2 W (20 min); (2) 200 V, 2 mA, 2 W (80 min), (3) 400 V, 2 mA, 2 W (80 min), and (4) 600 V, 2 mA, 2 W (80 min) using the ZOOM IEF Fractionator (Thermo Fisher, Waltham, MA). The resulting fractionation produced samples corresponding to the predicted IEF pH ranges for the fractionator (pH 3.0–4.6, pH 4.6–5.4, pH 5.4–6.2, pH 6.2–7.0, and pH 7.0–9.1) as judged by pH testing using pH strips. 1-dimensional gel electrophoresis and Coomassie staining (see below) were used to confirm equivalent fraction profiles for the naïve and blast samples and to verify equivalent protein concentrations for the naïve and blast samples of the same pH range.

*2.4. 1-Dimensional Gel Electrophoresis.* IEF fractions were further resolved by molecular weight fractionation using conventional sodium dodecyl sulfate polyacrylamide gel electrophoresis (SDS-PAGE). This two-step reduction in

the complexity of the proteome by IEF and SDS-PAGE was important for the visualization of deiminated proteins by western blot analysis. Briefly, IEF samples were diluted in 4x reducing loading buffer (10% LDS, 10% glycerol, 0.4 M DTT, 250 mM Tris buffer, 20 $\mu$L bromphenol blue (10 mg/mL), pH 8.4), heated at 70°C (10 min), and then fractionated in NuPage 4–12% Bis-Tris gels (Novex, Thermo Fisher, Waltham, MA), using 1x MES (2-[N-morpholino] ethanesulfonic acid) running buffer (9.76 gm/L MES, 60.6 gm/L Tris Base, 0.3 gm/L disodium ethylenediaminetetraacetic acid (EDTA), and 1 gm/L SDS, pH 8). Proteins were transferred to nitrocellulose using an iBlot transfer system (Thermo Fisher, Waltham, MA).

### 2.5. Immunoblotting

*2.5.1. Protein Deimination.* Nitrocellulose membranes were blocked with 5% nonfat dry milk/Tris-buffered saline/Tween 20 (TBS-T) (25 mM Tris Base, 0.115 M NaCl, 25 mM KCl, 0.1% Tween20, and pH 7.5) for 2 h at room temperature and then incubated overnight at 4°C with mouse monoclonal anti-protein citrulline primary antibody 6B3 [31, 38] (stock = 1.79 mg/mL) diluted (1 : 500) in 5% nonfat dry milk/TBS-T. Membranes were then washed in TBS-T (3 times over 60 min), incubated with secondary antibody (HRP-conjugated goat anti-mouse IgG (H+L), 31430, 1 : 2500 in TBS-T; Thermo Fisher, Waltham, MA) at room temperature for 2 h. Membranes were then washed in TBS-T (3 times over 60 min) and then visualized with enhanced chemiluminscence (ECL) (Novex ECL HRP Chemiluminescent Substrate Reagent Kit; WP20005, Invitrogen, Thermo Fisher, Waltham, MA) using the ChemiDoc Touch imaging system (Bio-Rad Laboratories, Hercules, CA). The specificity of the 6B3 mAb for detecting deiminated proteins was verified as described previously [31]. Images collected were analyzed using Image Lab software (v5.2.1, Bio-Rad Laboratories; Hercules, CA). Anti-peptidyl-citrulline, clone F95 antibody, was obtained commercially from Millipore (ab# MABN328, Darmstadt, Germany) and used similarly.

*2.5.2. Tissue IgG.* Nitrocellulose membranes were blocked with 5% nonfat dry milk in TBS-T (2 h, room temperature) and then incubated with goat anti-porcine IgG (H+L), HRP-conjugated antibody (1 : 2500 in TBS-T, EMD Millipore, Billerica, MA, AP166P) at room temperature for 2 h. Membranes were then washed in TBS-T (3 times over 60 min) and then visualized and analyzed as described for protein deimination above. Quantitation of the ECL Western blot signals was based upon standardization to protein load for each sample, as determined by the signal density for equivalent samples visualized on Coomassie-stained gels. ImageJ (Mac Version 1.50i, National Institutes of Health) was used to determine both ECL and Coomassie data; signal densities of immunoreactive ECL features (heavy and light chain bands) were summed and adjusted for protein load based upon a percent difference from a reference protein load (highest protein load of control samples = 100%).

*2.6. Protein Identification and Mapping of Deimination Sites.* Immunoreactive signals of interest were mapped to corresponding banding patterns of the Coomassie-stained gels. The bands were excised and analyzed by peptide mass finger printing and tandem mass spectrometry (MS-MS) using the proteomic services of the W.M. Keck Foundation Biotechnology Resource Laboratory (New Haven CT, USA). Briefly, gel bands were cut into smaller pieces, digested with trypsin, peptides extracted and desalted, and analyzed by liquid chromatography (LC) MS-MS using an Orbitrap Fusion Tribrid mass spectrometer (Thermo Fisher, Waltham, MA). Both MS and MS/MS scans were acquired in an Orbitrap analyzer. MS scans were of m/z range 350–1550, resolution of 120000, AGC (automatic gain control) target of 2e5, and maximum injection time of 60 ms, while MS/MS scans were with fixed first mass of m/z 120, resolution of 60000, AGC target of 5e4, and maximum injection time of 110 ms. Precursor ions were fragmented by high energy collision-induced dissociation collision energy (%) set to 28.

The raw files were processed using Proteome Discoverer v2.1 software (Thermo Fisher, Waltham, MA). The files were searched with Sequest HT algorithm against pig UniProt database (downloaded June 2016). The fragment ion mass tolerance of 0.02 Da, parent ion tolerance of 10 ppm, and digestion enzyme trypsin were specified in the Sequest analysis parameters. Oxidation of methionine, deamidation of asparagine and glutamine, deimination (citrullination) of arginine, and propionamide of cysteine were specified in Sequest as variable modifications.

Scaffold software (v4.6.1, Proteome Software) was used to validate peptide and protein identifications. Initial protein analysis was performed with a protein threshold of 99%, a minimum of 3 peptides, and a peptide threshold of 95%. The inclusion criteria for peptides with a deiminated arginine were an Xcorr of 2 or more and a deltaCn of >0.4. Peptides meeting these criteria were then assessed for a 43 Da neutral loss assessing for the loss of isocyanic acid (HNCO) through spectrometric analysis described by Hao et al. [37]. All spectra were visually reviewed to insure quality and clear presence of the 43 Da neutral loss signature for deimination.

The expected mass of the neutral loss of isocyanic acid was determined by subtracting the product of a 43 Da loss divided by the peptide charge from the observed mass of the peptide sequence [37]. Peaks corresponding to the expected neutral loss were identified in the spectrum data and included if an observed peak was less than 2 Da from the expected peak. The only exception to this was GABA transaminase (4-aminobutyrate aminotransferase) that had peaks identified at approximately 3 Da from the expected neutral loss mass. This tentative identification was included here based on the high quality of the spectrum, Xcorr, and deltaCn.

*2.7. Statistical Analysis.* The quantitation of the IgG ECL western blot signals was based on standardization to protein load for each sample, as determined by the signal density for equivalent samples visualized on Coomassie-stained gels. ImageJ (Mac version 1.50i, National Institutes of Health) was used to determine both ECL and Coomassie data; signal densities of immunoreactive ECL features (heavy and light chain bands) were summed and adjusted for protein load based on a percent difference from a reference protein load

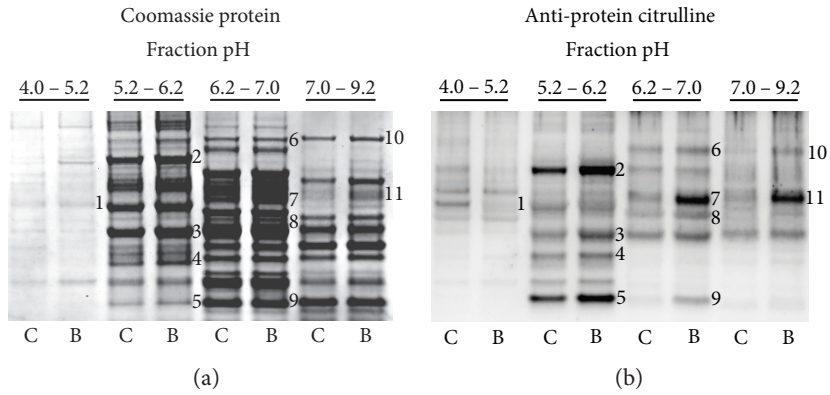


Figure 2: Blast-induced deimination of proteins in porcine brain. Brain samples were collected 2 weeks following a single blast exposure (average pressure = 46 psi). Homogenates of control (C) and the blast-exposed (B) cerebral cortex were prefractionated by LP-IEF. The resulting pH fractions were further fractionated by 1-dimensional SDS-PAGE (a) and analyzed for protein deimination by western blotting (b) using the mouse monoclonal 6B3 anti-protein citrulline antibody. Immunoreactive features affected by TBI (numbered, panel (b)) were mapped to corresponding bands in a Coomassie-stained protein gel (numbered, panel (a)). These were collected, identified, and mapped for site-specific deimination by peptide mass fingerprinting using liquid chromatography and tandem mass spectrometry (LC MS/MS).

(highest protein load of control samples = 100%). Analysis of the combined relative signal intensity of the IgG naïve and blast results was performed using Prism 7 for Mac OS X (v7.0a, GraphPad Software Inc.). An unpaired *t*-test was performed with the standard variance assumed to be equal in the population. Statistical significance was determined using the Holm-Sidak method with an alpha of 0.05.

## 3. Results

Figure 2 shows the effects of blast exposure on the status of protein deimination in the porcine cerebral cortex. Brains were collected 2 weeks postblast exposure, and cerebral cortex homogenates were prepared from each subject. Treatment group pools of sham and blast samples, representing 4 animals each, underwent two-dimensional fractionation involving liquid phase isoelectric focusing (LP-IEF) followed by molecular weight fractionation using 1-dimensional sodium dodecyl sulfate polyacrylamide gel electrophoresis (SDS-PAGE). These steps for reducing the complexity of the proteome were necessary to clearly reveal western blot signals in the analyses of protein deimination. Panel (a) shows the Coomassie-stained protein profiles for the control and blast groups over the four LP-IEF pH fractions. The data show that LP-IEF yielded pH fractions with distinct protein profiles, indicating the effectiveness of the IEF procedure to separate a complex proteome into subfractions having reduced protein complexity. It was also observed that within a given pH fraction, there was no apparent difference in the Coomassie-banding profile between the control and blast samples with the exception of feature 11. This feature, which had increased Coomassie staining in the blast-exposed fraction, was determined to contain IgG by both mass spectrometric and western blot analyses.

The effects of blast exposure on the profile of protein deimination, using 6B3 antibody western blotting, is shown in panel (b). These data indicate that there is a basal level of protein deimination in the control condition that involves a small subset of the proteins making up the entire brain proteome. Further, blast exposure dramatically affected the deimination status of several, but not all of these features. In most cases, blast exposure resulted in a pronounced increase in the observed deimination signal (features 2–11), in some cases increasing from virtually no signal in the control condition (feature 9). There was also evidence for blast exposure in reducing the degree of protein deimination within a protein band, as can be most clearly seen for feature 1. Preliminary findings with an alternative anti-protein citrulline antibody, F95, identified some features that were not revealed by antibody 6B3 and vice versa (not shown), suggesting that the amino acid context of a deimination site contributes to its antibody recognition. Additionally, it was observed that deimination signals observed by western blot were reduced upon repeated freeze-thaw cycles of the samples, indicating the importance of preparing sample aliquots for storage and repeat analyses.

Immunoreactive features identified by 6B3 western blotting (panel (b), features 1–11) were mapped to corresponding protein bands in a replicate Coomassie-stained protein gel (panel (a), features 1–11). These bands were collected and analyzed proteomically to identify the proteins present and to map their respective deimination sites. Site-specific deimination was confirmed by the demonstration of neutral loss of 43 Da representing the signature deimination fragment isocyanic acid [37] (Figure 3) (see Materials and Methods for details). Table 1 presents a list of the 6 proteins definitively identified and their respective deimination sites. The findings include deiminated GFAP and vimentin, both of which are recognized as autoantigens in neuropathology [39] and rheumatoid arthritis [40], respectively. Western blotting for protein deimination employed an anti-mouse IgG detection antibody that was subsequently shown to cross-react with porcine IgG. This reagent revealed an intense signal in feature 11 of the blast brain pool (Figure 2

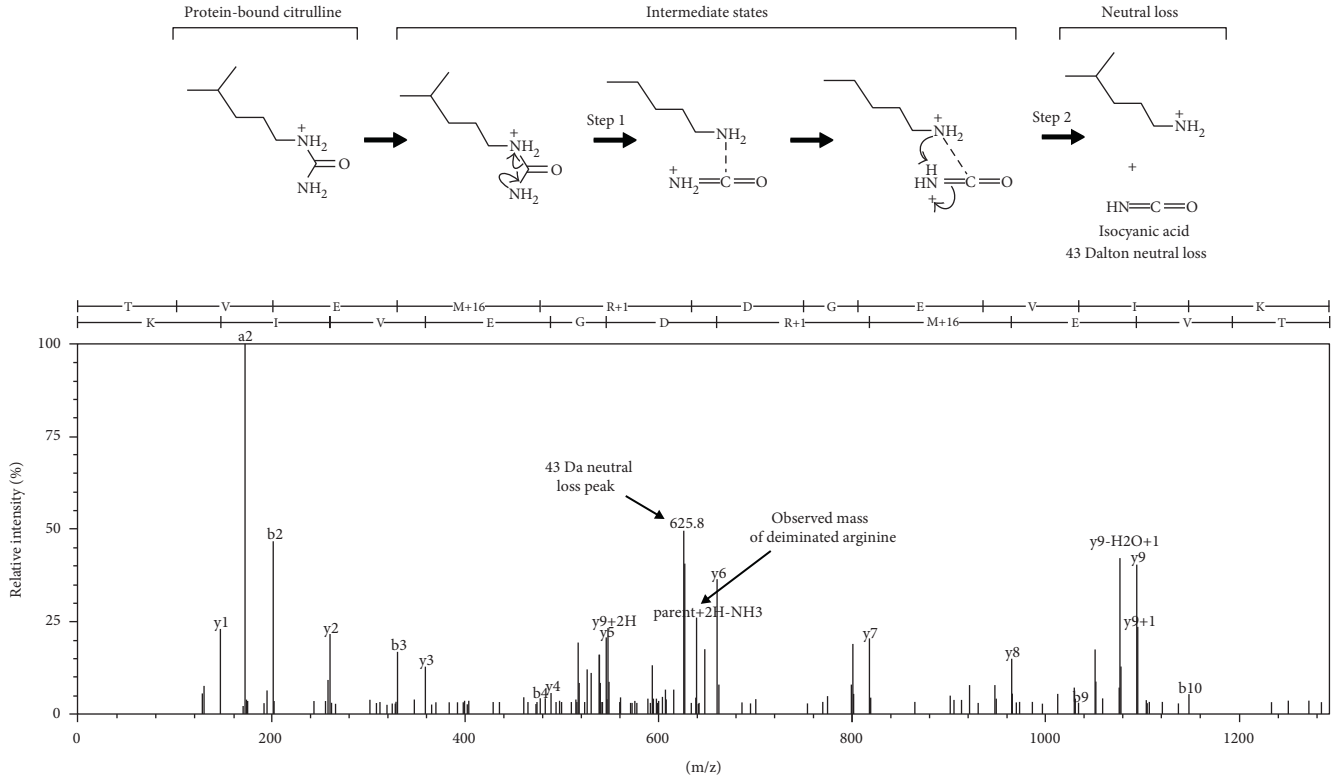


Figure 3: Mapping of protein deimination sites by neutral loss. Tryptic peptides were fragmented by collision-induced dissociation, and resulting spectra were analyzed for a neutral loss of 43 Da, reflecting the loss of isocyanic acid as a fragmentation product of citrulline (upper panel). The representative spectrum shown here depicts the Y and B ion spectra of GFAP peptide, TVEMrDGEVIK, with the neutral loss peak observed for the deiminated arginine (r) at 625.8 Da. Because the parent peptide ion was doubly charged in this case, the observed neutral loss in the spectrum was 21.5 Da, reflecting 43 Da/2.

Table 1: Mapping deimination sites in brain proteins of swine exposed to repeated mild blast exposure.

| Protein | Peptide sequence | Observed mass | Charge state | Expected mass with neutral loss | Mass of peak detected |
|---|---|---|---|---|---|
| GABA transaminase | LVQQPQNVSTFIN**R**PALGILPPENFVEK | 1050.57 | 3 | 1036.24 | 1033.28 |
| Aconitate hydratase | LN**R**PLTLSEK | 391.23 | 3 | 376.89 | 376.67 |
| Glial fibrillary acidic protein | ITIPVQTFSNLQI**R**ETSLDTK | 802.43 | 3 | 788.10 | 789.75 |
| | TVEM**R**DGEVIK | 647.32 | 2 | 625.82 | 625.82 |
| Glutathione S-transferase | AFLASPEHVN**R**PINGNGK | 481.25 | 4 | 470.50 | 469.23 |
| Histone H4 | ISGLIYEET**R**GVLKVFLENVIRDAVTYTEHAK | 733.80 | 5 | 725.20 | 726.32 |
| Vimentin | TVET**R**DGQVINETSQHHDDLE | 808.70 | 3 | 794.37 | 794.37 |

**R** = deimination site.

feature 11) that was not pronounced in the control pool. Proteomic analysis determined that the dominant protein in this immunoreactive feature was, indeed, porcine IgG as opposed to another protein that had reacted with the 6B3 primary antibody. The increased presence of IgG in the injured cortex was further verified by using a separate detection antibody specific to porcine IgG (Figure 4), suggesting that an adaptive immune response to blast injury may have occurred in these animals. An analysis of the individual samples making up the pools of naïve and blast-injured brain tissue further confirmed that blast injury was associated with significantly elevated levels of IgG in the cerebral cortex. The Coomassie-stained protein profile for each sample is presented in panel (a). The corresponding western blot for porcine IgG is shown in panel (b) (Figure 4). Panel (c) represents an integration analysis of the western blot signal intensities for IgG heavy and light chains (panel (b)), standardized to total protein load (panel (a)). The data show that blast significantly increased the amount of IgG detected in the cerebral cortex of blast-exposed swine. Variations in this response were observed among subjects, possibly reflecting variations in the degree of injury caused by the blast exposure.

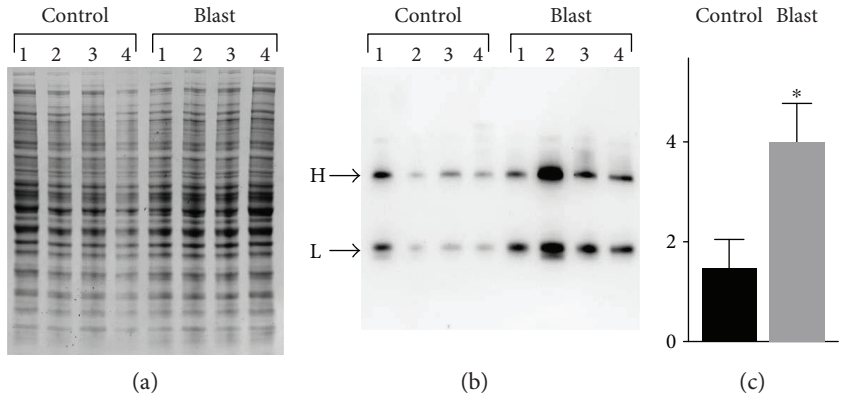


Figure 4: Effects of blast exposure on the presence of IgG expression in the cerebral cortex of swine. Homogenates of control and the blast-exposed (2 weeks postinjury) cerebral cortex (N-4/group) were fractionated by (a) 1-dimensional SDS-PAGE and (b) analyzed for IgG content by western blotting. Immunoreactive heavy (H) and light (L) chain IgGs were visualized using an anti-porcine IgG detection antibody. The values for the total IgG chemiluminescence signal (H+L) (c) for each sample were standardized to protein load (a) by densitometry analysis using ImageJ, and resulting values were analyzed statistically. The relative signal intensity is shown on the $y$-axis as densitometry values ×100. Data are presented as the mean ± standard error; $^{*}p \leq 0.005$.

## 4. Discussion

Brain injury can result in long-term symptomologies that include impaired learning and memory; poor concentration/attention; slowed thinking; emotional and mood imbalances including increased anxiety, depression, disorientation, and headaches; and emotional and cognitive dysfunction. These problems can persist for years after injury, often in the absence of any detectable neuropathology [14, 15]. At the cellular level, however, brain injury can result in a sustained state of neuroinflammation that is reflected in the pro-inflammatory, M1 phenotype of microglia [41, 42]. The persistence of these responses is consistent with the involvement of the adaptive immune system [29, 30]. The present findings raise the possibility that aberrant deimination of specific brain proteins, with the resulting generation of antigenic epitopes, may be an important mechanism in this phenomenon.

The data presented here demonstrate that blast injury upregulates the deimination of a small subset of the proteins making up the entire brain proteome. Additionally, it was also observed that the deimination status of certain protein features was reduced following blast exposure. Together, these observations indicate that (i) protein deimination normally takes place in the brain, (ii) aberrant deimination occurs in response to brain injury, and (iii) protein deimination may be reversible, analogous to phosphorylation. While the extent to which aberrant protein deimination contributes to injury-induced neuropathology has yet to be determined, recent findings in humans show that a history of concussions or documented brain injury is associated with the expression of brain-specific autoantibodies against GFAP [39] and S100b [43]. An important question facing this research area concerns the potential role of deimination in establishing the autoimmune response to these and other proteins following brain injury.

A working model for the sequence of events that could result in a brain-specific autoimmune response to injury is presented in Figure 5. Central to this model are injury-induced oxidative stress and calcium excitotoxicity, activation of PADs and aberrant protein deimination, T- and B-cell activation in response to novel deiminated autoantigens, and the resulting establishment of a chronic inflammatory state via sustained activation of the adaptive immune system. This potential mechanism involving the adaptive immune system presents a substantial concern for long-term pathogenesis, as well as a target for therapy. Also depicted in the model are three avenues for therapeutic intervention that address the inhibition of PAD, as well as T- and B-cell activation. To date, PAD inhibitors have not been tested in humans, although one or more prototype drugs are expected to reach clinical trials soon. Recent evidence indicates that the therapeutic effectiveness of the autoimmune therapies, abatacept [44] and rituximab [45, 46], in rheumatoid arthritis is directly related to the titer of autoantibodies reactive to deiminated proteins. Accordingly, models of long-term brain injury involving an autoimmune response to deiminated proteins may benefit from these therapies.

The relations between protein deimination and the adaptive immune system in rheumatoid arthritis and neurodegenerative diseases suggest that these states may share a common mechanism. As reported for rheumatoid arthritis, multiple sclerosis [47], Alzheimer's disease [48], and prion disease [49] have distinctive profiles of protein deimination. The vimentin sequence of TVET**r**DGQVINETSQHHDDLE identified here in blast injury precisely matches the site (indicated by "**r**") found to be deiminated in rheumatoid arthritis [40]. Moreover, the deimination site in GFAP observed here, TVEM**r**DGEVIK, was reported as a possible deimination site in Alzheimer's disease [33, 34] and the core sequence of this peptide, EM**r**DGEVIK, has also been shown to be reactive with circulating autoantibodies in a patient with relapsing-remittent multiple sclerosis [32]. On the basis of these findings, it is proposed that aberrant protein deimination and subsequent involvement of the adaptive immune system

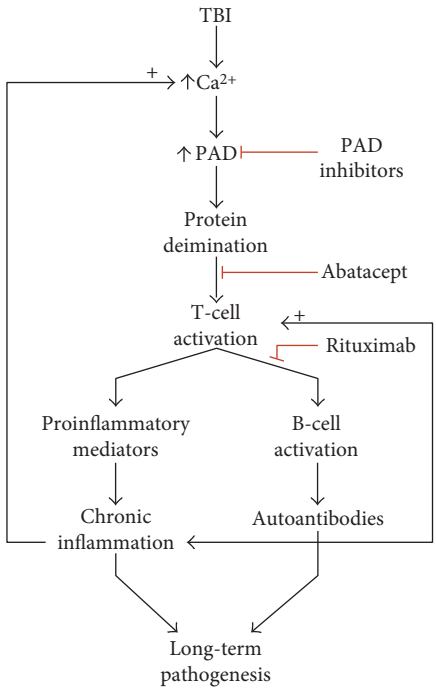


Figure 5: Proposed mechanism for the role of aberrant protein deimination in an autoimmune response to brain injury. TBI-induced calcium excitotoxicity hyperactivates PAD resulting in an abnormal pattern of protein deimination. Cells of the adaptive immune system process the modified proteins to reveal antigenic epitopes created by deimination. Antigen presentation and T-cell activation subsequently lead to the activation of B-cells for the production of autoantibodies and chronic neuroinflammation. It is proposed that these mechanisms contribute to long-term pathologies that can result from TBI. Potential therapeutic interventions that inhibit protein deimination and T-cell and B-cell activation are depicted with red lines.

may be an underlying mechanism shared by chronic neurodegenerative diseases and classical autoimmune diseases.

Finally, this study has several limitations that should be noted. Among these are a relatively small N size (4 animals per group), the presence of only one time point (2 weeks postblast), one blast condition (40–52 psi), and one gender (male). Additionally, by necessity, the discovery proteomic analyses were performed on treatment group pools and evaluated one, albeit major brain region, the frontal cortex. As such, this research does not account for individual differences and the likelihood that blast injury effects may vary across animals and brain regions. This potential for animal variation is suggested by differences in the presence of IgGs, possibly autoantibodies, in the brain samples from individual animals (Figure 4). Nevertheless, our preliminary study identified a short list of specific proteins and their respective epitopes that can be used to focus further investigations into the questions raised here.

In summary, the research presented here shows that blast injury affects the deimination status of select brain proteins. This finding provides the basis for a mechanistic link between the acute processes of brain injury and the expression of sustained neuropathology involving activation of the adaptive immune system. The potential role for abnormally deiminated proteins in this mechanism is supported by the firmly established role for protein deimination in the hallmark autoimmune disease, rheumatoid arthritis. Recent evidence that abnormal protein deimination may play a similar role in multiple sclerosis and other neurodegenerative diseases [25, 27, 28, 50] indicates that the use of acute therapies targeting protein deimination may be of value in mitigating the long-term consequences of blast and perhaps other forms of brain injury.

## 5. Conclusions

Blast-induced brain injury can result in long-term sequelae for which there is no known underlying mechanism. Here, we propose a role for the adaptive immune system in mediating chronic pathologies of brain injury. Blast injury establishes a cellular environment that promotes aberrant protein deimination via activation of the calcium-dependent enzymes involved. The deimination modification can generate antigenic epitopes for activation of a sustained autoimmune response. The present findings show that blast exposure selectively increases the deimination of a small segment of the brain proteome, which includes proteins known to be involved in the autoimmune-based pathologies of multiple sclerosis and possibly, Alzheimer's disease. The data further demonstrate that blast injury is associated with an increase in IgG levels in the brain, possibly representing autoantibodies directed against novel deiminated protein epitopes. Together, these findings provide support for a mechanistic link between injury-induced protein deimination and pathogenic responses of the adaptive immune system.

## Ethical Approval

Animal handling and treatments were conducted in compliance with the Animal Welfare Act and other Federal statutes and regulations related to animals and experiments involving animals and adhered to principles stated in the Guide to the Care and Use of Laboratory Animals, National Research Council. The facilities are fully accredited by the Association for Assessment and Accreditation of Laboratory Animal Care International.

## Disclosure

The views, opinions, and/or findings contained herein are those of the authors and should not be interpreted as the official views or policies, either expressed or implied, of DARPA, the Uniformed Services University, the Department of the Army, or the Department of Defense. The paper is approved for public release; distribution is unlimited.

## Conflicts of Interest

The authors declare no conflict of interest.

## Acknowledgments

The authors would like to acknowledge Drs. G. Martinelli and G. Holstein for providing the 6B3 monoclonal antibody used here. They also wish to acknowledge funding by USUHS Intramural Grant no. 92-447 (to Gregory P. Mueller), DMRDP Grant W81XWH-13-C-0196 (to R. Diaz-Arrastia and Gregory P. Mueller), and DARPA PREVENT (to Denes Agoston).

## References

[1] M. A. Ansari, K. N. Roberts, and S. W. Scheff, "Oxidative stress and modification of synaptic proteins in hippocampus after traumatic brain injury," *Free Radical Biology & Medicine*, vol. 45, no. 2, pp. 443–452, 2008.

[2] R. S. Darwish, N. Amiridze, and B. Aarabi, "Nitrotyrosine as an oxidative stress marker: evidence for involvement in neurologic outcome in human traumatic brain injury," *The Journal of Trauma*, vol. 63, no. 2, pp. 439–442, 2007.

[3] L. E. Goldstein, A. M. Fisher, C. A. Tagge et al., "Chronic traumatic encephalopathy in blast-exposed military veterans and a blast neurotrauma mouse model," *Science Translational Medicine*, vol. 4, no. 134, p. 134ra160, 2012.

[4] W. O. Opii, V. N. Nukala, R. Sultana et al., "Proteomic identification of oxidized mitochondrial proteins following experimental traumatic brain injury," *Journal of Neurotrauma*, vol. 24, no. 5, pp. 772–789, 2007.

[5] N. C. de Lanerolle, F. Bandak, D. Kang et al., "Characteristics of an explosive blast-induced brain injury in an experimental model," *Journal of Neuropathology and Experimental Neurology*, vol. 70, no. 11, pp. 1046–1057, 2011.

[6] D. Shlosberg, M. Benifla, D. Kaufer, and A. Friedman, "Blood-brain barrier breakdown as a therapeutic target in traumatic brain injury," *Nature Reviews. Neurology*, vol. 6, no. 7, pp. 393–403, 2010.

[7] I. Fineman, D. A. Hovda, M. Smith, A. Yoshino, and D. P. Becker, "Concussive brain injury is associated with a prolonged accumulation of calcium: a 45Ca autoradiographic study," *Brain Research*, vol. 624, no. 1, pp. 94–102, 1993.

[8] D. A. Sun, L. S. Deshpande, S. Sombati et al., "Traumatic brain injury causes a long-lasting calcium (Ca2+)-plateau of elevated intracellular Ca levels and altered Ca2+ homeostatic mechanisms in hippocampal neurons surviving brain injury," *The European Journal of Neuroscience*, vol. 27, no. 7, pp. 1659–1672, 2008.

[9] H. G. Belanger, Z. Proctor-Weber, T. Kretzmer, M. Kim, L. M. French, and R. D. Vanderploeg, "Symptom complaints following reports of blast versus non-blast mild TBI: does mechanism of injury matter?" *The Clinical Neuropsychologist*, vol. 25, no. 5, pp. 702–715, 2011.

[10] G. A. Elder, N. P. Dorr, R. De Gasperi et al., "Blast exposure induces post-traumatic stress disorder-related traits in a rat model of mild traumatic brain injury," *Journal of Neurotrauma*, vol. 29, no. 16, pp. 2564–2575, 2012.

[11] H. S. Levin, E. Wilde, M. Troyanskaya et al., "Diffusion tensor imaging of mild to moderate blast-related traumatic brain injury and its sequelae," *Journal of Neurotrauma*, vol. 27, no. 4, pp. 683–694, 2010.

[12] B. A. Schultz, D. X. Cifu, S. McNamee, M. Nichols, and W. Carne, "Assessment and treatment of common persistent sequelae following blast induced mild traumatic brain injury," *NeuroRehabilitation*, vol. 28, no. 4, pp. 309–320, 2011.

[13] R. D. Vanderploeg, H. G. Belanger, R. D. Horner et al., "Health outcomes associated with military deployment: mild traumatic brain injury, blast, trauma, and combat associations in the Florida National Guard," *Archives of Physical Medicine and Rehabilitation*, vol. 93, no. 11, pp. 1887–1895, 2012.

[14] K. Blennow, D. L. Brody, P. M. Kochanek et al., "Traumatic brain injuries," *Nature Reviews Disease Primers*, vol. 2, p. 16084, 2016.

[15] H. Zetterberg and K. Blennow, "Fluid biomarkers for mild traumatic brain injury and related conditions," *Nature Reviews. Neurology*, vol. 12, no. 10, pp. 563–574, 2016.

[16] G. L. Iverson, A. J. Gardner, P. McCrory, R. Zafonte, and R. J. Castellani, "A critical review of chronic traumatic encephalopathy," *Neuroscience and Biobehavioral Reviews*, vol. 56, pp. 276–293, 2015.

[17] B. P. Lucke-Wold, R. C. Turner, A. F. Logsdon, J. E. Bailes, J. D. Huber, and C. L. Rosen, "Linking traumatic brain injury to chronic traumatic encephalopathy: identification of potential mechanisms leading to neurofibrillary tangle development," *Journal of Neurotrauma*, vol. 31, no. 13, pp. 1129–1138, 2014.

[18] A. C. McKee, R. C. Cantu, C. J. Nowinski et al., "Chronic traumatic encephalopathy in athletes: progressive tauopathy after repetitive head injury," *Journal of Neuropathology and Experimental Neurology*, vol. 68, no. 7, pp. 709–735, 2009.

[19] K. L. Bicker and P. R. Thompson, "The protein arginine deiminases: structure, function, inhibition, and disease," *Biopolymers*, vol. 99, no. 2, pp. 155–163, 2013.

[20] B. Gyorgy, E. Toth, E. Tarcsa, A. Falus, and E. I. Buzas, "Citrullination: a posttranslational modification in health and disease," *The International Journal of Biochemistry & Cell Biology*, vol. 38, no. 10, pp. 1662–1677, 2006.

[21] E. Girbal-Neuhauser, J. J. Durieux, M. Arnaud et al., "The epitopes targeted by the rheumatoid arthritis-associated antifilaggrin autoantibodies are posttranslationally generated on various sites of (pro)filaggrin by deimination of arginine residues," *Journal of Immunology*, vol. 162, no. 1, pp. 585–594, 1999.

[22] Z. Reyes-Castillo, C. A. Palafox-Sanchez, I. Parra-Rojas et al., "Comparative analysis of autoantibodies targeting peptidylarginine deiminase type 4, mutated citrullinated vimentin and cyclic citrullinated peptides in rheumatoid arthritis: Associations with cytokine profiles, clinical and genetic features," *Clinical and Experimental Immunology*, vol. 182, no. 2, pp. 119–131, 2015.

[23] G. A. Schellekens, B. A. de Jong, F. H. van den Hoogen, L. B. van de Putte, and W. J. van Venrooij, "Citrulline is an essential constituent of antigenic determinants recognized by rheumatoid arthritis-specific autoantibodies," *The Journal of Clinical Investigation*, vol. 101, no. 1, pp. 273–281, 1998.

[24] A. Mastrangelo, T. Colasanti, C. Barbati et al., "The role of posttranslational protein modifications in rheumatological diseases: focus on rheumatoid arthritis," *Journal of Immunology Research*, vol. 2015, p. 712490, 2015.

[25] C. M. Bradford, I. Ramos, A. K. Cross et al., "Localisation of citrullinated proteins in normal appearing white matter and lesions in the central nervous system in multiple sclerosis," *Journal of Neuroimmunology*, vol. 273, no. 1, pp. 85–95, 2014.

[26] A. P. Nicholas, T. Sambandam, J. D. Echols, and W. W. Tourtellotte, "Increased citrullinated glial fibrillary acidic protein in

secondary progressive multiple sclerosis," *The Journal of Comparative Neurology*, vol. 473, no. 1, pp. 128–136, 2004.

[27] C. Stadelmann, "Multiple sclerosis as a neurodegenerative disease: pathology, mechanisms and therapeutic implications," *Current Opinion in Neurology*, vol. 24, no. 3, pp. 224–229, 2011.

[28] L. Yang, D. Tan, and H. Piao, "Myelin basic protein citrullination in multiple sclerosis: a potential therapeutic target for the pathology," *Neurochemical Research*, vol. 41, no. 8, pp. 1845–1856, 2016.

[29] J. Kipnis, "Multifaceted interactions between adaptive immunity and the central nervous system," *Science*, vol. 353, no. 6301, pp. 766–771, 2016.

[30] C. A. McKee and J. R. Lukens, "Emerging roles for the immune system in traumatic brain injury," *Frontiers in Immunology*, vol. 7, p. 556, 2016.

[31] R. C. Lazarus, J. E. Buonora, M. N. Flora et al., "Protein citrullination: a proposed mechanism for pathology in traumatic brain injury," *Frontiers in Neurology*, vol. 6, p. 204, 2015.

[32] M. Hecker, B. Fitzner, M. Wendt et al., "High-density peptide microarray analysis of IgG autoantibody reactivities in serum and cerebrospinal fluid of multiple sclerosis patients," *Molecular & Cellular Proteomics*, vol. 15, no. 4, pp. 1360–1380, 2016.

[33] A. Ishigami, H. Masutomi, S. Handa et al., "Mass spectrometric identification of citrullination sites and immunohistochemical detection of citrullinated glial fibrillary acidic protein in Alzheimer's disease brains," *Journal of Neuroscience Research*, vol. 93, no. 11, pp. 1664–1674, 2015.

[34] Z. Jin, Z. Fu, J. Yang, J. Troncosco, A. D. Everett, and J. E. Van Eyk, "Identification and characterization of citrulline-modified brain proteins by combining HCD and CID fragmentation," *Proteomics*, vol. 13, no. 17, pp. 2682–2691, 2013.

[35] F. Ahmed, A. Gyorgy, A. Kamnaksh et al., "Time-dependent changes of protein biomarker levels in the cerebrospinal fluid after blast traumatic brain injury," *Electrophoresis*, vol. 33, no. 24, pp. 3705–3711, 2012.

[36] A. Gyorgy, G. Ling, D. Wingo et al., "Time-dependent changes in serum biomarker levels after blast traumatic brain injury," *Journal of Neurotrauma*, vol. 28, no. 6, pp. 1121–1126, 2011.

[37] G. Hao, D. Wang, J. Gu, Q. Shen, S. S. Gross, and Y. Wang, "Neutral loss of isocyanic acid in peptide CID spectra: a novel diagnostic marker for mass spectrometric identification of protein citrullination," *Journal of the American Society for Mass Spectrometry*, vol. 20, no. 4, pp. 723–727, 2009.

[38] G. P. Martinelli, V. L. Friedrich Jr., and G. R. Holstein, "L-citrulline immunostaining identifies nitric oxide production sites within neurons," *Neuroscience*, vol. 114, no. 1, pp. 111–122, 2002.

[39] Z. Zhang, J. S. Zoltewicz, S. Mondello et al., "Human traumatic brain injury induces autoantibody response against glial fibrillary acidic protein and its breakdown products," *PloS One*, vol. 9, no. 3, article e92698, 2014.

[40] A. J. Ytterberg, V. Joshua, G. Reynisdottir et al., "Shared immunological targets in the lungs and joints of patients with rheumatoid arthritis: identification and validation," *Annals of the Rheumatic Diseases*, vol. 74, no. 9, pp. 1772–1777, 2015.

[41] S. L. Aungst, S. V. Kabadi, S. M. Thompson, B. A. Stoica, and A. I. Faden, "Repeated mild traumatic brain injury causes chronic neuroinflammation, changes in hippocampal synaptic plasticity, and associated cognitive deficits," *Journal of Cerebral Blood Flow and Metabolism*, vol. 34, no. 7, pp. 1223–1232, 2014.

[42] D. J. Loane and A. Kumar, "Microglia in the TBI brain: the good, the bad, and the dysregulated," *Experimental Neurology*, vol. 275, no. Pt 3, pp. 316–327, 2016.

[43] N. Marchi, J. J. Bazarian, V. Puvenna et al., "Consequences of repeated blood-brain barrier disruption in football players," *PloS One*, vol. 8, no. 3, article e56805, 2013.

[44] J. E. Gottenberg, P. Ravaud, A. Cantagrel et al., "Positivity for anti-cyclic citrullinated peptide is associated with a better response to abatacept: data from the 'Orencia and Rheumatoid Arthritis' registry," *Annals of the Rheumatic Diseases*, vol. 71, no. 11, pp. 1815–1819, 2012.

[45] K. Chatzidionysiou, E. Lie, E. Nasonov et al., "Highest clinical effectiveness of rituximab in autoantibody-positive patients with rheumatoid arthritis and in those for whom no more than one previous TNF antagonist has failed: pooled data from 10 European registries," *Annals of the Rheumatic Diseases*, vol. 70, no. 9, pp. 1575–1580, 2011.

[46] P. Lal, Z. Su, C. T. Holweg et al., "Inflammation and autoantibody markers identify rheumatoid arthritis patients with enhanced clinical benefit following rituximab treatment," *Arthritis and Rheumatism*, vol. 63, no. 12, pp. 3681–3691, 2011.

[47] G. Harauz and A. A. Musse, "A tale of two citrullines—structural and functional aspects of myelin basic protein deimination in health and disease," *Neurochemical Research*, vol. 32, no. 2, pp. 137–158, 2007.

[48] A. Ishigami, T. Ohsawa, M. Hiratsuka et al., "Abnormal accumulation of citrullinated proteins catalyzed by peptidylarginine deiminase in hippocampal extracts from patients with Alzheimer's disease," *Journal of Neuroscience Research*, vol. 80, no. 1, pp. 120–128, 2005.

[49] B. Jang, A. Ishigami, N. Maruyama, R. I. Carp, Y. S. Kim, and E. K. Choi, "Peptidylarginine deiminase and protein citrullination in prion diseases: strong evidence of neurodegeneration," *Prion*, vol. 7, no. 1, pp. 42–46, 2013.

[50] C. Louw, A. Gordon, N. Johnston, C. Mollatt, G. Bradley, and C. G. Whiteley, "Arginine deiminases: therapeutic tools in the etiology and pathogenesis of Alzheimer's disease," *Journal of Enzyme Inhibition and Medicinal Chemistry*, vol. 22, no. 1, pp. 121–126, 2007.

Hindawi
Oxidative Medicine and Cellular Longevity
Volume 2017, Article ID 5175249, 11 pages
https://doi.org/10.1155/2017/5175249

*Research Article*

# Distinguishing the Unique Neuropathological Profile of Blast Polytrauma

**W. Brad Hubbard,[1] Shaylen Greenberg,[2] Carly Norris,[1] Joseph Eck,[1] Erin Lavik,[3] and Pamela VandeVord[1,4]**

[1]*Biomedical Engineering and Mechanics, Virginia Tech, Blacksburg, VA 24061, USA*
[2]*Translational Biology, Medicine, and Health, Virginia Tech, Blacksburg, VA 24061, USA*
[3]*Department of Chemical, Biochemical and Environmental Engineering, University of Maryland, Baltimore County, Baltimore, MD 21250, USA*
[4]*Research Services, Salem VAMC, Salem, VA 24153, USA*

Correspondence should be addressed to Pamela VandeVord; pvord@vt.edu

Received 20 January 2017; Accepted 28 February 2017; Published 23 March 2017

Academic Editor: Valentina Pallottini



Traumatic brain injury sustained after blast exposure (blast-induced TBI) has recently been documented as a growing issue for military personnel. Incidence of injury to organs such as the lungs has decreased, though current epidemiology still causes a great public health burden. In addition, unprotected civilians sustain primary blast lung injury (PBLI) at alarming rates. Often, mild-to-moderate cases of PBLI are survivable with medical intervention, which creates a growing population of survivors of blast-induced polytrauma (BPT) with symptoms from blast-induced mild TBI (mTBI). Currently, there is a lack of preclinical models simulating BPT, which is crucial to identifying unique injury mechanisms of BPT and its management. To meet this need, our group characterized a rodent model of BPT and compared results to a blast-induced mTBI model. Open field (OF) performance trials were performed on rodents at 7 days after injury. Immunohistochemistry was performed to evaluate cellular outcome at day seven following BPT. Levels of reactive astrocytes (GFAP), apoptosis (cleaved caspase-3 expression), and vascular damage (SMI-71) were significantly elevated in BPT compared to blast-induced mTBI. Downstream markers of hypoxia (HIF-1$\alpha$ and VEGF) were higher only after BPT. This study highlights the need for unique therapeutics and prehospital management when handling BPT.

## 1. Introduction

A traumatic event that causes multiple injuries, or polytrauma, is a complex challenge for clinicians [1]. Recently, polytrauma has been reported in military populations with a direct link to blast exposure [2]. A rise in terrorism worldwide also fuels the polytrauma epidemic for civilian casualties. Reports from terrorist activity in the Middle East and Europe in the late twentieth century highlight the growing issues and prevalence of primary blast lung injury (PBLI) [3–9]. With the increased use of improvised explosive devices (IEDs) in warfare, blast loading produces debilitating effects on victims from military conflicts and acts of terrorism [10, 11].

Blast-induced polytrauma (BPT) poses a unique obstacle to physicians due to the complex systematic interactions. Diagnosing traumatic brain injuries (TBIs) is a significant task as the amount of concomitant injuries overshadows signs of neurotrauma. There is limited knowledge regarding the early stage management of polytrauma and the sensitive underlying systemic mechanisms that contribute to ongoing neuropathology. Injuries, such as pneumothorax or uncontrolled bleeding, take precedence in early stage trauma care. While these concerns are severe and need immediate treatment, TBIs often cause the most long-term harm to the surviving victims of blast exposure. In order to guide trauma management, as well as initial treatment for TBI, a preclinical model characterizing the intricate aspects of polytrauma is needed. McDonald et al. reported evidence that additional injuries, concomitant to impact-related TBI, can increase both peripheral and central inflammatory response as well

as exacerbate TBI pathology [12]. We expect that BPT models will show exacerbated vascular and inflammatory neuropathology due to these concomitant injuries.

A major objective of this study was to assess the role that subsequent hypoxia after blast exposure has on the outcomes of blast-induced TBI. Downstream neurological regulators of hypoxia and blood-brain barrier (BBB) disruption were examined as critical measures. Hypoxia likely contributes to exacerbating the injury progression after BPT due to impairment of pulmonary gas exchange in the lung, resulting in secondary effects on cerebral vasculature [13, 14]. Primary blast exposure to the brain also causes BBB disruption leading to a myriad of molecular cascades [15]. This cyclical relationship is highlighted with the finding that BBB disruption following TBI is biphasic, occurring at multiple time points after injury [16]. Comparing our BPT model to an established blast-induced mTBI model allows for the elucidation of molecular pathways triggered by the additive hypoxic environment. Examining how systemic pathology after lung injury impacts neuropathology is crucial to understanding mechanisms of blast-induced polytrauma and these results will aid in the development of injury-specific pharmacological targets that may be more effective in treating BPT.

## 2. Materials and Methods

*2.1. Experimental Set-Up.* All the experiments are in accordance with the Virginia Tech Institutional Animal Care and Use Committee and all the experimental protocols described herein have been approved. Prior to all experiments, male Sprague Dawley rats (~325 g, Harlan Labs, San Diego) were acclimated to a 12-hour light/dark cycle with food and water provided ad lib. As described previously, the shock front static and dynamic overpressures were generated using a custom-built Advanced Blast Simulator (200 cm × 30.48 cm × 30.48 cm) that consists of a driving compression chamber attached to a rectangular transition and testing chamber with an end wave eliminator (EWE) (ORA Inc., Fredericksburg, VA) located at the Center for Injury Biomechanics of Virginia Tech University. The passive EWE, installed at the venting end of the ABS, minimizes the shock wave outflow by means of a specially designed plate system. Patterns in the EWE plate system were created to mirror reflected shocks and rarefactions, which tend to cancel each other out and diminish unwanted effects within the test section. A peak static overpressure was produced with compressed helium and calibrated acetate sheets (Grafix Plastics, Cleveland, OH). Three pressure measurements were collected at 250 kHz using a Dash 8HF data acquisition system (Astro-Med, Inc., West Warwick, RI) and peak overpressures were calculated by determining wave speed (m/s) at the specimen position. A mesh sling, used to hold the animal during the exposure, allowed for minimal hindrance of the wave through the chamber. Shock wave profiles were verified to maintain consistent exposure pressures between subjects. Animals from the mTBI group were anesthetized with 3% isoflurane before being placed in a rostral cephalic orientation towards the shock wave. Whole body exposure is considered "on-axis" with the animal facing rostral cephalic orientation towards the blast. This exposure has minimal effect on the lungs, as the shock streamlines around the body. Thus, resulting exposure in this study creates a relatively specific brain injury and minimal polyorgan trauma. The mTBI rodent group was exposed to a single incident pressure profile resembling a "free-field" blast exposure, single Friedlander-like waveform that is in mild-moderate range at 117 kPa (17 psi) with a positive duration of 2.5 ms.

For the BPT group, rats were anesthetized with a ketamine/xylazine solution, in accordance with the rodent weight, for sedation during blast. BPT animals were exposed to a single incident pressure profile resembling a "free-field" blast exposure at a range of 170 to 210 kPa (24.5 to 30.5 psi) peak overpressure with 2.5 ms positive phase duration to ensure severe levels of PBLI [17, 18]. Rodents in the BPT group were positioned in a prone orientation with the right side of the thorax facing the shock front. The animals were not allowed to impact any solid surface in order to prevent secondary injuries and this was confirmed using high-speed video (Phantom Miro eX2, Vision Research). All animals were randomly assigned to one of three groups: mTBI, BPT, and sham ($n$ = 8–12/group). Sham animals underwent all procedures, including ketamine/xylazine sedation, as the BPT group except for blast exposure.

*2.2. Open Field Test.* Seven days after injury, animals performed an open field thigmotaxis assessment [19, 20]. Briefly, an opaque black acrylic box with dimensions 80 × 80 × 36 cm was used for the task. Animals were acclimated in the open field box before the injury and two days after injury. The acclimation ensures that any anxiety-like traits would be due to the blast and subsequent injury progression. Activity changes were detected using EthoVision XT™ software tracking. Thigmotaxia, or the animal's preference of proximity to the arena walls, tends to decrease after a period of acclimation but is continuously displayed in animals with anxiety. Time spent along the chamber wall reflects an increased level of anxiety and is a common method of determining anxiety levels [20]. Rats were videotaped for five minutes and avoidance of center square activity (i.e., anxiety-related behavior) was measured by determining the amount of time and frequency of entries into the central portion of the open field.

*2.3. Tissue Processing.* After seven days, animals were euthanized by transcardial perfusion of saline and 4% paraformaldehyde. Following collection, brains were stored in a 4% paraformaldehyde fixative solution. After 48 hours in fixative, whole brains were placed in 30% sucrose solution for tissue sectioning preparation. Whole brains were embedded in Tissue-Tek® optimal cutting temperature embedding medium (Sakura Finetek USA, Inc., Torrance, CA) for cryostat processing in the coronal plane. Samples were then cut (40 $\mu$m) and sections containing amygdala nuclei were isolated (bregma: −2.28 mm).

*2.4. Immunofluorescent Staining.* Immunohistochemistry was performed on amygdalar sections to evaluate levels of markers: glial fibrillary acidic protein (GFAP), cleaved caspase-3, ionized calcium-binding adaptor molecule 1

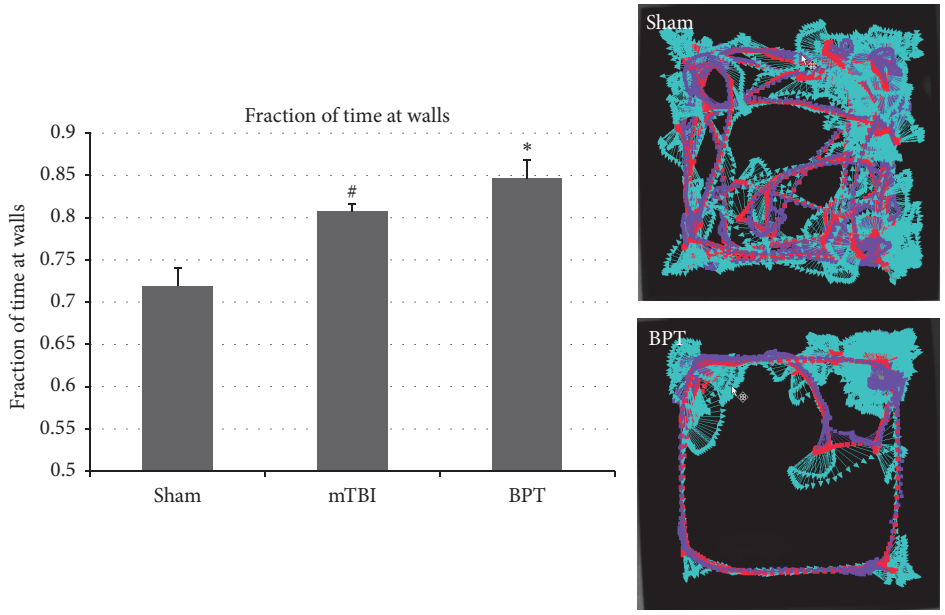


Figure 1: Fraction of time spent at the walls of the open arena was significantly higher in the mTBI and BPT groups compared to sham at 7 days after blast ($^{*}p < 0.02$, $^{\#}p < 0.05$). Representative images show animal tracking over five minutes.

(IBA-1), SMI-71, hypoxia inducible factor-1$\alpha$ (HIF-1$\alpha$), and vascular endothelial growth factor (VEGF). Samples were rinsed three times with PBS and incubated in 2% bovine serum albumin (BSA) in PBS for one hour at room temperature. Sections were then incubated with a primary antibody: anti-GFAP (1 : 500; Invitrogen, Carlsbad, California), anti-caspase-3 (1 : 500; Cell Signaling Technologies, Danvers, Massachusetts), anti-IBA-1 (1 : 500; Biocare Medical, Concord, California), anti-SMI-71 (1 : 250; Covance, Princeton, New Jersey), anti-HIF-1$\alpha$ (1 : 250; Novus Biologicals, Littleton, Colorado), or anti-VEGF (1 : 250; Santa Cruz, Dallas, Texas) overnight at 4°C. Primary antibodies were labeled separately on different amygdalar sections. After a PBS wash, the samples were incubated for 1.5 hours with fluorescein isothiocyanate (FITC) anti-rat, Alexa Fluor 555 anti-rabbit, Alexa Fluor 488 anti-mouse, or Alexa Fluor 594 anti-mouse. After three PBS washes (five minutes each), samples were mounted, air-dried, and coverslipped with ProLong Antifade Gold Reagent with 4′,6-diamidino-2-phenylindole (DAPI; Invitrogen, Carlsbad, CA). Sections were examined under a Zeiss fluorescence microscope at 20x magnification under appropriate fluorescent filters and images were taken by Zeiss AxioCam ICc 1. For all images, quantification (ImageJ software; NIH, Bethesda, MD) was based on fluorescence intensity after thresholding to eliminate background color. For average intensity, the output variable corresponds to the average fluorescent intensity per pixel (a number between 0 and 255). Percent area gives an indication of the amounts of pixels with signal divided by the total amount of pixels.

*2.5. Statistical Analysis.* Statistical differences between the treatment groups were assessed with analysis of variance, or ANOVA, using LSD post hoc test. All statistical analysis was performed using JMP Pro 10 (SAS Institute, Cary, NC) and $p < 0.05$ was considered statistically significant. Unless indicated otherwise, data are presented as mean ± standard error of the mean, or SEM.

## 3. Results

*3.1. Anxiety Assessment.* The fraction of time spent at the walls of the open field box for the BPT group was significantly increased ($p < 0.02$) compared to sham (Figure 1). The mTBI group also displayed elevated anxiety ($p < 0.05$) compared to sham. Representative image of animal activity over the five-minute period in the open arena demonstrates global exploration by the sham group and proximity to the walls in the BPT group (Figure 1). This display of anxiety-like behavior in the BPT group could be the neurological manifestation of injury pathology.

*3.2. Astrocyte Activation.* GFAP is a reliable marker to examine astrocyte morphology, as it is constitutively expressed in astrocytes. Higher expression of GFAP is seen in reactive astrocytes and is a standard method to assess astrogliosis [21]. While only slight elevation is seen in the mTBI group compared to sham, the BPT group is significantly different compared to sham (Figure 2). Images show astrocyte populations in each group, though more GFAP expression due to astrogliosis is seen qualitatively in the BPT group.

*3.3. Apoptosis.* Cleaved caspase-3 is a protein that is expressed in cells undergoing apoptotic signaling events, which makes it a reliable marker for apoptosis. Expression of cleaved caspase-3 was elevated in both blast groups, although only significantly different in the BPT group (Figure 3). Amygdalar images show an elevated number of apoptotic cells in the blast groups compared to sham.

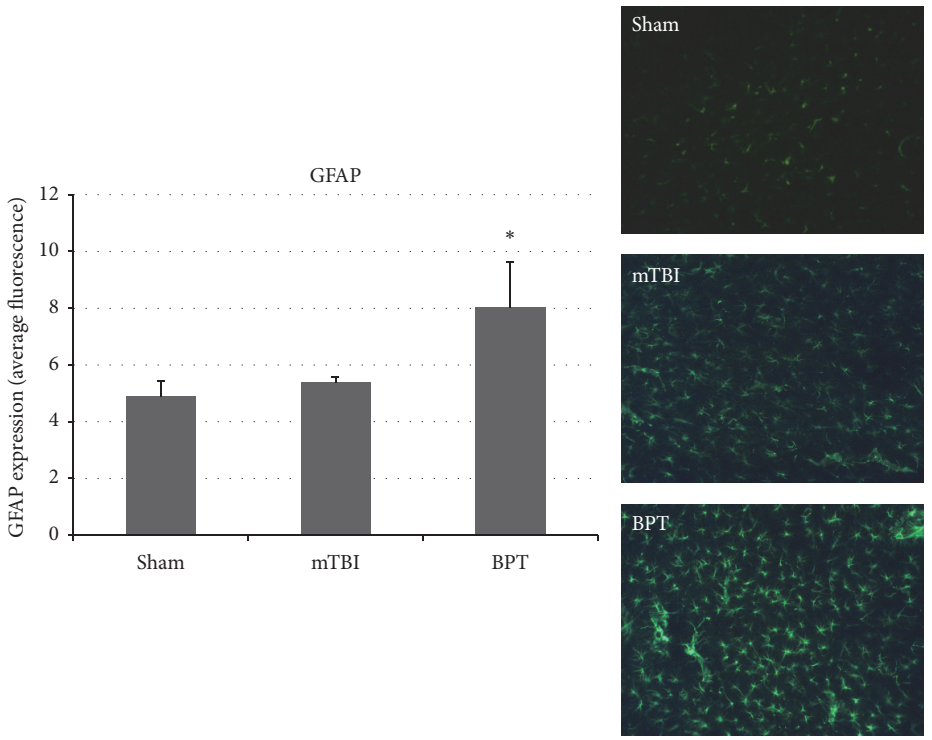


Figure 2: Representative images show reactive glia present seven days after blast in the BPT group. GFAP expression, examining astrocytosis, was significantly elevated in the BPT group compared to sham ($^{*}p < 0.05$).

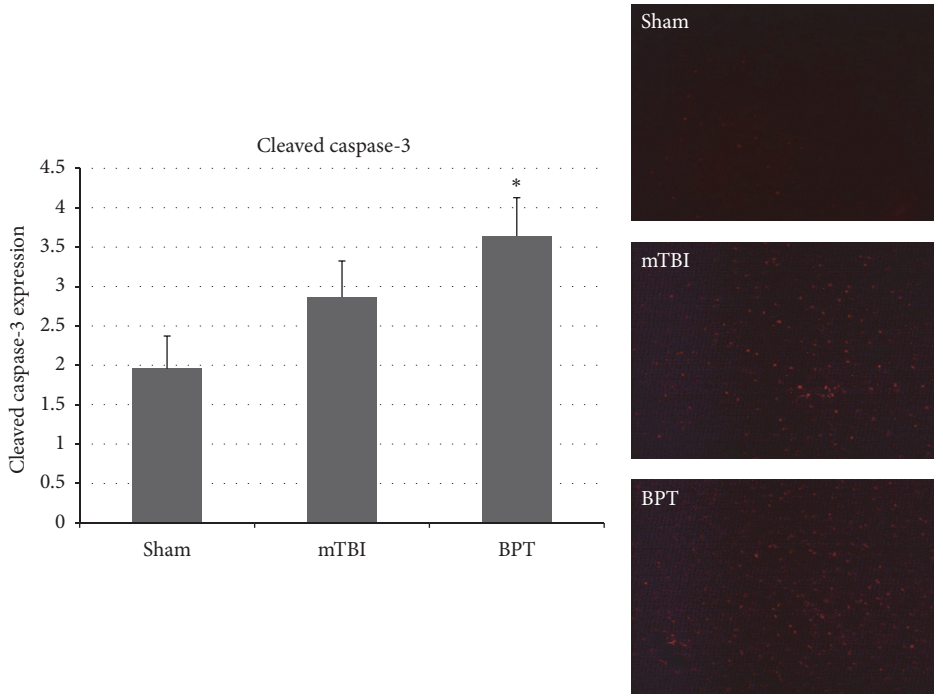


Figure 3: Representative images depict higher number of cells undergoing apoptosis in the mTBI and BPT groups. Cleaved caspase-3 expression was significantly elevated in the BPT compared to the sham group ($^{*}p < 0.05$). mTBI group are elevated compared to sham, though not significant ($p < 0.24$).

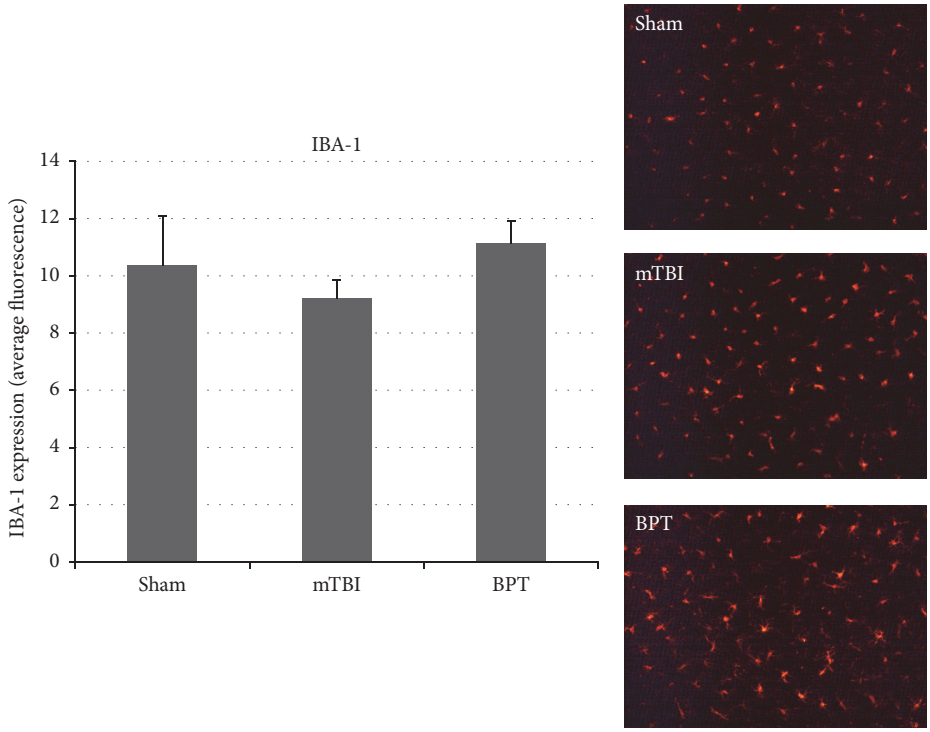


Figure 4: Images show similar number of microglia. IBA-1 expression, marking microglia, in the amygdala was not significantly different between groups.

*3.4. Microglia Activation.* IBA-1, which is involved in phagocytosis and actin reorganization in microglia, is constitutively expressed in microglia. Though not specific to activated microglia, IBA-1 is usually used to assess morphology (ramified or ameboid), which gives information about microglial modulation in disease states. Although there is no significant difference between the BPT group and sham, there is slight elevation in IBA-1 expression in the BPT group compared to sham (Figure 4).

*3.5. Blood-Brain Barrier Disruption.* SMI-71 is an established antibody against rat endothelial barrier antigen [22, 23]. This antibody binds to EBA, which is not present in vessels with BBB disruption [23]. Figure 5 depicts the decreased staining found within the injury group compared to sham due to decrease in vessel count with EBA expressed. The expression of SMI-71 was decreased in the BPT group, which has been shown previously to signify a compromised BBB [24], compared to the sham group ($p$ value $< 0.001$).

*3.6. HIF-1α.* HIF-1$\alpha$ is a transcription factor that is involved in several injury modalities where hypoxia occurs, including TBI [25]. HIFs are heterodimeric transcription factors composed of an oxygen-sensitive $\alpha$-subunit and a constitutively expressed $\beta$-subunit. Under normoxia, the HIF-1$\alpha$ subunit is constitutively transcribed but constantly targeted for degradation. As oxygen tension drops, the degradation enzymes are inhibited, which results in cytoplasmic stabilization of the $\alpha$-subunits. For the BPT group, HIF-1$\alpha$ expression was increased in the amygdala at seven days after blast compared to the sham group (Figure 6). In Figure 6, HIF-1$\alpha$ appears to be colocalized with DAPI around major vessels, showing that hypoxia is potentially being sensed first due to low blood oxygen concentration and this could be an ongoing mechanism.

*3.7. VEGF Expression.* VEGF, a signal protein, is produced to exert angiogenic stimulation. VEGF usually has a downstream role in response to HIF-1$\alpha$ transcription in hypoxic cells [26]. Overexpression of VEGF has been shown to contribute to neurological disease [27–29]. Expression of VEGF was elevated though not statistically different in the BPT group compared to sham (Figure 7).

## 4. Discussion

*4.1. Polytrauma Rodent Model.* Preclinical models designed for investigation of lung injury and neurotrauma sustained from blast exposure are scarce in the literature [18, 30]. As such, there is a lack of identifiable polytraumatic-specific injury markers for clinical use. Primary blast exposure has been correlated with varying TBI injury severities with assessment of physiology and lung injury in the rodent model shown by Mishra et al. [31]. BBB damage, signified by immunoglobulin G (IgG), has been characterized following blast trauma but exact mechanisms and time of BBB repair have not been elucidated [30]. In a lateral/side-on blast exposure to unanesthetized rodents, pulmonary hemorrhage was reported after 116 kPa exposure in addition to motor function impairment with an absence of axonal injury [32]. Another BPT model was created by exposing the animal to a blast wave

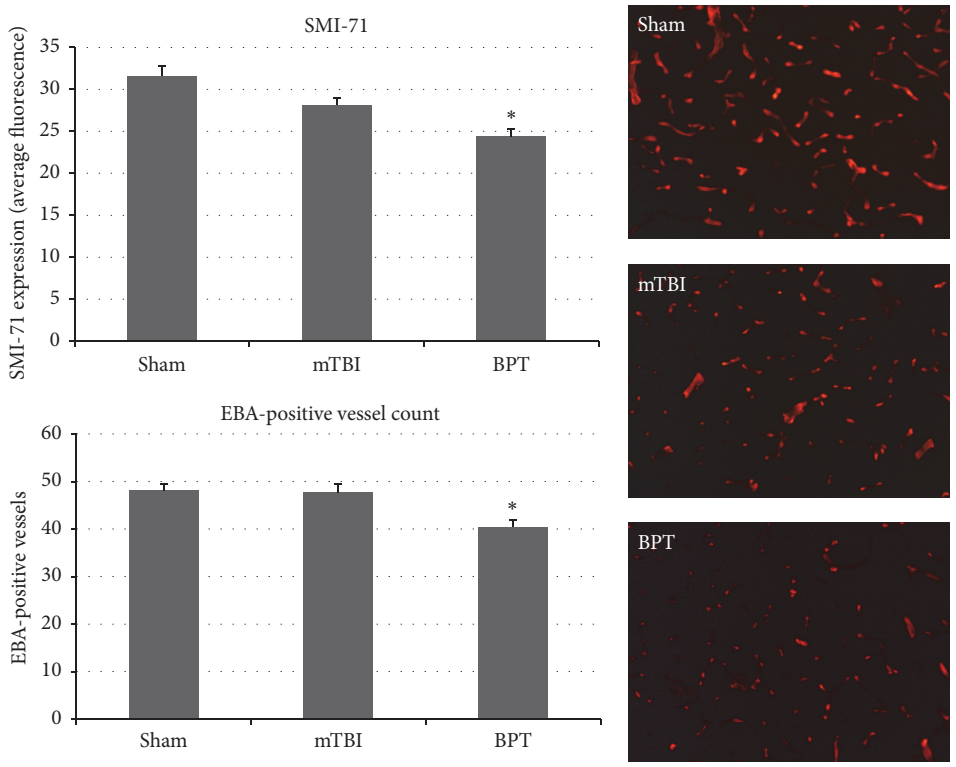


Figure 5: Representative images show lower number of vessels with EBA (BBB competent) in the BPT group. SMI-71 average fluorescence and marking of EBA+ vessels both show significant decrease in the BPT group compared to sham ($^{*}p < 0.001$).

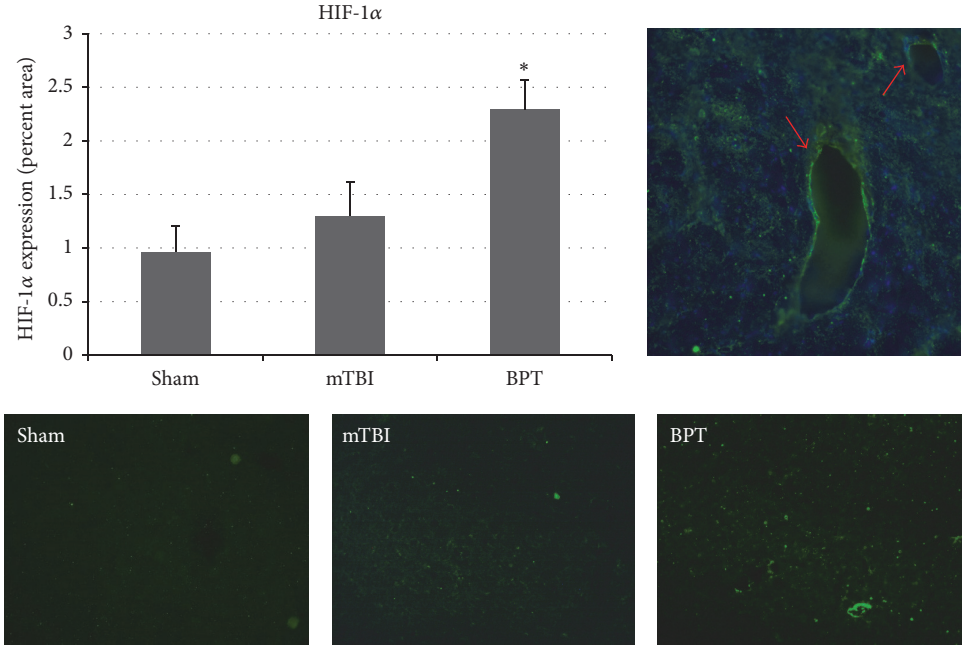


Figure 6: Representative images show HIF-1$\alpha$ expression is elevated in the BPT group ($^{*}p < 0.05$) when compared to the sham group. (Top right) HIF-1$\alpha$ was colocalized with DAPI around the vessels in the BPT group.

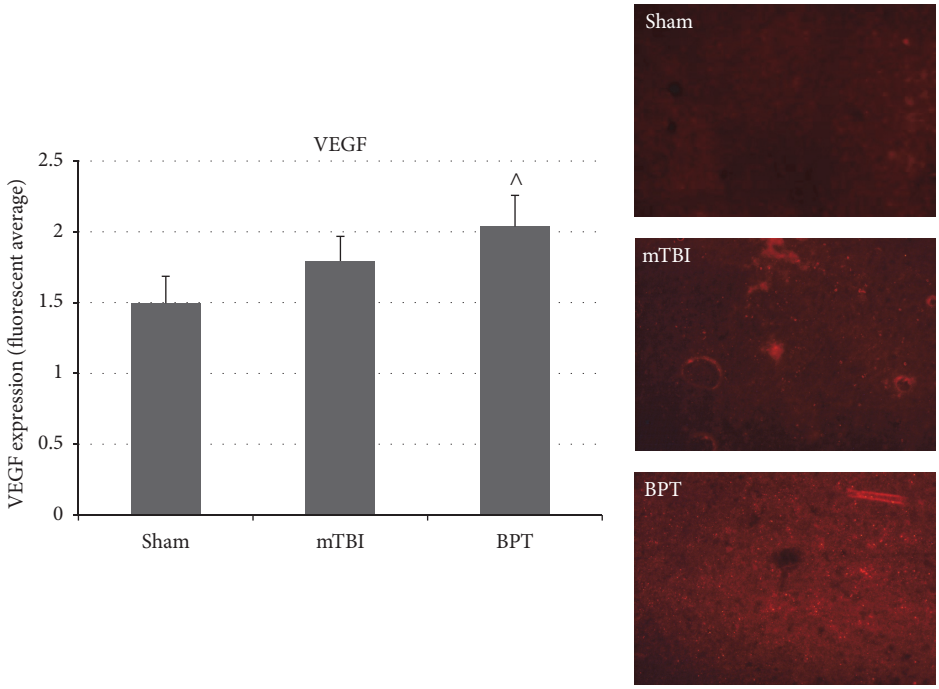


Figure 7: VEGF expression in the amygdala of the BPT group was elevated over sham, though not significant ($^{\wedge}p = 0.064$). Representative images depict VEGF expression in the amygdala.

directed at the thorax [33]. This model relied on the "vascular pulse" blast injury mechanism where blast overpressure causes pressure differentials in vasculature and produces a wave to the cerebrovasculature. Lung injury and perivenular neuroinflammation were found in this study [33], highlighting the importance of systemic circulation in polytrauma. Our model has been previously characterized and blast-induced lung injury mechanisms, as well as apparent pathology, have been deduced [17, 18]. Decreased oxygen saturation due to lung injury has been reported acutely, which is the major premise of hypoxia in the current BPT model.

*4.2. Polytrauma Worsens Behavioral Deficits.* The open field test is a standard test to measure anxiety-like behavior [34]. Rodents exposed to BPT displayed more time against the walls of the open field arena, or elevated anxiety-like behavior, compared to other groups. Anxiety has been reported seven to nine days after blast exposure [35, 36]. In a blast-induced TBI model, anxiety was seen in open field activity at seven days after following 25–40 psi blast exposure [37]. In a rat model of blast-induced mTBI, minocycline was administered and negated anxiety seen in injured animals at eight days after injury [38]. The BPT group displays worsened behavior outcome compared to mTBI animals, pointing to neural dysregulation due to systemic influence in the BPT group.

*4.3. Exacerbated Pathology after Polytrauma.* The results showed that our BPT model has unique neuropathological features compared to the blast-induced mTBI model. While similar markers are increased in both injury models, injury markers in general are exacerbated in the polytrauma model. Elevated GFAP expression and cleaved caspase-3 have been reported over the course of multiple time points after blast in the amygdala [39, 40]. Higher expression of GFAP and cleaved caspase-3 in the BPT model shows that there are more astrogliosis and apoptosis with higher injury severity. While differences in IBA-1 are not seen in this model, activation-specific antibodies, such as CD68 or CD11b, could be investigated to assay microglia activation after BPT. An antibody, like CD68, would be more sensitive as it has a distinct role in phagocytosis during the activation process. There is a potential that microglia at seven days after blast are in a retracted process activation state [41] and this morphology would be difficult to quantify with IBA-1.

A major finding was that BBB disruption, highlighted by a reduction in EBA+ vessels at seven days after injury, plays a distinct role in BPT injury pathology. Disruption of the BBB is a common finding in models of polytrauma but the exact mechanisms have not been deduced [30, 31, 33]. This could be a crucial upstream event in an ongoing injury cascade, involving hypoxia and subsequent BBB modulation. Along with secondary mechanisms of neuroinflammation and apoptosis, BBB disruption has been examined in blast-induced mTBI studies and has been reported acutely with recovery at 30 days after blast [42–46]. Hypoxia can produce BBB disruption and increased permeability, according to Kaur and Ling [47]. Clinically, compromise of astrocytic endfeet coverage of blood vessels in the brain has been reported in depressive disorders [48]. Exact blast injury thresholds have yet to be determined to produce consistent BBB breakdown but levels in this study indicated BBB compromise, subsequently leading to debilitating neurological consequence [43, 49]. SMI-71, as

a marker for BBB disruption, has been correlated with FITC-albumin infiltration [23]. Lower number of EBA+ vessels and stained vessel area were associated with regions of BBB dysfunction in the BPT group.

In addition to BBB damage that occurs from the primary blast wave, hypoxic conditions are present when lung injury has occurred which contributes to BBB disruption [50]. HIF-1$\alpha$ is a transcription factor that is involved in several injury modalities where hypoxia occurs, including TBI [51]. Even though HIF-1$\alpha$ has been shown to play a role in TBI progression and cerebral ischemia, few studies have examined its role after mTBI and it has not been investigated in relation to BPT [52, 53]. Delayed opening of the BBB, that is, only after HIF-1$\alpha$ was already stabilized, suggested barrier stability is mediated via one or more HIF-1$\alpha$ effectors [54]. HIF-1$\alpha$ is a mediator of disruption of the BBB and has been shown to have detrimental effects on injury pathology in the brain [55]. Inhibition of HIF-1$\alpha$ has been reported to reduce BBB damage and improve recovery from cerebral ischemia in rats [28, 55], possibly by reducing levels of VEGF and attenuating the expression of cleaved caspase-3 and p53, which are key molecules in the apoptosis pathway [56]. Inhibition of VEGF has shown to restore integrity of the BBB after an insult, possibly through modulation of matrix metalloproteinases (MMPs) [27]. VEGF, a downstream factor, can cause a leaky BBB [54]. Overall, BBB disruption is based on many factors during and after hypoxia with enhanced production of VEGF and inflammatory cytokines constituting ongoing pathways [47]. This injury pathway in the amygdala can potentially lead to neurologic impairment, such as anxiety [35]. Characterizing the role of secondary markers in BPT pathology would contribute to understanding of injury pathways, such as BBB dysfunction, and lead to novel therapeutic options.

Even though no significant difference was found in VEGF staining in BPT compared to sham, this factor could still play a role in the pathology at different time points. The role of VEGF, a downstream factor in injury cascades, in BBB disruption has been established in models of brain injury [29, 57]. Preclinical studies of mTBI reported increased levels of VEGF five days after injury in the amygdala [39]. As VEGF is a potential downstream marker after HIF-1$\alpha$ presence, it is possible that VEGF has significantly elevated expression after the seven-day time point. After multiple blast exposure, VEGF levels in plasma were upregulated at two hours after multiple injuries but not at 22 days after injury [58]. In a repeated mild blast TBI model, long lasting (42 days after injury) elevated levels of HIF-1$\alpha$ and VEGF in plasma were reported and due to hypoxia at time of injury [59]. After severe TBI in a rat model, HIF-1$\alpha$ level in serum steadily increased from one day to 28 days after injury, showing delayed response and release into the bloodstream [60]. HIF-1$\alpha$ has been shown to play a distinct role in apoptosis and BBB disruption after TBI in several models [51, 61]. Acute presentation of hypoxic factors would validate the findings of secondary mechanisms of hypoxic insult to the amygdala seven days after blast. More studies need to be conducted to fill in these knowledge gaps.

*4.4. Mechanical Damage to the Brain by the Blast Wave.* The mechanics of how primary blast exposure specifically injures the brain, usually in an inhomogeneous way, are poorly understood and are likely to be dependent upon orientation to the blast. Since the BPT model has a lateral orientation to the origin of the blast source, it is possible that mechanical transmission of blast energy differs compared to other orientations. Extensive evidence has been provided that skull dynamics contribute to blast-induced TBI [62–66]. Vibration of the skull from the shock wave causes secondary brain tissue displacement and injury stems from susceptibility of the viscoelastic brain to shear forces [62, 64, 67]. Other studies speculate that vascular surge, or venous pressure pulse that is transmitted to the brain through the jugular veins after blast exposure to the thorax, is a mechanism of blast-induced brain injury [33, 68]. This mechanism could rationalize a biophysical basis of ongoing BBB disruption after BPT due to lung injury. Our BPT model also highlights the importance of cerebrovasculature due to its impedance, density gradient, and systemic connection. Multiple studies have confirmed that microcontusion and microhemorrhaging of the BBB occurs with a lower threshold of 200 kPa peak overpressure in direct cranial and lateral blast exposure models [49, 69]. Also, sudden regional-specific changes in cerebral blood flow caused by increased intracranial pressure [46, 63, 64] can cause a rapid ischemic event, contributing to hypoxic cascade later on [70]. The amygdala has been shown to be hypervascularized, indicating increased dysregulation of neural networks susceptible to vascular mechanisms [71].

Blast polytrauma is a complex injury that can encompass trauma to several specific areas of the body. For our experimental model, we focused on replicating injuries that play the largest role acutely, lung injury, and chronically, brain injury. This model is also unique due to the multiple mechanisms of injury to the brain. Mechanical insult by the blast wave on the brain has been documented by several researchers [62, 63, 66]. Though the BPT model in this study has an increased input blast overpressure compared to the mTBI model, our research group has previously shown that this relationship can be nonlinear with neuropathology [40]. To exacerbate the direct injury from blast, there is a gradual acute response of systemic hypoxia on the brain in this polytrauma model. Our group has reported that there are minimal effects on the lungs and therefore an absence of systemic hypoxia after blast-induced mTBI [35, 72]. Future studies will examine oxidative stress and susceptibility of blast-induced BBB breakdown in hypoxic environments.

*4.5. Future Directions and Unique Therapeutic Solutions.* As polytrauma incidence increases due to terrorism activities, there has been a lack of characterizing the neuropathological aspects of blast polytrauma. Understanding specific mechanisms in this unique injury mode can impact the approach to treating polytrauma. While polytraumatic injury can be complex, the time course of systemic inflammation and other systemic effects on the brain can be crucial to therapeutic intervention and prehospital management. While these findings give a general view of mechanisms present at this time point, more detail on neuroinflammation is needed

to investigate specific pathways after BPT. Also, determining which components of the BBB are disrupted could point to how it is being damaged and at what point it is involved in injury pathology. MMPs have been implicated to play a major role in HIF-1$\alpha$/VEGF cascade and BBB disruption. Examining the role of MMPs could elucidate therapeutic strategies.

In addition to the effect on acute lung trauma, the primary injury mechanisms of blast-induced TBI can be influenced by orientation of the animal within the blast tube. Acute hypoxemia can produce immediate cerebrovascular pathology. Expansion of physiology recording is needed to see how long hypoxia is present after initial injury. This could solidify hypoxia as a major concern after systemic injury. This will also give an idea of the best time window for therapeutics designed to mitigate early factors in place to aggravate injury pathology at later stages. Blood biomarkers are another way to further characterize this polytrauma, specifically targeting astrogliosis (GFAP/S100$\beta$), BBB breakdown (VEGF), and hypoxia (HIF-1$\alpha$).

## 5. Conclusion

While many overlapping mechanisms in blast polytrauma coincide with that of blast-induced TBI, specific markers, such as BBB dysfunction and hypoxic factors, can play a larger role in neuropathology. For BPT, the combination of mechanically driven and hypoxic-driven neuropathology can worsen neurological outcomes. In this study, it is shown that BPT has a unique pathology and should have a different therapeutic approach compared to mTBI.

## Conflicts of Interest

The authors of this manuscript declare that there are no conflicts of interest regarding the publication of this paper.

## Acknowledgments

The authors would like to thank Dr. Michael Urban, Zachary Bailey, Bryce Dunn, and Ryan Brady for their technical assistance during blast testing. They would like to acknowledge funding support by the DOD CDMRP Program W81XWH-11-1-0014.

## References

[1] G. P. Liao and J. B. Holcomb, "Trauma resuscitation and fluid considerations in the polytrauma patient with CNS injury," in *Neurotrauma Management for the Severely Injured Polytrauma Patient*, J. M. Ecklund and L. E. Moores, Eds., pp. 51–59, Springer, Cham, Switzerland, 2017.

[2] P. A. Toyinbo, R. D. Vanderploeg, H. G. Belanger, A. M. Spehar, W. A. Lapcevic, and S. G. Scott, "A systems science approach to understanding polytrauma and blast-related injury: bayesian network model of data from a survey of the florida national guard," *American Journal of Epidemiology*, vol. 185, no. 2, pp. 135–146, 2017.

[3] M. Hirsch and J. Bazini, "Blast injury of the chest," *Clinical Radiology*, vol. 20, no. 4, pp. 362–370, 1969.

[4] W. A. Hadden, W. H. Rutherford, and J. D. Merrett, "The injuries of terroist bombing: a study of 1532 consecutive patients," *British Journal of Surgery*, vol. 65, no. 8, pp. 525–531, 1978.

[5] B. Brismar and L. Bergenwald, "The terrorist bomb explosion in Bologna, Italy, 1980: an analysis of the effects and injuries sustained," *Journal of Trauma—Injury, Infection and Critical Care*, vol. 22, no. 3, pp. 216–220, 1982.

[6] G. J. Cooper, R. L. Maynard, N. L. Cross, and J. F. Hill, "Casualties from terrorist bombings," *Journal of Trauma*, vol. 23, no. 11, pp. 955–967, 1983.

[7] E. R. Frykberg and J. J. Tepas III, "Terrorist bombings. Lessons learned from Belfast to Beirut," *Annals of Surgery*, vol. 208, no. 5, pp. 569–576, 1988.

[8] E. Katz, B. Ofek, J. Adler, H. B. Abramowitz, and M. M. Krausz, "Primary blast injury after a bomb explosion in a civilian bus," *Annals of Surgery*, vol. 209, no. 4, pp. 484–488, 1989.

[9] R. Pizov, A. Oppenheim-Eden, I. Matot et al., "Blast lung injury from an explosion on a civilian bus," *Chest*, vol. 115, no. 1, pp. 165–172, 1999.

[10] J. M. Wightman and S. L. Gladish, "Explosions and blast injuries," *Annals of Emergency Medicine*, vol. 37, no. 6, pp. 664–678, 2001.

[11] CDC, "Bombings: injury patterns and care. Blast curriculum: one-hour module," 2006.

[12] S. J. McDonald, M. Sun, D. V. Agoston, and S. R. Shultz, "The effect of concomitant peripheral injury on traumatic brain injury pathobiology and outcome," *Journal of Neuroinflammation*, vol. 13, no. 1, article 90, 2016.

[13] D. S. Dewitt and D. S. Prough, "Blast-induced brain injury and posttraumatic hypotension and hypoxemia," *Journal of Neurotrauma*, vol. 26, no. 6, pp. 877–887, 2009.

[14] E. Kirkman and S. Watts, "Characterization of the response to primary blast injury," *Philosophical Transactions of the Royal Society B: Biological Sciences*, vol. 366, no. 1562, pp. 286–290, 2010.

[15] A. Chodobski, B. J. Zink, and J. Szmydynger-Chodobska, "Blood-brain barrier pathophysiology in traumatic brain injury," *Translational Stroke Research*, vol. 2, no. 4, pp. 492–516, 2011.

[16] M. K. Başkaya, A. M. Rao, A. Doğan, D. Donaldson, and R. J. Dempsey, "The biphasic opening of the blood-brain barrier in the cortex and hippocampus after traumatic brain injury in rats," *Neuroscience Letters*, vol. 226, no. 1, pp. 33–36, 1997.

[17] W. B. Hubbard, C. Hall, V. Siva Sai Suijith Sajja, E. Lavik, and P. VandeVord, "Examining lethality risk for rodent studies of primary blast lung injury," *Biomedical Sciences Instrumentation*, vol. 50, pp. 92–99, 2014.

[18] W. B. Hubbard, M. M. Lashof-Sullivan, E. B. Lavik, and P. J. Vandevord, "Steroid-loaded hemostatic nanoparticles combat lung injury after blast trauma," *ACS Macro Letters*, vol. 4, no. 4, pp. 387–391, 2015.

[19] E. Huang, M. Ngo, S. Yee et al., "Repeated blast exposure alters open field behavior recorded under low illumination," *Brain Research*, vol. 1529, pp. 125–133, 2013.

[20] H. Darwish, A. Mahmood, T. Schallert, M. Chopp, and B. Therrien, "Simvastatin and environmental enrichment effect on recognition and temporal order memory after mild-to-moderate traumatic brain injury," *Brain Injury*, vol. 28, no. 2, pp. 211–226, 2014.

[21] M. V. Sofroniew and H. V. Vinters, "Astrocytes: biology and pathology," *Acta Neuropathologica*, vol. 119, no. 1, pp. 7–35, 2010.

[22] B. Lin and M. D. Ginsberg, "Quantitative assessment of the normal cerebral microvasculature by endothelial barrier antigen (EBA) immunohistochemistry: application to focal cerebral ischemia," *Brain Research*, vol. 865, no. 2, pp. 237–244, 2000.

[23] J. Pelz, W. Härtig, C. Weise et al., "Endothelial barrier antigen-immunoreactivity is conversely associated with blood-brain barrier dysfunction after embolic stroke in rats," *European Journal of Histochemistry*, vol. 57, no. 4, article e38, 2013.

[24] J. E. Westin, H. S. Lindgren, J. Gardi et al., "Endothelial proliferation and increased blood-brain barrier permeability in the basal ganglia in a rat model of 3,4-dihydroxyphenyl-L-alanine-induced dyskinesia," *Journal of Neuroscience*, vol. 26, no. 37, pp. 9448–9461, 2006.

[25] Y. Li, M. Chavko, J. L. Slack et al., "Protective effects of decay-accelerating factor on blast-induced neurotrauma in rats," *Acta Neuropathologica Communications*, vol. 1, no. 1, article 52, 2013.

[26] J. A. Forsythe, B.-H. Jiang, N. V. Iyer et al., "Activation of vascular endothelial growth factor gene transcription by hypoxia-inducible factor 1," *Molecular and Cellular Biology*, vol. 16, no. 9, pp. 4604–4613, 1996.

[27] H. Zhang, P. Zhang, Y. Gao et al., "Early VEGF inhibition attenuates blood-brain barrier disruption in ischemic rat brains by regulating the expression of MMPs," *Molecular Medicine Reports*, vol. 15, no. 1, pp. 57–64, 2017.

[28] W.-L. Yeh, D.-Y. Lu, C.-J. Lin, H.-C. Liou, and W.-M. Fu, "Inhibition of hypoxia-induced increase of blood-brain barrier permeability by YC-1 through the antagonism of HIF-1$\alpha$ accumulation and VEGF expression," *Molecular Pharmacology*, vol. 72, no. 2, pp. 440–449, 2007.

[29] M. K. Sköld, C. Von Gertten, A.-C. Sandberg-Nordqvist, T. Mathiesen, and S. Holmin, "VEGF and VEGF receptor expression after experimental brain contusion in rat," *Journal of Neurotrauma*, vol. 22, no. 3, pp. 353–367, 2005.

[30] M. Skotak, F. Wang, A. Alai et al., "Rat injury model under controlled field-relevant primary blast conditions: acute response to a wide range of peak overpressures," *Journal of Neurotrauma*, vol. 30, no. 13, pp. 1147–1160, 2013.

[31] V. Mishra, M. Skotak, H. Schuetz, A. Heller, J. Haorah, and N. Chandra, "Primary blast causes mild, moderate, severe and lethal TBI with increasing blast overpressures: experimental rat injury model," *Scientific Reports*, vol. 6, Article ID 26992, 2016.

[32] S. T. Ahlers, E. Vasserman-Stokes, M. C. Shaughness et al., "Assessment of the effects of acute and repeated exposure to blast overpressure in rodents: toward a greater understanding of blast and the potential ramifications for injury in humans exposed to blast," *Frontiers in Neurology*, vol. 3, article 32, 2012.

[33] J. M. Simard, A. Pampori, K. Keledjian et al., "Exposure of the thorax to a sublethal blast wave causes a hydrodynamic pulse that leads to perivenular inflammation in the brain," *Journal of Neurotrauma*, vol. 31, no. 14, pp. 1292–1304, 2014.

[34] L. Prut and C. Belzung, "The open field as a paradigm to measure the effects of drugs on anxiety-like behaviors: a review," *European Journal of Pharmacology*, vol. 463, no. 1–3, pp. 3–33, 2003.

[35] V. S. Sajja, W. B. Hubbard, and P. J. VandeVord, "Subacute oxidative stress and glial reactivity in the amygdala are associated with increased anxiety following blast neurotrauma," *Shock*, vol. 44, supplement 1, pp. 71–78, 2015.

[36] H. O. Awwad, L. P. Gonzalez, P. Tompkins et al., "Blast overpressure waves induce transient anxiety and regional changes in cerebral glucose metabolism and delayed hyperarousal in rats," *Frontiers in Neurology*, vol. 6, article 132, 2015.

[37] S. A. Heldt, A. J. Elberger, Y. Deng et al., "A novel closed-head model of mild traumatic brain injury caused by primary overpressure blast to the cranium produces sustained emotional deficits in mice," *Frontiers in Neurology*, vol. 5, article 2, 2014.

[38] E. Kovesdi, A. Kamnaksh, D. Wingo et al., "Acute minocycline treatment mitigates the symptoms of mild blast-induced traumatic brain injury," *Frontiers in Neurology*, vol. 3, article 111, 2012.

[39] A. Kamnaksh, E. Kovesdi, S.-K. Kwon et al., "Factors affecting blast traumatic brain injury," *Journal of Neurotrauma*, vol. 28, no. 10, pp. 2145–2153, 2011.

[40] P. J. VandeVord, R. Bolander, V. S. Sajja, K. Hay, and C. A. Bir, "Mild neurotrauma indicates a range-specific pressure response to low level shock wave exposure," *Annals of Biomedical Engineering*, vol. 40, no. 1, pp. 227–236, 2012.

[41] B. R. Huber, J. S. Meabon, Z. S. Hoffer et al., "Blast exposure causes dynamic microglial/macrophage responses and microdomains of brain microvessel dysfunction," *Neuroscience*, vol. 319, pp. 206–220, 2016.

[42] R. D. Readnower, M. Chavko, S. Adeeb et al., "Increase in blood-brain barrier permeability, oxidative stress, and activated microglia in a rat model of blast-induced traumatic brain injury," *Journal of Neuroscience Research*, vol. 88, no. 16, pp. 3530–3539, 2010.

[43] P. M. Abdul-Muneer, H. Schuetz, F. Wang et al., "Induction of oxidative and nitrosative damage leads to cerebrovascular inflammation in an animal model of mild traumatic brain injury induced by primary blast," *Free Radical Biology and Medicine*, vol. 60, pp. 282–291, 2013.

[44] C. D. Hue, F. S. Cho, S. Cao et al., "Time course and size of blood-brain barrier opening in a mouse model of blast-induced traumatic brain injury," *Journal of Neurotrauma*, vol. 33, no. 13, pp. 1202–1211, 2016.

[45] J. R. Perez-Polo, H. C. Rea, K. M. Johnson et al., "A rodent model of mild traumatic brain blast injury," *Journal of Neuroscience Research*, vol. 93, no. 4, pp. 549–561, 2015.

[46] U. Kawoos, M. Gu, J. Lankasky, R. M. McCarron, M. Chavko, and M. A. Deli, "Effects of exposure to blast overpressure on intracranial pressure and blood-brain barrier permeability in a rat model," *PLoS ONE*, vol. 11, no. 12, Article ID e0167510, 2016.

[47] C. Kaur and E. A. Ling, "Blood brain barrier in hypoxic-ischemic conditions," *Current Neurovascular Research*, vol. 5, no. 1, pp. 71–81, 2008.

[48] G. Rajkowska, J. Hughes, C. A. Stockmeier, J. Javier Miguel-Hidalgo, and D. Maciag, "Coverage of blood vessels by astrocytic endfeet is reduced in major depressive disorder," *Biological Psychiatry*, vol. 73, no. 7, pp. 613–621, 2013.

[49] S. Yeoh, E. D. Bell, and K. L. Monson, "Distribution of blood-brain barrier disruption in primary blast injury," *Annals of Biomedical Engineering*, vol. 41, no. 10, pp. 2206–2214, 2013.

[50] G. Mohaddes, J. Abdolalizadeh, S. Babri, and F. Hossienzadeh, "Ghrelin ameliorates blood-brain barrier disruption during systemic hypoxia," *Experimental Physiology*, vol. 102, no. 3, pp. 376–382, 2017.

[51] A. Li, X. Sun, Y. Ni, X. Chen, and A. Guo, "HIF-1$\alpha$ involves in neuronal apoptosis after traumatic brain injury in adult rats," *Journal of Molecular Neuroscience*, vol. 51, no. 3, pp. 1052–1062, 2013.

[52] F. Ahmed, I. Cernak, S. Plantman, and D. V. Agoston, "The temporal pattern of changes in serum biomarker levels reveal complex and dynamically changing pathologies after exposure

to a single low-intensity blast in mice," *Frontiers in Neurology*, vol. 6, article 114, 2015.

[53] M. Liu, C. Zhang, W. Liu et al., "A novel rat model of blast-induced traumatic brain injury simulating different damage degree: implications for morphological, neurological, and biomarker changes," *Frontiers in Cellular Neuroscience*, vol. 9, article 168, 2015.

[54] S. Engelhardt, A. J. Al-Ahmad, M. Gassmann, and O. O. Ogunshola, "Hypoxia selectively disrupts brain microvascular endothelial tight junction complexes through a hypoxia-inducible factor-1 (HIF-1) dependent mechanism," *Journal of Cellular Physiology*, vol. 229, no. 8, pp. 1096–1105, 2014.

[55] O. O. Ogunshola and A. Al-Ahmad, "HIF-1 at the blood-brain barrier: a mediator of permeability?" *High Altitude Medicine and Biology*, vol. 13, no. 3, pp. 153–161, 2012.

[56] C. Chen, Q. Hu, J. Yan et al., "Early inhibition of HIF-1$\alpha$ with small interfering RNA reduces ischemic-reperfused brain injury in rats," *Neurobiology of Disease*, vol. 33, no. 3, pp. 509–517, 2009.

[57] S. Okada, R. Okeda, S. Matsushita, and A. Kawano, "Histopathological and morphometric study of the late effects of heavy- ion irradiation on the spinal cord of the rat," *Radiation Research*, vol. 150, no. 3, pp. 304–315, 1998.

[58] A. Kamnaksh, S.-K. Kwon, E. Kovesdi et al., "Neurobehavioral, cellular, and molecular consequences of single and multiple mild blast exposure," *Electrophoresis*, vol. 33, no. 24, pp. 3680–3692, 2012.

[59] F. A. Ahmed, A. Kamnaksh, E. Kovesdi, J. B. Long, and D. V. Agoston, "Long-term consequences of single and multiple mild blast exposure on select physiological parameters and blood-based biomarkers," *Electrophoresis*, vol. 34, no. 15, pp. 2229–2233, 2013.

[60] E. P. Thelin, A. Frostell, J. Mulder et al., "Lesion size is exacerbated in hypoxic rats whereas hypoxia-inducible factor-1 alpha and vascular endothelial growth factor increase in injured normoxic rats: a prospective cohort study of secondary hypoxia in focal traumatic brain injury," *Frontiers in Neurology*, vol. 7, article 23, 2016.

[61] T. Higashida, C. W. Kreipke, J. A. Rafols et al., "The role of hypoxia-inducible factor-1$\alpha$, aquaporin-4, and matrix metalloproteinase-9 in blood-brain barrier disruption and brain edema after traumatic brain injury," *Journal of Neurosurgery*, vol. 114, no. 1, pp. 92–101, 2011.

[62] R. Bolander, B. Mathie, C. Bir, D. Ritzel, and P. Vandevord, "Skull flexure as a contributing factor in the mechanism of injury in the rat when exposed to a shock wave," *Annals of Biomedical Engineering*, vol. 39, no. 10, pp. 2550–2559, 2011.

[63] A. Dal Cengio Leonardi, N. J. Keane, C. A. Bir, A. G. Ryan, L. Xu, and P. J. VandeVord, "Head orientation affects the intracranial pressure response resulting from shock wave loading in the rat," *Journal of Biomechanics*, vol. 45, no. 15, pp. 2595–2602, 2012.

[64] A. D. C. Leonardi, C. A. Bir, D. V. Ritzel, and P. J. VandeVord, "Intracranial pressure increases during exposure to a shock wave," *Journal of Neurotrauma*, vol. 28, no. 1, pp. 85–94, 2011.

[65] C. E. Hampton and P. J. VandeVord, "Vibrational frequency response to impact loading of skull models," *Biomedical Sciences Instrumentation*, vol. 48, pp. 157–164, 2012.

[66] A. D. Gean, *Brain Injury: Applications from War and Terrorism*, Wolters Kluwer, 2014.

[67] W. C. Moss, M. J. King, and E. G. Blackman, "Skull flexure from blast waves: a mechanism for brain injury with implications for helmet design," *Physical Review Letters*, vol. 103, no. 10, Article ID 108702, 2009.

[68] R. A. Bauman, G. Ling, L. Tong et al., "An introductory characterization of a combat-casualty-care relevant swine model of closed head injury resulting from exposure to explosive blast," *Journal of Neurotrauma*, vol. 26, no. 6, pp. 841–860, 2009.

[69] R. Kuehn, P. F. Simard, I. Driscoll et al., "Rodent model of direct cranial blast injury," *Journal of Neurotrauma*, vol. 28, no. 10, pp. 2155–2169, 2011.

[70] F. Adhami, G. Liao, Y. M. Morozov et al., "Cerebral ischemia-hypoxia induces intravascular coagulation and autophagy," *The American Journal of Pathology*, vol. 169, no. 2, pp. 566–583, 2006.

[71] G. N. Neigh, M. J. Owens, W. R. Taylor, and C. B. Nemeroff, "Changes in the vascular area fraction of the hippocampus and amygdala are induced by prenatal dexamethasone and/or adult stress," *Journal of Cerebral Blood Flow and Metabolism*, vol. 30, no. 6, pp. 1100–1104, 2010.

[72] V. S. S. S. Sajja, W. B. Hubbard, C. S. Hall, F. Ghoddoussi, M. P. Galloway, and P. J. VandeVord, "Enduring deficits in memory and neuronal pathology after blast-induced traumatic brain injury," *Scientific Reports*, vol. 5, Article ID 15075, 2015.

Hindawi
Oxidative Medicine and Cellular Longevity
Volume 2017, Article ID 7063874, 10 pages
https://doi.org/10.1155/2017/7063874

*Research Article*

# Nicotinamide Adenine Dinucleotide Protects against Spinal Cord Ischemia Reperfusion Injury-Induced Apoptosis by Blocking Autophagy

**Lei Xie,[1,2] Sifei Yu,[1,2] Zhenfei Wang,[1,2] Kai Yang,[1,2] Zhuochao Liu,[1,2] Changwei Li,[1,2] and Yu Liang[1,2]**

[1]*Department of Orthopedics, Ruijin Hospital, Shanghai Jiao Tong University School of Medicine, 197 Ruijin 2nd Road, Shanghai 200025, China*
[2]*Shanghai Key Laboratory for Prevention and Treatment of Bone and Joint Diseases with Integrated Chinese-Western Medicine, Shanghai Institute of Traumatology and Orthopedics, Ruijin Hospital, Shanghai Jiao Tong University School of Medicine, 197 Ruijin 2nd Road, Shanghai 200025, China*

Correspondence should be addressed to Changwei Li; changwei393331@163.com and Yu Liang; ly10334@rjh.com.cn

Received 18 September 2016; Accepted 12 February 2017; Published 7 March 2017

Academic Editor: Andreas Büttner



The role of autophagy, neuroprotective mechanisms of nicotinamide adenine dinucleotide ($NAD^+$), and their relationship in spinal cord ischemic reperfusion injury (SCIR) was assessed. Forty-eight Sprague-Dawley rats were divided into four groups: sham, ischemia reperfusion (I/R), 10 mg/kg $NAD^+$, and 75 mg/kg $NAD^+$. Western blotting, immunofluorescence, and immunohistochemistry were used to assess autophagy and apoptosis. Basso, Beattie, and Bresnahan (BBB) scores were used to assess neurological function. Expression levels of Beclin-1, Atg12-Atg5, LC3B-II, cleaved caspase 3, and Bax were upregulated in the I/R group and downregulated in the 75 mg/kg $NAD^+$ group; p-mTOR, p-AKT, p62, and Bcl-2 were downregulated in the I/R group and upregulated in the 75 mg/kg $NAD^+$ group. Numbers of LC3B-positive, caspase 3-positive, Bax-positive, and TUNEL-positive cells were significantly increased in the I/R group and decreased in the 75 mg/kg $NAD^+$ group. The mean integrated option density of Bax increased and that of Nissl decreased in the I/R group, and it decreased and increased, respectively, in the 75 mg/kg $NAD^+$ group. BBB scores significantly increased in the 75 mg/kg $NAD^+$ group relative to the I/R group. No difference was observed between I/R and 10 mg/kg $NAD^+$ groups for these indicators. Therefore, excessive and sustained autophagy aggravates SCIR; administration of $NAD^+$ alleviates injury.

## 1. Introduction

Spinal cord ischemia reperfusion (I/R) injury (SCIR) is a disastrous complication in many pathophysiological situations, which may result in devastating paraplegia and paraparesis [1]. SCIR has been reported to occur in 3%–18% of patients undergoing descending thoracic and thoracoabdominal aneurysms surgery and endovascular aortic repair surgery [2]. SCIR should be regarded not only as a medical problem, but also as a socioeconomic burden. Considerable therapeutic interventions have been attempted to mitigate this problem, including cerebrospinal fluid drainage, reattachment of segmental arteries, intercostal vessel reimplantation [3, 4], and administering pharmaceuticals (steroids, oxygen-derived free radical scavengers, and vasodilators) and drugs [5, 6]. However, the results were not satisfactory [7].

Autophagy plays an important role for survival when cells encounter metabolic stress and for metabolic processes maintaining cytoplasmic compositions via the autophagosomal-lysosomal pathway. Autophagy is an intracellular catabolic mechanism which can promote cell survival through degrading and recycling damaged organelles and unwanted proteins but also induce cell death in some pathological conditions [8]. Currently, several studies have been conducted to explore the functional role of autophagy in SCIR. However, the results of these studies are inconsistent. Some studies reported

that activation and upregulation of autophagy reduce nerve damage after I/R [9, 10], whereas other studies found that autophagy contributed to neuronal death and inhibition of autophagy seemed to provide protective effects [11, 12]. In general, the precise role of autophagy remains controversial in SCIR and requires further investigation.

Nicotinamide adenine dinucleotide ($NAD^+$) is a vital cofactor for metabolizing energy and a substrate for various enzymes [13]. Mounting evidence suggests that $NAD^+$ plays an essential role in calcium homeostasis, mitochondrial, and immunological functions [14, 15]. Previous studies showed that cerebral I/R results in reduction of $NAD^+$ levels [16, 17]. Repletion of $NAD^+$ could alleviate I/R injury and prevent astrocyte death in the brain [18]. In a previous study, we have shown that $NAD^+$ protects against SCIR injury via reducing oxidative stress-induced neuronal apoptosis [19]. However, whether $NAD^+$ can alleviate SCIR injury by restraining autophagic apoptosis remains to be elucidated.

The primary goal of our study was to investigate the role of autophagy and its potential signaling pathway in SCIR. Furthermore, we aimed to examine the protective effect and the internal mechanism of $NAD^+$ involved in SCIR, as well as to explore the underlying relationship between autophagy and $NAD^+$.

## 2. Materials and Methods

*2.1. Animals.* Forty-eight male Sprague-Dawley rats (180–250 g body weight), obtained from the Shanghai Laboratory Animal Corporation (Shanghai, China), were used in this study. The rats were acclimatized to laboratory conditions (25°C, 12 h/12 h light/dark, 50% humidity, and ad libitum access to food and water) for one week prior to experiments. All procedures involving animals were reviewed and approved by the Institutional Animal Care and Use Committee of Ruijin Hospital, Shanghai Jiao Tong University, Shanghai, China [IACUC protocol number: SYXK (Shanghai) 2011-0113].

*2.2. Surgical Procedure of Spinal Cord Ischemic Reperfusion Injury.* SCIR was modeled using a modified method from Zhang et al. [20]. Briefly, all rats were neurologically intact before the experiment and anesthetized with 2.5% sodium pentobarbital (60 mg/kg) administered intraperitoneally. After opening the retroperitoneum through the midline incision, the abdominal aorta was blocked above the right renal artery near the heart using a 50 g aneurysm clip for 60 min. The clips were removed just before closure. Sham-operated rats underwent the same procedure, but no occlusion of the aorta was performed. All operated rats were placed in a box at 28°C until anesthetic recovery and subsequently placed in separated cages with ad libitum access to food and water.

*2.3. Experimental Protocol.* A total of 48 rats were randomly divided into four groups. The sham group ($n = 12$) underwent the surgical procedure without aortic clipping. The I/R group ($n = 12$) received abdominal aortic exposure and cross-clamping for 60 min followed by intraperitoneal injection of equivalent volume of 0.9% saline solution immediately after reperfusion. Rats in the 10 mg/kg $NAD^+$ group ($n = 12$) and 75 mg/kg $NAD^+$ group ($n = 12$) underwent the same surgical procedure as those in the I/R group but were treated with different doses of $NAD^+$ immediately after I/R injury.

*2.4. $NAD^+$ Preparation and Treatment.* $NAD^+$ (Roche, Mannheim, Germany) was dissolved in 0.9% saline solution and injected intraperitoneally. To investigate whether $NAD^+$ has protective effects in SCIR, rats were treated with 10 mg/kg and 75 mg/kg $NAD^+$ intraperitoneally. The control group was treated with equivalent volume of 0.9% saline solution. Dosage of $NAD^+$ was decided based on previous studies with minor modification [19, 21].

*2.5. Tissue Preparation.* A total of 24 rats (randomly 6 rats from each group) were euthanized 24 h after reperfusion by an intraperitoneal injection of overdosed (100 mg/kg) sodium pentobarbital. The rats were transcardially perfused with 0.9% saline, followed by 4% paraformaldehyde in 0.1 M PBS, pH 7.4. Spinal cord segments (L1-2) were collected, post-fixed in the same fixative overnight at 4°C, and divided into two parts. One part was embedded in paraffin and the other was embedded in optimal cutting temperature (OCT) compound (Sakura, Torrance, USA). Serial, 6 $\mu$m, transverse sections were mounted on slides. Paraffin sections were used for histology and frozen sections for immunofluorescence and terminal deoxynucleotidyl transferase-mediated dUTP nick end labeling (TUNEL) as described below. The L1-2 segments of spinal cords of the remaining 24 rats were rapidly collected and deep-frozen at −80°C in preparation for western blot analysis.

*2.6. Assessment of Neurological Function.* Locomotor function of rats was recorded at different time points (1, 6, 12, and 24 h) after reperfusion using the Basso, Beattie, and Bresnahan (BBB) open-field locomotor scale [22] ranging from 0 (complete paralysis) to 21 (normal locomotion). Two blind observers scored each animal, respectively, and any discrepancies between the two scores were resolved by discussion.

*2.7. Nissl Staining.* All paraffin sections were deparaffinized and rehydrated. The sections were washed in distilled water three times, then stained with 0.25% toluidine blue at 50°C for 3 h, and bleached using 95% ethanol. Subsequently, sections underwent 100% ethanol dehydration, xylene transparency, and neutral gum mounting. In each experiment, all sections were stained at the same time.

*2.8. Immunohistochemical Staining of Bax.* Paraffin sections were deparaffinized and rehydrated. Antigen retrieval was performed according to the manufacturer's instructions for the Citrate Antigen Retrieval Solution (Beyotime, China). Sections were incubated in hydrogen peroxide to quench any endogenous peroxidases and then blocked with 5% bovine serum albumin (Sigma) for 30 min at room temperature. Sections were incubated in primary rabbit anti-Bax antibodies

(1 : 100; Abcam) diluted in PBS overnight at 4°C. The Vectastain Elite ABC Kit (Vector Laboratories, USA) was used according to the manufacturer's instructions. Positive staining was visualized with DAB (ImmPACT DAB, Vector Laboratories, USA). Sections were counterstained with hematoxylin for 10 s and dipped in acid alcohol as needed before being dehydrated and mounted on coverslips.

*2.9. Counting and Calculation of Mean Integrated Option Density of Nissl and Bax.* Digital photographs of all sections were taken using a ZEISS Axioskop microscope. The images were analyzed using Image-Pro Plus 6.0 software (Media Cybernetics, USA), and sum of area and integrated option density (IOD) were measured. The mean integrated option density was calculated by dividing the IOD sum by the area sum. The above information was collected in three sections for each rat by three blind observers.

*2.10. Immunofluorescence Staining of Bax, Caspase 3, and LC3.* Frozen sections were washed with PBS for 10 min and then with PBS containing 0.1% Tween (PBST) for 10 min and then blocked with 5% bovine serum albumin (Sigma) for 30 min at room temperature. Sections were incubated in permeabilization solution (1% Triton X-100) for 15 min at room temperature and then incubated in primary rabbit anti-Bax antibodies (1 : 100; Santa Cruz Biotechnology), primary rabbit anti-caspase 3 antibodies (1 : 100; Santa Cruz Biotechnology), or primary rabbit anti-LC3B antibodies (1 : 200; Cell Signaling Technology) diluted in PBS overnight at 4°C. After rinsing with PBST, sections were incubated with goat anti-rabbit IgG Alexa Fluor 488 secondary antibody (1 : 500; Molecular Probes) for 2 h at room temperature. The sections were mounted with ProLong® Gold antifade reagent with DAPI to label the nuclei (Molecular Probes).

*2.11. Terminal Deoxynucleotidyl Transferase-Mediated dUTP Nick End Labeling (TUNEL) Assay.* In order to identify DNA fragmentation, TUNEL was performed. Apoptotic cells in the frozen spinal cord sections were stained using the in situ Cell Death Detection kit (TMR red; Roche Diagnostics GmbH), according to the manufacturer's instructions. Briefly, sections were washed in PBS and incubated in permeabilization solution for 15 min at room temperature and then in the TUNEL solution containing TMR-dUTP for 1 h at 37°C. After labeling, cell nuclei were labeled with ProLong Gold antifade reagent with DAPI (Molecular Probes). After the immunofluorescence staining protocol described above, all sections were scanned using a confocal microscope (LSM 710, ZEISS, Germany). To quantify Bax, caspase 3, LC3 expression levels, and TUNEL in the spinal cord, labeled cells and mean fluorescence intensity were recorded in each spinal cord transverse section. The average of the numbers in the three sections was compared between groups. The above analysis was performed by three blinded investigators.

*2.12. Western Blot Analysis.* L1-2 segments of spinal cords were homogenized in Radio-Immunoprecipitation Assay (RIPA) buffer (Beyotime, China) with phenylmethanesulfonyl fluoride (PMSF) protease and Phosphatase Inhibitor Cocktail (CWBIO, China). Homogenates were clarified using centrifugation at 12000 ×g for 15 min at 4°C. The concentration of protein samples was determined using the BCA protein assay kit (Beyotime, China). Aliquots of protein (50 $\mu$g/lane) were fractionated using 10% sodium dodecyl sulfate polyacrylamide gel electrophoresis (SDS-PAGE). After electrophoresis, the proteins on the gel were transferred to polyvinylidene difluoride membranes (0.45 $\mu$m, Millipore, USA). The membranes were blocked in Tris-buffered saline/Tween (20 mmol/L Tris, pH 7.5, 0.5 mol/L NaCl, and 0.1% Tween 20) containing 5% nonfat dry milk for 1 h at room temperature and subsequently incubated with primary antibodies overnight at 4°C. Membranes were incubated with secondary antibody for 90 min at room temperature. Chemiluminescence results were recorded using an imaging system (Imagequant LAS4000mini, General Electric, USA). Signal intensities were quantified using Image-Pro Plus software. The antibodies used were as follows: rabbit anti-mTOR (1 : 1000; Cell Signaling Technology), rabbit anti-p-mTOR (1 : 1000; Cell Signaling Technology), rabbit anti-AKT (1 : 1000; Cell Signaling Technology), rabbit anti-p-AKT (1 : 1000; Cell Signaling Technology), mouse anti-SQSTM1/p62 (1 : 1000; Abcam), rabbit anti-Atg12 (1 : 1000; Cell Signaling Technology), rabbit anti-cleaved caspase 3 (1 : 1000; Cell Signaling Technology), rabbit anti-Bcl-2 (1 : 1000; Cell Signaling Technology), rabbit anti-Bax (1 : 1000; Cell Signaling Technology), rabbit anti-LC3B (1 : 1000; Cell Signaling Technology), mouse anti-$\beta$-actin (1 : 1000; Cell Signaling Technology), and horseradish peroxidase- (HRP-) conjugated secondary antibodies (1 : 5000; Jackson).

*2.13. Statistical Analysis.* All data were expressed as mean ± standard deviation (mean ± SD) and analyzed by Statistical Package for Social Sciences software (version 19.0). Groups were analyzed using the one-way analysis of variance (ANOVA), followed by Newman-Keuls post hoc analysis. Threshold for statistical significance was set at $P < 0.05$.

## 3. Results

*3.1. $NAD^+$ Inhibits Autophagy Activation after I/R Injury.* Our previous study [19] revealed that $NAD^+$ with the concentration higher than 50 mg/kg significantly alleviated spinal cord ischemia-reperfusion injury via reducing oxidative stress-induced neuronal apoptosis; however, 10 mg/kg $NAD^+$ showed no obvious therapeutic effect on this damage. So, we chose 75 mg/kg $NAD^+$ as an effective therapeutic dosage and chose 10 mg/kg $NAD^+$ as an invalid ineffective concentration in this study. To detect whether $NAD^+$ exerted an effect on autophagy activation in SCIR injury, it is essential to measure the level of protein LC3, p62, and Atg12-Atg5 proteins. Our result shows that expression levels of LC3-II in spinal cords of the I/R group were significantly larger at 24 h than in sham-operated rats. Treatment with 75 mg/kg $NAD^+$ could decrease the LC3-II protein expression at 24 h. However, no significant difference was observed between the 10 mg/kg $NAD^+$ group and the I/R group (Figure 1). Atg12-Atg5 was upregulated in the I/R and 10 mg/kg $NAD^+$ group and downregulated

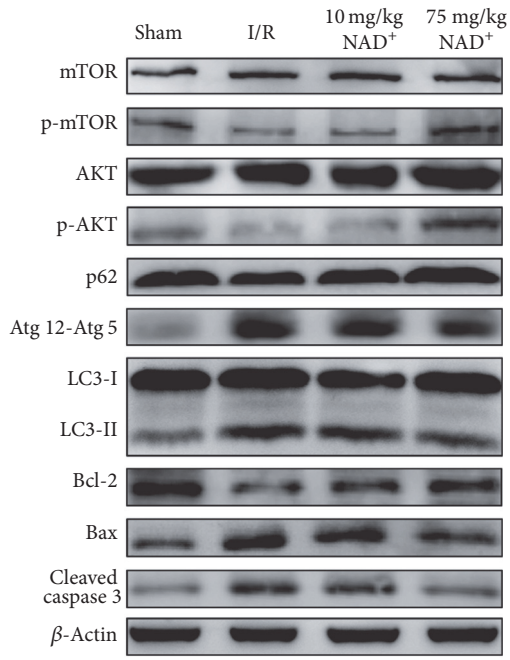


Figure 1: Changes in protein expression after spinal cord ischemia reperfusion (I/R) injury and treatment with different dose of nicotinamide adenine dinucleotide ($NAD^+$) ($n = 6$ per group).

in the 75 mg/kg $NAD^+$ group (Figure 1). However, LC3-II gave similar results. Conversely, the expression of p62 decreased in the I/R and 10 mg/kg $NAD^+$ group. However, no significant decrease in expression was observed in the 75 mg/kg $NAD^+$ group (Figure 1). The above changes in protein expression could indicate an activation of autophagy in SCIR. To further explore autophagy activation in neuronal cells, immunofluorescence staining of LC3 was performed (Figure 2(a)). The results showed that mean fluorescence intensity of LC3 increased significantly in neuronal cells of the I/R group ($P < 0.01$, versus sham), indicating autophagy activation in neurons. Compared with the I/R group, the mean fluorescence intensity of LC3 decreased in the 75 mg/kg $NAD^+$ group ($P < 0.01$). No significant difference was detected in the 10 mg/kg $NAD^+$ group compared with I/R group ($P > 0.05$; Figure 2(b)). These results confirmed that autophagy was activated in neuronal cells after SCIR. Administration of $NAD^+$ could inhibit autophagy to a certain extent.

*3.2. $NAD^+$ Ameliorates Deteriorated Neurological Functions after Autophagy Activation after I/R Injury.* Motor functions of rats were evaluated using BBB scores. Figure 3 showed the trends in the different groups. All rats experienced severe paraplegia in the first few hours after reperfusion, except rats from the sham group. The 75 mg/kg $NAD^+$ group showed faster and better recovery of motor functions than the I/R group ($P < 0.01$); however, I/R rats treated with 10 mg/kg $NAD^+$ showed no significant improvement in motor functions compared with the I/R group ($P > 0.05$). These results were in accordance with results from Nissl staining (Figure 4(a)). The mean IOD of Nissl was significantly smaller in the I/R and 10 mg/kg $NAD^+$ group ($P < 0.01$, versus sham) and larger in the 75 mg/kg $NAD^+$ group compared with I/R group ($P < 0.01$; Figure 4(b)). These results indicate that neurological function deteriorated after I/R injury and was gradually restored with the administration of $NAD^+$.

*3.3. Autophagy Can Aggravate and $NAD^+$ Can Alleviate Cell Apoptosis in I/R Injury.* To investigate the interaction between autophagy and apoptosis in ischemic reperfusion injury, we examined the protein expression levels of cleaved caspase 3 and immunofluorescence signals of TUNEL and caspase 3. Our results indicate that expression of cleaved caspase 3 was distinctly lower in the 75 mg/kg $NAD^+$ group than the I/R and 10 mg/kg $NAD^+$ group (Figure 1). Immunofluorescence staining gave similar results (Figures 5(a) and 5(b)). Greater number of TUNEL-positive neurons and higher mean fluorescence intensity of caspase 3 were detected in the I/R and 10 mg/kg $NAD^+$ group ($P < 0.01$ versus sham). In contrast, both parameters were dramatically lower in the 75 mg/kg $NAD^+$ group ($P < 0.01$; Figures 5(c) and 5(d)). Therefore, we concluded that autophagy aggravated neuronal apoptosis in I/R injury and $NAD^+$ decreased neuronal apoptosis.

*3.4. The Pathway of Autophagy Activation and Neuroprotective Mechanisms of $NAD^+$.* The PI3K/AKT/mTOR pathway is an intracellular signaling pathway important in regulating the cell cycle. A recent study has shown that AKT/mTOR signaling pathway is essential in the activation of autophagy [8]. To explore the role of the AKT/mTOR pathway, western blot analysis was performed. Our results indicate that expression of p-AKT and p-mTOR was significantly lower in I/R and 10 mg/kg $NAD^+$ group, but markedly higher in the 75 mg/kg $NAD^+$ group. The Bcl-2 family of apoptosis-related genes has been considered to play a central role in regulating apoptotic signaling cascade [23]. Bcl-2 exerts a survival function in response to a wide range of apoptotic stimuli through inhibition of mitochondrial cytochrome c release. Moreover, Bax is a key component for cellular induced apoptosis through mitochondrial stress. Therefore, we further evaluated whether the expression of these proteins was correlated with apoptosis. We found the increased Bax and decreased Bcl-2 in I/R and I/R + 10 mg/kg $NAD^+$ group, and the processes were significantly restrained after 75 mg/kg $NAD^+$ administration (Figure 1). Immunofluorescence and immunohistochemistry analysis of Bax further confirmed these results (Figure 6). Taken together, our data suggests that autophagy is partially regulated through the PI3K/AKT/mTOR pathway and apoptosis is partially regulated through the Bcl-2/Bax pathway. Furthermore, the protective effect of $NAD^+$ may occur in part through these pathways.

## 4. Discussion

SCIR involves a series of complex metabolic derangements including molecular and cellular events, such as oxidative stress, inflammatory response, apoptosis, and autophagy [24].

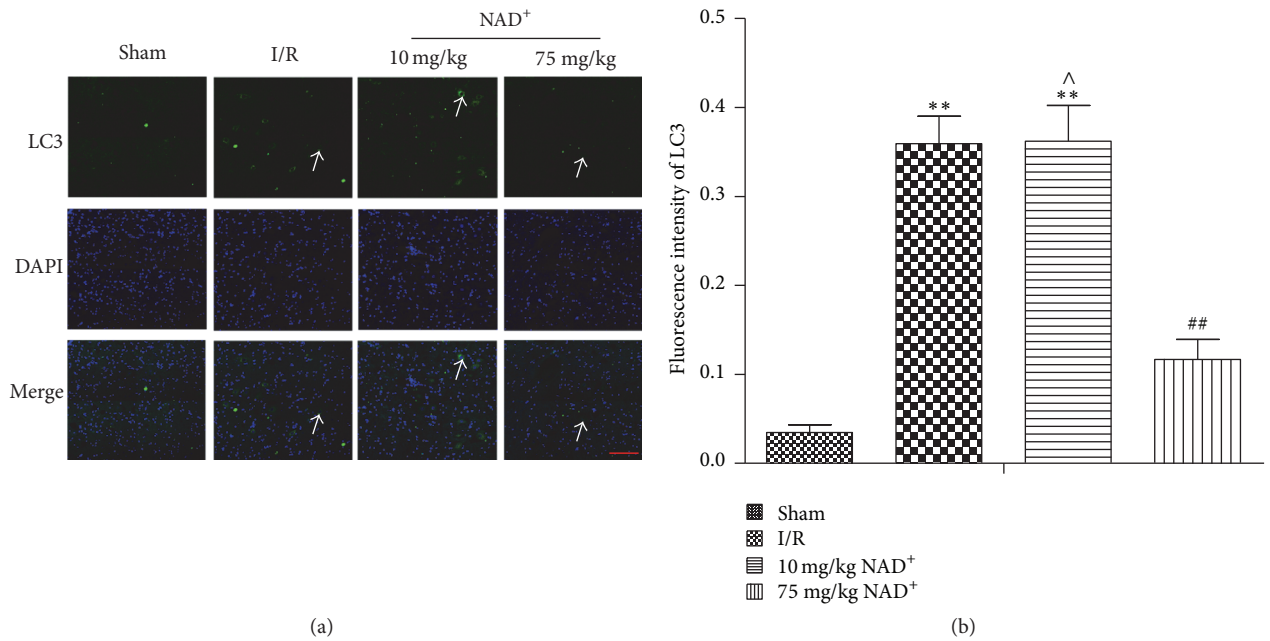


Figure 2: Immunofluorescence staining of LC3B in sham, ischemia reperfusion (I/R), 10 mg/kg nicotinamide adenine dinucleotide ($NAD^+$), and 75 mg/kg $NAD^+$ group. (a) LC3B-positive neurons (arrow) were observed in different groups (400x, scale bar = 50 $\mu$m). (b) Analysis of fluorescence intensity of LC3B-positive neurons in each group. Compared with the sham group, the fluorescence intensity of LC3B-positive neurons was significantly increased in the I/R group. Compared with the I/R group, the fluorescence intensity of LC3B-positive neurons was significantly decreased in the 75 mg/kg $NAD^+$ group. There was no significant difference in 10 mg/kg $NAD^+$ group. Values are means ± SD ($n = 6$ per group). $^{**}P < 0.01$ versus sham; $^{\#\#}P < 0.01$ versus I/R; $^{\wedge}P > 0.05$ versus I/R.

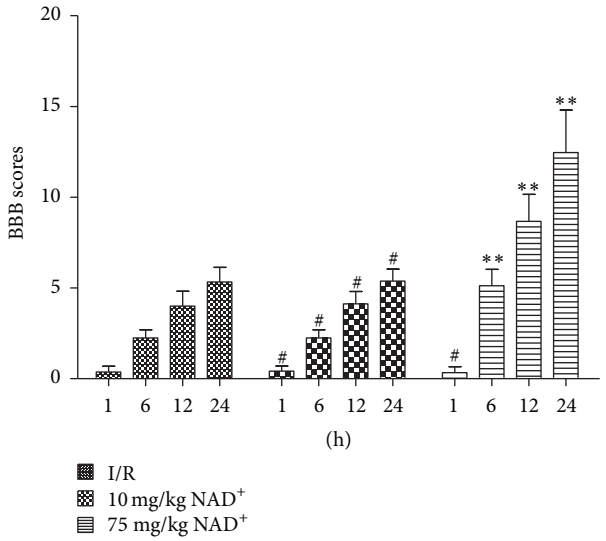


Figure 3: Basso, Beattie, and Bresnahan (BBB) scores of rats in ischemia reperfusion (I/R), 10 mg/kg nicotinamide adenine dinucleotide ($NAD^+$), and 75 mg/kg $NAD^+$ group at each time point. BBB scores were measured from 1 h to 24 h after I/R injury. Compared with the I/R group, BBB scores were consistently higher in 75 mg/kg $NAD^+$-treated rats from 6 to 24 h after I/R injury, whereas there were no significant differences in the 10 mg/kg $NAD^+$ group from 1 h to 24 h after injury. Values are means ± SD ($n = 12$ per group). $^{**}P < 0.01$ versus I/R; $^{\#}P > 0.05$ versus I/R.

In addition to primary ischemic injury, neuronal death induced by damage secondary to reperfusion is the major therapeutic conundrum in SCIR [25]. A growing body of experimental studies described the pathological derangement and molecular and cellular events in ischemic reperfusion injury and examined the efficacy of novel strategies [26–28]. A role of autophagy has been implicated not only in central nervous system diseases, including traumatic brain injury, cerebral ischemia, and neurodegeneration [28, 29], but also in other pathological conditions, such as cancer, myocardial infarction, and infections [26, 30]. However, the exact role of autophagy in these processes remains to be elucidated. Recently, an increasing number of studies have investigated the role of autophagy in I/R injury. Whether autophagy is neuroprotective in spinal cord injury has not yet been clarified. Therefore, we aimed to explore the types of neuronal death and potential signaling pathways involved in SCIR. An understanding of these mechanisms is critical for reliable protective therapeutic strategies.

Mounting evidence suggests that $NAD^+$ plays an important role in mitochondrial function, calcium homeostasis, and immunological functions [14, 15]. $NAD^+$ is a key cofactor for metabolizing energy and various enzymes [13]. $NAD^+$ repletion has been suggested to decrease astrocyte death [18]. However, studies regarding the effect of $NAD^+$ on SCIR and the role of $NAD^+$ involved in autophagy are scarce. In this study, for the first time, we investigate the role of autophagy

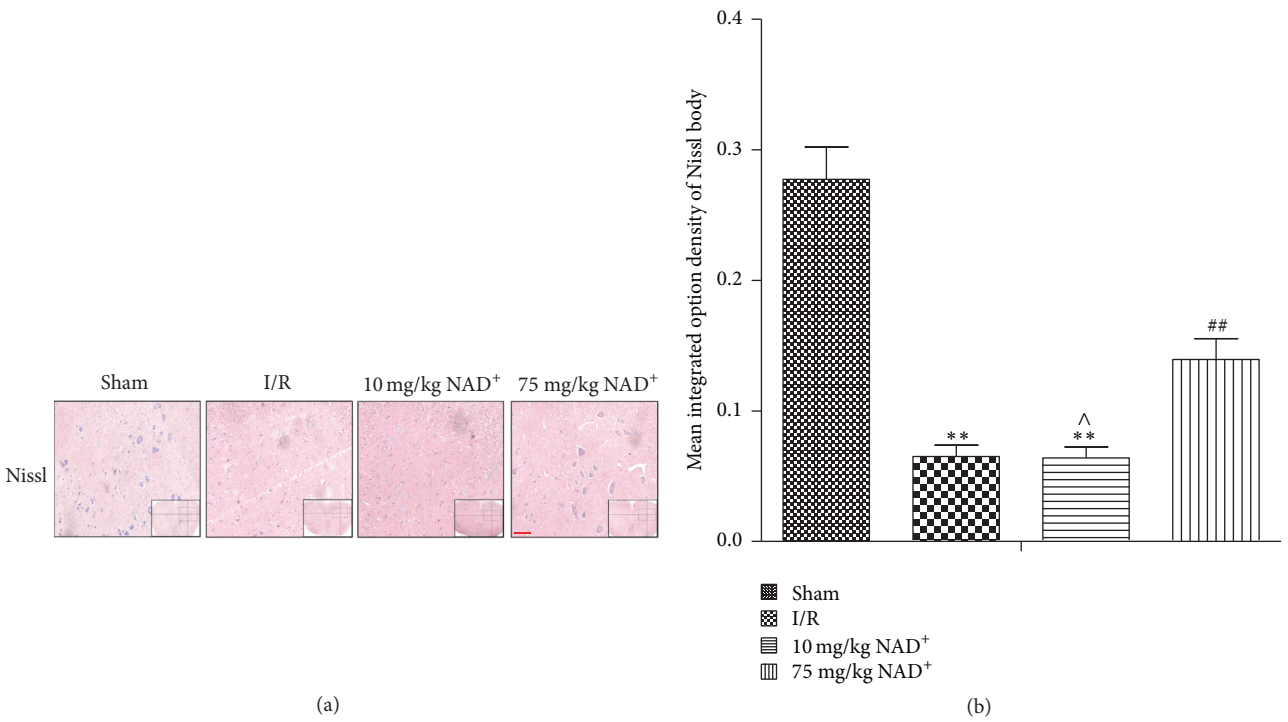


Figure 4: Nissl staining in sham, ischemia reperfusion (I/R), 10 mg/kg $NAD^+$, and 75 mg/kg nicotinamide adenine dinucleotide ($NAD^+$) group. (a) Nissl bodies were observed in different groups (100x, scale bar = 100 $\mu$m). (b) Analysis of the mean integrated option density (IOD) of Nissl bodies in each group. Compared with the sham group, the mean IOD of Nissl bodies was significantly decreased in the I/R group. Compared with the I/R group, the mean IOD of Nissl bodies was significantly increased in the 75 mg/kg $NAD^+$ group. No significant differences were observed in the 10 mg/kg $NAD^+$ group. Values are means ± SD ($n$ = 6 per group). $^{**}P < 0.01$ versus sham; $^{\#\#}P < 0.01$ versus I/R; $^{\wedge}P > 0.05$ versus I/R.

in SCIR and assess the effect of $NAD^+$ administration after SCIR. We found that expression of LC3-II was significantly increased in the I/R group and decreased in the 75 mg/kg $NAD^+$ group. Moreover, the level of p62 expression was decreased in I/R group, whereas it remained unchanged in the 75 mg/kg $NAD^+$ group. Moreover, the mean fluorescence intensity of LC3 was significantly increased in neurons of the I/R group and decreased in the 75 mg/kg $NAD^+$ group. These findings suggested that autophagy occurred after SCIR and that a high enough level of $NAD^+$ could inhibit it.

In this study, we focused on exploring the relationship between apoptosis and autophagy after SCIR. Our results show that cleaved caspase 3 was obviously increased in the I/R group and reduced in the 75 mg/kg $NAD^+$ group relative to the I/R group. The TUNEL and caspase 3 positive cells were neurons. Furthermore, the number of TUNEL-positive cells and mean fluorescence intensity of caspase 3 also increased in the I/R group and decreased in 75 mg/kg $NAD^+$ group. In conjunction with previous findings, we propose that activation of autophagy might promote neuronal apoptosis, whereas $NAD^+$ administration reduced neuronal loss by blocking autophagy. These results seem to contradict the results of some previous studies, which concluded that autophagy activation could prevent neuronal loss and had antiapoptotic effects in spinal cord injury [9, 10]. There are several possible explanations for the discrepancy: First, different experimental models were used to assess the function of autophagy and its relationship with apoptosis. Second, the degree of autophagy activation differs between the different studies, suggesting that autophagy may play a dual role: low levels of autophagy activation promote cell survival, while overactivation of autophagy leads to cell death. Surgical method, ischemic time, and reperfusion time are also potential confounding factors. This interpretation also explains the complex role of autophagy in SCIR. Further well-designed studies are warranted to clarify this issue.

Next, we focused on the signaling pathway activating autophagy and the protective mechanism of $NAD^+$. The formation of the autophagosome, elongation, maturation, and fusion are the major steps of autophagy. Various proteins are involved in this process; however only a small subset has been identified until now [31]. The PI3K/AKT/mTOR pathway is an intracellular signaling pathway important in cell cycle regulation. PI3K/AKT/mTOR pathway is the most classical activation pathway of autophagy. Akt activates the downstream mTOR signaling pathway. mTOR is inactivated by nutrient deprivation and then regulates downstream proteins to facilitate nucleation, the first step of autophagic vesicle formation [8]. The molecular mechanism of mTOR regulation in SCIR is still controversial. In this study, we

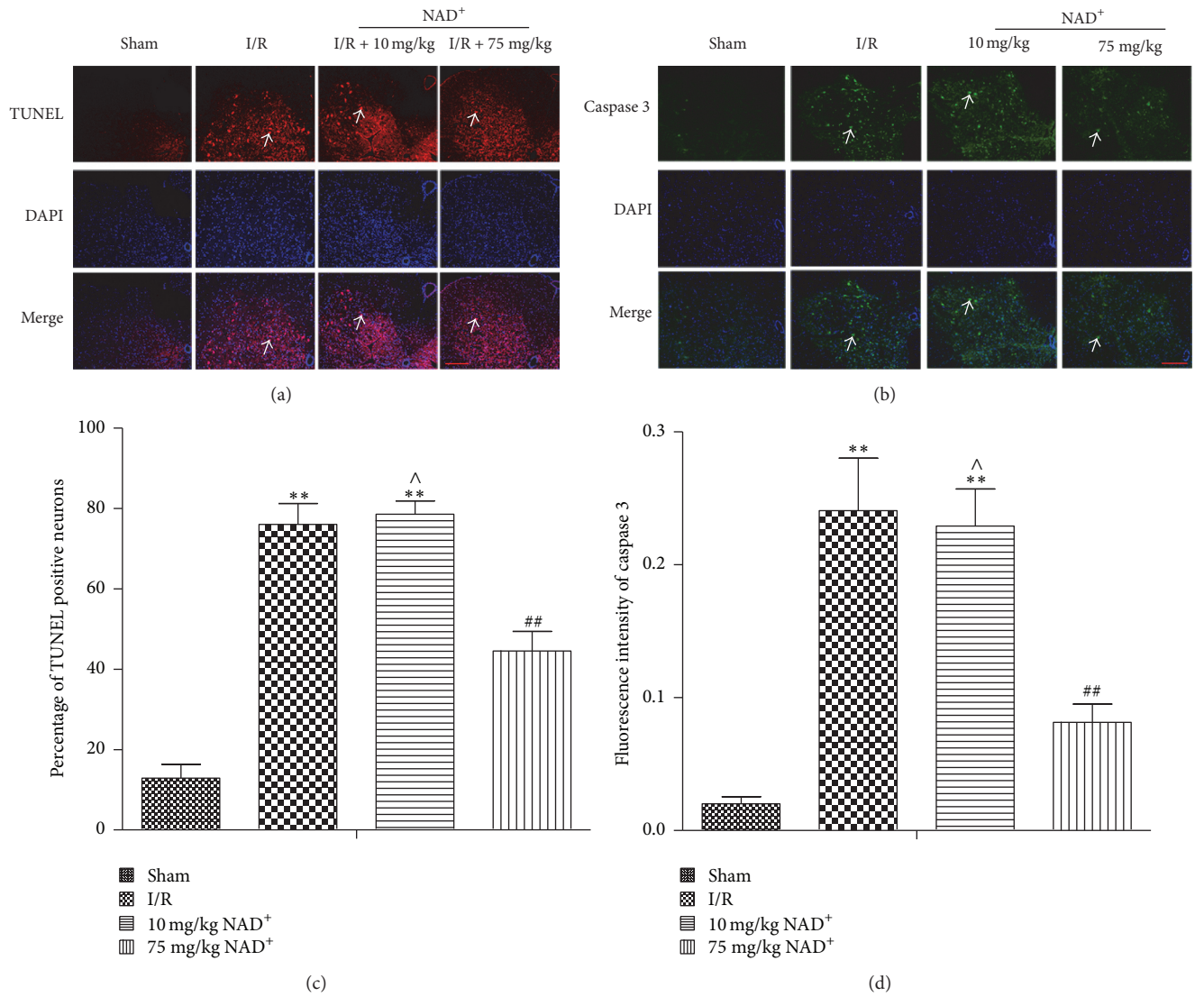


FIGURE 5: Immunofluorescence staining of terminal deoxynucleotidyl transferase-mediated dUTP nick end labeling (TUNEL) and caspase 3 in sham, ischemia reperfusion (I/R), 10 mg/kg nicotinamide adenine dinucleotide ($NAD^+$), and 75 mg/kg $NAD^+$ group. (a) TUNEL-positive neurons (arrow) were observed in different groups (200x, scale bar = 100 $\mu$m). (b) Caspase 3-positive neurons (arrow) were observed in different groups (200x, scale bar = 100 $\mu$m). (c, d) Analysis of the percentage of TUNEL-positive neurons and fluorescence intensity of caspase 3-positive neurons in each group, respectively. Compared with the sham group, the percentage of TUNEL-positive neurons and fluorescence intensity of caspase 3-positive neurons were significantly increased in the I/R group. Compared with the I/R group, the percentage of TUNEL-positive neurons and fluorescence intensity of caspase 3-positive neurons significantly were decreased in the 75 mg/kg $NAD^+$ group. No significant differences were observed in the 10 mg/kg $NAD^+$ group. Values are means ± SD ($n = 6$ per group). $^{**}P < 0.01$ versus sham; $^{\#\#}P < 0.01$ versus I/R; $^{\wedge}P > 0.05$ versus I/R.

found that phosphorylation of AKT and mTOR was inhibited in I/R group and activated in the 75 mg/kg $NAD^+$ group. We also analyzed expression levels of Atg12-Atg5, p62, and LC3B. Our results supported the above hypothesis that PI3K/AKT/mTOR is included in the activation pathway of autophagy in SCIR. Furthermore, we investigated Beclin-1 expression, because previous studies have indicated that Beclin-1-independent autophagy was alternative pathway [8, 32, 33]. Our results confirmed these observations. Taken together, both PI3K/AKT/mTOR and Beclin-1-independent pathway regulated autophagy and higher doses of $NAD^+$ could block these two pathways.

Previous studies have shown that Bax can induce apoptosis, whereas Bcl-2 exerts an antiapoptotic effect [23]. In the present study, we assessed the expression of Bcl-2 and Bax and immunofluorescence/immunohistochemistry signals of Bax. In the I/R group, expression of Bcl-2 decreased, whereas expression of Bax, mean fluorescence intensity, and mean IOD of Bax increased. Opposite effects were observed in 75 mg/kg $NAD^+$ group compared with the I/R group. These

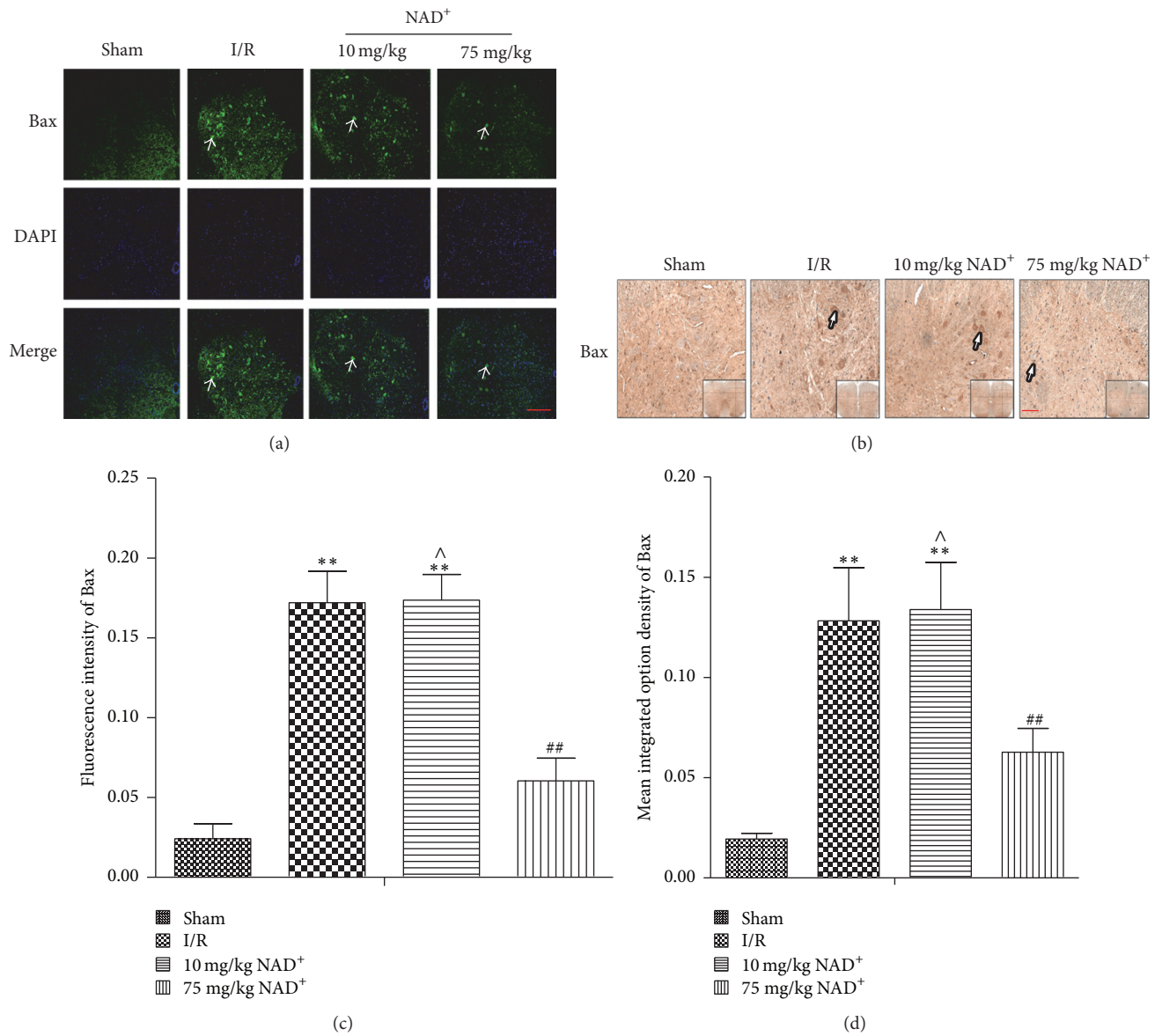


FIGURE 6: Immunofluorescence and immunohistochemical staining of Bax in sham, ischemia reperfusion (I/R), 10 mg/kg nicotinamide adenine dinucleotide ($NAD^+$), and 75 mg/kg $NAD^+$ group. (a) Bax-positive neurons (arrow) were observed in different groups (200x, scale bar = 100 $\mu$m). (b) Bax-positive neurons (arrow) were observed in different groups (100x, scale bar = 100 $\mu$m). (c, d) Analysis of fluorescence intensity of Bax-positive neurons and the mean integrated option density (IOD) of Bax in each group, respectively. Compared with the sham group, the fluorescence intensity of Bax-positive neurons and the mean IOD of Bax were significantly increased in the I/R group. Compared with the I/R group, the fluorescence intensity of Bax-positive neurons and the mean (IOD) of Bax-positive neurons were significantly decreased in the 75 mg/kg $NAD^+$ group and were not significantly different in the 10 mg/kg $NAD^+$ group. Values are means ± SD ($n$ = 6 per group). $^{**}P < 0.01$ versus sham; $^{\#\#}P < 0.01$ versus I/R; $^{\wedge}P > 0.05$ versus I/R.

findings indicate that the Bcl-2/Bax pathway is related to neuronal apoptosis in SCIR and $NAD^+$ may decrease apoptosis partially through this pathway.

In our study, in the I/R group, the expression of Beclin-1 was significantly increased and the number of neurons apoptosis was the highest. This phenomenon largely resulted from the proapoptotic function of Beclin-1, which was consistent with previously reported studies indicating the involvement of Beclin-1 in mitochondria-mediated apoptosis [8]. Recently, growing interest has focused on the role of Bcl-2 in autophagy, which is thought to be an important factor for crosstalk between autophagy and apoptosis [10, 32, 34]. Our results indicate the transition from autophagy to apoptosis might be via deregulation of Bcl-2 protein and upregulation of Bax protein. Therefore, we suggest that the neuroprotective mechanism of $NAD^+$ is inhibiting the conversion of autophagy to apoptosis by increasing the phosphorylation of AKT/mTOR and decreasing the expression of Beclin-1.

It is essential to comprehensively understand the complex function of autophagy and its relationship with apoptosis in SCIR.

Although we present important findings in this study, several limitations need to be addressed. First, although the SCIR model used in this study has been widely used due to the segmental blood supply of the spine, the model has its own shortcomings, such as lower limbs ischemia. Different modified models should be considered in future studies. Second, the period of postoperative observations was 24 h in our study. This period was not sufficient to determine whether $NAD^+$ had long-lasting neuroprotective effects. In addition, $NAD^+$ was administrated only at two predetermined doses (10 and 75 mg/kg) in this study, although our previous work has demonstrated $NAD^+$ with the concentration higher than 50 mg/kg exerted a protective role in SCIR injury. Moreover, although no obvious side effects of 75 mg/kg $NAD^+$ were identified until the predetermined observation time point, the lack of adverse response could be due to the limited observation time in our study; further studies with different dosages of $NAD^+$ as well as longer observation time are needed to strengthen and extend our present work.

## 5. Conclusion

In summary, this study suggests excessive and sustained activation of autophagy in SCIR. Administration of $NAD^+$ can decrease I/R induced injury and inhibit neuronal cell apoptosis. Further studies are needed to explore the implications of these findings.

## Abbreviations

| | |
|---|---|
| I/R: | Ischemia reperfusion |
| SCIR: | Spinal cord ischemia reperfusion injury |
| TUNEL: | Terminal deoxynucleotidyl transferase-mediated dUTP-biotin nick end labeling assay |
| LC3: | Microtubule-associated protein 1 light chain 3 |
| $NAD^+$: | Nicotinamide adenine dinucleotide |
| BBB score: | Basso-Beattie-Bresnahan score |
| IOD: | Integrated option density. |

## Competing Interests

The authors declare no competing financial interests.

## Authors' Contributions

Lei Xie, Sifei Yu, and Zhenfei Wang contributed equally to this work.

## Acknowledgments

This work was supported by Shanghai Sailing Program [Grant no. 16YF1410100].

## References

[1] C. D. Etz, E. Weigang, M. Hartert et al., "Contemporary spinal cord protection during thoracic and thoracoabdominal aortic surgery and endovascular aortic repair: a position paper of the vascular domain of the European association for cardio-thoracic surgery," *European Journal of Cardio-thoracic Surgery*, vol. 47, no. 6, Article ID ezv142, pp. 943–957, 2014.

[2] J. S. Coselli, S. A. LeMaire, C. C. Miller III et al., "Mortality and paraplegia after thoracoabdominal aortic aneurysm repair: a risk factor analysis," *Annals of Thoracic Surgery*, vol. 69, no. 2, pp. 409–414, 2000.

[3] M. F. Conrad, J. Y. Ye, T. K. Chung, J. K. Davison, and R. P. Cambria, "Spinal cord complications after thoracic aortic surgery: long-term survival and functional status varies with deficit severity," *Journal of Vascular Surgery*, vol. 48, no. 1, pp. 47–53, 2008.

[4] R. P. Cambria, D. Clouse, J. K. Davison et al., "Thoracoabdominal aneurysm repair: results with 337 operations performed over a 15-year interval," *Annals of Surgery*, vol. 236, no. 4, pp. 471–479, 2002.

[5] M. S. Bischoff, G. Di Luozzo, E. B. Griepp, and R. B. Griepp, "Spinal cord preservation in thoracoabdominal aneurysm repair," *Perspectives in Vascular Surgery and Endovascular Therapy*, vol. 23, no. 3, pp. 214–222, 2011.

[6] B. Herlambang, K. Orihashi, T. Mizukami et al., "New method for absolute spinal cord ischemia protection in rabbits," *Journal of Vascular Surgery*, vol. 54, no. 4, pp. 1109–1116, 2011.

[7] J. Wang and D. D. Pearse, "Therapeutic hypothermia in spinal cord injury: the status of its use and open questions," *International Journal of Molecular Sciences*, vol. 16, no. 8, pp. 16848–16879, 2015.

[8] D. J. Klionsky, K. Abdelmohsen, A. Abe et al., "Guidelines for the use and interpretation of assays for monitoring autophagy (3rd edition)," *Autophagy*, vol. 12, no. 1, pp. 1–222, 2016.

[9] H. Hou, L. Zhang, L. Zhang, and P. Tang, "Acute spinal cord injury in rats should target activated autophagy: laboratory investigation," *Journal of Neurosurgery: Spine*, vol. 20, no. 5, pp. 568–577, 2014.

[10] P. Tang, H. Hou, L. Zhang et al., "Autophagy reduces neuronal damage and promotes locomotor recovery via inhibition of apoptosis after spinal cord injury in rats," *Molecular Neurobiology*, vol. 49, no. 1, pp. 276–287, 2014.

[11] H. Hou, L. Zhang, L. Zhang et al., "Acute spinal cord injury in rats induces autophagy activation," *Turkish Neurosurgery*, vol. 24, no. 3, pp. 369–373, 2014.

[12] H.-Y. Zhang, Z.-G. Wang, F.-Z. Wu et al., "Regulation of autophagy and ubiquitinated protein accumulation by bFGF promotes functional recovery and neural protection in a rat model of spinal cord injury," *Molecular Neurobiology*, vol. 48, no. 3, pp. 452–464, 2013.

[13] P. Belenky, K. L. Bogan, and C. Brenner, "$NAD^+$ metabolism in health and disease," *Trends in Biochemical Sciences*, vol. 32, no. 1, pp. 12–19, 2007.

[14] Y. Ma, H. Chen, X. He et al., "NAD+ metabolism and NAD+-dependent enzymes: promising therapeutic targets for neurological diseases," *Current Drug Targets*, vol. 13, no. 2, pp. 222–229, 2012.

[15] W. Ying, "NAD+ and NADH in cellular functions and cell death," *Frontiers in Bioscience*, vol. 11, no. 3, pp. 3129–3148, 2006.

[16] S.-W. Yu, H. Wang, M. F. Poitras et al., "Mediation of poly(ADP-ribose) polymerase-1-dependent cell death by apoptosis-inducing factor," *Science*, vol. 297, no. 5579, pp. 259–263, 2002.

[17] M. Endres, Z.-Q. Wang, S. Namura, C. Waeber, and M. A. Moskowitz, "Ischemic brain injury is mediated by the activation of poly(ADP- ribose)polymerase," *Journal of Cerebral Blood Flow and Metabolism*, vol. 17, no. 11, pp. 1143–1151, 1997.

[18] C. C. Alano, W. Ying, and R. A. Swanson, "Poly(ADP-ribose) polymerase-1-mediated cell death in astrocytes requires NAD+ depletion and mitochondrial permeability transition," *Journal of Biological Chemistry*, vol. 279, no. 18, pp. 18895–18902, 2004.

[19] L. Xie, Z. Wang, C. Li, K. Yang, and Y. Liang, "Protective effect of nicotinamide adenine dinucleotide (NAD+) against spinal cord ischemia–reperfusion injury via reducing oxidative stress-induced neuronal apoptosis," *Journal of Clinical Neuroscience*, vol. 36, pp. 114–119, 2017.

[20] Q. Zhang, C. Huang, B. Meng, T. Tang, Q. Shi, and H. Yang, "Acute effect of ghrelin on ischemia/reperfusion injury in the rat spinal cord," *International Journal of Molecular Sciences*, vol. 13, no. 8, pp. 9864–9876, 2012.

[21] C. Zheng, J. Han, W. Xia, S. Shi, J. Liu, and W. Ying, "NAD+ administration decreases ischemic brain damage partially by blocking autophagy in a mouse model of brain ischemia," *Neuroscience Letters*, vol. 512, no. 2, pp. 67–71, 2012.

[22] D. M. Basso, M. S. Beattie, and J. C. Bresnahan, "A sensitive and reliable locomotor rating scale for open field testing in rats," *Journal of Neurotrauma*, vol. 12, no. 1, pp. 1–21, 1995.

[23] N. Volkmann, F. M. Marassi, D. D. Newmeyer, and D. Hanein, "The rheostat in the membrane: BCL-2 family proteins and apoptosis," *Cell Death and Differentiation*, vol. 21, no. 2, pp. 206–215, 2014.

[24] M. S. Beattie, "Inflammation and apoptosis: linked therapeutic targets in spinal cord injury," *Trends in Molecular Medicine*, vol. 10, no. 12, pp. 580–583, 2004.

[25] M. M. Wynn and C. W. Acher, "A modern theory of spinal cord ischemia/injury in thoracoabdominal aortic surgery and its implications for prevention of paralysis," *Journal of Cardiothoracic and Vascular Anesthesia*, vol. 28, no. 4, pp. 1100–1111, 2014.

[26] T. Aoyagi, Y. Kusakari, C.-Y. Xiao et al., "Cardiac mTOR protects the heart against ischemia-reperfusion injury," *American Journal of Physiology - Heart and Circulatory Physiology*, vol. 303, no. 1, pp. H75–H85, 2012.

[27] B.-L. Chen, L.-T. Wang, K.-H. Huang, C.-C. Wang, C.-K. Chiang, and S.-H. Liu, "Quercetin attenuates renal ischemia/reperfusion injury via an activation of AMP-activated protein kinase-regulated autophagy pathway," *Journal of Nutritional Biochemistry*, vol. 25, no. 11, pp. 1226–1234, 2014.

[28] B.-Y. Chiu, C.-P. Chang, J.-W. Lin et al., "Beneficial effect of astragalosides on stroke condition using PC12 cells under oxygen glucose deprivation and reperfusion," *Cellular and Molecular Neurobiology*, vol. 34, no. 6, pp. 825–837, 2014.

[29] B. D. S. Clarkson, C. Ling, Y. Shi et al., "T cell-derived interleukin (IL)-21 promotes brain injury following stroke in mice," *Journal of Experimental Medicine*, vol. 211, no. 4, pp. 595–604, 2014.

[30] R. Ojha, S. Bhattacharyya, and S. K. Singh, "Autophagy in cancer stem cells: a potential link between chemoresistance, recurrence, and metastasis," *BioResearch Open Access*, vol. 4, no. 1, pp. 97–108, 2015.

[31] Z. Surviladze, R. T. Sterk, S. A. DeHaro, and M. A. Ozbun, "Cellular entry of human papillomavirus type 16 involves activation of the phosphatidylinositol 3-kinase/Akt/mTOR pathway and inhibition of autophagy," *Journal of Virology*, vol. 87, no. 5, pp. 2508–2517, 2013.

[32] Z.-Y. Wang, J.-H. Lin, A. Muharram, and W.-G. Liu, "Beclin-1-mediated autophagy protects spinal cord neurons against mechanical injury-induced apoptosis," *Apoptosis*, vol. 19, no. 6, pp. 933–945, 2014.

[33] H. Kanno, H. Ozawa, A. Sekiguchi, and E. Itoi, "Spinal cord injury induces upregulation of Beclin 1 and promotes autophagic cell death," *Neurobiology of Disease*, vol. 33, no. 2, pp. 143–148, 2009.

[34] S. Mukhopadhyay, P. K. Panda, N. Sinha, D. N. Das, and S. K. Bhutia, "Autophagy and apoptosis: where do they meet?" *Apoptosis*, vol. 19, no. 4, pp. 555–566, 2014.